UNIVERSITY OF WEST ATTICA
SCHOOL OF ENGINEERING
DEPARTMENT OF NAVAL ARCHITECTURE

Strength study of the foredeck and reinforcements of composite construction (Sandwich type) using the Finite Element Method for marine crane installation

Apostolos Galanis

submitted to the Department of Naval Architecture of the University of West Attica in partial fulfillment of the requirements for the degree in Naval Architecture and Marine Engineering

Athens, May 2022

Πανεπιστημιούπολη
Άλσους Αιγάλεω
Αγίου Σπυρίδωνος, Αιγάλεω 12243
τηλ: 210 5385100

ΠΑΝΕΠΙΣΤΗΜΙΟ ΔΥΤΙΚΗΣ ΑΤΤΙΚΗΣ
ΣΧΟΛΗ ΜΗΧΑΝΙΚΩΝ
ΤΜΗΜΑ ΝΑΥΠΗΓΩΝ ΜΗΧΑΝΙΚΩΝ

Μελέτη αντοχής του πρωραίου καταστρώματος και ενισχυτικών απο σύνθετη κατασκευή (τυπου Sandwich) με χρήση της Μεθόδου των Πεπερασμένων Στοιχείων για την τοποθέτηση γερανού

Απόστολος Γαλάνης

Διπλωματική Εργασία υποβληθείσα στο Τμήμα Ναυπηγών Μηχανικών του Πανεπιστημίου Δυτικής Αττικής ως μέρους των απαιτήσεων για την απόκτηση του πτυχίου Ναυπηγού Μηχανολόγου Μηχανικού.

Αθήνα,Μάιος 2022

Πανεπιστημιούπολη
Άλσους Αιγάλεω
Αγίου Σπυρίδωνος, Αιγάλεω 12243
τηλ: 210 5385100

Σελίδα Τριμελούς Εξεταστικής Επιτροπής

- Δημήτριος Δραγατογιάννης (Επιβλέπων)

Digitally signed by DIMITRIOS DRAGATOGIANNIS
Date: 2023.07.19 10:40:56 EEST

-Ισίδωρος Ιακωβίδης

Isidoros Iakovidis
Digitally signed by Isidoros Iakovidis
Date: 2023.07.25 21:31:56 +03'00'

-Θεοδουλίδης Αλέξανδρος

Alexandros Theodoulidis
Digitally signed by Alexandros Theodoulidis
Date: 2023.07.25 00:03:55 +03'00'

Ημερομηνία εξέτασης: 29/06/2023

Πανεπιστημιούπολη
Άλσους Αιγάλεω
Αγίου Σπυρίδωνος, Αιγάλεω 12243
τηλ: 210 5385100

Δήλωση Συγγραφέα Διπλωματικης Εργασίας

Ο κάτωθι υπογεγραμμένος Γαλάνης Απόστολος του Κωνσταντίνου, με αριθμό μητρώου 51117059, φοιτητής του Πανεπιστημίου Δυτικής Αττικής της Σχολής Μηχανικών του Τμήματος Ναυπηγών Μηχανικών, δηλώνω υπεύθυνα ότι: «Είμαι συγγραφέας αυτής της διπλωματικής εργασίας και ότι κάθε βοήθεια την οποία είχα για την προετοιμασία της είναι πλήρως αναγνωρισμένη και αναφέρεται στην εργασία. Επιπλέον, οι όποιες πηγές από τις οποίες έκανα χρήση δεδομένων, ιδεών ή λέξεων, είτε ακριβώς είτε παραφρασμένες, αναφέρονται στο σύνολό τους, με πλήρη αναφορά στους συγγραφείς, τον εκδοτικό οίκο ή το περιοδικό, συμπεριλαμβανομένων και των πηγών που ενδεχομένως χρησιμοποιήθηκαν από το διαδίκτυο. Επίσης, βεβαιώνω ότι αυτή η εργασία έχει συγγραφεί από μένα αποκλειστικά και αποτελεί προϊόν πνευματικής ιδιοκτησίας τόσο δικής μου, όσο και του Ιδρύματος.

Παράβαση της ανωτέρω ακαδημαϊκής μου ευθύνης αποτελεί ουσιώδη λόγο για την ανάκληση του πτυχίου μου».

Ο Δηλών

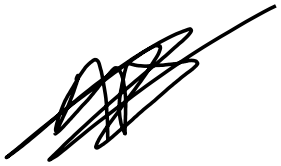

Γαλάνης Απόστολος

Πανεπιστημιούπολη
Άλσους Αιγάλεω
Αγίου Σπυρίδωνος, Αιγάλεω 12243
τηλ: 210 5385100

Acknowledgments

I express my heartfelt gratitude to my thesis advisor, Professor Dimitrios Dragatogiannis, for his invaluable guidance, support, and encouragement throughout my research. His expertise, insightful feedback, and unwavering dedication to excellence have been critical to the success of this work. I would also want to extend a sincere thank you to Professor Isidoros Iakovidis for his assistance and effort in making the experiments for the PVC core material a success.

I also thank the faculty and staff of the Naval Architecture and Marine Engineer at the University of West Attica for providing me with an exceptional learning environment and the resources I needed to pursue my research interests. Their unwavering commitment to academic excellence and research has been a constant source of inspiration and motivation. The finite element analysis software ANSYS® was provided by National Technical University of Athens - School of Chemical Engineering which I also warmly thank.

I am much obligated to my family and friends who have provided me with emotional support, encouragement, and motivation throughout my academic journey. Their unwavering faith in me has been a constant source of inspiration and has given me the strength to overcome any obstacle.

Finally, I would like to thank all participants who contributed their time and expertise to my research. Their willingness to share their experience and knowledge has been critical to the success of this study.

I am deeply grateful for everyone who has supported me in this endeavor and helped me achieve my academic goals.

Strength study of the foredeck and reinforcements of composite construction (Sandwich type) using the Finite Element Method for marine crane installation

Keywords: Structural design, Strength Analysis, Classification Society, DNV, Yacht, Marine crane, Finite element analysis, Composite sandwich structure, T-Joint

Abstract

This thesis presents a study on the installation of a yacht crane at the bow weather deck according to register regulations, by evaluating the strength and structural performance of the foredeck and reinforcements, using the Finite Element Method (FEM). Three geometry models are developed to analyze different configurations: Model (A) representing the existing bow region, Model (B) incorporating a T-Joint reinforcement, and Sub-Model (C) featuring a defected T-Joint. The two panels (bulkhead and deck) constitute a T-Joint reinforced locally by GFRP attachment laps at the region of cranes' installation.

The total deformation, normal and shear stresses, principal stresses, and the safety factor according to Tsai-Wu failure criterion are calculated. The results show that the incorporation of GFRP attachment laps at the region of cranes' installation significantly reduces local deformations and stresses, resulting in increased safety factor. Model (B), with the T-Joint, outperforms Model (A) in terms of deformation, stress distribution, and safety factor. The findings contribute to enhancing the understanding of the structural performance evaluation of yacht crane installations at the bow weather deck.

By employing Virtual Crack Closure Technique (VCCT) and analyzing Energy Release Rates, the study provides information on the influence of construction-related defects on the structural integrity. Within Sub-Model (C), a crack is located between the over laminated skin and the deck region of the T-Joint. Although fracture-related analysis is limited but provides valuable information on crack behavior and the potential implications of defects in a T-joint.

By considering the structural performance and safety aspects, designers and engineers can make optimum decisions regarding yacht crane installation and proper reinforcing, leading to safer and more efficient structures.

After extensive research of reliable information in the field of Marine Cranes and in particular application to yachts made of sandwich composite materials, it was noted that there is a serious lack of data and studies on this issue. This finding is one of the reasons why this study was conducted with as much information as possible included. Therefore, this study is based on data and guidance provided by the classification societies and rules of offshore structures.

Μελέτη αντοχής του πρωραίου καταστρώματος και ενισχυτικών απο σύνθετη κατασκευή (τυπου Sandwich) με χρήση της Μεθόδου των Πεπερασμένων Στοιχείων για την τοποθέτηση γερανού

Λέξεις Κλειδιά: Structural design, Strength Analysis, Classification Society, DNV, Yacht, Marine crane, Finite element analysis, Composite sandwich structure, T-Joint

Περίληψη

Η παρούσα διπλωματική εργασία παρουσιάζει μια μελέτη σχετικά με την εγκατάσταση ενός γερανού σκαφών αναψυχής στο κατάστρωμα της πλώρης σύμφωνα με τους κανονισμούς νηογνώμονα, αξιολογώντας την αντοχή του πρωραίου καταστρώματος και των ενισχύσεων, χρησιμοποιώντας τη μέθοδο πεπερασμένων στοιχείων (FEM). Για την μελέτη,αναπτύσσονται τρία γεωμετρικά μοντέλα: Το μοντέλο (Α) που αναπαριστά την υπάρχουσα περιοχή της πλώρης, το μοντέλο (Β) που ενσωματώνει την τοπική ενίσχυση T-Joint και το υπομοντέλο (Γ) το οποίο περιέχει ένα ελαττωματικό T-Joint. Τα δύο πάνελ (φρακτή και κατάστρωμα) αποτελούν ένα T-Joint ενισχυμένο τοπικά με GFRP attachment laps στην περιοχή εγκατάστασης του γερανού.

Υπολογίζονται η συνολική παραμόρφωση, οι ορθές και διατμητικές τάσεις, οι κύριες τάσεις και ο συντελεστής ασφαλείας σύμφωνα με το κριτήριο αστοχίας Tsai-Wu. Τα αποτελέσματα δείχνουν ότι η ενσωμάτωση των GFRP attachment laps στην περιοχή εγκατάστασης των γερανών μειώνει σημαντικά τις τοπικές παραμορφώσεις και τάσεις, με αποτέλεσμα την αύξηση του συντελεστή ασφαλείας. Το μοντέλο (Β), με την σύνδεση Τ, υπερτερεί του μοντέλου (Α) όσον αφορά την παραμόρφωση, την κατανομή των τάσεων και τον συντελεστή ασφαλείας. Τα αποτελέσματα συμβάλλουν στη βελτίωση της κατανόησης και αξιολόγησης της αντοχής των εγκαταστάσεων γερανών σκαφών αναψυχής στο κατάστρωμα της πλώρης.

Με τη χρήση της τεχνικής Virtual Crack Closure Technique (VCCT) και την ανάλυση του ρυθμού απελευθέρωσης ενέργειας, η μελέτη παρέχει πληροφορίες σχετικά με την επιρροή των ελαττωμάτων κατά την κατασκευαστική διαδικασία. Στο πλαίσιο του υποδείγματος (Γ), μια ρωγμή δημιουργείται μεταξύ του over laminated skin και της περιοχής του καταστρώματος στο T-Joint. Αν και η ανάλυση που σχετίζεται με τη θραύση είναι περιορισμένη, παρέχει πολύτιμες πληροφορίες σχετικά με τη συμπεριφορά της ρωγμής και τις πιθανές επιπτώσεις των ατελειών σε ένα T-joint.

Λαμβάνοντας υπόψη την αντοχή και τις πτυχές της ασφάλειας, οι σχεδιαστές και οι μηχανικοί μπορούν να λάβουν βέλτιστες αποφάσεις σχετικά με την εγκατάσταση ενός γερανού σε σκάφη αναψυχής και την κατάλληλη ενίσχυση, οδηγώντας σε ασφαλέστερες και αποδοτικότερες κατασκευές.

Μετά από εκτεταμένη έρευνα στον τομέα των ναυτικών γερανών και ειδικότερα της εφαρμογής σε σκάφη αναψυχής από σύνθετα υλικά σάντουιτς, διαπιστώθηκε ότι υπάρχει σοβαρή έλλειψη δεδομένων και μελετών για το θέμα αυτό. Η διαπίστωση αυτή είναι ένας από τους λόγους για τους οποίους διεξήχθη η παρούσα μελέτη με τη συμπερίληψη όσο το δυνατόν περισσότερων πληροφοριών. Ως εκ τούτου, η παρούσα μελέτη βασίζεται σε δεδομένα και οδηγίες που παρέχονται από τους νηογνώμονες και τους κανόνες των υπεράκτιων κατασκευών.

Table of Contents

List of Figures

List of Tables

Introduction

One of the main goals of a naval architect is to construct an optimal ship as possible. Optimization concerns both the strength and weight of the construction. A lighter ship that can meet the necessary strength conditions can operate at higher speeds with less fuel consumption and at the same time carry more payload.

In recent years, composite materials have gained an increasing position in the marine industry, finding applications in many different parts of the ship. The most common types of ships made of composite materials are high speed vessels, pleasure and patrol craft, mine hunters and generally military purpose vessels [1]. The most important components found in composite materials are the main hulls, decks, superstructures, bulkheads, propeller masts, etc. For example, the superstructure constructed by composite materials for cruise vessels or passenger vessels lowers the center of gravity of the structure by improving both stability and other parameters.

The joining of the various components and the structural integrity of the construction, it depends on various factors such as the type of joint, the materials and their mechanical properties, the joining area, etc. Joining between dissimilar materials, such as composites and metals, is more complex, due to the different mechanical properties [2]. The optimum joint transfers the loads between the components and ensures the uniform distribution of the stresses throughout the construction. Local stress concentration due to the discontinuity of the load transfer at the region of the joint is critical making a joint the weakest point of a construction. An optimum design policy suggests to avoid or limit the use of joining taking into account time and cost, as well [3].

In the marine industry, composite materials are joined mainly through adhesive bonding, over-lamination and mechanical joint techniques. As far as adhesive bonding is concerned, it is one of the relatively modern connection techniques, giving the construction many advantages compared to the rest, one of which is a uniform stress distribution. Adhesive bonding is essentially the connection of two materials using adhesives and has largely replaced the traditional joining techniques in both composite and metal constructions. In general, it offers high ratio of strength-to-weight and reduced production costs. For these reasons adhesive bonding is one effective way to join various structural parts to yachts, pleasure boats ferries, offshore boats and generally to any kind of marine application. Another important advantage is the fatigue resistance of the joint. Due to the elasticity and thermal expansion the impact energy of the waves or other factors is absorbed. In addition, they can offer easy assembly and disassembly, inspection, and maintenance. On the other hand, the increased weight, concentration of stress combined with the weakening of composite material and the creation of galvanic corrosion due to different materials are limitations in respect to the use of this type of joints. In over-lamination the connection is achieved by a further hand lamination of the parts. The over-lamination joint is an important connection technique that is mainly used in the bulkhead component of the ship. Overlapping is created from resin reinforced with fiberglass layers arranged so that the two

components are connected forming a T-type cross-section. The most critical point in over-lamination is the first layer. If a gap is created in this layer, then the joint of the two components becomes weaker, increasing the risk of failure of the connection. The fact that the over-lamination orientation does not affect the mechanical properties of the joint is key information [2].

A general description of the components made of composite materials is that in the case of single skin constructions the components consist of layers of reinforcement fabric in polymer resin matrix, while in the case of sandwich constructions the component consists of two single skin laminates and a core is contained between them which essentially connects the two skin laminates creating a single construction. More specifically, the materials used per element category are:

Glass (E glass, R glass, S glass), aramids (Kevlar, Twaron), carbon, polyester, high-performance polyethylene (HPPE), and combinations of all of the above are the major fiber materials used in reinforcing textiles. Chopped strand mat, continuous strand mat (randomly arranged fibres), woven roving (plain weave, satin, twill), uniaxial and "multiaxial" configurations are among the fabric types employed (layers of uniaxials stitched together, also known as non-crimp fabrics). Polyesters, vinylesters, epoxies and different modifications of these resins and phenolics are examples of matrix materials or resins. Polymer foams, end-grain balsa wood, honeycombs and corrugated FRP cores are some of Sandwich core components. PVC (different varieties), polymethacrylimide (PMI), polyetherimide (PEI) and phenolic are the most common foams used. Metal or aramid paper ("Nomex") are commonly used in honeycombs [3].

Talking exclusively about the ship structure made of composite materials, the available hull types that can be found in commercial application so far are unstiffened monocoque hull, single skin-framed hull (top hat), corrugated hull, as well as hybrid designs. The single-skin framed hull is similar to the usual metal ship constructions since the only difference is the fact that the shell and stiffeners are composed of composite materials. Monocoque hull structures are usually sandwich-type constructions. Due to that, they are thick enough to absorb impact loads and achieve the appropriate hull stiffness. As in any other sandwich-type construction skins are used to offer high strength, while the core offers high stiffness, light weight and resistance to shear loads, thus creating an overall construction of excellent durability. An evolution of monocoque hull is the corrugated hull which is designed with external longitudinal corrugations. This contributes to both the reduction of weight and construction costs and hull strengthening. This type of hull is applied to specific parts of the monocoque hull, mainly in the bottom and side shell. An integral component of the hull is the bulkhead with which the desired compartmentation is achieved on ship construction. The connection between the bulkhead and the hull allows the transport of many types of loads throughout the hull. The types of loads that a bulkhead receives are mainly divided into tensile, shear and bending. For example, the flooding of a compartment causes the development of hydrostatic pressure in the watertight bulkhead and as a result the creation of bending and shear load in the join between bulkhead and hull. The connection between the hull and the bulkhead is known as T-Joint and aims to transport tensile, flexural and shear loads between the hull and the bulkhead. Since the T-joint is a link by its nature, it tends to be the weakest point of construction and presents failures. The most common types that are presented are fillet cracking, disbond between overlaminates with the fillet materials, disbond between overlaminates in the area of

the bulkhead or hull and delamination of plies within the overlaminates. When there is a crack on a T-Joint there are two possible scenarios of the evolution of the phenomenon. The first is the crack to become larger than the one that already exists, while the second is to have a fracture mechanism. Regarding the safety measures against cracks, two basic parameters are calculated. One of them is the crack size that determines the fracture toughness of each material. The second one is the critical load. Fracture toughness is an important value for studies, since it essentially shows the resistance to the fracture of the material when there are cracks in it. On the basis of fracture toughness, the materials are categorized into brittle or ductile materials. Brittle materials show low fracture toughness and high yield strength while, on the other hand, ductile materials show high fracture toughness and low yield strength [4].

Taking into consideration the mechanics of adhesively bonded joints, as well as the geometry and materials of the components to be connected, service loads, environmental conditions and inspection requirements for the completed connection, are necessary for a successful design. Concerning the joint analysis, there is a variety of closed-form solutions accessible that are included in [5]. These may be used to determine how strong a bond is. However, these formulas are ineffective for complicated joint geometry. Due to this the only option is to conduct a FE study. Special attention must be paid to failure criteria, non-linear material modeling, modeling assumptions and simplifications and boundary conditions when performing FE analysis [1].

Finally, the evolution of composite materials and joints in the marine industry has a bright future, since the change in international rules away from prescriptive requirements and toward formal safety evaluation and probabilistic design techniques make it easier to utilize unique and sophisticated solutions by properly crediting them and making them appealing.

This study will be carried out taking into consideration all the above for a T-Joint stiffening of yacht bow region construction, inspired from a bulkhead-hull (deck or bottom) joint. It will also be representative for any other T-joint application.

The T-Joint studies are categorized according to the application, the type of connection, the loads exerted on the construction, the failure mode and the fracture behavior of the joint. The most common type of connections found, in respect to the construction of a T-joint are adhesively bond, z-pin and stitched connections.

An overview of an adhesively bonded T-Joint and adhesively bonded joints is given in [6]. The factors that affect the adhesion and the types of adhesives that exist are explained in detail while all possible joints, including the T-Joint geometry, are presented. All type of failure modes of adhesive materials is also discussed. To improve the resistance of the T-joint structure against adhesion failure, several methods are used, such as changing the anisotropy of the material stacking sequence of the laminated composite structure and adjusting the number of layers. In [8,9] an analysis of the strength of an adhesively bonded T-joint under fatigue using experimental and numerical analysis is studied by investigating two types of gluing, a flat joint and a grooved joint. The results showed that the grooved joint in fatigue is more durable than

the flat joint. Within the same framework, the structural behavior of the adhesively bonded composite sandwich T-Joint for aerospace applications is tested under quasi-static and dynamic loading conditions [10,11]. The same authors, in [12] conducted a significant numerical analysis of adhesively bonded T-joints with sandwich materials and a study of design parameters. The design parameters concern the fillet geometry and the core material of the sandwich panels. Whereas, for the study of geometrical models, different base fillet angles (25,30,35,40,45,50,55,60 and 70 degrees) were used. The base angle of fillets is one of the most important geometry parameters of T-Joint. In terms of sandwich panels, different types of foam with different stiffness (Divinycell H100 and Divinycell HCP70) were used, while the simulation of adhesive joints in numerical analysis is using contact elements and a cohesive zone material model.

In [13] a novel way to connect a sandwich panel and an aluminum plate in the T-joint form, using adhesive as a means of gluing, was carried out on behalf of the marine industry for two types of joints in different geometrical configurations. The first model follows the design of the joint according to the classification society Det Norske Veritas for high-speed light crafts, while the second model emerges from the first having made appropriate modifications in terms of durability, thus creating the new design configuration of the T-Joint. The new design has better load-carrying capacity than the previous one using 10% less adhesive which results in a more economical construction solution with better durability. By L. F. M. da Silva et al. [14], the effect of water on the fracture of adhesive joints was studied, by analyzing modes I, II and III of fracture failure in the following environments: dry, salt water and distilled water. In the salt water environment, there was an increase in mechanical properties, whereas in the distilled water environment there was a decrease. This provides the important information that the adhesive SikaPower-4720(of company Sika Vila Nova de Gaia, Portugal) and other similar materials are ideal for constructions immersed in salt water environments.

Another type of T-joint configuration is that of z-pin and stitch where in essence, it becomes a combination of adhesive and some kind of riveting as reinforcement of joint. The A. P. Mouritz.et al. [15],[16] mention that one of the serious problems of T -Joint is the delamination between the horizontal and vertical components caused by the transverse loads. Therefore, the delamination resistance of the composite joint can be improved in the direction of the thickness of the material using z-pins in the bonded region which increase the strength of the connection. The numerical results obtained using FEM were validated against experimental results. FEM analysis is carried out for failure mode I and II of the structure that contains the z-pin. The study by J. Bigaud et al. [17],[18] provides an analysis of the mechanical behavior of composite T-Joint reinforced by stitching. The results showed that, due to crack bridging that delamination toughness was increased, the energy release rate was better restrained in stitched structures, especially in the crucial area (delta-fillet). In comparison to the reference, the stitched T-joints had higher ultimate strength and load recovery post-ultimate strength.

In [19] is investigated the mechanical behavior of an ordinary adhesive, z-pin reinforcement and stitching reinforcement under tension loading in the vertical component of the structure. The tensile strength, damage failure mechanism and failure mode, are compared for the three types of joints. the z-pin reinforcement is the optimal solution in tensile strength compared to the stitching reinforcement. Similar results were obtained for the deformation of the construction, with the z-pin reinforcement again being the best solution. Regarding the failure mode, the ordinary adhesive T-Joint exhibits brittle failure, whereas the other two joints showed ductile damage behavior. Finally, an optimal and efficient way to enhance a T-Joint construction is definitely the z-pin reinforcement.

The main type of loads, that are exerted on a T-joint are tensile, pull-of or pull-out load.

The most common load exerted on such connections is the tensile load. As far as tensile forces are concerned, whenever these are applied to the vertical component of T-Joint they are called as pull-off or pull-out load in literature. The main failure mechanisms are fracture or delamination by creating and spreading a crack in one of the parts of the structure (adhesive region, core of panel, etc.). This local failure is capable of causing total failure in the construction once the load reaches a maximum value or even earlier.

In their widely acclaimed work, [20] discuss the design and test of sandwich t-joints for naval ships in the context of the EUCLID project “Survivability, Durability, and Performance of Naval Composite Structures”. This research studies improved T-Joint geometries subject to tensile load to improve strength or reduce the weight of the structure. The T-Joint consists of sandwich panels with PVC foam core and glass fiber /vinyl ester skin laminates, while for the connection of the panels, core triangles (fillets) are used made of PVC foam and filler (adhesive). In the FE analysis performed, the sandwich skin materials were assumed to be orthotopic and linear-elastic, when in fact all the other materials were considered linear-elastic and isotropic. An important observation was that the failure was initiated by a shear failure in the base panel of the joint. The main conclusion is that the base angle of the core triangle is the most important geometry parameter of the T-Joint and the 45 degrees angle is the optimal choice. The optimized design has far more durability and less weight than the original design.

An effective technique is using 3D woven reinforcements to increase the load-bearing capabilities of composite T-joints over laminates. This improvement may be optimized in terms of fiber architecture. Another type of T-Joint with delta-filler and L-ribs at tension load is studied in the research works [21]– [29]. The reduction of the fillet-fill ratio, the initiation and propagation paths of the delamination cracks are parameters that change the failure mode. The 3D braided composite fillers provide high transverse strength, high multidirectional loading capacity and high damage tolerance. The weakest area was found to be the filling area. A-Progressive Damage Model based on mixed criterion for failure has better results than those from Hou, Chang-Chang, and Hashin criteria for predicting mechanical behaviors under tensile load. The triangular zone filler and boundary angle radius are important parameters for construction with the triangular zone from resin showing the best behavior. A novel design of T-Joint using ply promises to strengthen the construction, altering the ply orientation in the

radius bend area and giving encouraging results to improve the mechanical properties of the joint.

The key failure modes are attributed to: i) cracking in the core of sandwich panel (core shear failure), ii) debonding between the connection fillet and sandwich panel, iii) debonding (interfacial failure) between the two sandwich panels (web and flange) [30-31]. Regarding the first study, an investigation is carried out for an original U-channel aluminum connection. It is placed in the base panel where the vertical component of T-Joint is placed inside it. This architecture hands out improved results compared to a conventional circular fillet T-Joint. Two more bolted joints are being studied in order to prove their efficiency in the phenomenon of debonding. Satisfactory results are not provided by the use of bolted joints in combination with a circular fillet failure of the panel since the core starts earlier. Therefore, it would be advisable that bolted joints should be avoided in a T-Joint construction even though they suppress debonding. While, on the other hand, the existence of the attachment lap in the construction is crucial since it distributes the load in a more efficient way throughout the construction. The authors in [32] propose a reinforcement of the T-Joint construction with thermoplastic composite fasteners which may reduce shear failure. The results showed that the bond strength of the T-Joint increased compared to that of the T-Joint without fasteners. In [33] an insight on the naval applications of T-joints is given taking into account dynamic loading conditions. An important conclusion is the fact that the fracture modes, under dynamic tensile loading, are similar to those of the static condition. Based on the above and considering that the construction will present failure between the overlaminates and the base panel, or core shear failure in the base panel, the following conclusions are drawn: i) core shear failure strength of the base panel is sensitive to all failure modes, ii) the failure load increases with larger fillet radius, iii) the fabrication defects reduce the strength of the structure and the failure load by 37-50%.

Focusing mainly on the marine section [34], the geometry studied is a T-Joint in which a static pull-off load is applied and which represents the bulkhead of the ship. The study is mainly conducted with finite element analysis (MSC Nastran) using virtual closure technique (VCCT) tools to investigate fracture behavior. Moreover, it is assumed that there is already some kind of debonding in the construction. With the use of strain energy release rate (SERR) theorem in the crack tips the propagation mechanism of the crack is created and failure loads are predicted. For verification purposes, the corresponding experimental procedures shall be performed. The results showed that the change of direction in the pull-off load determine the failure load and more detailed study should be done. The extension of the previous study in the form of comparative results is that of [35],[36] in which the comparison is made between two study techniques, the Crack Tip Element method and the VCCT method. Initially, the Crack Tip Element method can offer a study of fairly good accuracy in predicting damage at very low computational cost under the right conditions. More specifically, the use of this method in thick marine T-Joint composite structures is investigated, since the thickness of the structure is a critical parameter for the application of the method. It was observed that between the three modes of fracture the major one is Mode I (opening fracture mode). To apply the analysis above to a thicker structure, the researchers came across a specific way to work with the data used in FEM analysis that yielded the

desired results. The models examined relate to thin and thick T-Joint using the CTE and VCCT method. The SERR results are presented in tables, making an accurate comparison for each case. Including these conclusions, it is understood that the CTE analysis for thin T-Joints can be used in disbonding problems, with the 3D CTE method having advantages over other methods. If the thick structure has dimensions similar to those required by classical laminate plate theory (CLPT), then CTE can be applied without any changes in geometry, giving significant benefits. If the CLPT criteria are not met, then there should be some kind of modification similar to that of the study. The study of G.Di Bella et al. [37] inspired by T-joints manufactured in a shipyard, highlights the effect of basic construction parameters on tensile load, such as adhesive, the material of the joined sections and the over-lamination sequence. The cases examined in the fillet area concern two over-lamination sequences, one with 0/90 degrees, one with +45/-45 degrees and a methacrylate adhesive under the brand name Adekit A 310NF as a material of joined sections. Both experimental and numerical results showed that: i) the models 0/90-GRP-GRP and +45/-45-GRP-GRP fail in the same way. The over-lamination sequence does not affect the joint, when the tensile load is exerted, ii) the methacrylate adhesive-GRP-GRP initially presented shear crack propagation in the horizontal component and then led to failure of the joint. For the reason why the fracture was detected in the substrate it is suggested that the adhesion was efficient iii) The 0/90-GRP-Wood and +45/-45-GRP-Wood models had exactly the same behavior. No shear core failure was observed, but there was a failure in the interface between wood and over-lamination. iv) The methacrylate adhesive-GRP-Wood model initially presented shear failure of the horizontal component and then a horizontal-vertical component and adhesive-vertical component failure. In a real sea state, the load alternates from tensile to compression creating buckling phenomena in a T-Joint construction, as shown in [38],[39]. To avoid core shear, it is suggested to use some other material with better mechanical properties for shear forces than Polyvinyl chloride (PVC). Regarding the design of T-Joints, it is worth mentioning the study of [40-43], where the design and testing of a new T-type connection for marine applications is investigated in order to overcome issues in the connection between bulkhead and deck. The behavior of T-Joints and failure modes mainly depend on geometry and construction material. The predominant geometric parameters that affect the joint are the radius of fillet and the thickness of the overlaminate, while the gap between the panels and the edge of preparation of the tee part has a secondary effect. More generally, increasing the radius of the fillet enables the joint to withstand higher loads. In addition, the choice of over-laminating resin proved to be an important manufacturing variable. However, increasing the stiffness of the joints did not lead to higher joint strengths. Prediction of failure values using FEM requires careful selection of material data, otherwise there is a high risk of failure of the study. In an effort to optimize the performance of T-Joint, it was proved that the large radius flexible resin fillet with an overlaminate of minimal thickness is the most efficient model, mainly for tensile load. As far as fatigue failure analysis is concerned, the study is done for the same models with tensile load in a direction of 45 degrees which resembles combined moments and forces in the joint. As shown in a study by another author mentioned earlier, the failure mechanisms under fatigue loading are the same as those at static load. Failure refers to delamination in the boundary angle and dislocation of the fillet from the boundary angle, thus creating crack in the fillet. The analysis of damage and fatigue

life showed a linear combination of these two. These two studies complement one another and provide a bigger picture for the study of T-Joints. The extension of the same study for more models is [44]. The additional conclusions that emerged were that the number of over-laminations is also an important study parameter, since lowering this number reduces the weight and cost of construction. Vibration transmission and noise on ships are not desirable and must exist in some way to be reduced. The study of [45] sheds light on such phenomena, using a viscoelastic insert in the T-Joint construction.

Theotokoglou and T. Moan [46], [47] studied the failure of a composite sandwich T-Joint, using lap joint by means of connecting the two panels under the influence of pull-out load. The connection of this type is widely found in high-speed marine ships as a connection between bulkheads or bulkhead and the side of ship. It is emphasized that such a study is very complex because it involves several types of materials. The study uses non-linear material laws for the core of the panels and the glue. The main goal is to better understand the response and failure of sandwich T-Joints. For this reason, the following design parameters are being considered which may affect the strength and flexibility of T-Joint: i) Extension of the lap, and ii) Thickness of the lap (i.e., the number of layers) which seemed to have almost no effect on pull-out strength. Further research was done at the points where the glue, the laminate and the panel core meet each other, as well as the points where the glue, the laminate and the lap meet. The main conclusions that were drawn from this study are the following: the most critical points for stress and strain states are in the core of the horizontal panel and in the core of the vertical panel near the interface corner where the three materials meet each other. The finite element analysis gave important results for the crack initiation and propagation between lap and laminate, at the vertical core panel near the interface corner with horizontal panel and glue and the horizontal core panel with failure Mode II. The length and thickness of the attachment determine the failure mode that occurs. The longer and thicker laps exist, fracture mode II prevails. It is also understood that, compared to other parameter configurations, the higher strength core material provides optimal results in terms of load capacity. Numerical analysis [48], [49] showed that increasing the number of layers in the lap reduces the maximum principal stresses in the attachment lap, while the thickness through stresses increases to a lower limit than that of tensile strength. For this reason, the attachment lap should not consist of a single layer but of at least two or more. In addition, the number of layers in the lap does not greatly affect the maximum shear and principal stresses inside the cores of the panels, although it creates a slight weakness in strength. In terms of finite element analysis [50], the crack initiation occurs at the interface between the fillet and the connected laminate and then propagates along the interface. The technique used is the crack closure technique using intensity factors K_I, K_{II}. The model for the propagation of the crack refers to the extension of the lap and the angle ω which is essentially the radius of the fillet. It was observed that, with an increase up to a specific value in the radius of the fillet, the crack propagation stops.

The most important points related to the literature review are the following:

1. The base angle of the fillets is one of the most important geometry parameters of the T-Joint.
2. One of the most serious issues of the T-Joint is the delamination between the horizontal and vertical components caused by the loads across the thickness.
3. The delamination resistance of the composite T- joint can be improved in the direction of the thickness of the material using z-pins in the bonded region.
4. The reinforcement of the construction with z-pin is better than that of the rivets. The z-pins can successfully strengthen the entire lap area while the rivets can only strengthen an area around themselves.
5. Stitched T-joints had higher ultimate strength and load recovery post ultimate strength
6. The adhesive T-joint shows brittle failure, in contrast to the z pin and the stitched, which show ductile damage behavior.
7. The most common load exerted on such connections is the tensile load. The main failure mechanisms are fracture or delamination by creating and spreading a crack in one of the parts of the structure (adhesive region, core of panel, etc.).
8. Using 3D woven reinforcements to increase the load-bearing capabilities of composite T-joints over-laminates is an effective technique.
9. The fracture modes under dynamic tensile loading are similar to those of the static case.
10. The core shear failure strength of the base panel is sensitive to all failure modes.
11. The geometric parameters that affect the joint are the radius of fillet and the thickness of the overlaminate, while the gap between the panels and the edge of preparation of the tee part have secondary effects. More generally, increasing the radius of the fillet enables the joint to withstand higher loads.
12. The most critical points in respect to stress and strain distributions are in the center of the horizontal panel and in the center of the vertical panel near the interface corner where the three materials meet each other.

Table 1 T-Joint Literature Summary by sections

Type of Connection Between T Components	Parametric Study	Marine Applications
[6 – 11] **[13]** **[15]** **[16-19]**	**[12]** **[18-19]** **[20-29]** **[30-32]** **[43-44]** **[46-47]** **[49]**	**[14]** **[20-21]** **[33-50]** **.**

1 T Joint Sandwich Composites

Several meters of T-joints are not unusual in larger sandwich constructions, such as ships. As a result, a lot of studies focused on T-joints to create a low-cost design. The transfer of force from the hull to the bulkhead is the underlying principle behind transverse stiffening of the hulls of ships. The significant stiffness of the bulkhead face sheets will respond as two parallel line loads on the hull inner face sheet since the bulkhead is often perpendicular to the hull. The materials used in ship building are of four main types: reinforcement materials, resin materials, core materials and adhesives.

1.1 Reinforcement Materials

1.1.1 Fibers

The fiber type used for this study is E-Glass with the following characteristics [51]:

1. Glass

The two main types of glass used in composite shipbuilding are E and R types. Glass monofilaments have the same molecular arrangement as glass plates and are considered as isotropic materials, which means that the mechanical properties are the same in the length and cross directions. The primary benefits are strong stiffness, tensile strength and compression resistance, whereas the main drawback is the comparatively low impact resistance.

		Glass		Carbon			Para-aramid
		E	R	HS	IM	HM	
Density ρ_f		2,57	2,52	1,79	1,75	1,88	1,45
Tensile in fibre direction	Poisson coefficient ν_f	0,238	0,20	0,30	0,32	0,35	0,38
	Young modulus $E_{f0°}$ (N/mm²)	73100	86000	238000	350000	410000	129000
	breaking strain (%)	3,8	4,0	1,5	1,3	0,6	2,2
	breaking stress (N/mm²)	2750	3450	3600	4500	4700	2850
Tensile normal to fibre direction	Poisson coefficient	0,238	0,20	0,02	0,01	0,01	0,015
	Young modulus $E_{f90°}$ (N/mm²)	73100	86000	15000	10000	13800	5400
	breaking strain (%)	2,40	2,40	0,90	0,70	0,45	0,70
	breaking stress (N/mm²)	1750	2000	135	70	60	40
Compression in fibre direction	breaking strain (%)	2,40	2,40	0,90	0,60	0,45	0,40
	breaking stress (N/mm²)	1750	2000	2140	2100	1850	500
Shear	Modulus G_f (N/mm²)	30000	34600	50000	35000	27000	12000
	breaking strain (%)	5,6	5,6	2,4	3,0	3,8	4,0
	breaking stress (N/mm²)	1700	1950	1200	1100	1000	500

Figure 1:Typical Mechanical properties of fibers [51]

1.1.2 Fabrics

Typically, fabric items are constructed using reinforcing fibers. The fabric used for this study is [51]:

1. Chopped fibers chemically gathered into sheets (Chopped Strand Mats CSM)

The fibers used to create chopped strand mats (CSM) are chemically grouped into a web. There is no primary direction since the fibers are randomly arranged in the web and CSM are regarded as isotropic reinforcements. Fibers 50mm or longer may be used to create CSM. In general, only CSM with fibers greater than 50 mm should be used. The kind and length of the fibers, as well as the area weight, are the primary properties of mats.

1.2 Resin Materials

The resin material used for this study is [51]:

1.2.1 Polyester resin

Unsaturated polyester resin, unsaturated monomer (also known as a copolymer), a catalyst and occasionally an accelerator are combined to create polyester resin systems. Co-polymerization is the name of this process. These combined components have the functions of monomer, catalyst, and accelerator.

The typical mechanical properties of resins are given in the table below:

	Polyester	Vinylester	Epoxy
Density ρ_r	1,20	1,10	1,25
Poisson coefficient ν_r	0,38	0,26	0,39
Tg (°C)	around 60°	around 100°	between 80° and 150°
Tensile Young modulus E_r (N/mm²)	3550	3350	3100
Tensile or compression breaking stress (N/mm²)	55	75	75
Tensile or compression breaking strain (%)	1,8	2,2	2,5
Shear modulus G_r (N/mm²)	1350	1400	1500
Shear breaking stress (N/mm²)	around 50	around 65	around 80
Shear breaking strain (%)	3,8	3,7	5,0

Figure 2: Typical Mechanical properties of commonly used resins [51]

1.3 Core Materials

To increase the overall moment of inertia of the laminate sandwich core materials are included. Sandwich laminates are constructed from two reinforced faces, also known as skins, joined together at the core. The core substance of a laminate is intended to thicken the laminate in order to enhance stiffness. The core material essentially experiences shear stresses because of how it behaves like the web of a beam. Low density, shear strength and the ability to handle compression and shear loads without failure of buckling are the essential properties of a core material. The core material used for this study is:

1.3.1 Foam Cores

In a wide range of densities and thicknesses foam cores may be produced using a wide spectrum of synthetic resins. Closed cells must be present in all foam cores to prevent water migration. Foam cores must tolerate the temperatures for pre-preg or post-cure procedures and be compatible with the resin systems and adhesives being applied [51]

1. *PolyVinyl Chloride PVC foam:* are very resistant to chemical compounds and water absorption, especially styrene found in polyester and vinylester resin systems. PVC foams come in two varieties: cross-linked PVC and uncross-linked PVC, often known as linear PVC. Compared to cross-connected PVC foam, linear PVC foam has lower mechanical qualities and is more flexible. However, cross-linked PVC is more brittle than linear PVC.

The mechanical properties of the foams are given in the table below:

Foam type	Density (kg/m³)	Modulus			Poisson coefficient	Breaking stresses		
		Tensile E_1 , E_2 (N/mm²)	Compression E_3 (N/mm²)	Shear G_{12} , G_{13} , G_{23} (N/mm²)	ν_{12} , ν_{21}	Tensile σ_1, σ_2 (N/mm²)	Compression σ_1, σ_2 (N/mm²)	Shear τ_{12} , τ_{13} , τ_{23} (N/mm²)
Linear PVC	50	21	18	8	0,36	0,7	0,3	0,3
	60	29	28	11	0,31	0,9	0,4	0,5
	70	37	38	14	0,27	1,1	0,6	0,7
	80	44	49	18	0,25	1,3	0,7	0,8
	90	52	59	21	0,24	1,4	0,9	1,0
	100	59	69	24	0,23	1,6	1,0	1,2
	110	67	79	27	0,22	1,8	1,2	1,3
	130	82	99	34	0,21	2,2	1,5	1,7
	140	89	109	37	0,21	2,4	1,6	1,9
Cross linked PVC	50	37	40	18	0,02	1,0	0,6	0,6
	60	47	51	22	0,05	1,4	0,8	0,8
	70	57	63	27	0,07	1,8	1,1	1,0
	80	67	75	31	0,08	2,2	1,4	1,1
	90	78	88	36	0,09	2,5	1,7	1,3
	100	88	102	40	0,10	2,9	1,9	1,5
	110	98	116	44	0,11	3,3	2,2	1,6
	130	118	145	53	0,12	3,9	2,8	2,0
	140	129	161	57	0,12	4,3	3,0	2,2
	170	159	209	71	0,13	5,2	3,8	2,7
	190	180	243	79	0,13	5,8	4,4	3,0
	200	190	260	84	0,13	6,1	4,7	3,2
	250	241	352	105	0,14	7,4	6,0	4,1
SAN	50	52	29	13	0,11	0,9	0,4	0,7
	60	65	37	16	0,18	1,2	0,5	0,8
	70	78	44	18	0,20	1,5	0,6	0,9
	80	92	50	21	0,19	1,7	0,8	1,0
	90	107	55	23	0,17	1,9	0,9	1,1
	100	122	60	26	0,15	2,0	1,1	1,2
	110	137	64	29	0,12	2,2	1,2	1,3
	130	168	71	34	0,06	2,5	1,6	1,5
	140	184	74	36	0,03	2,6	1,8	1,6
	170	234	83	43	0,03	2,9	2,4	1,9
	190	268	88	48	0,03	3,1	2,8	2,1
	200	285	90	51	0,03	3,1	3,0	2,1
PET	60	69	35	13	0,32	1,14	0,67	0,43
	70	79	49	15	0,32	1,45	0,84	0,52
	80	89	61	18	0,38	1,72	1,01	0,61
	90	100	74	21	0,38	1,95	1,20	0,70
	100	111	86	24	0,38	2,16	1,39	0,79
	110	121	99	27	0,32	2,36	1,59	0,89
	130	144	122	33	0,27	2,69	2,02	1,09
	150	168	145	40	0,22	3,98	2,47	1,29
	200	230	196	59	0,22	3,55	3,72	1,83
	250	298	241	80	0,12	4,00	5,11	2,39
PMI	50	54	59	21	0,40	1,9	0,8	0,8
	60	69	76	24	0,60	2,1	1,1	1,0
	70	84	94	28	0,60	2,3	1,5	1,2
	80	101	112	33	0,70	2,6	1,9	1,5
	90	119	132	39	0,70	2,9	2,3	1,8
	100	137	152	45	0,70	3,2	2,7	2,1
	110	155	173	52	0,60	3,6	3,2	2,4
	130	195	217	71	0,50	4,5	4,2	3,1
	140	215	239	83	0,40	5,0	4,8	3,5
	170	280	311	131	0,20	6,8	6,7	4,7

Figure 3:Typical Mechanical properties of foam cores [51]

1.4 Adhesives

An adhesive is a polymeric material that when applied to surfaces may adhere to them and prevent their separation. Structural adhesives are used in order to provide the structural contributing factors of strength and stiffness when a significant load and a wide range of stresses applied over an extended period of time are required to cause separation. The structural elements of the bond that the adhesives keep together are the adherents. This concept of adhesion is widely used when describing maritime structures. Observe that every joining technique has weak points at [52].

The material characteristics of the adherents and adhesives, their geometric relationships, thickness and finally overlap are the main determinants of the joint strength of adhesively joined surfaces. In view of the fact that the load is distributed unevenly throughout the bonded region in adhesive joints, the average shear stress may be significantly lower than the local maximum stress. Shear stress is a traditional standard for identifying a structural adhesive and must be more than $10\frac{N}{mm^2}$ at room temperature. There are common recommendations whose goal is to improve joint strength by reducing stress concentrations [53]:

1. Use an adhesive that exhibits ductile behavior and low modulus.
2. Use similar adherends, or if not possible, balance the stiffness.
3. Use a thin adhesive layer.
4. Use a large bonded area.

The difference between joint strength and adhesive strength must be made clearly. If a stronger adhesive is used, the strength of the joint would not improve. High-ductility and flexibility adhesives typically have low strength. When applied in a joint, however, their capacity to spread stress uniformly throughout the overlap and to bend plastically. This can result in a joint strength that is significantly higher than that with adhesives that appear to be robust, but are less ductile. In contrast to a stiff adhesive, which has a large stress concentration at the overlap endpoints, a low-modulus adhesive provides a more equal distribution of stress. Adhesives can be durable, brittle and stiff, or they can be weaker, ductile and elastic. A durable, ductile and flexible adhesive would be excellent. Additionally, compared to brittle adhesives, ductile adhesives are more resistant to crack spread, increasing their level of toughness. The fatigue life of joints with ductile adhesives is significantly longer than that of joints with brittle adhesives if the fatigue limit is expressed as a percentage of the static maximum joint strength. This is because ductile adhesives have a higher damping energy and a more uniform stress distribution [53].

The adhering modulus and its strength are the most crucial. The smaller the deformation at the endpoints of the overlap, where load transfer occurs, and the lesser the impact of the adhesive's differential straining, the higher the adherend modulus. Another important factor that assists to explain many joint failures is the adhesion strength. Strength increases proportionally as the width of the joint increases. However, the effect is small.

The overlap length varies depending on the type of adherent and whether the adhesive is brittle or ductile. The ability to connect different materials, such as aluminum and carbon fiber-reinforced polymers (CFRP), is one of the key benefits of adhesive bonding. However, various adherents could have extremely different thermal expansion coefficients. Thus, in addition to the loads exerted externally, temperature fluctuations may also cause thermal stresses. Internal strains may also be created by the thermal shrinkage that results from bond curing. There may be deformations or even fractures [53].

In conclusion, an adhesive joint is a method for permanently connecting two surfaces through a polymeric material layer using chemical, mechanical, or a mixture of mechanical and chemical interfacial forces. Adhesive assembly refers to the process of joining pieces or adherents, which may or may not be formed of the same material. The figure below shows the various loads that can be placed on an adhesive joint. Manufacturers have created a great number and diversity of adhesives to offer products to attach an equally wide range of materials in the maritime sector. The core material used for this study is:

1.4.1 Epoxy-based adhesive

The following are the primary characteristics of epoxy adhesives [54]:

1. This is one of the most popular and effective thermoset families among structural adhesives.
2. Dependent on the formulation (mostly the kind of hardener) and the curing process, stiff bond and strong mechanical qualities
3. Available in single, two-component or film form
4. Excellent adhesion to a variety of substrates

1.5 Load Transfers

The hull inner face sheet may be severely bent and the hull core may be compressed due to the relatively direct transfer of force between the bulkhead face sheets and the hull core. A minimal amount of tensile force can also be transferred when only a thin layer of adhesive holds the bulkhead to the hull as a result of high stress concentration. The mechanics of a fast boat going at slamming speed increases the possibility of developing tensile force, which may be considerable and not insignificant. A T-joint should therefore spread the loads to ensure that there are not too many interface strains between the panels [55].

A T-Joint is illustrated below with a number of parts that may be combined or used separately. The gap filler distributes force between the bulkhead face sheets and the hull panel by filling the space between the hull and the bulkhead, which is crucial. Normally, a fillet and a gap-filler are used in addition to the glued tapered laminate. As a result, the force spreads and the joint may transfer moment. Such a joint should not be put under fatigue stresses. The load transverse to the hull panel is distributed across a wider area of the core owing to the reinforcement of the inner face sheet of the hull, which enhances the bending stiffness. The nearby high-density core can also sustain a greater local stress that develops.

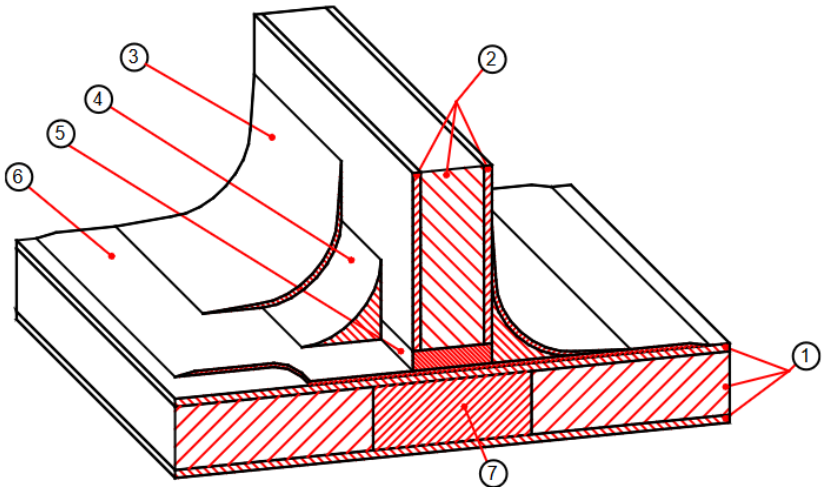

Figure 4:T-Joint structural components: (1) hull panel (face-sheets and core), (2) bulkhead (face-sheets and core), (3) bonded tapered laminate, (4) fillet (5) gap filler, (6) reinforcement of hull inner face-sheet and (7) local high density hull core. [55]

The joint's function is to distribute reactions among the linked panels. The following are the responses for the T-Joint:

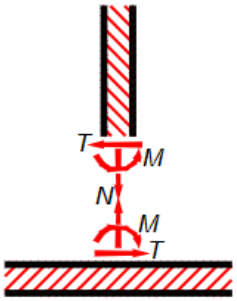

Figure 5:T-Joint reaction loads

Typically, sandwich panels should behave as following:

i. The face sheets act as membranes and transfer the in-plane force N directly and the moment M as force couples.
ii. The core transfers the transverse reaction T

2 Mechanics of Composite Materials (Quasi-Orthotropic Material)

2.1 Definition of composite materials and quasi-orthotropic Material

Composite materials are designed materials composed of two or more constituent materials that, when combined, generate a material with qualities that are distinct from the sum of the separate elements. The individual components of the resulting structure are maintained to be distinct and independent, distinguishing composites from combinations and solid solutions [88].

A particular class of composite material is called a quasi-orthotropic material. In two dimensions they have orthotropic properties and in the third dimension they are isotropic. A symmetrically stacked composite where each layer is orthotropic, but the stacking sequence expresses the composite as a whole quasi-orthotropic behavior, is a common example of a quasi-orthotropic material [89].

2.2 Stress and Strain Tensor

2.2.1 Definition of stress and strain tensor

The distribution of stress and strain in the material in various directions is described by the stress and strain tensors for quasi-orthotropic materials.

The stress tensor, in the context of quasi-orthotropic materials, indicates the state of stress at a particular location within the material. The tension in three dimensions is represented by a second-order tensor. The stress tensor for quasi-orthotropic materials is a 3x3 matrix that includes normal stresses and shear stresses in three mutually orthogonal directions [89].

In the context of a quasi-orthotropic material the stress tensor can be written as:

$$[\sigma] = \begin{bmatrix} \sigma_{11} & \sigma_{12} & 0 \\ \sigma_{12} & \sigma_{22} & 0 \\ 0 & 0 & \sigma_{66} \end{bmatrix} \quad (1)$$

In this tensor, σ_{11} and σ_{22} represent the normal stresses in the longitudinal and transverse directions, respectively. σ_{12} represents the shear stress between the longitudinal and transverse directions. σ_{66} represents the in-plane shear stress.

However, the deformation or deformation at a specific location within the material, is described by the strain tensor. It is likewise a second-order tensor and has a 3 x 3 matrix representation. For quasi-orthotropic materials, the shear deformation, longitudinal and transverse elongation and contraction are all accounted for by the strain tensor.[88].

The strain tensor for a quasi-orthotropic material can be represented as:

$$[\varepsilon] = \begin{bmatrix} \varepsilon_{11} & \varepsilon_{12} & 0 \\ \varepsilon_{12} & \varepsilon_{22} & 0 \\ 0 & 0 & \gamma_{66} \end{bmatrix} \quad (2)$$

In this tensor, ε_{11} and ε_{22} represent the normal strains in the longitudinal and transverse directions, respectively. ε_{12} represents the shear strain between the longitudinal and transverse directions. γ_{66} represents the in-plane shear strain.

For analyzing the mechanical behavior of quasi-orthotropic materials in various loading situations and predicting their reaction to applied forces, an understanding of the stress and strain tensors is essential.

2.2.2 Description of Hook's law in the context of quasi-orthotropic materials

The linear relationship between stress and strain in a material is defined by Hooke's law, a fundamental principle in the study of material mechanics. In the study of elastic materials, including composites like quasi-orthotropic materials, this relationship is quite critical.

Hooke's law offers a mathematical approach that combines the stress matrix and the strain matrix in the setting of quasi-orthotropic materials. The equation provides this relationship:

$$\varepsilon = [S] \cdot \sigma \quad (3)$$

where ε represents the strain matrix, σ is the stress matrix and [S] is the compliance matrix. The compliance matrix is the inverse of the stiffness matrix [Q], and contains the material properties of the compound, taking into account the effects of the orientations of the fiber and the matrix and the volume fractions.

In the case of quasi-orthotropic materials, the compliance matrix [S] would have nine independent entries, corresponding to the nine independent material properties of the material.

The compliance matrix [S] for a quasi-orthotropic material can be represented as following:

$$[S] = \begin{bmatrix} \frac{1}{E_1} & \frac{-\nu_{12}}{E_2} & 0 \\ \frac{-\nu_{12}}{E_1} & \frac{1}{E_2} & 0 \\ 0 & 0 & \frac{1}{G_{12}} \end{bmatrix} \quad (4)$$

In this compliance matrix, E_1 and E_2 represent the longitudinal and transverse elastic moduli, respectively. ν_{12} is the Poisson's ratio, and G_{12} represents the in-plane shear modulus.

This understanding of Hooke's law in the context of quasi-orthotropic materials is essential in predicting the behavior of these materials under various loading conditions [90].

2.3 Rule of Mixture

2.3.1 Explanation of rule of mixture

The rule of mixtures, commonly referred to as the law of mixtures, is a theoretical model for calculating the properties of composite materials. According to the rule of mixtures, a composite property is the volume-weighted average of the individual attributes of its parts. When predicting the elastic modulus and tensile strength of unidirectional composites, it is especially advantageous.

For a composite material composed of a fiber and a matrix, the mixture rule can be used to calculate longitudinal and transverse moduli (E_1 and E_2, respectively) as following:

$$E_1 = E_f \cdot V_f + E_m \cdot V_m \quad (5)$$

$$E_2 = \frac{(E_f \cdot E_m)}{(V_m \cdot E_f + V_f \cdot E_m)} \quad (6)$$

where:

E_f and E_m are the elastic moduli of the fiber and the matrix, respectively,

V_f and V_m are the volume fractions of the fiber and the matrix, respectively.

This criterion presupposes that there is no porosity within the composite and that the matrix and fibers are perfectly bonded. Although the rule of mixtures offers a simple and straightforward technique to estimate the qualities of the composites, due to its simplifications and assumptions, it may not precisely predict all events in the real world [89].

2.3.2 Rule of mixture of quasi-orthotropic materials

The properties of quasi-orthotropic materials can be predicted using the rule of mixtures. The law of mixtures is used to calculate the longitudinal and transverse moduli (E_1 and E_2, respectively), as well as the shear modulus (G_{12}) for the materials which have orthotropic properties in two dimensions and isotropic characteristics in the third dimension.

Another essential characteristic in the investigation of quasi-orthotropic materials is the shear modulus G_{12}, which may also be predicted using a modified version of the rule of mixtures or other empirical connections.

It is crucial to remember that the rule of mixtures only provides an initial estimate of the properties of composite materials and may not be entirely accurate because it is predicated on a number of untested establishments, including perfect bonding between the matrix and fibers and the absence of any voids or flaws in the substance. On the basis of practical facts, or more complicated theoretical models, adjustments may need to be made [89].

2.4 Quasi-Orthotropic Material

2.4.1 Description of the structure and behavior of quasi-orthotropic materials.

Materials having a quasi-orthotropic structure have many layers, each with a unique fiber orientation. Although the third dimension is isotropic, these layers are stacked symmetrically to maintain balanced qualities in two dimensions. This layered structure gives the composite a range of strength and stiffness characteristics in various directions, enabling customized mechanical behavior.

The characteristics of the layers that make up quasi-orthotropic materials and the order in which they are stacked determine how they behave. The orientation and arrangement of the individual layers are determined by the stacking order, which in turn, affects the composite's overall mechanical response. Specific qualities such as stiffness, strength

and anisotropy can be produced by intentionally changing the stacking order. Anisotropic behavior, or the variation of mechanical properties with direction, is exhibited by quasi-orthotropic materials. The composite exhibits various stiffnesses, strengths and thermal expansion coefficients in the two orthotropic planes. However, the composite behaves uniformly in all directions in the third isotropic plane. For their design and analysis quasi-orthotropic materials require an understanding of their structure and behavior. This allows engineers to take advantage of the customized qualities of these composites for applications in fields such as marine technology [89].

2.4.2 Stiffness matrix for quasi-orthotropic materials.

In the research and characterization of composite materials, particularly quasi-orthotropic materials, the stiffness matrix is vital. It provides crucial details on the mechanical behavior of the material and describes how stress and strain interact in the material.

For quasi-orthotropic materials the stiffness matrix is given by the following:

$$[Q] = \begin{bmatrix} Q_{11} & Q_{12} & 0 \\ Q_{12} & Q_{22} & 0 \\ 0 & 0 & Q_{66} \end{bmatrix} \quad (7)$$

In this matrix, Q_{11}, Q_{22}, and Q_{66} represent the longitudinal, transverse, and in-plane shear stiffness coefficients, respectively. Q_{12} is the coupling stiffness coefficient. The qualities of the constituent materials, such as the fiber and matrix, as well as the volume fractions and orientations of the fibers, determine the stiffness of the matrix components. The longitudinal and transverse stiffness coefficients, Q_{11} and Q_{22}, can be estimated using the rule of mixtures, as discussed earlier. The coupling stiffness coefficient Q_{12} accounts for the interaction between the longitudinal and transverse directions and depends on the specific fiber and matrix materials. The in-plane shear stiffness coefficient, Q_{66}, is typically calculated as the product of the in-plane shear modulus and the thickness of the quasi-orthotropic material. The prediction of a material's mechanical response under various loading situations is made possible by the stiffness matrix which offers useful information about the anisotropic behavior of quasi-orthotropic materials.[88].

2.4.3 Limitations of quasi-orthotropic material model

Understanding the mechanics of quasi-orthotropic materials is of significant importance for several reasons:

1. Design Optimization: Engineers can optimize their designs for particular applications by understanding the mechanical behavior of quasi-orthotropic materials. The mechanical properties of the composite can be tailored to suit the required specifications, such as strength, stiffness and durability, by adjusting the fiber orientations and layer stacking order.
2. Structural Analysis: Analyzing and modeling the structural response of composite components requires a precise understanding of the mechanics of quasi-orthotropic materials. Designers can create safe and effective designs using this knowledge to evaluate the load-bearing capability, deflections and failure modes of quasi-orthotropic structures.
3. Material Selection: The choice of suitable constituent materials, such as fibers and matrices, depending on the required qualities and performance criteria, is made easier with an understanding of quasi-orthotropic material mechanics. This guarantees that the materials are capable of offering the required stiffness, strength and other mechanical properties for the specified application.
4. Performance Prediction: Designers can estimate the behavior of these composites under varied loading circumstances with accuracy if they have a strong grasp of the mechanics of quasi-orthotropic materials. This involves evaluating how they react to thermal, dynamic and static loads in addition to anticipating fatigue behavior and long-term durability.

Designers can use the unique features of quasi-orthotropic materials to construct lightweight, high-performance structures for a variety of applications by fully understanding their mechanics [89].

It is important to recognize the limits of the models used to describe the behavior of quasi-orthotropic materials, such as the stiffness matrix approach and rule of mixtures. These limitations include:

1. Assumptions of Homogeneity: Numerous theories presuppose that the composite material is homogeneous and that all areas of the construction have the same qualities. However, in practice, small differences in characteristics might be introduced by changes in fiber orientations, resin distribution and interfacial bonding, deviating from the expected behavior.
2. Neglecting Complex Interactions: Complex interactions between fiber and matrix, such as fiber / matrix debonding, interfacial slipping, or fiber breakage, are frequently ignored in simplified models. Especially under conditions of high loads or stress, these interactions can have a considerable impact on the overall mechanical behavior.
3. Lack of Material Variability Consideration: Due to manufacturing procedures, material defects and environmental factors, composite materials have significant property variability. Simplicified models frequently ignore this unpredictability which could result in errors when predicting how quasi-orthotropic materials will behave in practical situations.
4. Influence of Manufacturing Defects: Models often assume a composite construction free of flaws, ignoring the effects of production flaws such as voids, porosity, or fiber misalignment. The mechanical characteristics of the material and how it reacts to external loads can be significantly impacted by these flaws.
5. Nonlinear Behavior: Simplicified models frequently assume linear elastic behavior, ignoring the quasi-orthotropic materials' nonlinear response to high stresses or complex loading conditions. The mechanical behavior of the material can be significantly impacted by nonlinear events such as fiber/matrix damage, plastic deformation, or matrix cracking.

It is crucial to be aware of these restrictions and to take into account more sophisticated modeling methods, such as micromechanics or finite element analysis, to more precisely depict the complicated behavior of quasi-orthotropic materials. [89].

3 Composite Failure Criterion

3.1 Tsai-Wu

The Tsai-Wu failure criterion is an anisotropic failure criterion commonly used to assess the failure of composite materials. It considers the interaction between normal and shear stresses and provides a quantitative measure of the failure potential of the composite material. The Tsai-Wu failure criterion is expressed as following:

$$F = F_1 \cdot \sigma_1 + F_2 \cdot \sigma_2 + F_{11} \cdot \sigma_1^2 + F_{22} \cdot \sigma_2^2 + F_{66} \cdot \tau_{12}^2 + 2 \cdot F_{12} \cdot \sigma_1 \cdot \sigma_2 \leq 1 \quad (8)$$

In the expression above, σ1 and σ2 are the normal stresses, τ12 is the shear stress and F_1, F_2, F_{11}, F_{22}, F_{12}, and F_{66} are material properties known as Tsai-Wu interaction coefficients or Tsai-Wu constants. Each coefficient is dependent on the strength of the material under specific stress conditions (tension, compression, shear). The coefficients are calculated based on the strengths of the composite material in tension, compression and shear, which are typically obtained from laboratory testing. [89]. The coefficients are calculated as following:

$$F_1 = \frac{1}{\sigma_{1t}} - \frac{1}{\sigma_{1c}}, F_2 = \frac{1}{\sigma_{1t}} - \frac{1}{\sigma_{1c}}, F_{12} = -0.5 \cdot \sqrt{\frac{1}{(\sigma_{1t} \cdot \sigma_{1c})} \cdot \frac{1}{(\sigma_{2t} \cdot \sigma_{2c})}} \quad (9)$$

$$F_{11} = \frac{1}{\sigma_{1t} \cdot \sigma_{1c}}, F_{22} = \frac{1}{\sigma_{2t} \cdot \sigma_{2c}}, F_{66} = \frac{1}{\tau_{s12}^2} \quad (10)$$

Where: σ_{1t} and σ1c are the tensile and compressive strengths in the 1 direction (fiber direction), respectively. The σ_{2t} and σ_{2c} are the tensile and compressive strengths in the second direction (perpendicular to the fiber direction), respectively and τ_{s12} is the in-plane shear strength.

3.2 Application in the Marine Industry

In the marine industry, the Tsai-Wu failure criterion and the safety factor are widely used to build and assess composite constructions. They support analyses of laminated composites' tensile strength and failure potential under the complicated loading circumstances present in marine applications. Engineering professionals can identify whether a composite component is prone to failure or can safely resist the applied loads by comparing the calculated Tsai-Wu failure index with the unity value. By offering a safety factor that guarantees the structural reliability of composite materials under marine conditions, the Tsai-Wu safety factor directs the design process. To reach a desired safety margin and comply with regulatory criteria, it assists designers optimize the placement of the composite, fiber orientations and thickness of the laminate [92].

3.3 Limitations and Considerations

Although the Tsai-Wu failure criterion and the safety factor provide valuable information, it is important to recognize their limits. These models ignore the post-failure response and assume linear elastic material behavior. Furthermore, they do not take into account environmental degradation, manufacturing flaws, or material heterogeneity. Therefore, it is important to use additional analysis methods, such as finite element analysis, to take these elements into account and improve the precision of failure predictions. To determine the possibility of failure and guarantee the reliability of composite materials in the marine industry, the Tsai-Wu failure criterion and safety factor are useful tools. Designers can make accurate decisions to produce strong and long-lasting composite constructions, improving the performance and safety of marine vessels and components, including these models into the design process [91].

4 Yacht Crane Installation

The theory of sandwich composites and fracture mechanics finds application in the reinforcement of the bow under the crane base of a yacht made of composite materials. The expected effect of T reinforcement in construction includes the following:

i. Reduction of local stress on the crane base
ii. Reduction of stresses in transverse frames
iii. Smoother load distribution in construction through the T-Joint

The regulations to be used for the design and control of the T-connection are based on the DNV Classification Society and the American Petroleum Institute API with reference to their respective annexes. The uploading and downloading of the tender will be the main function of the crane, i.e., the load which interacts with the sea and contains dynamic charges. The regulations will also apply to the Offshore Standards.

4.1 Design of T Joint

The T-Joint consists of the longitudinal bulkhead and the deck, while the reinforcement of the T-Joint consists of the overlamination skin and the adhesive-filler. Essentially, this reinforcement connects the longitudinal bulkhead to the deck via the overlamination skin using the adhesive, with an angle of fillet between the deck and the longitudinal bulkhead, 45 degrees as an optimal, according to bibliographic references. The material specifications for this connection are presented in the following chapters.

The construction drawings in millimeters and its 3D illustration are shown below:

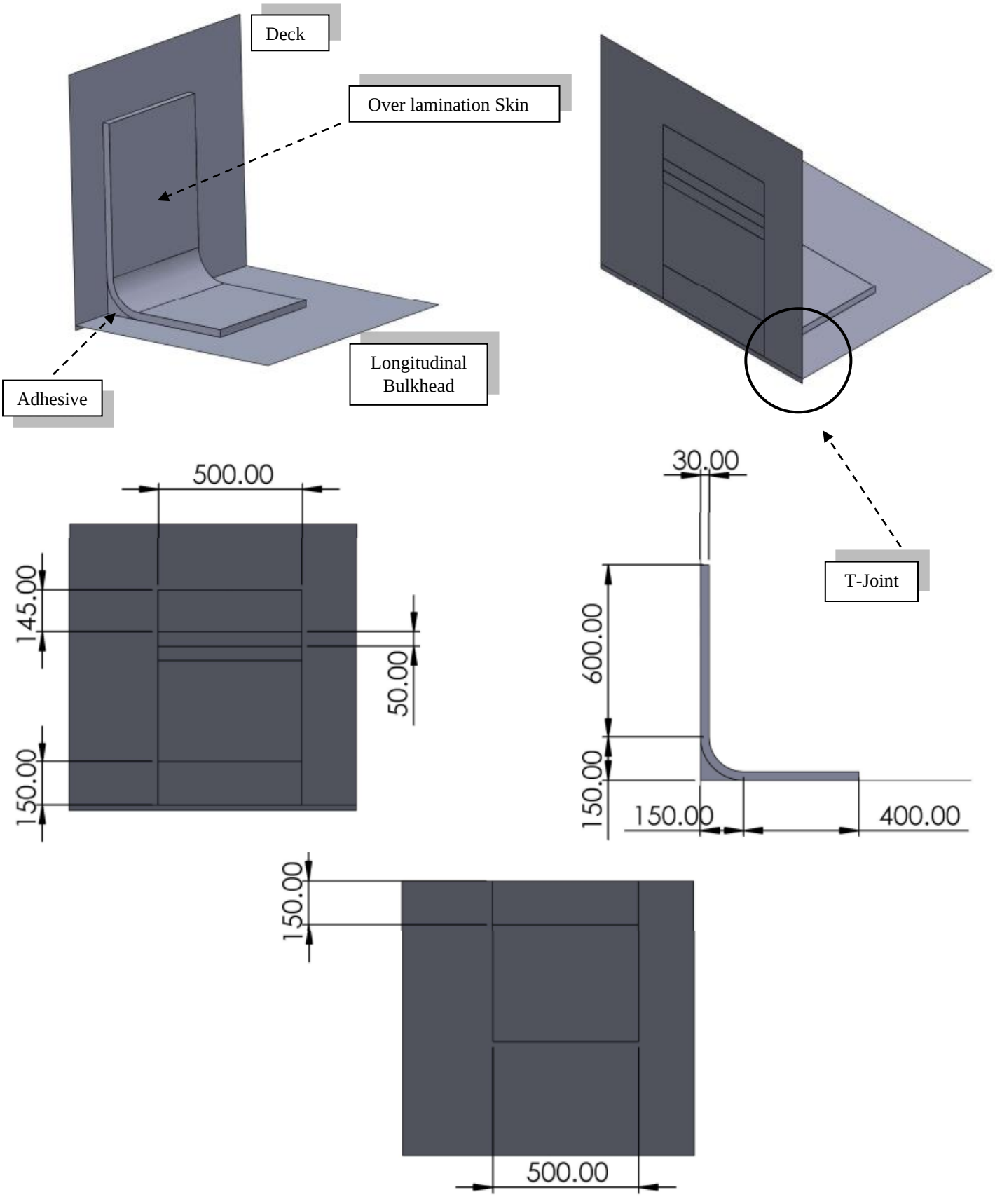

Figure 6:T-Joint Reinforcement Design

4.2 Design Regulations Yacht Crane

Typical loads considered in the analysis of deck and crane are:

Loads on crane:

i. Regular loads
   a. Dead loads: Dead loads are the weights of all fixed and mobile components of lifting appliances and loose gear permanently present during operation.
   b. Hoist loads: Sum of a lifting appliance's working load, the weight of its fixed load-lifting attachments and half of the weight of that part of hoist medium, which is arranged between rope exit point and fixed load-lifting attachments
   c. Dynamic forces due to drive systems at crane: They relate to the dynamic loads resulting from movements of the crane itself, i.e., lifting and rotating the load.
   d. Dynamic forces by ship motions at crane and structure: It refers to the dynamic loads applied to the crane components and the load when the ship is in a severe wave state.

ii. Irregular loads
   a. Wind loads: They relate to the wind-related charge values of the crane components and also to the load.

4.2.1 Crane Loads Calculation Procedure according to DNV and API2C

The general methodology for calculating the loads to be applied to the crane base in accordance with [80],[81] and [82] results is as following:

1. Calculation of the geometrical centers of the crane and tender
2. Find Dead load and Hoist Load from study data
3. Calculation of the components Dead Load and Hoist Load in the directions Longitudinal, Vertical and Transverse after the effect of the static List and Trim angles φ and θ respectively.
4. Calculation of inertial forces due to the movement of the crane itself during lifting of the load, multiplying Dead Load and Hoist Load by the dynamic coefficient ψ.
5. Calculation of inertial forces at the working ratio of the crane itself during transport-spin of the charge by multiplying the masses Dead Load and Hoist Load by the corresponding centrifugal and tangential accelerations of the crane.

6. Calculation of inertial forces in the crane's Dead Load when finding the ship in large ripples, multiplying the mass Dead Load by the corresponding roll, pitch and heave accelerations of the ship.
7. Calculation of the wind force exerted on the tender crane system taking into account the worst direction.
8. The above forces shall be summed by the respective components and multiplied by the safety factor c. The calculation of the above forces has been made in components Longitudinal, Vertical and Transverse according to the ship's coordinate system.
9. According to the geometric centers of the crane, these forces are transferred to the crane base along with the corresponding transfer moments.

The speeds of the ship as a floating body are determined by the corresponding annex of the DNV [83].

4.3 Calculation of Design Loads

The problem concerns strengthening the bow to mount a crane base on a 40m yacht made of sandwich composites. The bow in the crane area should be checked for its total strength for the design loads specified in the regulations according to the failure criteria for composite materials such as the Tsai-Wu. The strength is presented in the form of a safety factor. Also, the T-type connection is checked locally to a fracture effect assuming that during its construction voids have been created at specific points (in Appendix C). Initially, the loads are applied to the construction without the presence of the T-Joint reinforcement in order to check the strength of the existing construction. With the aim of improving the tendencies and the remaining mechanical properties of the bow, the T-Joint connection is placed in a strategic position and the strength of the construction is re-checked. These results can be compared later. Finally, considering that during the construction of the T-Joint the adhesive that connects the deck with the T-Joint overlamination has not become cured, a weak strip has been created from which a crack can spread that will make the T-connection nonfunctional.

For the remaining study parameters, the crane is studied while in service it is lifting and slewing the load at the same time. The ship is studied in when the bow falls into wave trough. Thus, a heel in port side direction and a trim in fore direction is generated. Wind loading is considered to allow wind forces and moments to be added to the direction of the most unfavorable situation.

4.3.1 Definitions

– A.1.Ship Coordinate System of motions sign convention

— positive surge is translation in the *X*-axis direction (positive forward)
— positive sway is translation in the *Y*-axis direction (positive towards port side of ship)
— positive heave is translation in the *Z*-axis direction (positive upwards)
— positive roll motion is positive rotation about a longitudinal axis through the COG (starboard down and port up)
— positive pitch motion is positive rotation about a transverse axis through the COG (bow down and stern up)
— positive yaw motion is positive rotation about a vertical axis through the COG (bow moving to port and stern to starboard).

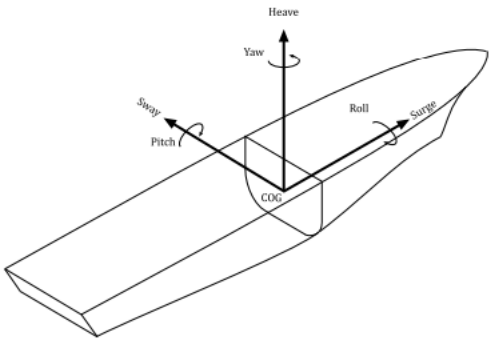

Figure 7:Ship Coordinate system [84]

– A.2.Trim and List sign convention

Trim is considered positive when the bow inclination is forward 'nose-down'.

The list is considered positive when the inclination of the ship is on the port side.

– A.3.Forces and Moments Coordinate system sign convention

VG: Force acting in Vertical direction on center G

LG: Force acting in Longitudinal direction on center G

TG: Force acting in Transverse direction on center G

MLV: Moment generated from Vertical force around Longitudinal Axis

MLT: Moment generated from Transverse force around Longitudinal Axis

MVL: Moment generated from Longitudinal force around Vertical Axis

MVT: Moment generated from Transverse force around Vertical Axis

MTL: Moment generated from Longitudinal force around Transverse Axis

MTV: Moment generated from Vertical force around Transverse Axis

- Crane in Service:

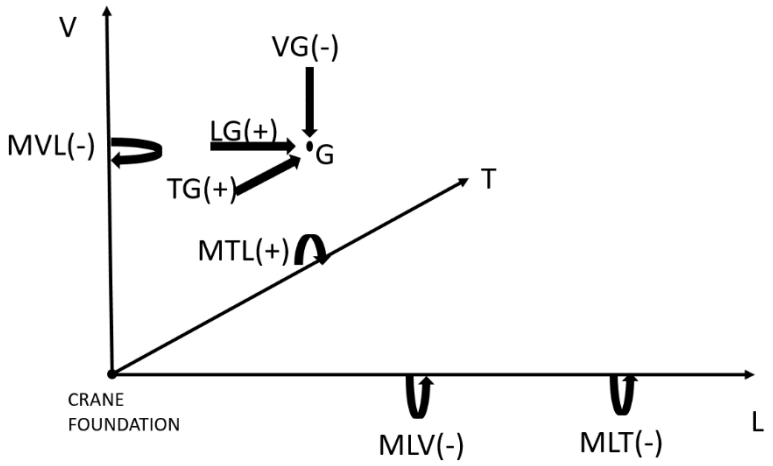

Table 2:Moments Sign Convention

MOMENTS IN SERVICE			
	ML	MT	MV
V-	-		
L+		+	-
L-		-	+
T+	-		
T-	+		

– A.4. Crane in service assumptions

- The crane extends in the transverse direction of the ship.
- Heel angle of 5 degrees port side
- Trim angle of 2 degrees fore
- Wind speed 25 m/s
- The ship is in mooring condition with two anchors.
- Sea state of significant wave height 3 m
- Hogging, Sagging and hydrodynamic loads (such as slamming) of bow region do not exist. Only the loads related to crane are taken into account.

– A.6.Dictionary

- Sea operation: The crane operates when the ship is mooring in an unsheltered location.
- Dynamic Hoist Load: The load of the hoist during the lifting operation multiplied by the dynamic amplification factor.
- Dynamic Amplification factor ψ: Safety factor that considers the dynamic phenomena during the lifting of a load.
- Partial safety factor M: Safety factor applied in load and crane, considered sea operation.

4.3.2 Crane Main Data

Table 3:Crane Data

Crane Main Data	
Hoist load=	**1500 kg**
Dead Load=	**2200 kg**
Area Comp1=	**0.49 m^2**
Area Comp2=	**1.59 m^2**
Area Comp3=	**1.2m^2**
Projected area for crane=	**3.288m^2**
Projected area of the tender=	**0.375 m^2**
Total projected Area A=	**3.66 $m^{2.}$**

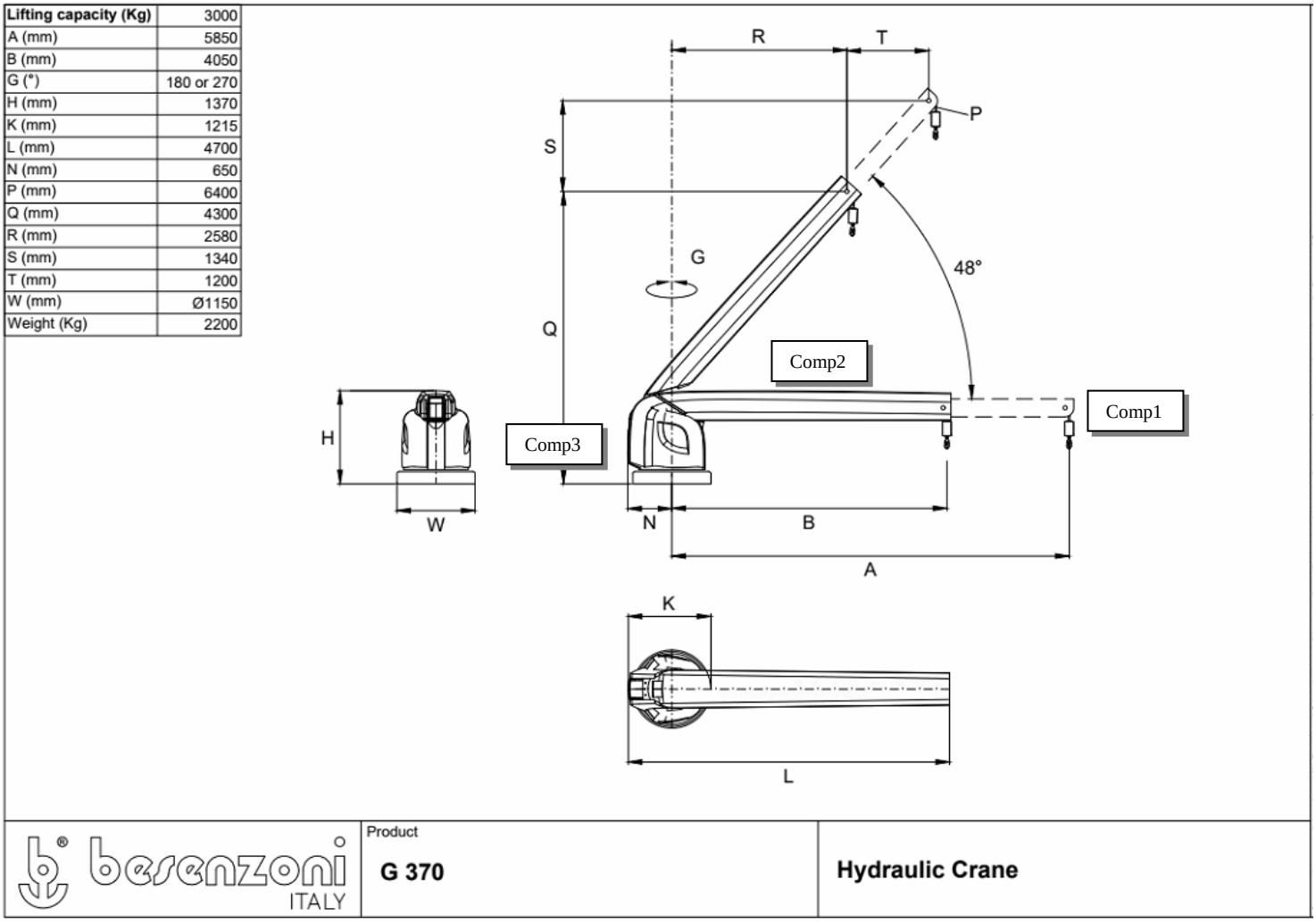

Figure 8:Crane Drawing

– B.1. Crane in Service

Table 4:Crane Geometric centers Crane Transverse Fully Extend +Tender Calculation Centers	
Transverse Center of Gravity TG=	**1.967 m**
Longitudinal Center of Gravity LG=	**0 m**
Vertical Center of Gravity VG=	**0.929 m**
Crane Boom Transverse Distance=	**5.85 m**
Crane Boom Vertical Distance=	**1.37 m.**

4.3.3 Yacht Main Data

Table 5:Yacht main data

SHIP DATA	
Length over all=	**40**
Scantling Lenght=	**39**
Length at water line=	**36**
Draft at full load T=	**2**
Height at the main deck D=	**4.1**
Beam B=	**8.3**
Lightship Displacement=	**180**
Full load Displacement=	**235**
Maximum speed at 200 tons=	**24**
Block coefficient CB=	**0.4.**

According to DNV YACHTS [84], the ship is in High Speed Craft Category.

Calculations for Design Loads at the base of the crane are made according to the regulations DNV Shipboard Lifting Appliances [80], DNV Offshore Lifting Appliances [81] and API2C [82].

The option of determining the loads through three different regulations was chosen in order to compare the results and to check the accuracy of the calculations. The results of the three regulations should not differ significantly.

4.3.4 Calculation according to DNV Shipboard Lifting Appliances

4.3.4.1 Regular Loads

Regular loads are the loads that are permanently present in each study situation.

4.3.4.1.1 Dead Loads

Dead loads refer to the structural components of the crane.

LE= 21582 N

4.3.4.1.2 Hoist load at sea operation

Hoist loads refer to the force acting on the crane boom due to working load.

LH= 15450.75N

4.3.4.2 Dynamic forces due to drive systems at load and crane

These forces consider the inertia of the lift load and the crane components during the movement of the total crane system. This calculation exists only when the condition is that the crane is in service. In crane in service operation, the initial position of crane extends at ships transverse direction.

4.3.4.2.1 Lifting of a load

Lifting load refer to the condition that the crane pulls vertically the hoist load with a dynamic amplification factor consider as ψ=1.4. The dynamic amplification factor is multiplied with Hoist Load LH.

At this operation the crane components may be considered inertia forces from static trim and list of ship, but without dynamic amplification factor.

The longitudinal and transverse forces components are resulted only from trim and list inclination of the ship during lifting of a load.

4.3.4.2.1.1. Force in Ships' Vertical direction including list and trim

The force induced on the hoist load or crane components when the ship has trim (2 degrees) and list (5 degrees) inclination and performs the lifting of the load. To include the most unfavorable angle situation we consider the angle $\varepsilon = \sqrt{(trim^2) + (list^2)}$ in the trim direction.

The general formulation of the above is given as following:

$$Load\ vertical\ inclination = Load \cdot \cos(\varepsilon) \qquad (11)$$

Hoist loads refer to the force act on crane boom due to working load after multiplied with dynamic amplification factor ψ=1.4 and the ship has inclination of 2 degrees trim and 5 degrees list.

Dynamic Hoist Load vertical inclination LHDI= 21831.823 N

Dead loads refer to the structural components of the crane after a 2 degree trim and a 5 degree list of the inclination of the ship.

Crane Dead load vertical inclination LEI= 21486.743 N

4.3.4.2.1.2. Force in Ships' Longitudinal direction including list and trim

The force induced on the hoist load or crane components when the ship has trim (2 degrees) and list (5 degrees) inclination and performs the lifting of the load. To include the most unfavorable angle situation we consider the angle $\varepsilon = \sqrt{(trim^2) + (list^2)}$ in the trim direction.

The general formulation of the above is given as following:

$$Load\ longitudinal\ inclination = Load\ \cdot \sin(\varepsilon) \quad (12)$$

The results are as following:

Dynamic Hoist Load Longitudinal inclination= 2058.012 N

Crane Dead load Longitudinal inclination= 2025.482 N

4.3.4.2.1.3. Force in Ships' Transverse direction including list and trim

The force induced on the hoist load or crane components when the ship has trim (2 degrees) and list (5 degrees) inclination and performs the lifting of the load.

The general formulation of the above is given as follows:

$$Load\ longitudinal\ inclination = Load\ vertical\ inclination \cdot \sin(heel) \quad (13)$$

The results are as following:

Dynamic Hoist Load Transverse inclination= 1902.769 N

Crane Dead load Transverse inclination= 1872.693 N

4.3.4.2.2 Suspended load

Suspended load refers to the condition that the crane rotates the hoist load in slewing radius to place it on the deck. In suspended load conditions no dynamic amplification factor ψ is considered. Additionally, this operation results in inertia forces due to tangential accelerations on the lifting load and the crane components. Trim and list contribution, as defined in Lifting of a load, is considered by vectorially addition at each force component.

4.3.4.2.2.1. Force in Ships' Vertical direction

Without a dynamic factor ψ, the value of Load vertical inclination over ψ must be taken into account.

Total Vertical load with inclination for Hoist Load=15382.55 N

Total Vertical load with inclination for Crane dead Load= 21486.7N

4.3.4.2.2.2 Force in Ships' Longitudinal direction

When the crane rotates from the transverse direction to the longitudinal direction, a tangential acceleration is induced at the lifting load and the crane components. This force has direction at ships longitudinal. Also, force components from ship inclination are added vectorially.

With the known value of the slewing radius r=5.85 m, the n=4 rpm of the slewing and calculates the tangential and centrifugal acceleration b_t,b_r respectively from the formula $b_t = b_r = b = \frac{r \cdot n^2}{91} = 1.029 \frac{m}{s^2}$ The general formulation is the following:

$$Load\ tangencial = Load \cdot b \tag{14}$$

The results are as following:

Total Longitudinal load with inclination for Hoist Load= 3749.26 N

Total Longitudinal load with inclination for Crane dead Load= 4401.5 N

4.3.4.2.2.3. Force in Ships' Transverse direction

Forces may induce in the transverse direction of the ships if centrifugal acceleration is considered. In this case, the centrifugal forces are not ignored and forces applied in this direction due to ship inclinations.

With the known value of the slewing radius r=5.85 m, the n=4 rpm of the slewing and calculate the tangential and centrifugal acceleration b_t,b_r respectively from the formula $b_t = b_r = b = \frac{r \cdot n^2}{91} = 1.029 \frac{m}{s^2}$ The general formulation is the following:

$$Load\ centrifugal = Load \cdot b \tag{15}$$

Total Transverse load with inclination for Hoist Load= 3530.4N

Total Transverse load with inclination for Crane dead Load= 4135.55 N

4.3.4.3 Dynamic forces by ship motions at crane and supporting structure

When the ship operates at sea the ship motions depend on the waves and the state of the sea. These motions create forces at the supporting structure of the crane and must be considered for the case study of crane in service and crane out of service. For the structural components of the crane only these forces are considered. The case study of crane in service contemplates accelerations based on the acceleration of the floating vessel body in the crane bases for the roll period of 9.8 seconds and the pitch period of 5.4 seconds for the oblique sea. Also, for specific accelerations for the equipment, as defined in DNV [83].

4.3.4.3.1 5.4.3.1.Force in Ships' Vertical direction

With vertical acceleration $a_V = 6.44 \frac{m}{s^2}$ The vertical inertia force for crane components is:

Extra Vertical Component due to crane base acceleration= 14175.7 N

4.3.4.3.2 5.4.3.2..Force in Ships' Longitudinal direction

With longitudinal acceleration $a_L = 2.16 \frac{m}{s^2}$ The longitudinal inertia force for crane components is:

Extra Longitudinal Component due to crane base acceleration = 4765.6 N

4.3.4.3.3 5.4.3.3. Force in Ships' Transverse direction

With longitudinal acceleration $a_T = 4 \frac{m}{s^2}$ The longitudinal inertia force for crane components is:

Extra Transverse Component due to crane basis acceleration = 8949.6N

4.3.4.4 Irregular loads

4.3.4.4.1 Wind loads

Wind induces forces in the structural components and the crane tender. These forces act on the center of the area of the crane-tender system. For crane in service case study the wind velocity is calculated as 25 m/s with direction at ships longitudinal. Notice that, in service, the crane position extends in the transverse direction of the ship.

Wind load crane in service= 2289.31N

4.3.4.5 Load combinations results and safety factors

Table 6:Load Combinations according to DNV Shipboard Lifting Appliances

Crane in service				
Category	**Loads**	**Components Base on Ships Coordinate System**	**Load combination II (Regular loads-Wind-Dynamic forces)**	
			Sea operation	
			II1 During lifting	**II2 Suspended load**
Regular loads	Hoist Load (Vertical) and Dynamic forces due to drive (Load) (N) (Inclination included)	Logitudinal	2058.012	3749.260
		Vertical	-21831.823	-15382.555
		Transverse	1902.769	3530.391
	Dead Load (Vertical) and Dynamic forces due to drive (Crane) (N) (Inclination included)	Logitudinal	2025.482	4401.482
		Vertical	-21486.743	-21486.743
		Transverse	1872.693	4135.550
	Extra Dynamic forces due to ship motions (Crane) (N)	Logitudinal	4765.575	4765.575
		Vertical	-14175.744	-14175.744
		Transverse	8949.571	8949.571
Irregular loads	Wind loads (N)	Logitudinal	2289.313	2289.313
		Vertical	0.000	0.000
		Transverse	0.000	0.000
Global safety factor γs=			1.34.	

The forces and moments at the crane foundation on the deck after transfer by distances of center of mass and area coordinates of the crane-tender system and safety factor are as follows:

Table 7:Loading Condition of Crane according to DNV Shipboard Lifting Appliances

Summary of Total Forces and Moments on Crane Foundation-Crane In Service			
Load Components	**Sea operation**		
	II1 During lifting	**II2 Suspended load**	**Average Combined**
Force Logitudinal (kN)	14.925	20.376	20
Force Veritcal (kN)	-77.042	-68.400	76
Force Transverse (kN)	17.052	22.265	22
Moment Around Longitudinal Axis (kNm)	-282.106	-186.571	-280
Moment Around Vertical Axis (kNm)	-40.066	-59.586	-64
Moment Around Transverse Axis(kNm)	15.087	21.151	22.

4.3.5 Calculation according to DNV Offshore Lifting Appliances

4.3.5.1 Principal loads

The dead weight of the crane components and the working load on the crane boom are considered principal loads. The weight of the crane boom is ignored.

4.3.5.1.1 Loads due to dead weight of crane

The load due to the dead weight of the crane components SG in kN is:

$$S_G = 21.582\ kN$$

4.3.5.1.2 Loads due to working load

The load due to the working load S_L in kN is:

$$S_L = 14.715\ kN$$

4.3.5.2 Principal loads after inclination

When static inclination is considered for the ship, the principal loads acquire different force components in the vertical, longitudinal and transverse direction of the ship. The trim inclination is defined by angle θ and the list inclination is defined by angle φ. In this study, consider the minimum angles θ=3 deg and φ=5 deg.

4.3.5.2.1 Ships vertical direction

The vertical component of the principal loads after inclination is calculated as:

$$S_{iV} = S_i \cdot \cos(\theta) \quad (16)$$

The force components in the vertical direction of the ship are:

S_{GV}= 21.57 kN

S_{LV}= 14.71 kN

4.3.5.2.2 Ships' Longitudinal direction

The longitudinal component of the principal loads after inclination is calculated as:

$$S_{iL} = S_i \cdot \sin(\theta) \quad (17)$$

The force components in the longitudinal direction of the ships are:

S_{GL}= 0.75 kN

S_{LL}= 0.51 kN

4.3.5.2.3 Ships' Transverse direction

The transverse component of principal loads after inclination is calculated as:

$$S_{iT} = S_i \cdot \sin(\theta) \quad (18)$$

The force components in the transverse direction of the ship are:

S_{GT}= 1.88 kN

S_{LT}= 1.28 kN

4.3.5.3 Vertical loads due to operational motions- Calculation of dynamic factor ψ

To determine the dynamic factor ψ one must take into account the stiffness of the crane, the work load and the relative velocity between the hook and load at the time of lift-off. The stiffness of the crane depends on the modulus of elasticity of the wire ropes, the nominal strength of the wire rope, the strain and the extension of the cable in unit length and can be calculated or provided as data from the manufacture of the crane. The relative velocity between hook and load depends on downward velocity, jib tip velocity and velocity of lifting off load from sea surface. Due to the lack of data on crane stiffness from the manufacturer and the exact determination of velocity, the factor is taken empirically from DNV [80].

The dynamic factor ψ takes the value:

$$\psi = 1.4 \tag{19}$$

4.3.5.3.1 Vertical Principal loads after dynamic factor

Multiply S_{GV}, S_{LV} with dynamic amplification ψ. The principal vertical loads after dynamic factor ψ are:

$\underline{S_{GV\psi} = 30.2\ kN}$

$\underline{S_{LV\psi} = 20.6\ kN}$

4.3.5.4 Horizontal loads due to operational motions

Horizontal loads take into account the slewing of the working load by the crane due to operational motions. Considering crane slewing with n= 4 rpm, a tangential force (side-lead) in the longitudinal direction of the ship and centrifugal force (off-lead) in the transverse direction of the ship is induced.

4.3.5.4.1 Ships' Longitudinal direction

The formulation of the tangential forces for crane and work load, considering the slewing radius r, the load Si and the sea state of the significant wave height H_s=3m is:

$$S_{iLS} = \frac{S_i}{100} \cdot [2.5 + 0.1 \cdot r \cdot n + H_s] \tag{20}$$

The results of the calculation are the following:

S_{GLS}= 1.37 kN

S_{LLS}= 1.61 kN

4.3.5.4.2 Ships' Transverse direction

The formulation for centrifugal forces for crane and working load considers the slewing radius r and the load Si as following:

$$S_{iTS} = \frac{S_i}{1000} \cdot n^2 \cdot r \tag{21}$$

The results of the calculation are the following:

S_{GLS}= 0.68 kN

S_{LLS}= 1.93 kN

4.3.5.5 Loads due to motion of vessel

When the ship operates at sea the ship motions depend on the waves and the state of the sea. These motions create forces at the supporting structure of the crane and must be considered for the case study of crane in service and crane out of service. For the structural components of the crane only these forces are considered. The case study of crane in service contemplates accelerations based on the acceleration of the floating vessel body in the crane bases for the roll period of 9.8 seconds and the pitch period of 5.4 seconds for the oblique sea. Also, for specific accelerations for the equipment, as defined in DNV [83].

4.3.5.5.1 Ships' Vertical direction

With vertical acceleration $a_V = 6.44 \frac{m}{s^2}$ The vertical inertia force for crane components is:

S_{GVI}= 19.83 kN

4.3.5.5.2 Ships' Longitudinal direction

With longitudinal acceleration $a_L = 2.16\frac{m}{s^2}$ The longitudinal inertia force for crane components is:

$$S_{GLI} = 4.76\ kN$$

4.3.5.5.3 Ships' Transverse direction

With longitudinal acceleration $a_T = 4\frac{m}{s^2}$ The longitudinal inertia force for crane components is:

$$S_{GTI} = 8.95\ kN$$

4.3.5.6 Loads due to wind

The wind loads are the same as calculated in the section Wind loads, because there has been no change in geometry or wind parameters.

4.3.5.6.1 Ships' Longitudinal direction

Wind induces forces in the structural components and the crane tender. These forces act on the center of the area of the crane-tender system. For crane in service case study the wind velocity is calculated as 25 m/s with direction at ships longitudinal. Notice that, in service, the crane position extends in the transverse direction of the ship.

$$Wind\ load = 2289.3\ N$$

4.3.5.7 Load combinations results and safety factors

The forces and moments on the crane foundation on deck, after their multiplication with the safety factor and transfer by distances from the center of mass and area coordinates of the crane-tender system, are as following:

Table 8:Loading Condition of Crane according to DNV Offshore Lifting Appliances

Load Case with wind and ship motion-Forces and Moments at crane base	
Forces and Moments	**Load combination sea operation crane in service combined lift off and slewing**
Vertical forces (kN)	74.4
Longitudinal forces(kN)	13.5
Transverse forces (kN)	17.66
Moment around vertical axis (kNm)	36.57
Moment around longitudinal axis(kNm)	280.73
Moment around Transverse axis(kNm)	11.17.

4.3.6 Calculation according to API2C

The American Petroleum Institute [82] provides a clear and understandable methodology for calculating crane loads. This methodology does not take into account the phenomenon of ship movement in terms of velocity, but considers these factors using the significant wave height Hs. For this reason, the forces and moment values of API2C are expected to be smaller than the DNV values.

The term side-lead refers to trim inclination and off-lead to heel inclination.

The calculations at the end of the methodology are converted from US unit system to SI unit system.

4.3.6.1 Vertical Design Load

The vertical design load results from the work load multiplied by the dynamic factor $C_{v.}$

As explained in the chapter "Vertical loads due to operational motions-Calculation of dynamic factor ψ", due to the lack of data on crane stiffness from the manufacturer and the exact definition of the velocity, the factor is taken empirically from DNV [80]

The dynamic factor Cv takes the value:

$$C_v = 1.45 \tag{22}$$

The vertical design load is as following:

$$\underline{V_{DL} = \quad 4795 \text{ lb force}}$$

4.3.6.2 Off-lead and side-lead due to other floating body motions.

When the load is lifted from a surface which is not calm but has relative motion compared to the ship, in this case the sea, off-lead and side-lead forces may be induced in the crane system.

Considering angle φ=48 deg between the horizontal plane and the end of the extended crane arm, vertical distance of the boom tip above the sea surface H_w=31.94 ft , length of the extended crane arm *BL*=19.2 ft and significant wave height of Hsig=9.84 ft , then the off-lead and side lead due to other motion of the floating body are provided by the formulas:

$$W_{offSB} = V_{DL} \cdot \frac{2.5 + 0.457 \cdot H_{sig}}{0.305 \cdot (H_w + BL \cdot sin\varphi)} \qquad (23)$$

$$W_{sideSB} = \frac{W_{offSB}}{2} \qquad (24)$$

The W_{sideSB} shall not be less than $0.02 \cdot V_{DL}$

The results of the calculations above are as following:

W_{offSB} =3416 lb force

W_{sideSB} =1708 lb force

4.3.6.3 Horizontal loads due to static crane inclination

When static inclination is considered for the ship, the principal loads acquire different force components in the longitudinal and transverse directions of the ships.

The trim inclination is defined by angle θ and the list inclination is defined by angle φ.

In this study, consider the minimum angles θ=2 deg and φ=5 deg.

For the hoist load consider as load the V_{DL}, while for the crane the dead load of components is in lb force.

The formulation for off-lead and side-lead is:

$$W_{sideCI} = V \cdot \tan(\theta) \qquad (25)$$

$$W_{offCI} = V \cdot \tan(\varphi) \qquad (26)$$

The results from the formulation above are:

$W_{sideCIL}$ =167.44 lb force

$W_{sideCIC}$ =169.37 lb force

W_{offCIL} =419.51 lb force

W_{offCIC} =424.33 lb force

4.3.6.4 Horizontal loads due to crane motions

The crane motions depend on the state of the sea and take into account the parameter of significant wave height to determine the acceleration for dynamic calculations. With a significant wave height of H_{sig}=9.84 ft, the crane dynamic acceleration is given from:

$$a = 0.01 \cdot H_{sig}^{1.1} = 0.01 \cdot 9.84^{1.1} \rightarrow a = 0.12\ g's \quad (27)$$

The crane base angle is equal to ε=45 degrees and is in the horizontal plane. For example, if the crane base angle was 0 degrees, then only the off-lead exists. Therefore, the dynamic force has off-lead and side-lead components on account of the 45 degree angle. Note that for the load calculations the V_{DL} is used.

The vertical component of the crane and load is given by:

$$W_{horizontalCM} = V \cdot \alpha \quad (28)$$

The off-lead and side-lead components are:

$$W_{offCM} = W_{horizontalCM} \cdot \cos(\varepsilon) \quad (29)$$

$$W_{sideCM} = W_{horizontalCM} \cdot \sin(\varepsilon) \quad (30)$$

The results of crane and load are:

$W_{horizontalCML}$ = 593 lb force

W_{offCML} =419.34 lb force

$W_{sideCML}$ =419.34 lb force

$W_{horizontalCMC}$ =599.86 lb force

W_{offCMC} =424.16 lb force

$W_{sideCMC}$ =424.16 lb force

4.3.6.5 Combination of Horizontal design loads

The horizontal design loads can be superimposed as following:

$$W_{sidedynL} = \sqrt{W_{sideSB}^2 + W_{sideCML}^2} \quad (31)$$

$$W_{offdynL} = \sqrt{W_{offSB}^2 + W_{offCML}^2} \quad (32)$$

$$W_{sidedynC} = W_{sideCMC} \quad (33)$$

$$W_{offdynC} = W_{offCMC} \quad (34)$$

The resultant horizontal design load for the lift load is:

$W_{sidedynL}$ =1758.74 lb force

$W_{offdynL}$ =3441.69 lb force

$W_{sidedynC}$ =424.16 lb force

$W_{offdynC}$ =424.16 lb force

4.3.6.6 Wind loads

The wind load, as shown in "Wind loads" and "Loads due to wind", is:

Wind load side-lead in hoist load =52.6 lb force

Wind load side-lead in crane =514.64 lb force

4.3.6.7 Inertia forces due to Crane dead weight components

In order to be more accurate according to the results above and to have a comparison of values, the vertical inertia force component due to ship motions in sea must be added to this analysis. According to DNV [83] the vertical acceleration is $a_V = 1.07\ g's$ and the vertical inertia load of crane is calculated as:

$$V_{CI} = a_v \cdot Vc \tag{35}$$

The inertia vertical force is:

V_{CI} *=5189.63 lb force*

4.3.6.8 Total forces-moments formulation and safety factors

The total loads for the hoist load including the safety factor SF are:

$$Total\ vertical\ load\ for\ hoist\ load = WTV_L = SF \cdot (V_{DL}) \tag{36}$$

$$Total\ offlead\ load\ for\ hoist\ load = WTO_L = SF \cdot \left(W_{offdynL}\right) \tag{37}$$

$$Total\ sidelead\ load\ for\ hoist\ load\ = WTS_L = SF \cdot \left(W_{sidedynL} + Wind\ load\ L\right) \tag{38}$$

The total loads for the crane including the safety factor SF are:

$$Total\ vertical\ load\ for\ crane = WTV_C = SF \cdot (V_c) \tag{39}$$

$$Total\ offlead\ load\ for\ crane = WTO_C = SF \cdot \left(W_{offdynC}\right) \tag{40}$$

$$Total\ sidelead\ load\ for\ crane\ = WTS_C = SF \cdot \left(W_{sidedynC} + Wind\ load\ C\right) \tag{41}$$

Knowing the center of gravity of the crane tender system (V_G,L_G,T_G), the radius (R) of the extended crane arm and the transverse and vertical distances of the crane boom (C_{BT},C_{BV}) from the center of rotation of the crane, the moments produced by loading and loading are:

$$Inplane\ moments(Around\ Longitudinal\ axis)\ Load = IMLVL = WTV_L \cdot R \quad (42)$$

$$Inplane\ moments(Around\ Longitudinal\ axis)\ Load = IMLOL = WTO_L \cdot C_{BV} \quad (43)$$

$$Inplane\ moments(Around\ Transverse\ axis)\ Load = IMTSL = WTS_L \cdot C_{BV} \quad (44)$$

$$Torque\ (Around\ Vertical\ axis)\ Load = TVL = WTS_L \cdot R \quad (45)$$

$$Inplane\ moments(Around\ Longitudinal\ axis)\ Load = IMLVC = WTV_C \cdot T_G \quad (46)$$

$$Inplane\ moments(Around\ Longitudinal\ axis)\ Load = IMLOC = WTO_C \cdot V_G \quad (47)$$

$$Inplane\ moments(Around\ Transverse\ axis)\ Load = IMTSC = WTS_C \cdot V_G \quad (48)$$

$$Torque\ (Around\ Vertical\ axis)\ Load = TVC = WTS_C \cdot T_G \quad (49)$$

Summarize the forces and moments:

$$Total\ vertical\ load = WTV_L + WTV_C \quad (50)$$

$$Total\ offlead\ load\ = WTO_L + WTO_C \quad (51)$$

$$Total\ sidelead\ load\ = WTS_L + WTS_C \quad (52)$$

$$Total\ Moments\ around\ longitudinal\ axis = IMLVL + IMLOL + IMLVC + IMLOC \quad (53)$$

$$Total\ Moments\ around\ transverse\ axis = IMTSL + IMTSC \quad (54)$$

$$Total\ Moments\ around\ vertical\ axis = TVL + TVC \quad (55)$$

4.3.6.9 Load combinations results SI unit System

The total load combination in the crane base is provided below in the SI unit system:

Table 9: Loading Condition of Crane according to API2C in SI

Load Case with wind and ship motion-Forces and Moments at crane base	
Forces and Moments	**Load combination sea operation crane in service combined lift off and slewing**
Vertical forces (kN)	**66623.44**
Transverse forces (kN)	**25795.25**
Longitudinal forces(kN)	**14788.74**
Moment around Longitudinal axis(kNm)	**194503.15**
Moment around Transverse axis(kNm)	**21215.89**
Moment around Vertical axis (kNm)	**31425.46**

4.3.7 Comparison between studies

From the three studies above, it is useful to compare the loading conditions between them in order to make a decision about which loads will be used in finite element analysis. The above cumulative table and figure show the results of each study:

Table 10:Comparison and decision making of loading conditions

Component	DNV [A]	API2C[B]	DNV OFFHORE [C]	Overestimate
Crane Foundation Force Longitudinal (kN)=	20	14.79	13.5	DNV[A]
Crane Foundation Force Vertical (kN)=	76	66.62	74.4	DNV[A]
Crane Foundation Force Transverse (kN)=	22	25.79	17.66	API2C[B]
Crane Foundation Longitudinal Axis Moments(kNm)=	280	194.5	280.73	DNV[C]
Crane Foundation Vertical Axis Moments(kNm)=	64	31.42	36.57	DNV[A]
Crane Foundation Transverse Axis Moments(kNm)=	22	21.21	11.17	DNV[A]

On the basis of the results above, the most unfavorable study situation is given from DNV [A] [80] and is used as the final loading condition of the crane base.

4.4 Finite Element Analysis

Three geometry models have been created. The first model(A) simulates the bow region, as it already exists, without the t-joint stiffener configuration. The second model(B) contains a T-Joint reinforcement between deck and longitudinal bulkhead. A fully solid connection between components without any crack or defection achieved. Finally, the third sub model(C) contains a cracked T-Joint reinforcement that is described above. It is assumed that the crack was created during the construction of T-Joint and that there is a crack propagation during the loading of the construction. The initial crack located between the over-lamination skin and the deck region of the T-Joint. The above three models are compared and analyzed below.

4.4.1 Simulation Materials

The simulation material data are imported into ANSYS Workbench according to the values below. The simulation materials remain the same for all models. The design of composite materials is done through the ComposeIT software [85] of the BV Classification Society and the ANSYS ACP Module. Setting up the fibers, resin system and core material, the following composite laminates are produced.

4.4.1.1 Mats

Table 11:Mechanical properties of Mats

Name	Fibre	Resin	Fibre %	in	Fibre mass/m² (g/m²)	Resin mass/m² (g/m²)	Mass/m² (g/m²)	Thickness (mm)	Density
Mat300 E Glass Polyester	E Glass	Polyester	60.00	Volume	300.00	93.39	393.39	0.7	2.022
Mat450 E Glass Polyester	E Glass	Polyester	50.00	Volume	450.00	210.12	660.12	1.050	1.885
Mat900 E Glass Polyester	E Glass	Polyester	50.00	Volume	900.00	420.23	1,320.23	1.475	1.885.

Table 12:Elastic coefficients of Mats

Name	E1 (MPa)	E2 (MPa)	G12 (MPa)	G13 (MPa)	G23 (MPa)	v12	v21
Mat300 E Glass Polyester	24674	24674	9490	2915	2915	0.300	0.300
Mat450 E Glass Polyester	19976	19976	7683	2282	2282	0.300	0.300
Mat900 E Glass Polyester	19976	19976	7683	2282	2282	0.300	0.300.

Table 13: Breaking stress of Mats

Name	σ1 T	σ1 C	σ2 T	σ2 C	τ12	τIL1	τIL2
Mat300 E Glass Polyester	247.71	247.71	247.71	247.71	122.93	39.25	39.25
Mat450 E Glass Polyester	275.27	275.27	275.27	275.27	136.61	44.2	44.2
Mat900 E Glass Polyester	305.95	305.95	305.95	305.95	151.84	50.15	50.15

4.4.1.2 Core

Table 14:Mechanical properties of PVC core

Name	Type	Core material	Thickness (mm)	Mass/m² (g/m²)	Density
Foam PVC Cross Linked, 80 kg/m3, 80mm	Foam PVC Cross Linked	Foam PVC Cross Linked, 80 kg/m3	80.000	6400	0.080
Foam PVC Cross Linked, 80 kg/m3, 30mm	Foam PVC Cross Linked	Foam PVC Cross Linked, 80 kg/m3	30.000	2400	0.080
Foam PVC Cross Linked, 80 kg/m3, 25mm	Foam PVC Cross Linked	Foam PVC Cross Linked, 80 kg/m3	25.000	2000	0.080.

Table 15: Elastic coefficients of PVC Core

Name	E1 (MPa)	E2 (MPa)	G12 (MPa)	G13 (MPa)	G23 (MPa)	v12	v21
Foam PVC Cross Linked, 80 kg/m3, 80mm	67	67	31	31	31	0.080	0.080
Foam PVC Cross Linked, 80 kg/m3, 30mm	67	67	31	31	31	0.080	0.080
Foam PVC Cross Linked, 80 kg/m3, 25mm	67	67	31	31	31	0.080	0.080.

Table 16: Breaking stress for PVC Core

Name	σ1 T	σ1 C	σ2 T	σ2 C	τ12	τIL1	τIL2
Foam PVC Cross Linked, 80 kg/m3, 80mm	2.20	1.40	2.20	1.40	1.10	1.10	1.10
Foam PVC Cross Linked, 80 kg/m3, 30mm	2.20	1.40	2.20	1.40	1.10	1.10	1.10
Foam PVC Cross Linked, 80 kg/m3, 25mm	2.20	1.40	2.20	1.40	1.10	1.10	1.10.

4.4.1.3 Adhesive

Table 17: Mechanical properties of Adhesive

Name	Resin	Thickness (mm)	Mass/m² (g/m²)	Density
Epoxy 125mm	Epoxy	125.000	156250	1.250.

Table 18: : Elastic coefficients of Adhesive

Name	E1 (MPa)	E2 (MPa)	G12 (MPa)	G13 (MPa)	G23 (MPa)	v12	v21
Epoxy 125mm	3100	3100	1500	1500	1500	0.390	0.390.

4.4.1.4 Laminates

4.4.1.4.1 Deck Lamination

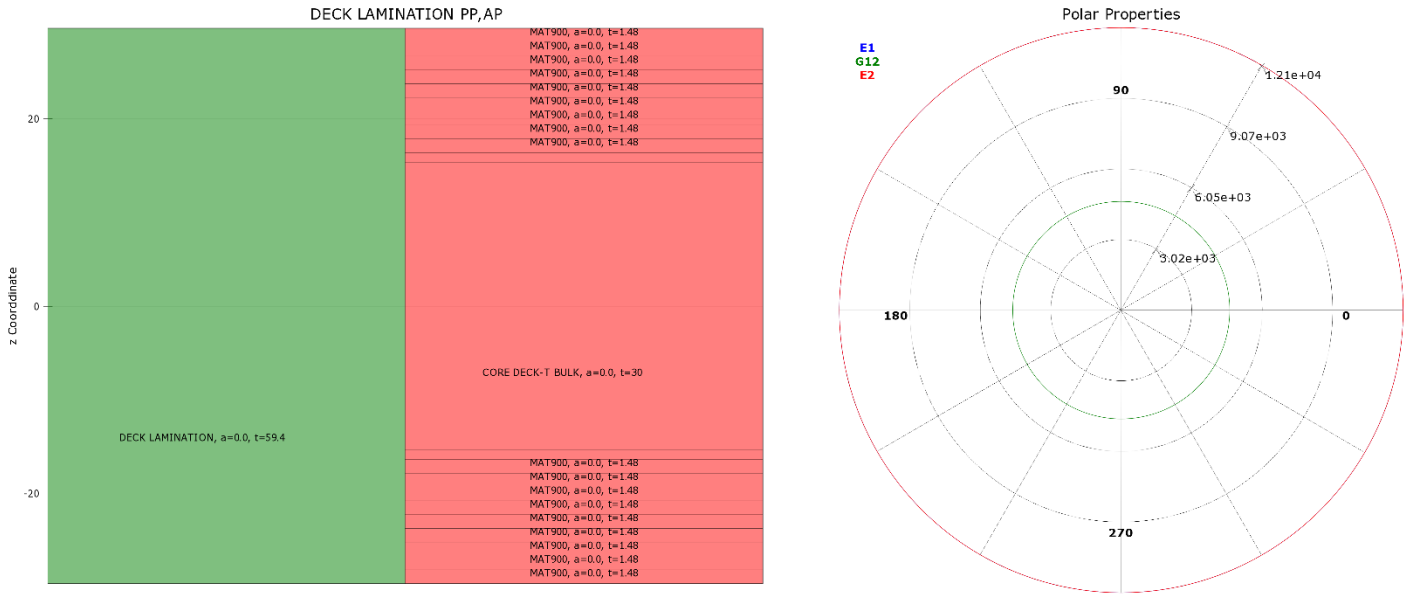

Figure 9:Deck Lamination layers and mechanical properties

4.4.1.4.2 Longitudinal Bulkhead Half Lamination

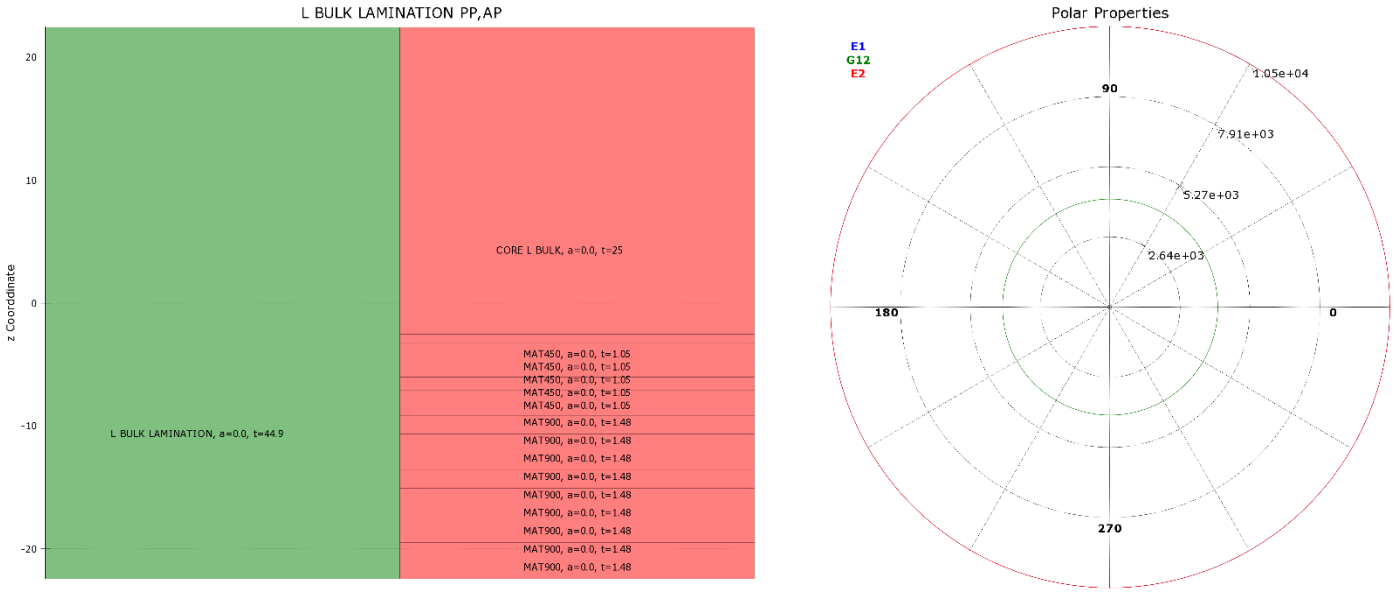

Figure 10: Longitudinal Bulkhead Lamination layers and mechanical properties

4.4.1.4.3 Transverse Bulkhead Lamination

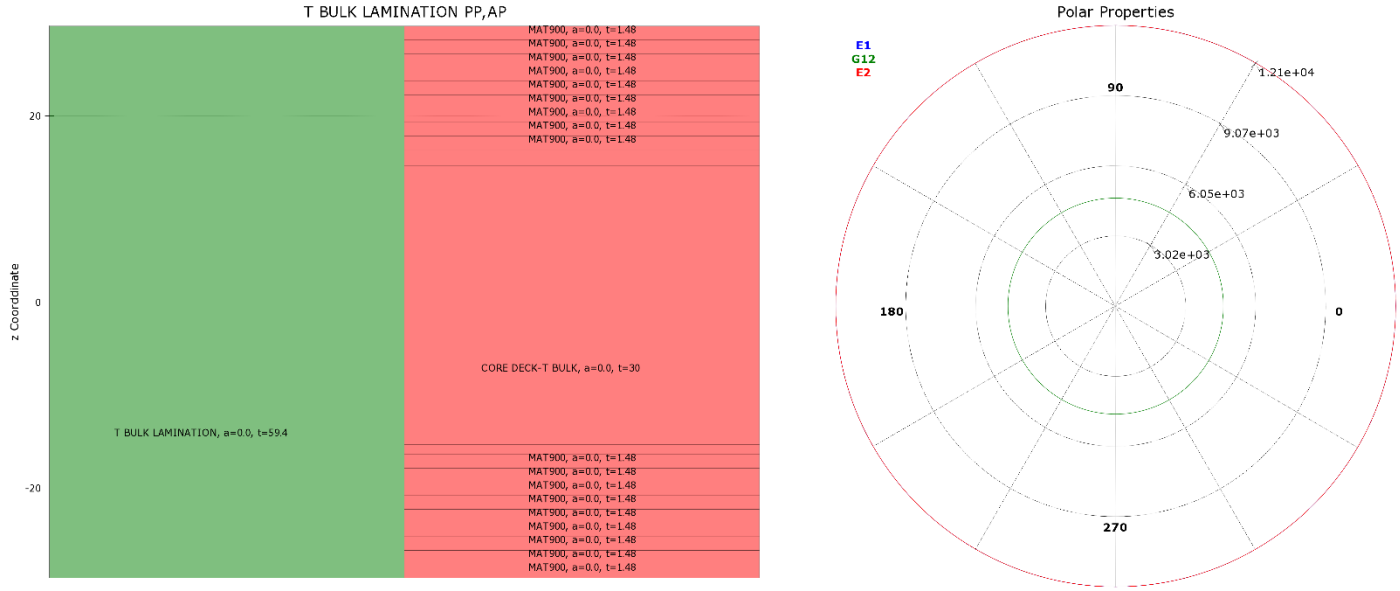

Figure 11: Transverse Bulkhead Lamination layers and mechanical properties

4.4.1.4.4 Transverse Frames Lamination

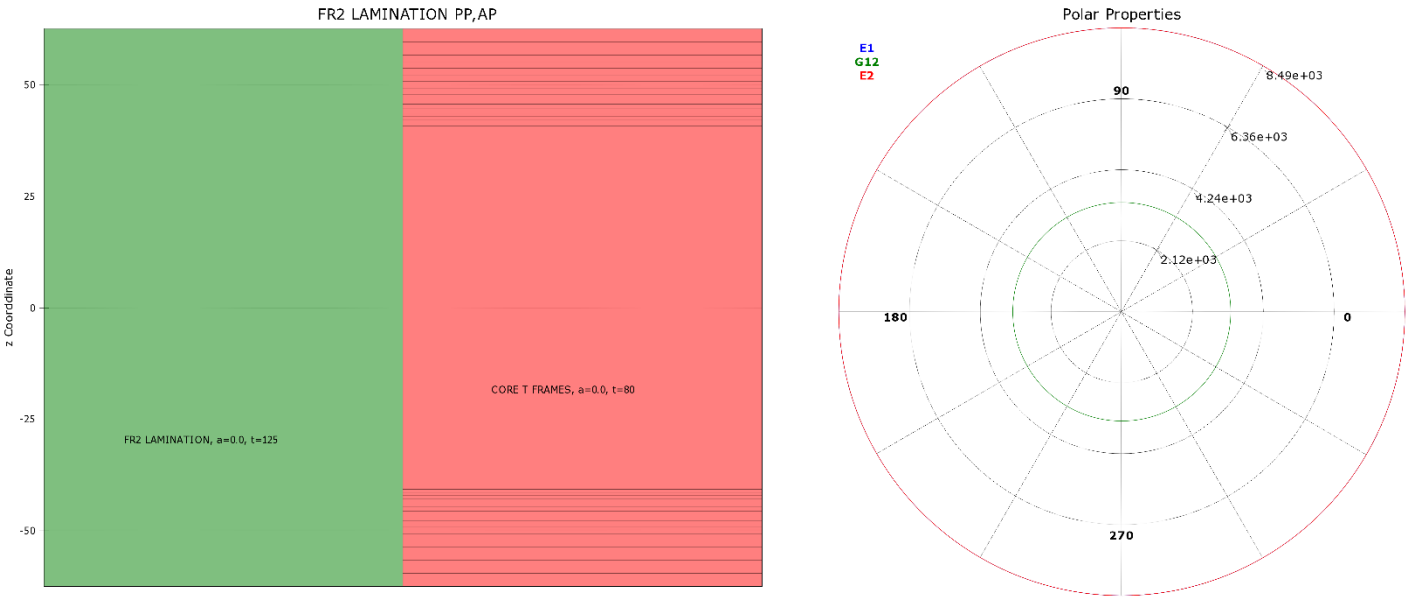

Figure 12: Transverse Frames Lamination layers and mechanical properties

4.4.1.4.5 T-Joint Over Lamination

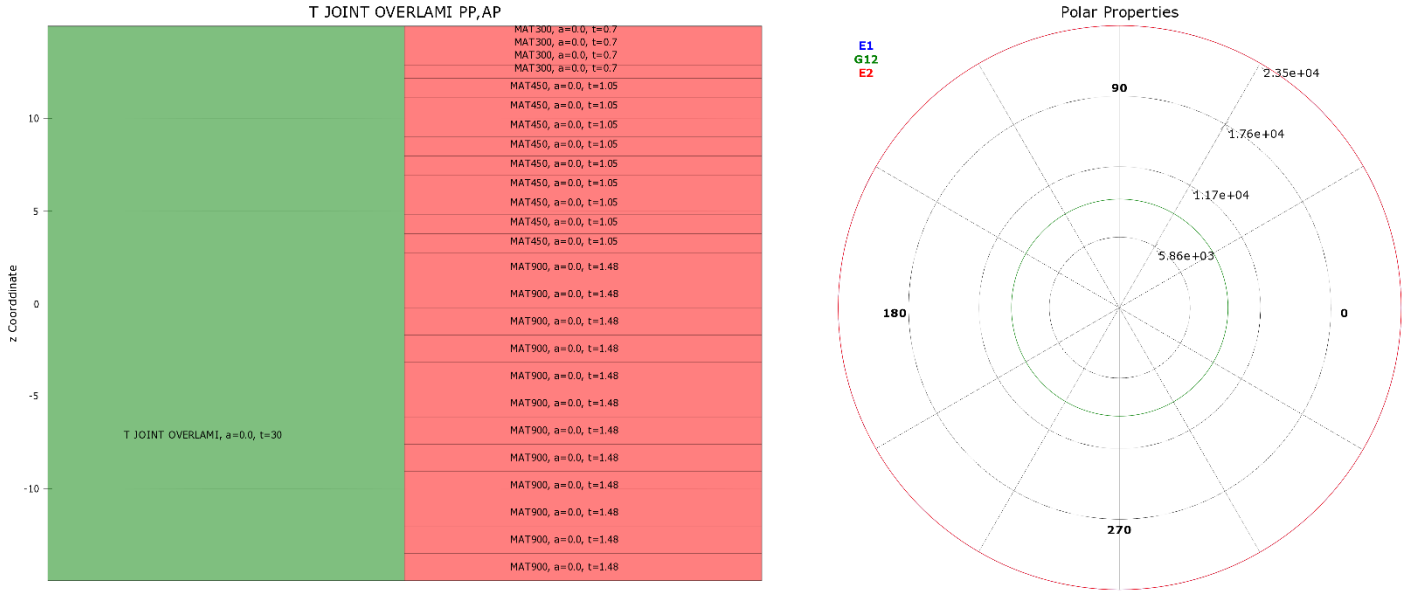

Figure 13: T-Joint Overlamination Lamination layers and mechanical properties

4.4.1.4.6 Adhesive Lamination

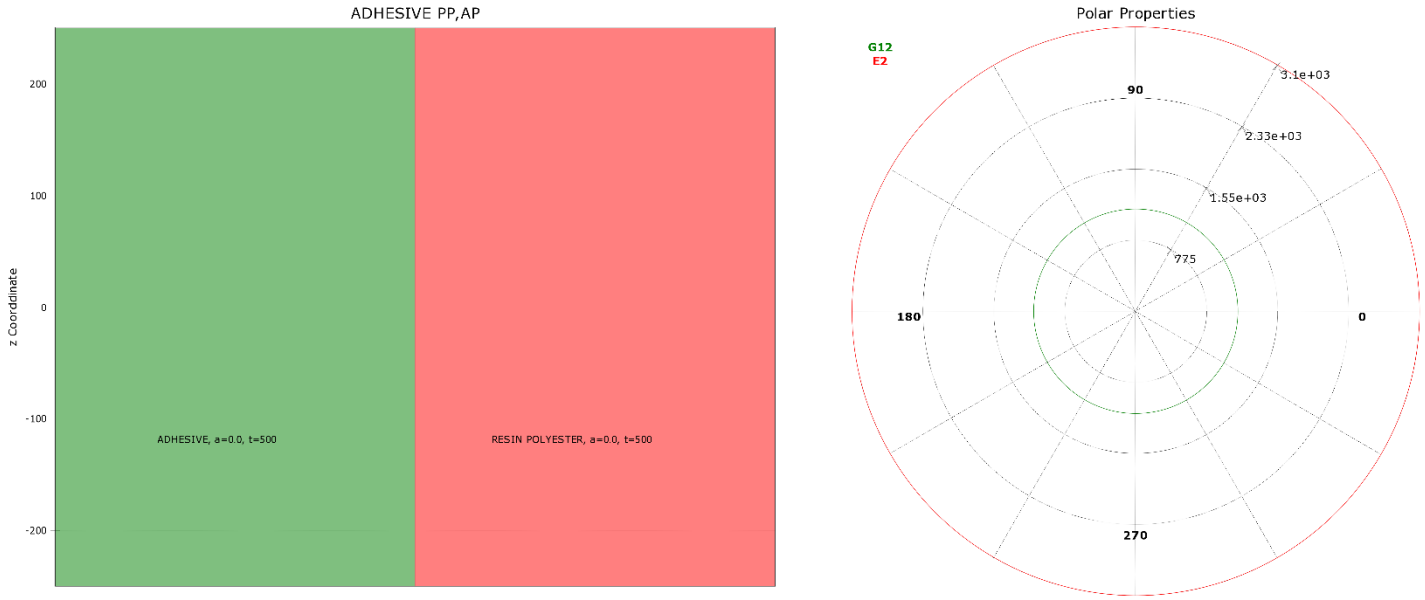

Figure 14:Adhesive Lamination layers and mechanical properties

4.4.2 Geometry of the bow region

The bow region consists of deck, longitudinal bulkhead, transverse bulkhead, transverse frames in simple form and t-joint stiffener configuration for the two last models. On the top skin of the deck, the circular crane base foundation pattern has been engraved to apply the loads calculated above. Also, crack fronts are created between the lamination skin and the deck. The 3D designs of yacht bow region are shown through ANSYS Space claim module as following:

4.4.2.1 Model(A)

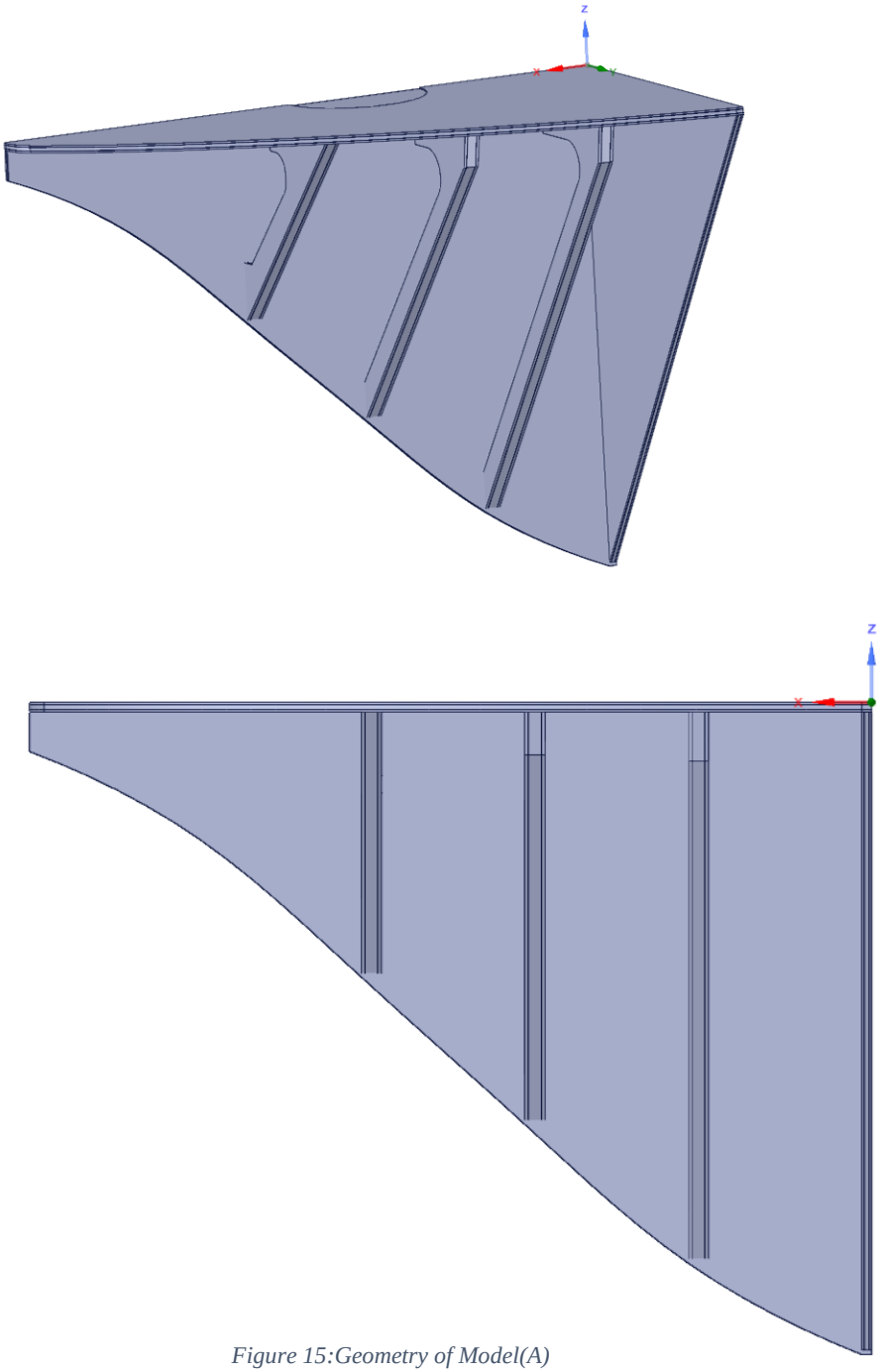

Figure 15:Geometry of Model(A)

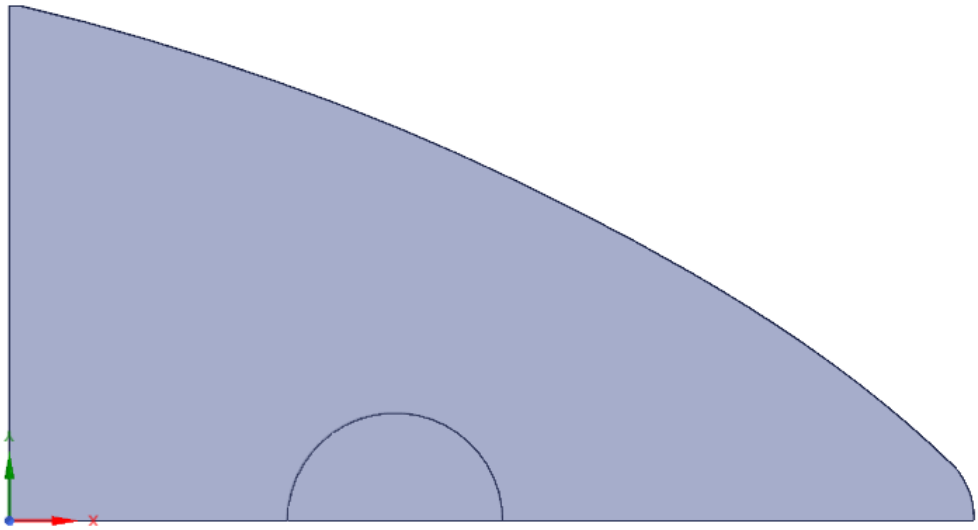

4.4.2.2 Model (B)

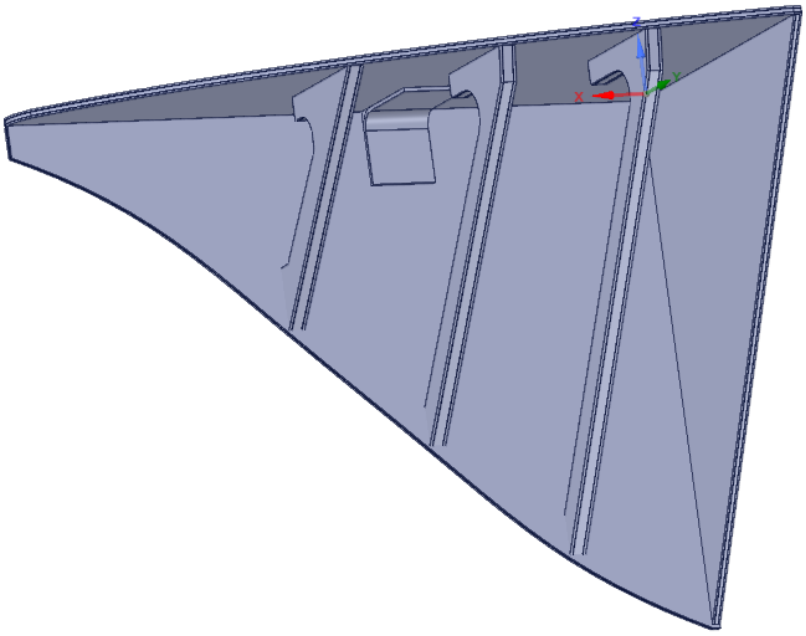

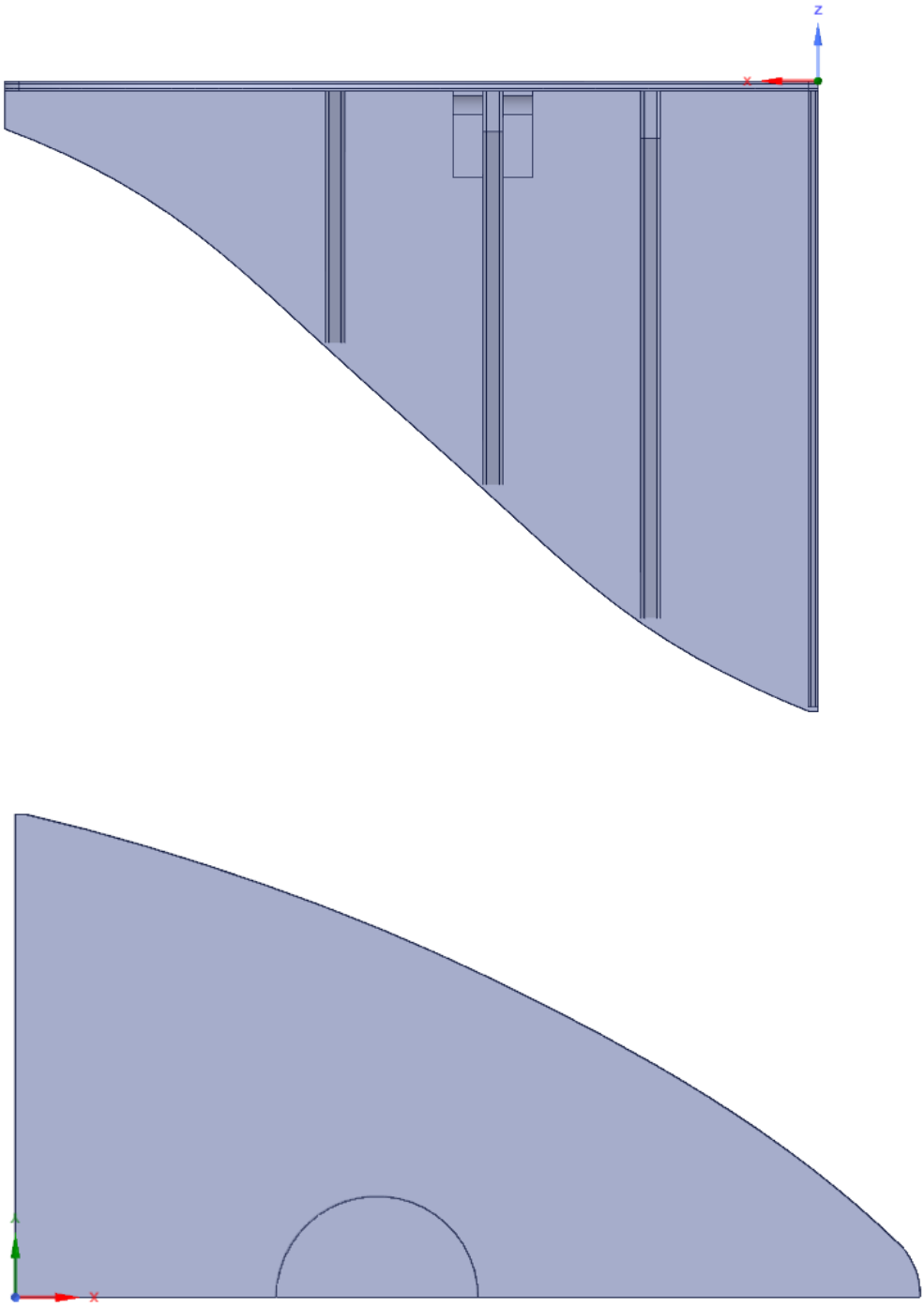

Figure 16:Geometry of Model(B)

4.4.3 Meshing and Boundary Conditions

4.4.3.1 Meshing

Meshing of model (A) consists of 216446 elements and 247147 nodes. Great importance has been given to the connection between the components. The nodes are connected to each other so that the grid is continuously and correctly defined. This process is done using a smaller mess size in the areas of interest. In the same manner, meshing of model (B) consists of 304065 elements and 341584 nodes. Particular emphasis has been placed on the meshing around the T-Joint area to properly carry the loads.

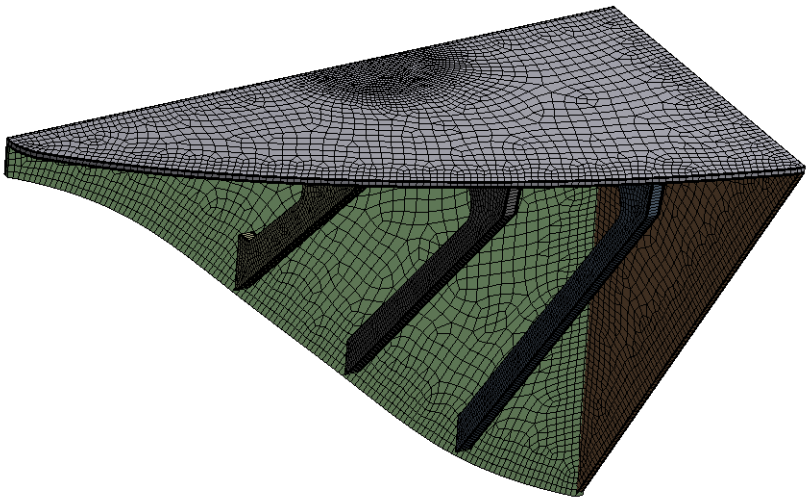

Figure 17:Meshing of model(A)

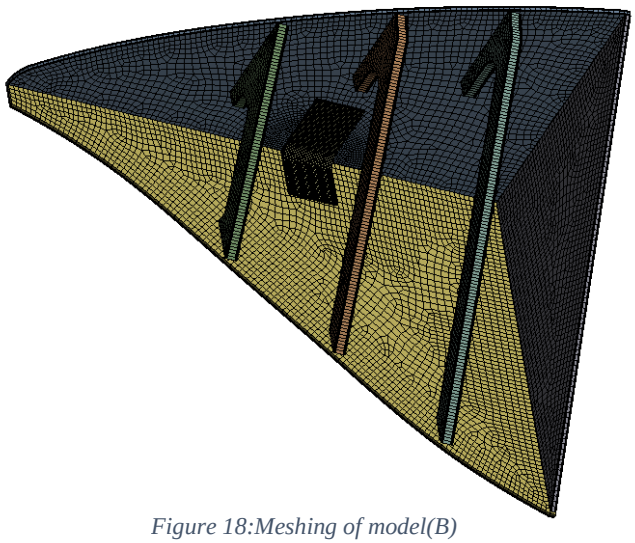

Figure 18:Meshing of model(B)

The mesh quality is checked for Model(B) which is corresponsive for all the Models. According to [86] the rule of thumb for mesh metrics is demonstrated below:

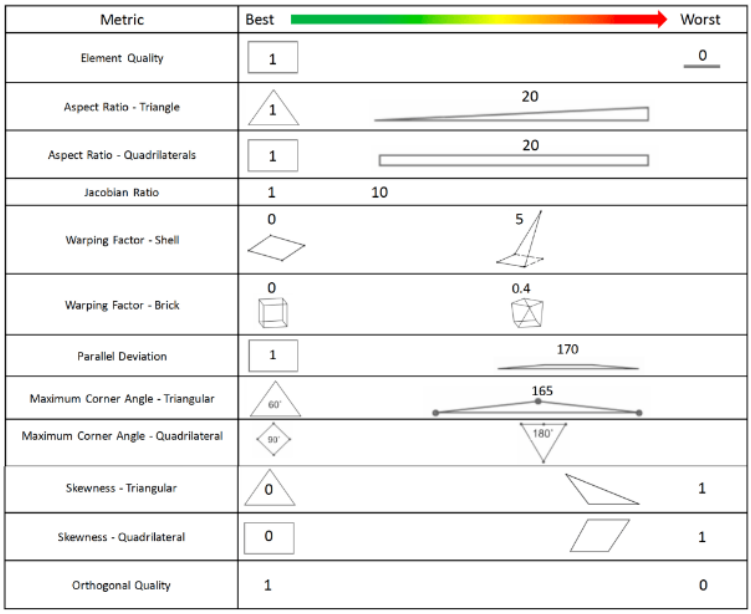

Figure 19:Mesh metrics check [86]

4.4.3.1.1 Element Quality

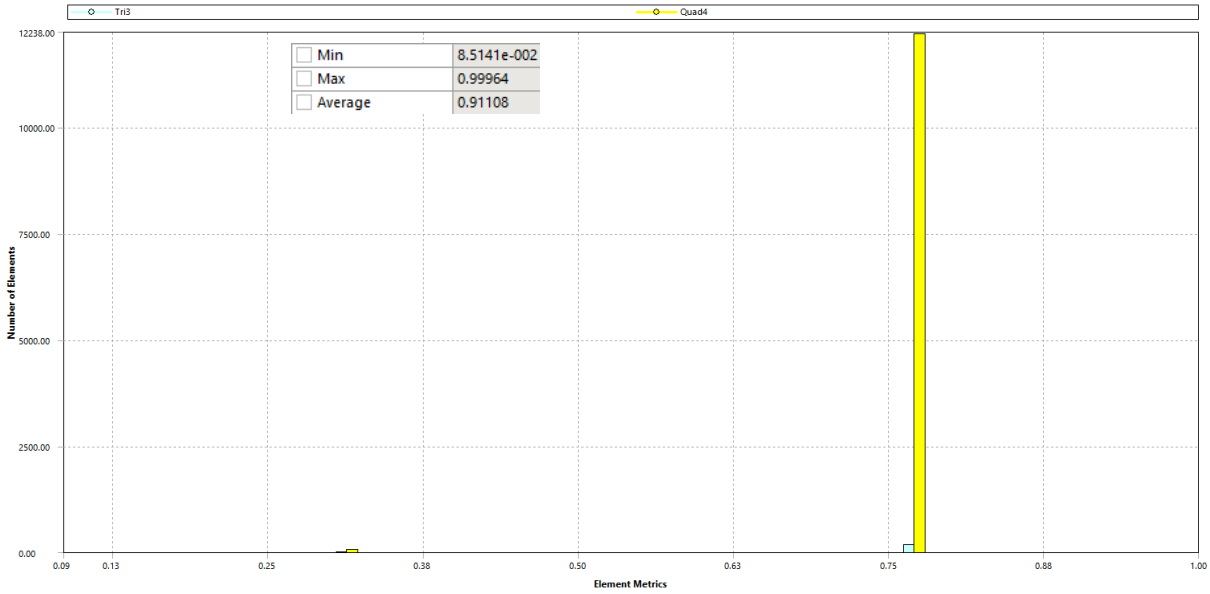

Figure 20:Element Quality Mesh Metrics

The average value of element quality is around 0.9, close to 1, so from the aspect of element quality the mesh is quite qualitative.

4.4.3.1.2 Aspect Ratio

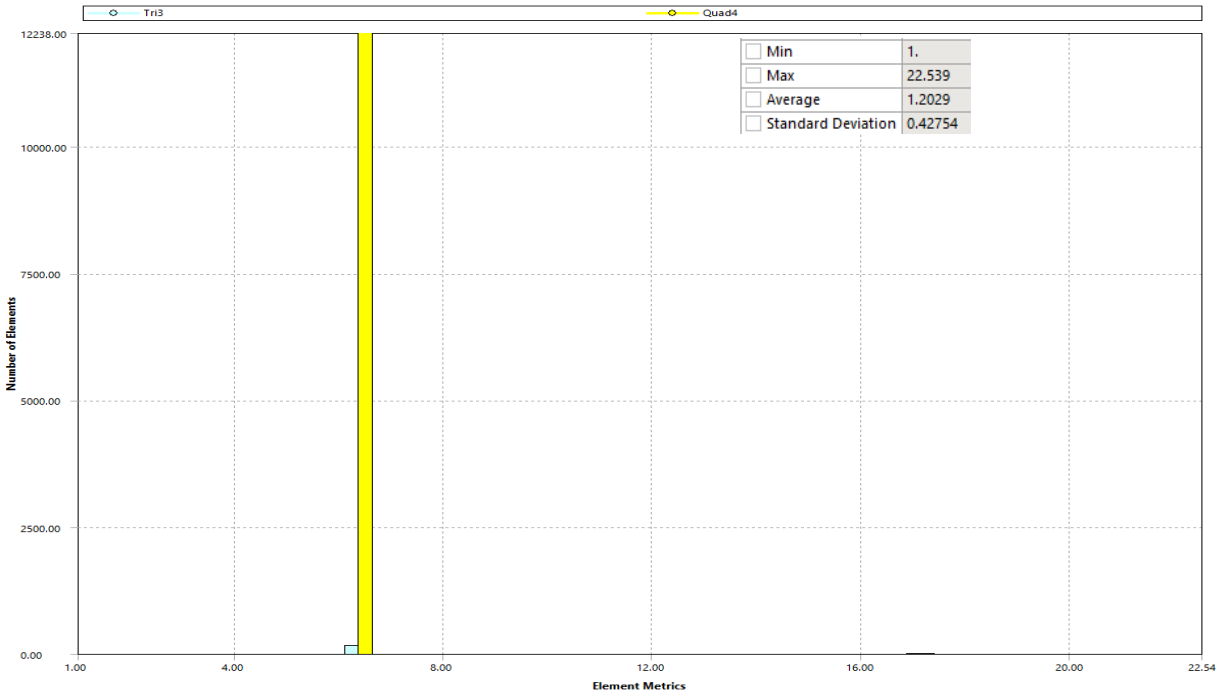

Figure 21:Aspect Ratio Mesh Metrics

The average value of aspect ratio is around 1.2, close to 1, so using the aspect ratio metric the mesh is quite qualitative.

4.4.3.1.3 Skewness

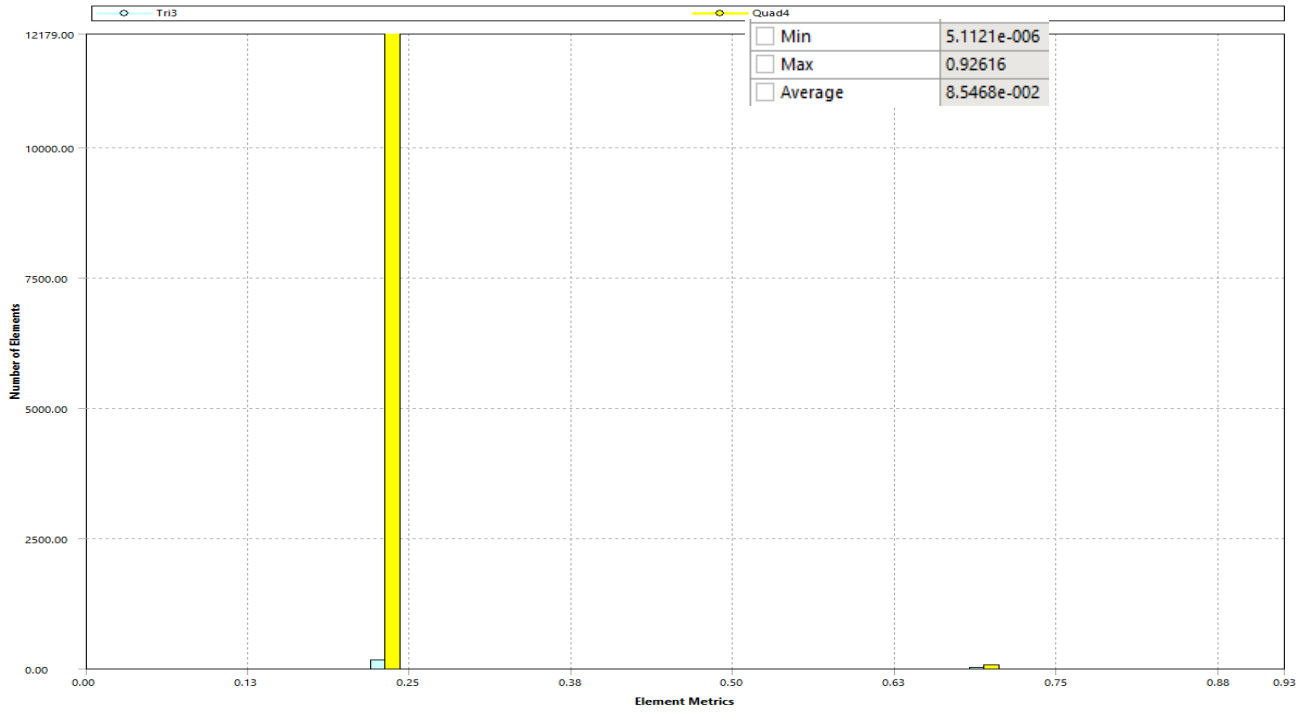

Figure 22:Skewness Mesh Metrics

The average value of skewness is around 0.085, close to 0, so using the skewness metric the mesh is quite qualitative.

4.4.3.1.4 Orthogonal Quality

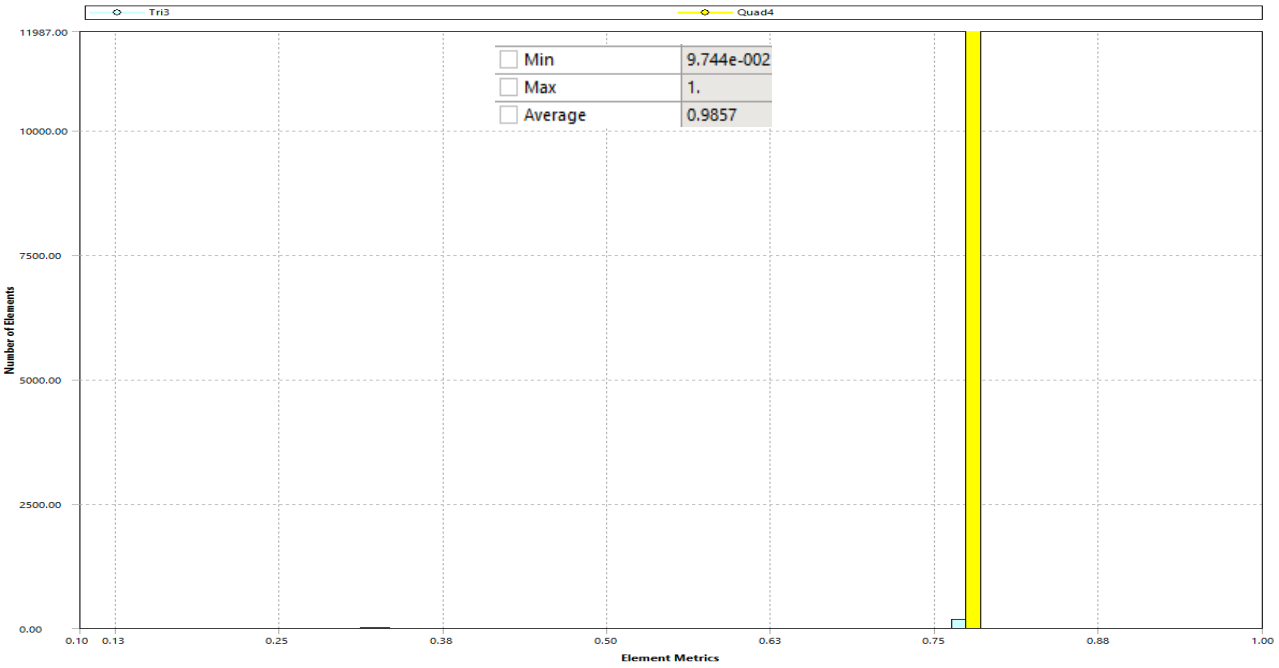

Figure 23:Orthogonal Quality Mesh Metrics

The average value of orthogonal quality is around 0.98, close to 1, so using the orthogonal quality metric the mesh is quite qualitative.

Based on the above Mesh Metrics, overall, the mesh of models seems to be qualitative enough to give corresponding results.

4.4.3.2 Boundary Conditions

Regarding boundary conditions, the supports used in model(A) and (B) are:

1. Longitudinal Bulkhead: y=0 (symmetry condition)
2. Transverse Bulkhead: x=0,y=0,z=0 (fixed support) on all edges

The boundary condition at the transverse bulkhead is similar to the fixed condition applied to the edges of the bulkhead.

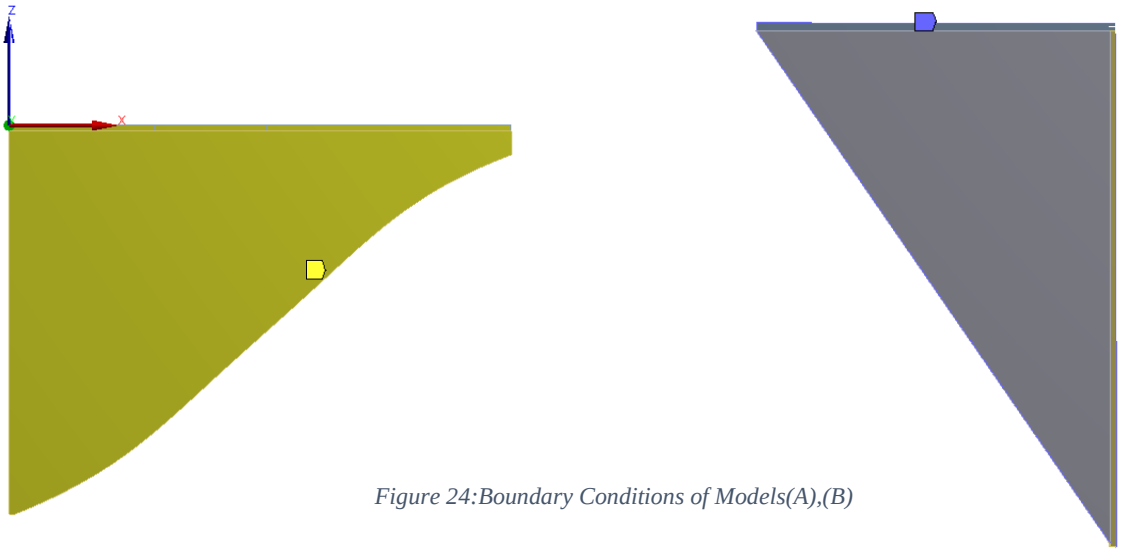

Figure 24:Boundary Conditions of Models(A),(B)

The forces applied to the area designated as the crane base are those calculated in "Calculation according to DNV Shipboard Lifting Appliances", as depicted below:

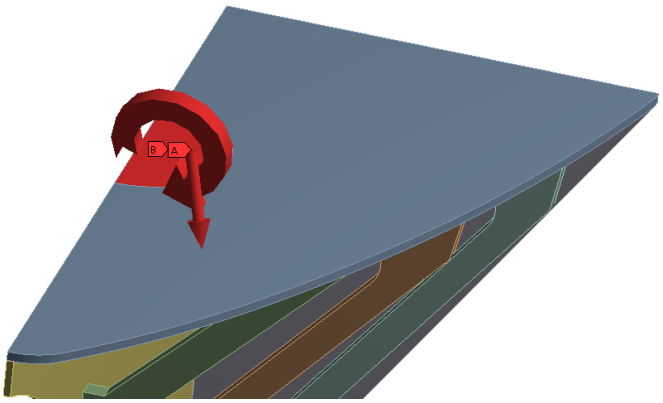

Figure 25:Forces and Moments for Models(A),(B)

Note that all components are bonded, as they are connected together.

4.5 ANSYS Coordinate Systems Definitions

This definition is necessary to understand the direction of stresses and deformations for the model. The effects of stresses are based on Global Coordinate System and the directions of sizes of each component are based on it.

4.5.1 Coordinate System of Normal and Shear Stresses

The symbols for normal and shear stresses accordingly are: s_1 or S_X, s_2 or S_Y and s_{12} or S_{XY}. The directions are shown below:

- Frame

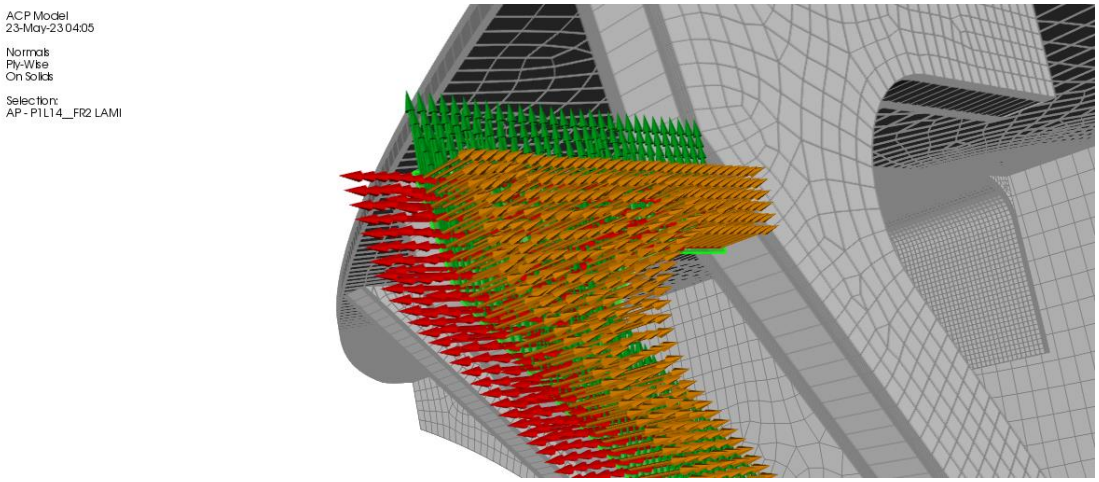

- Deck

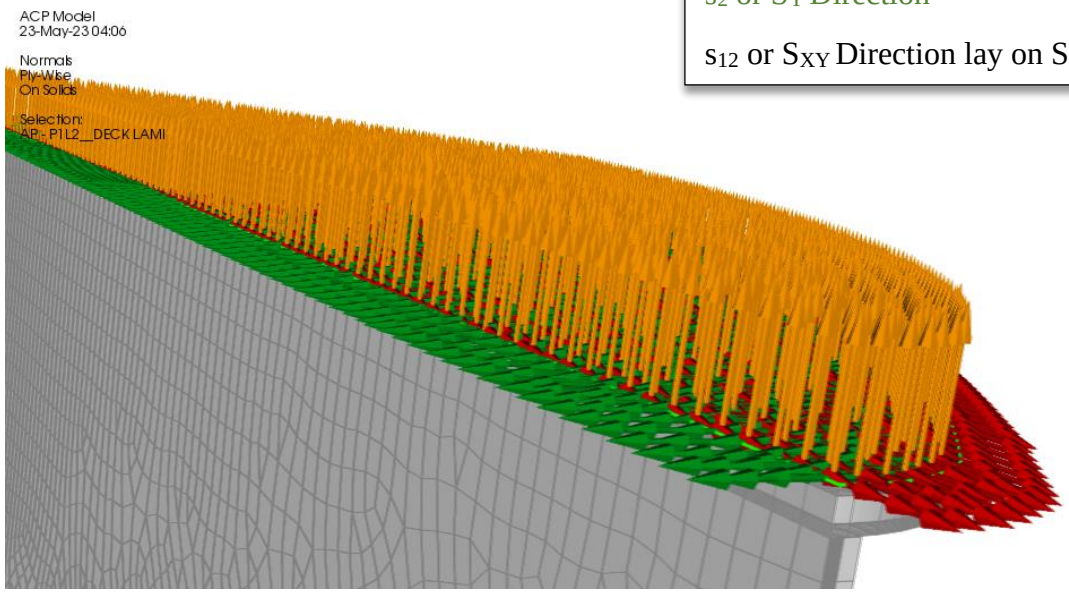

s_1 or S_X Direction

s_2 or S_Y Direction

s_{12} or S_{XY} Direction lay on S_X , S_Y Plane

Figure 26:Ansys ACP Coordinate System Definition of Normal and Shear Stresses

4.5.2 Coordinate System of Principal Stresses

The symbols for principal stresses accordingly are: Max Principal S_I, Middle Principal S_{II} and Minimum Principal S_{III}. The directions are shown below:

- Frame

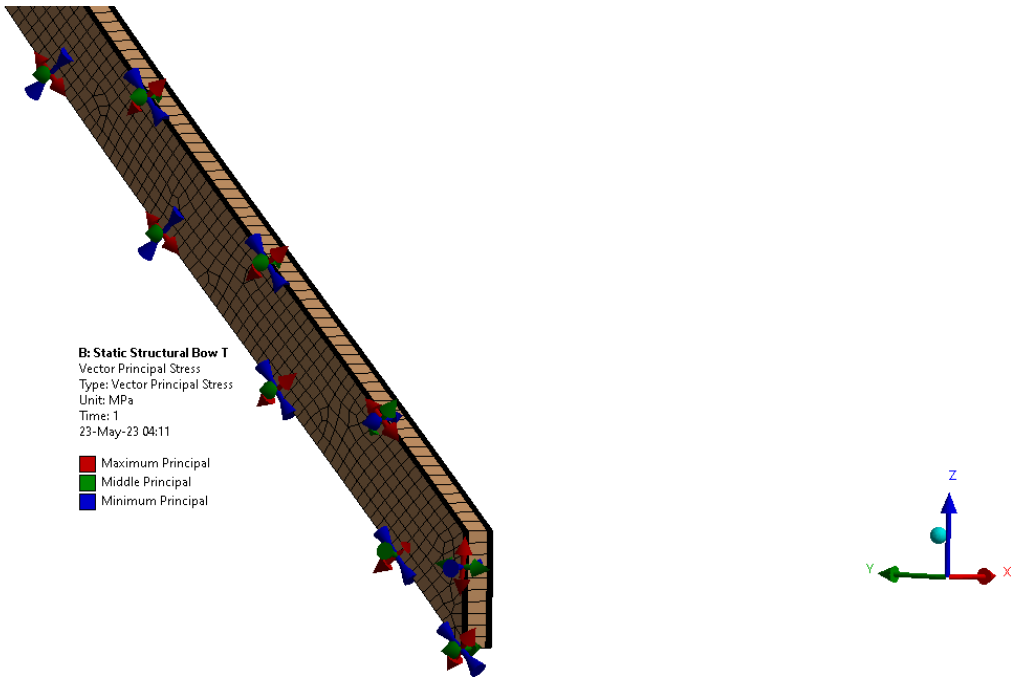

- Deck

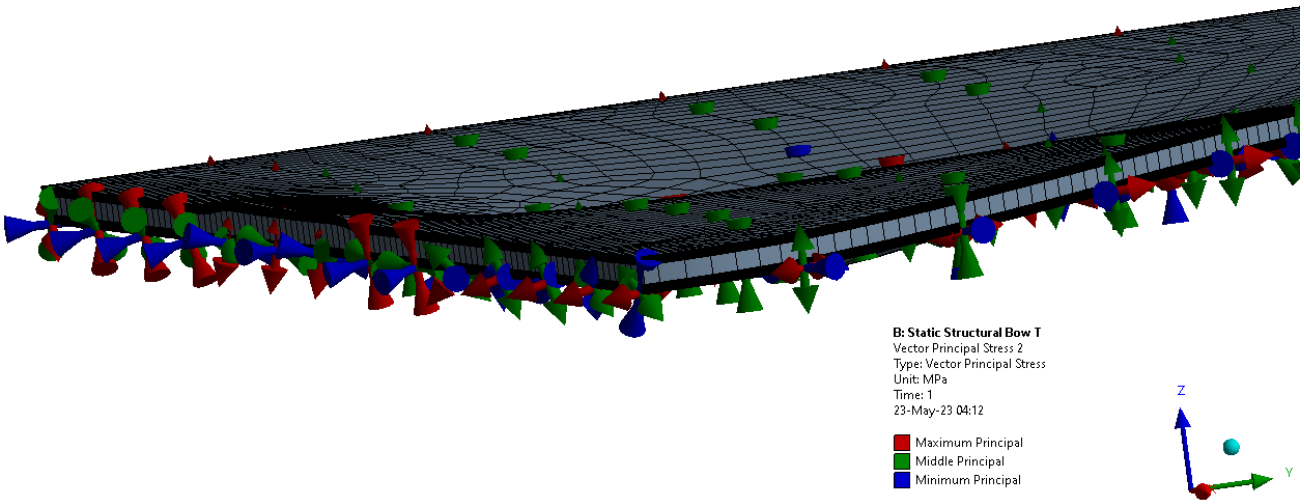

Figure 27:Ansys Mechanical Coordinate System Definition of Principal Stresses

5 Results

The results of this study mainly concern the strength analysis of the Model(A) and Model(B). A concept design of yacht crane base is established for specific loading conditions using DNV Shipboard Lifting Appliances rules [80]. The study of this crane base was conducted using three models. The Model(A) concerns the study of strength of the region at the bow of the yacht without T-Joint reinforcement, whereas the Model(B) is focused on the effect of T-Joint reinforcement.

The numerical results include the total deformation, normal and shear stresses distribution, principal stresses distribution and fracture results for the sub model(C) (Appendix(A)). By comparing the deformations and stresses results between the Models (A) & (B), significant conclusions are drawn for strength, structural performance and the effect of T-Joint reinforcement.

5.1 Total Deformation

In the context of finite element analysis (FEA), the deformation of a single element due to a load can be computed using the following general equation:

$$u = K^{-1} \cdot F \tag{56}$$

where:

u is the vector of nodal displacements

K is the stiffness matrix of the element

F is the vector of nodal forces

This formula assumes a linear elastic system and isotropic material behavior.

The Total Deformation in ANSYS Mechanical refers to the equivalent deformation, which combines the deformation in the x, y, and z directions at each node into a single scalar value using the formula:

$$Total\ Deformation = \sqrt{(Ux^2 + Uy^2 + Uz^2)} \tag{57}$$

where:

Ux, Uy, Uz are the displacements at a node in the x, y, and z directions respectively.

5.1.1 Bow Region

- Model(A):

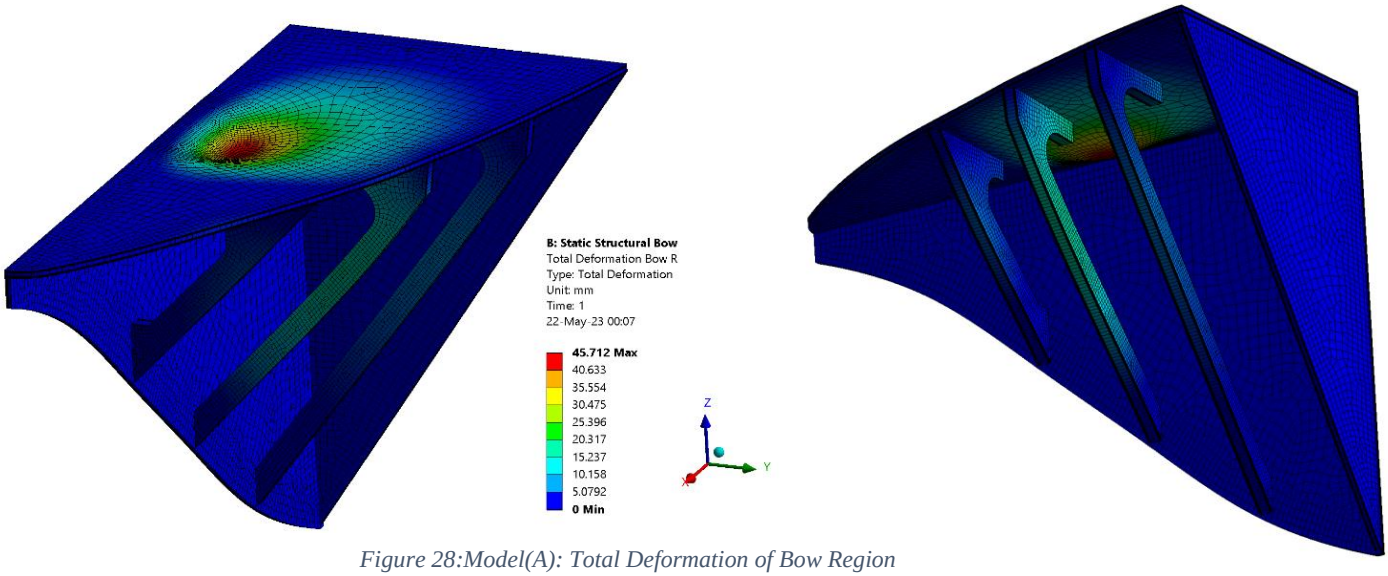

Figure 28:Model(A): Total Deformation of Bow Region

- Model(B):

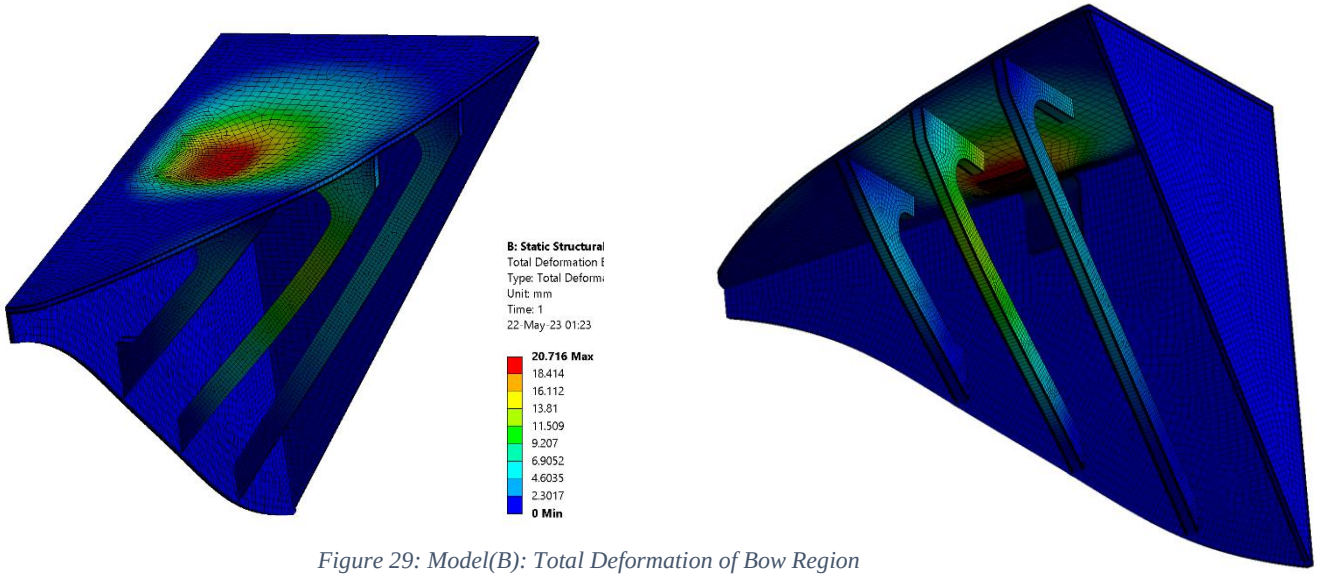

Figure 29: Model(B): Total Deformation of Bow Region

The largest deformations are located around the crane support area in the vertical direction and are distributed to the transverse frames through the deck. The reinforcement by GFRP attachment laps results in a reduction of deformations up to 50% in the middle transverse frame, as well as, in the deck. The z-directional deformation contributes to the greatest amount of total deformation.

5.2 Normal and Shear Stresses

The calculation of normal stresses in mechanics is imperative for ascertaining the capacity of a material or structure to withstand applied forces without undergoing failure. Normal and shear stresses are later included in failure criteria calculation therefore their magnitude (and orientation) is important for the evaluation of safety and reliability in design and engineering applications.

5.2.1 Bow Region

- Model(A):

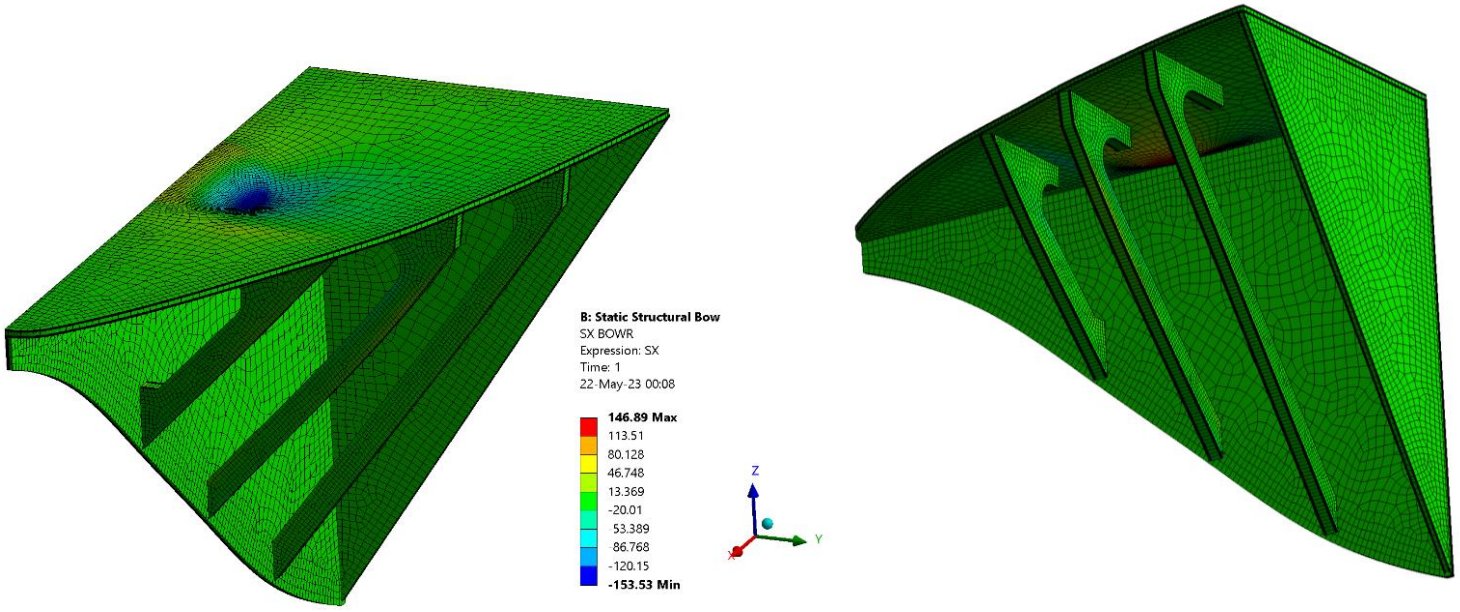

Figure 30:Model(A): Normal Stresses SX of Bow Region

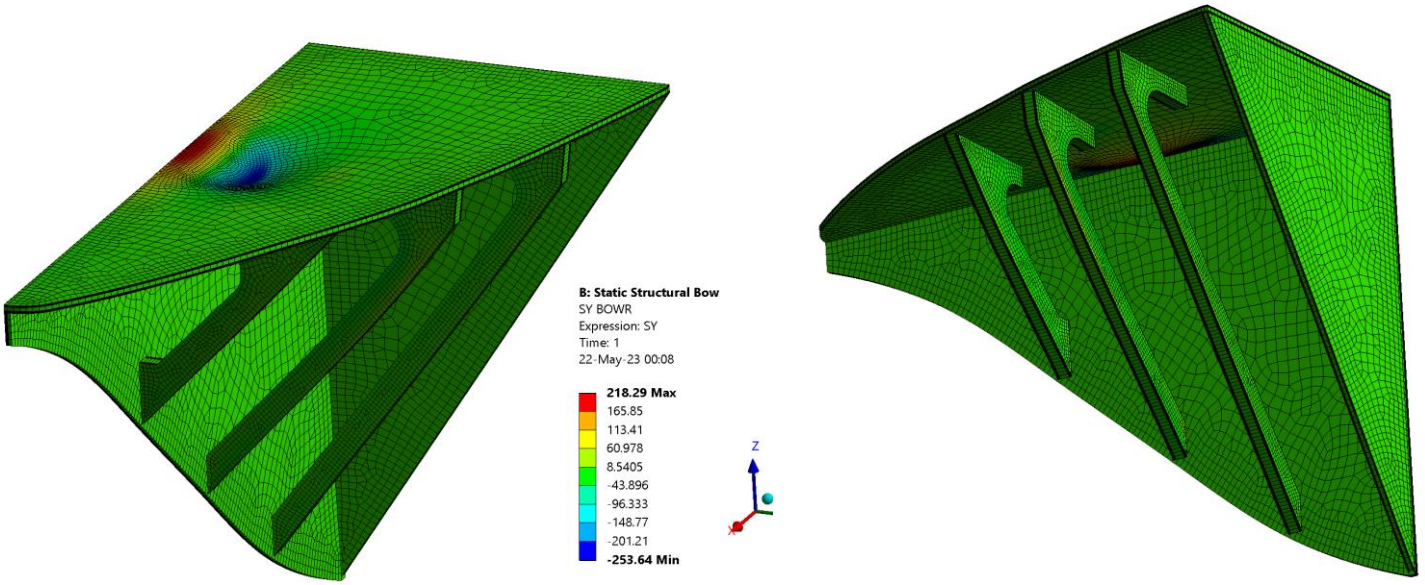

Figure 31:Model(A): Normal Stresses SY of Bow Region

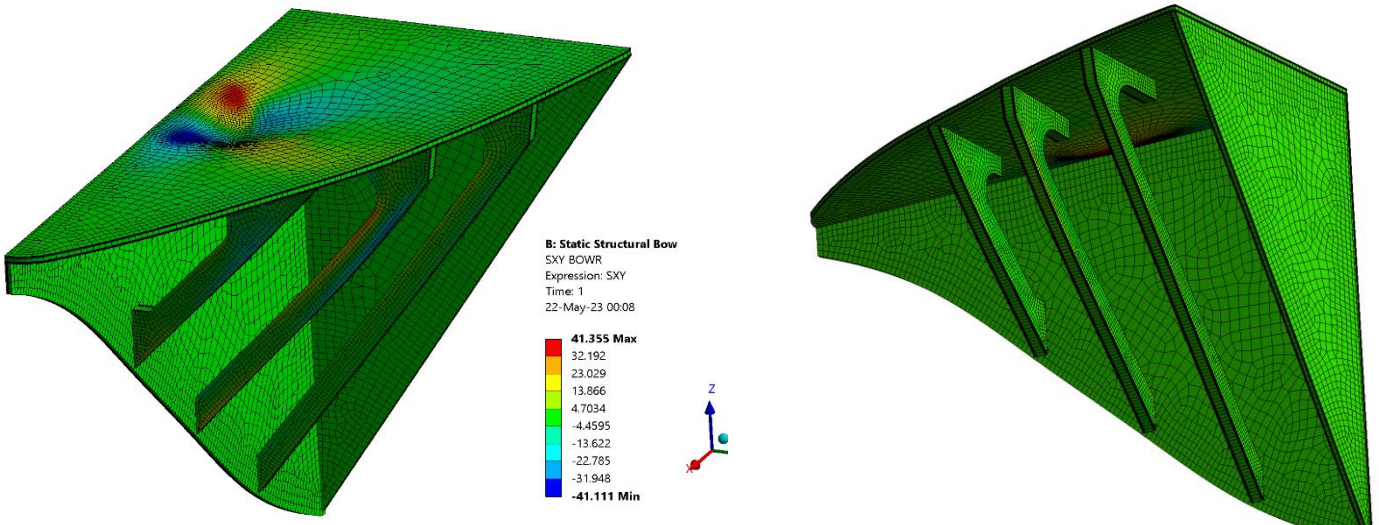

Figure 32: Model(A): Shear Stresses SXY of Bow Region

- Model(B):

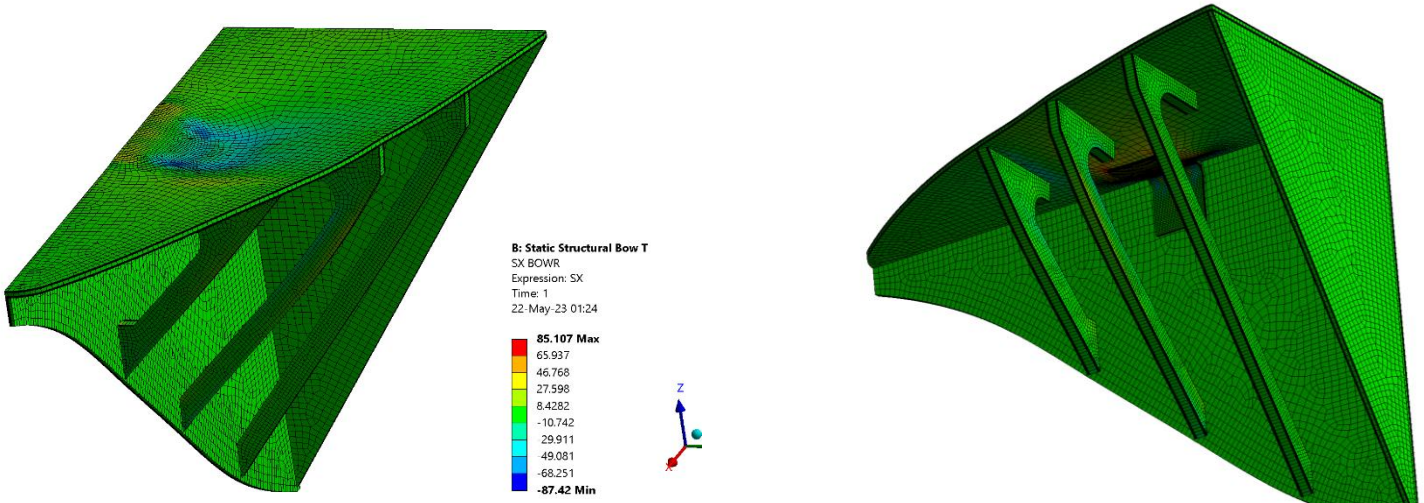

Figure 33: Model(B): Normal Stresses SX of Bow Region

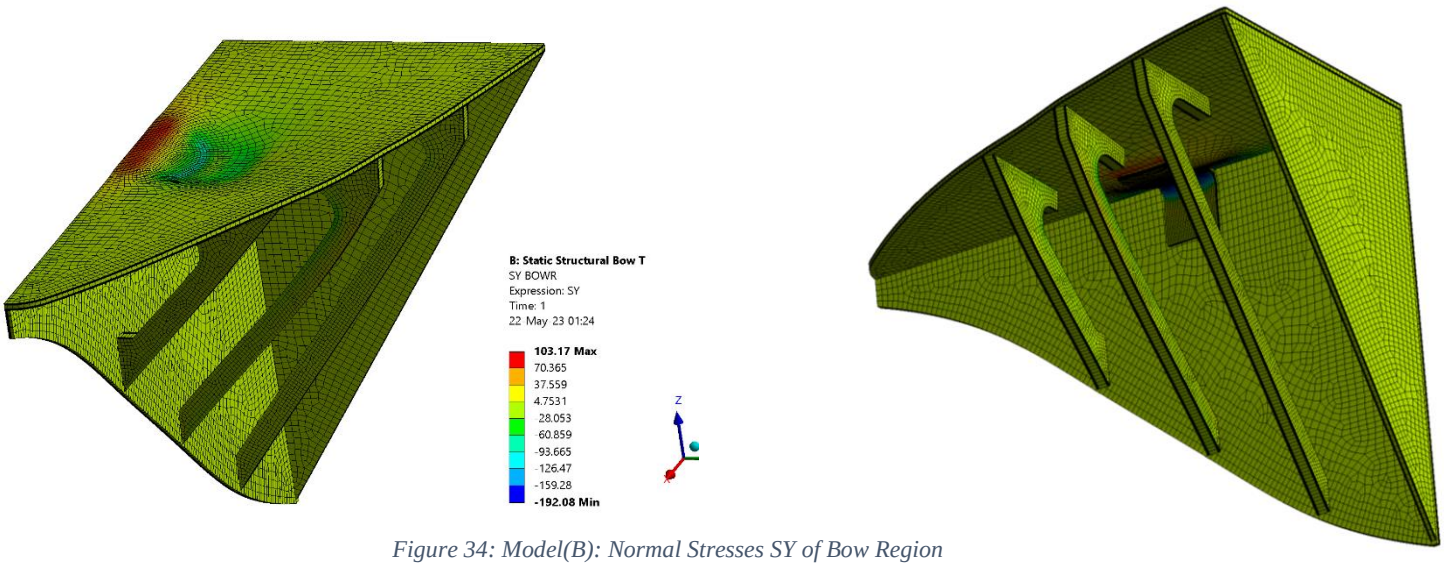

Figure 34: Model(B): Normal Stresses SY of Bow Region

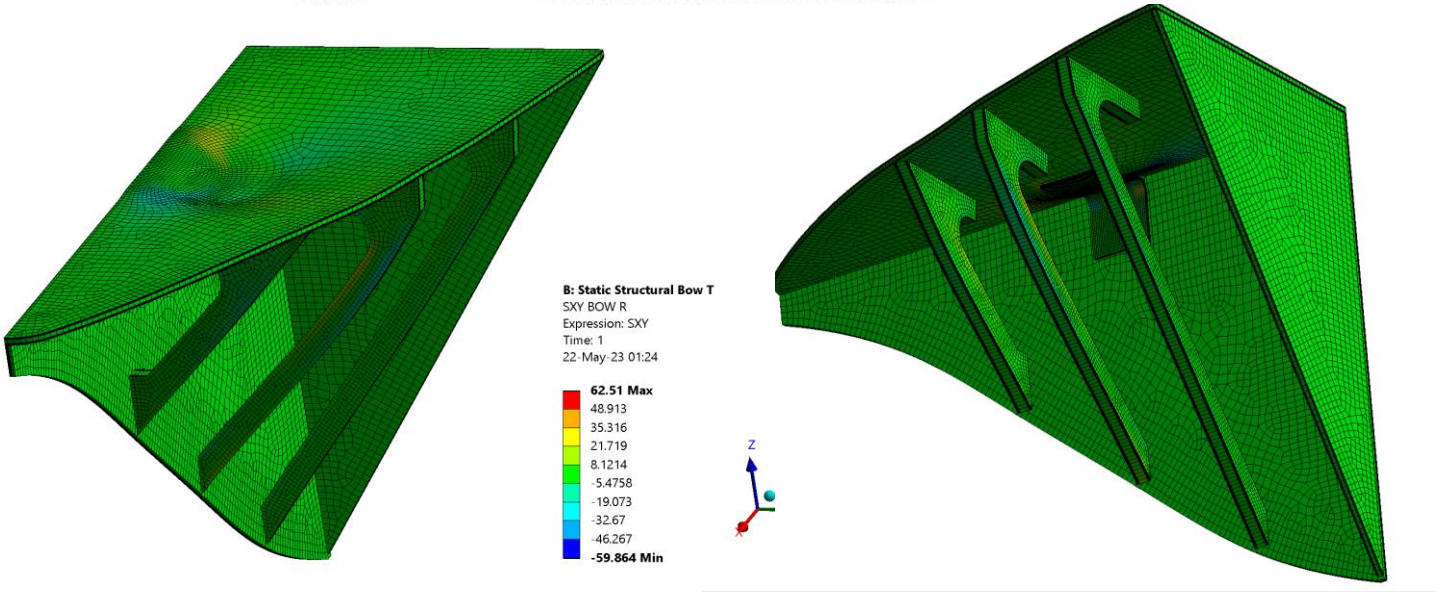

Figure 35: Model(B): Shear Stresses SXY of Bow Region

The reinforcement by a T-Joint results in a decrease of 50% in normal and shear stresses. More specifically, on the deck, there is also a decrease in the area that the stresses are distributed. Regarding the longitudinal bulkhead, a 20 % decrease of stresses is observed, the lower decrease compared to other areas. Also, a uniform stress distribution in longitudinal bulkhead is calculated and the load is distributed uniformly through middle transverse frame. Owing to high stress distribution the areas that need to be studied further are the deck in region of crane base and the medium transverse frame at middle of its height.

5.2.2 Middle Frame

- Model(A):

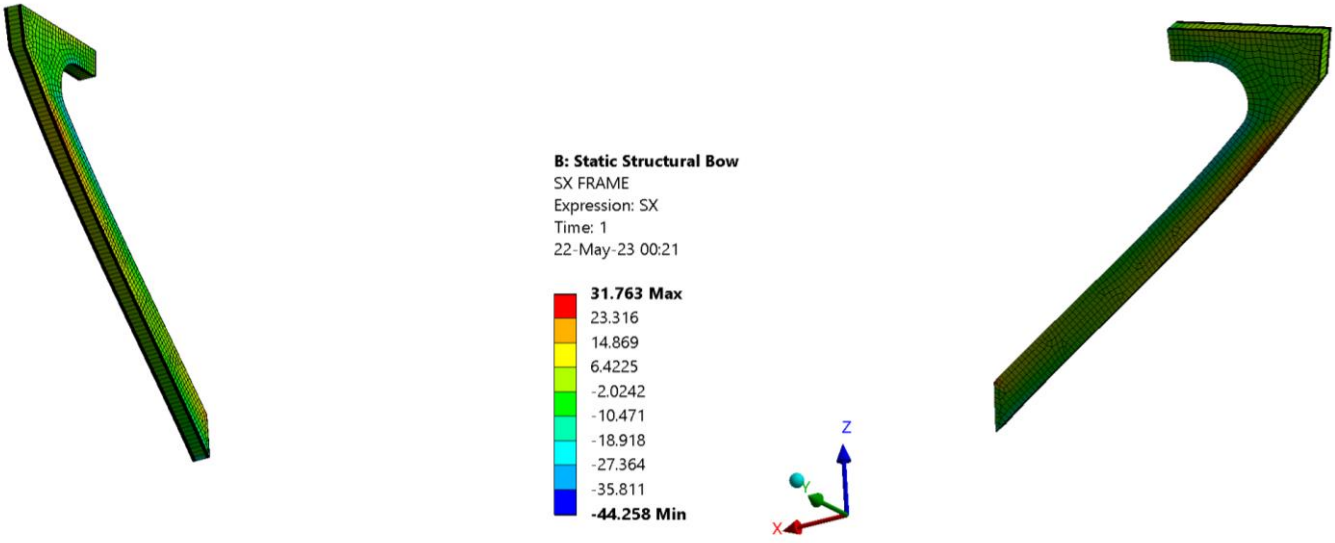

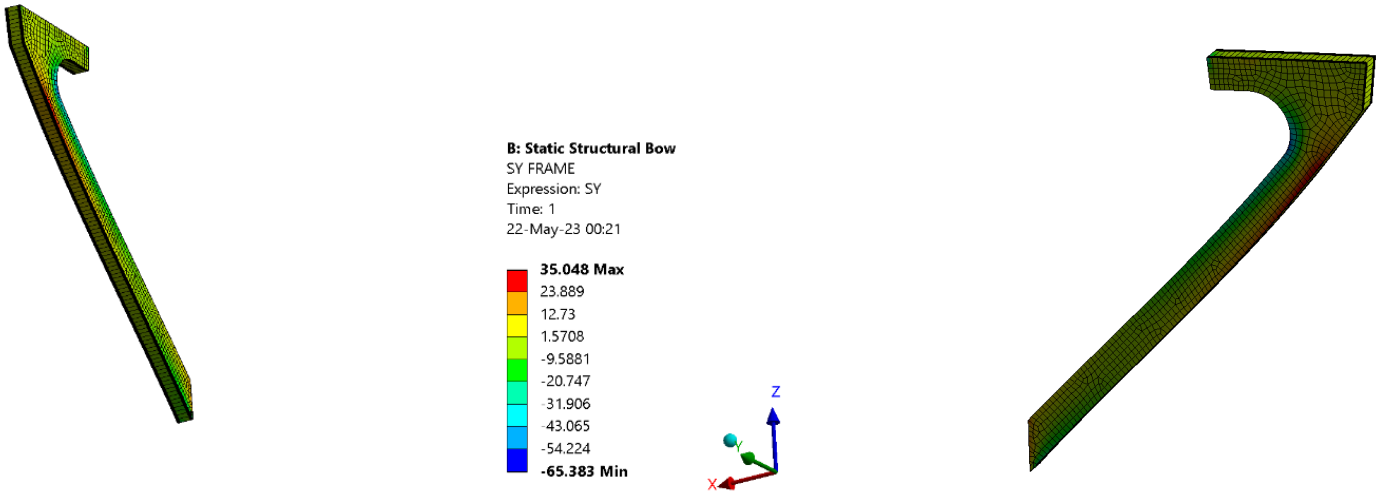

Figure 37: Model(A): Normal Stresses SY of Middle Frame

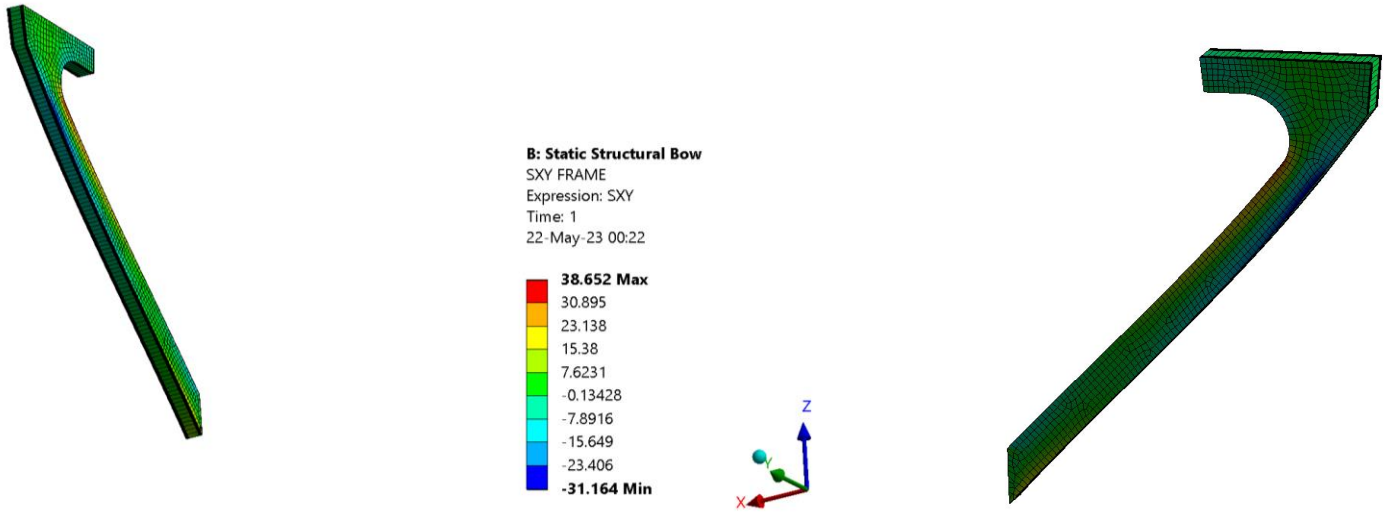

Figure 36: Model(A): Shear Stresses SXY of Middle Frame

In general, Transverse Middle Frame is significantly deformed by stresses, mainly at the ends and midway of its length. Stress analysis is further conducted per ply to understand the distribution of stresses and to find the critical layers that are at risk to fail first. The following diagram shows the distributions of normal stresses s_1, s_2 and shear stresses s_{12} in each ply as following:

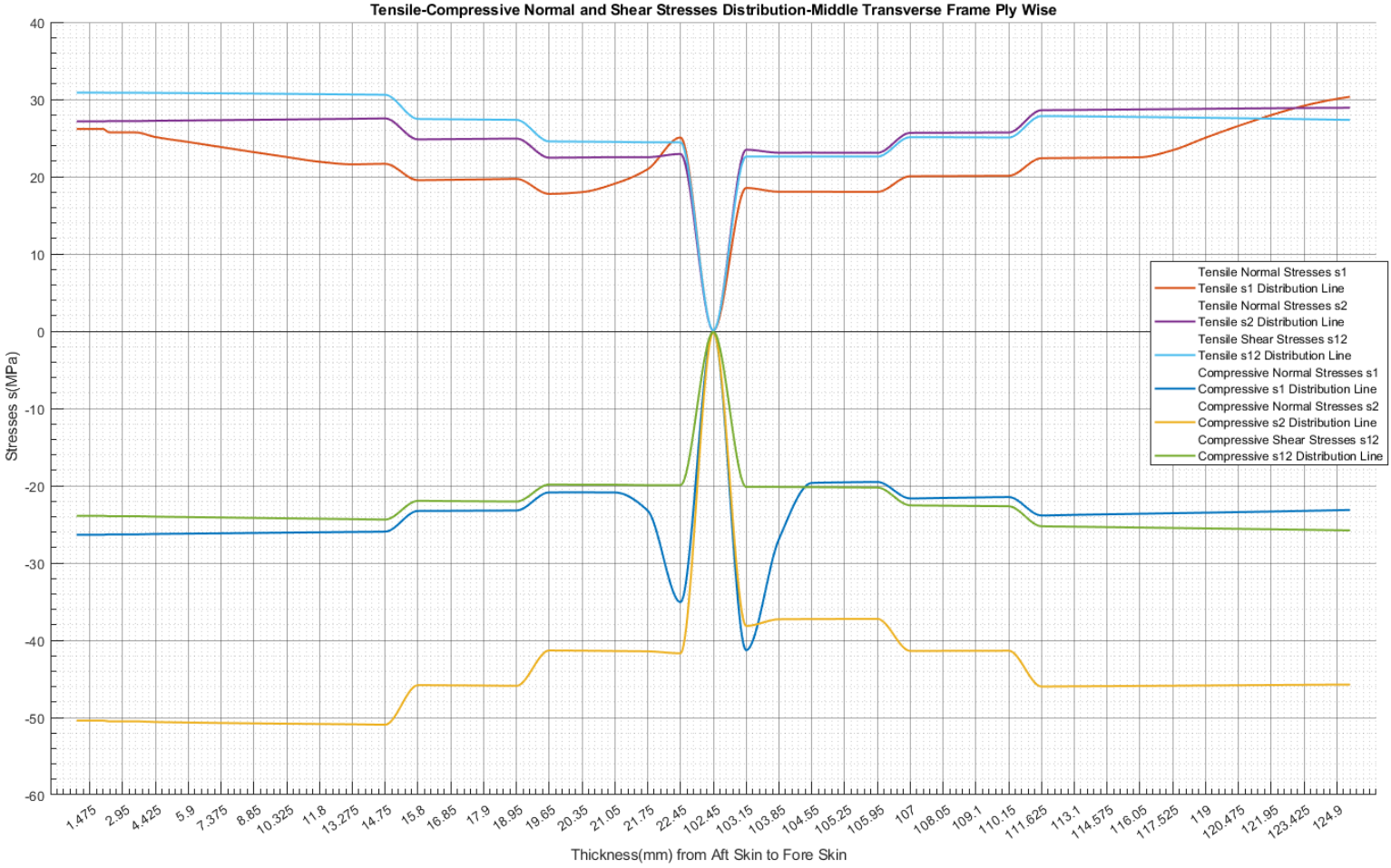

Figure 38:Model(A):Tensile-Compression Normal and Shear Stress Distribution of Middle Frame

From the Figures (36-39), for Model(A) it is observed that:

i. The highest stresses are s2 in compression mode, with a value of about -50MPa.
ii. In ply MAT300 next to the core, at a thickness of 103.15mm from the Aft Skin, there is a sharp increase in the compressive normal stress s1, with a value of -41.3 MPa, which is worth further investigation.
iii. For the tensile normal stresses in the x-axis s1, it is worth studying the location where the maximum value is presented.
iv. An important observation is the fact that the stresses in the core are exactly zero. So, the zero normal stress in the core signifies that the load is primarily borne by skins. This condition arises with bending loads. Undeniably, due to this phenomenon the core will present the highest safety factor. Instead, it can be assumed that the stresses relating to the core are approximated by the stresses in the layers adjacent to the core on either side. This comment applies to the deck, as well as to the principal stresses, as will be shown below.

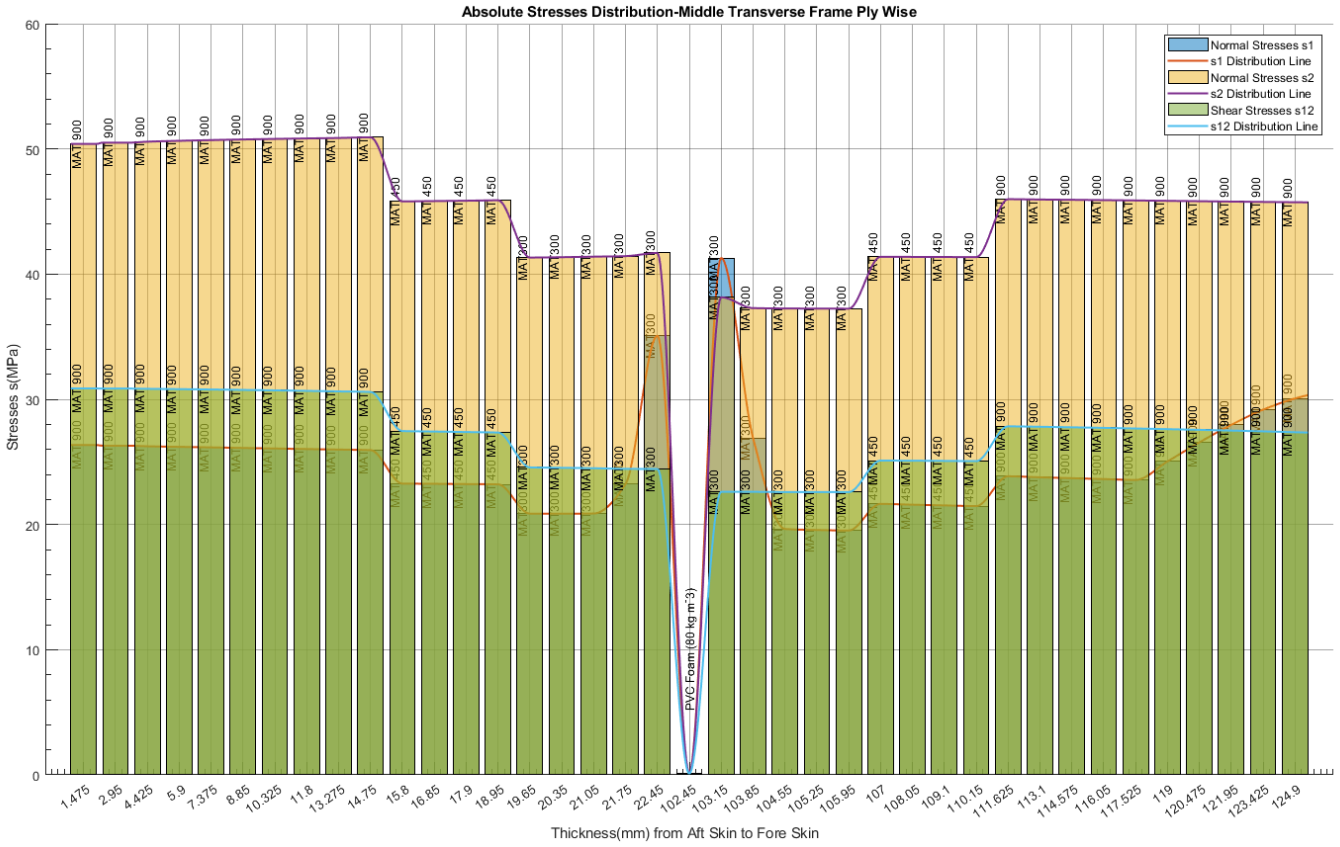

Figure 39: Model(A): Absolute Normal and Shear Stresses Distribution of Middle Frame

The absolute value chart (Figure 40) emerges from the analysis below. For each ply the maximum values are taken, which are presented in absolute terms:

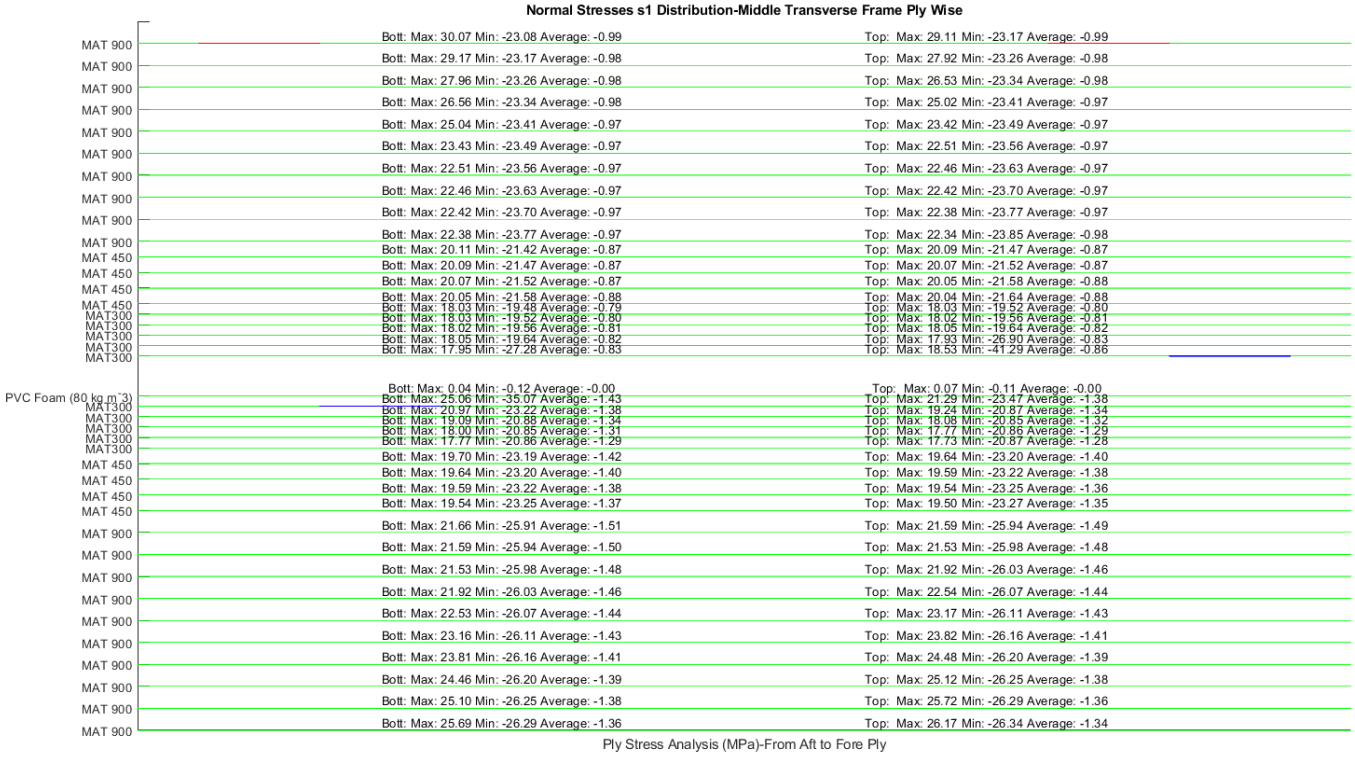

Figure 40: Model(A): Ply Analysis of Normal and Shear Stresses Distribution of Middle Frame

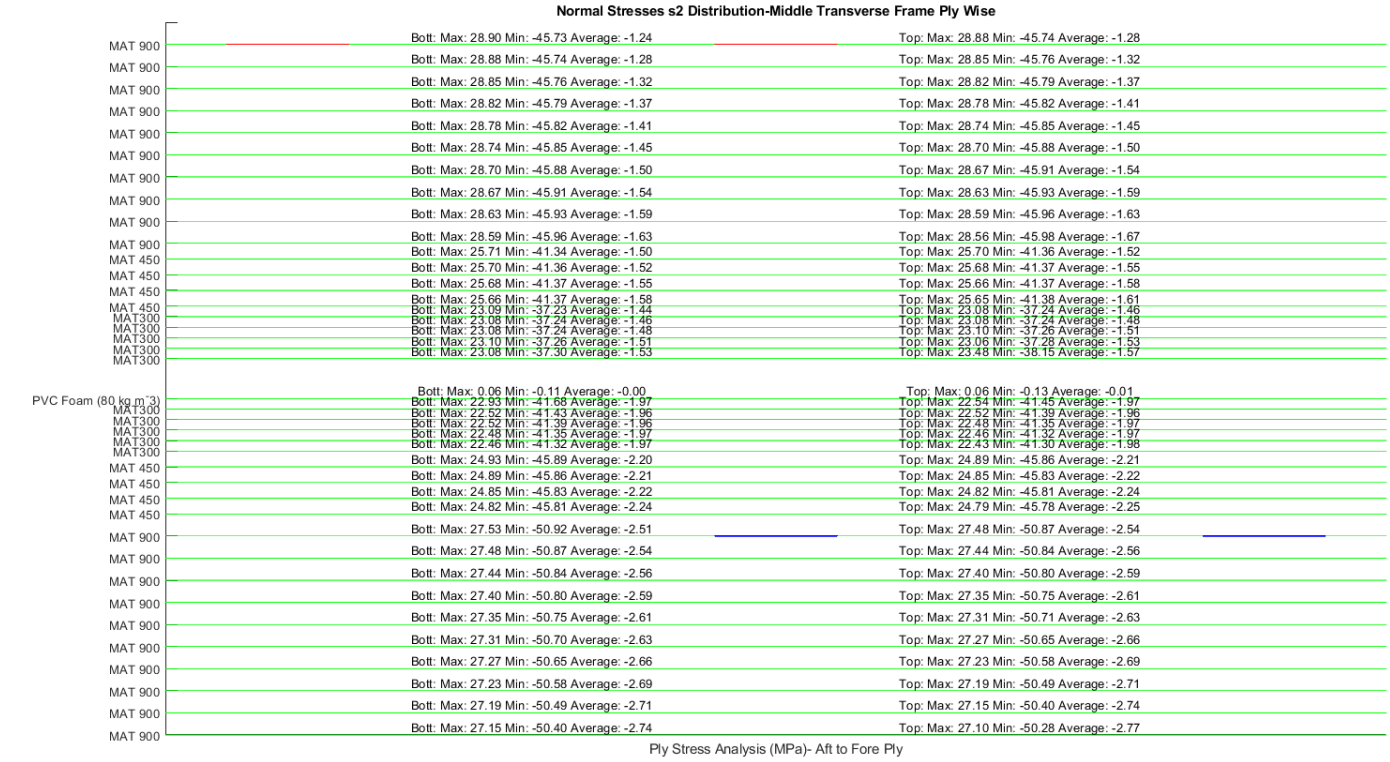

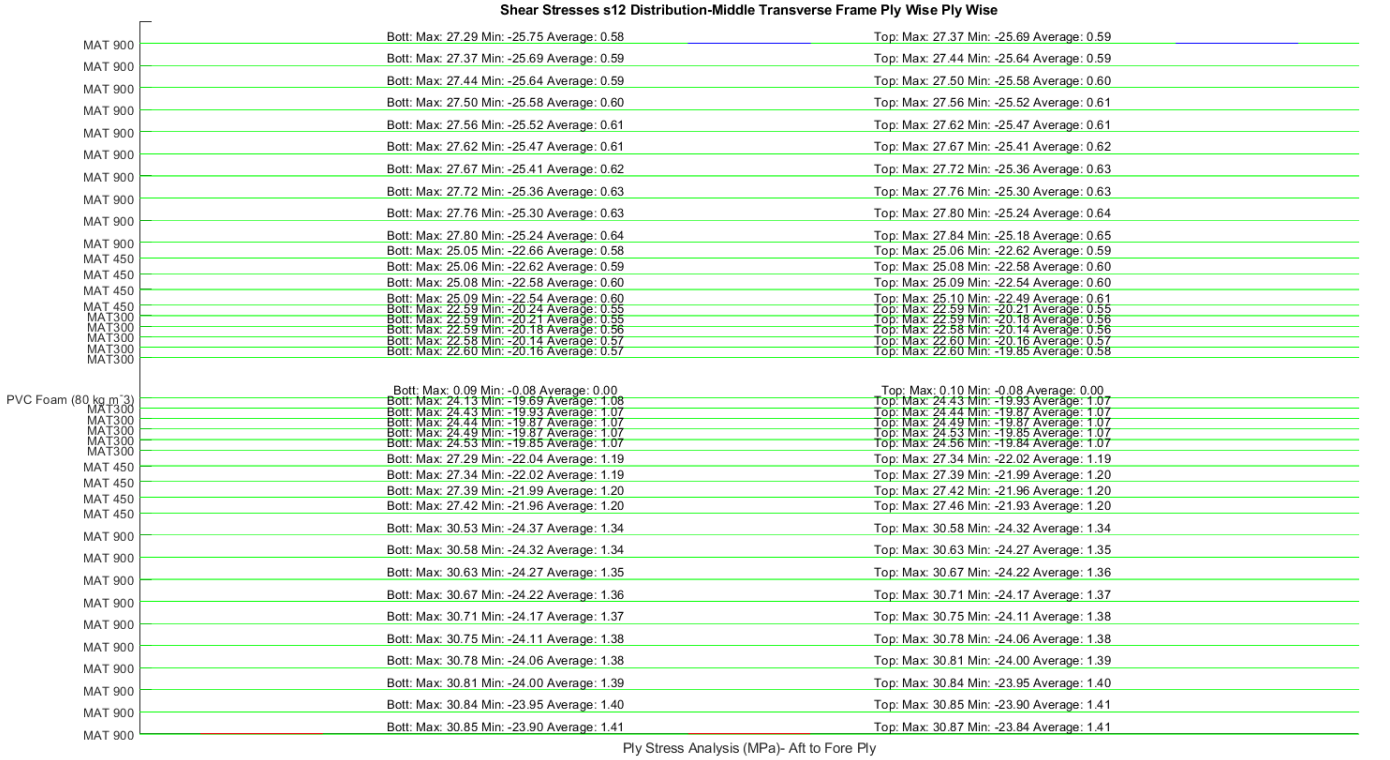

For further analysis and accurate values the other diagrams of this form for stress and failure are available in “C.Appendix of Ply Wise Analysis”.

The areas, indicated by a red circle, shown below, are locations of stress concentration. The stress concentrations result from peculiarities of the geometry and mesh and create results that are not representative of the study. For this reason, they should be investigated further.

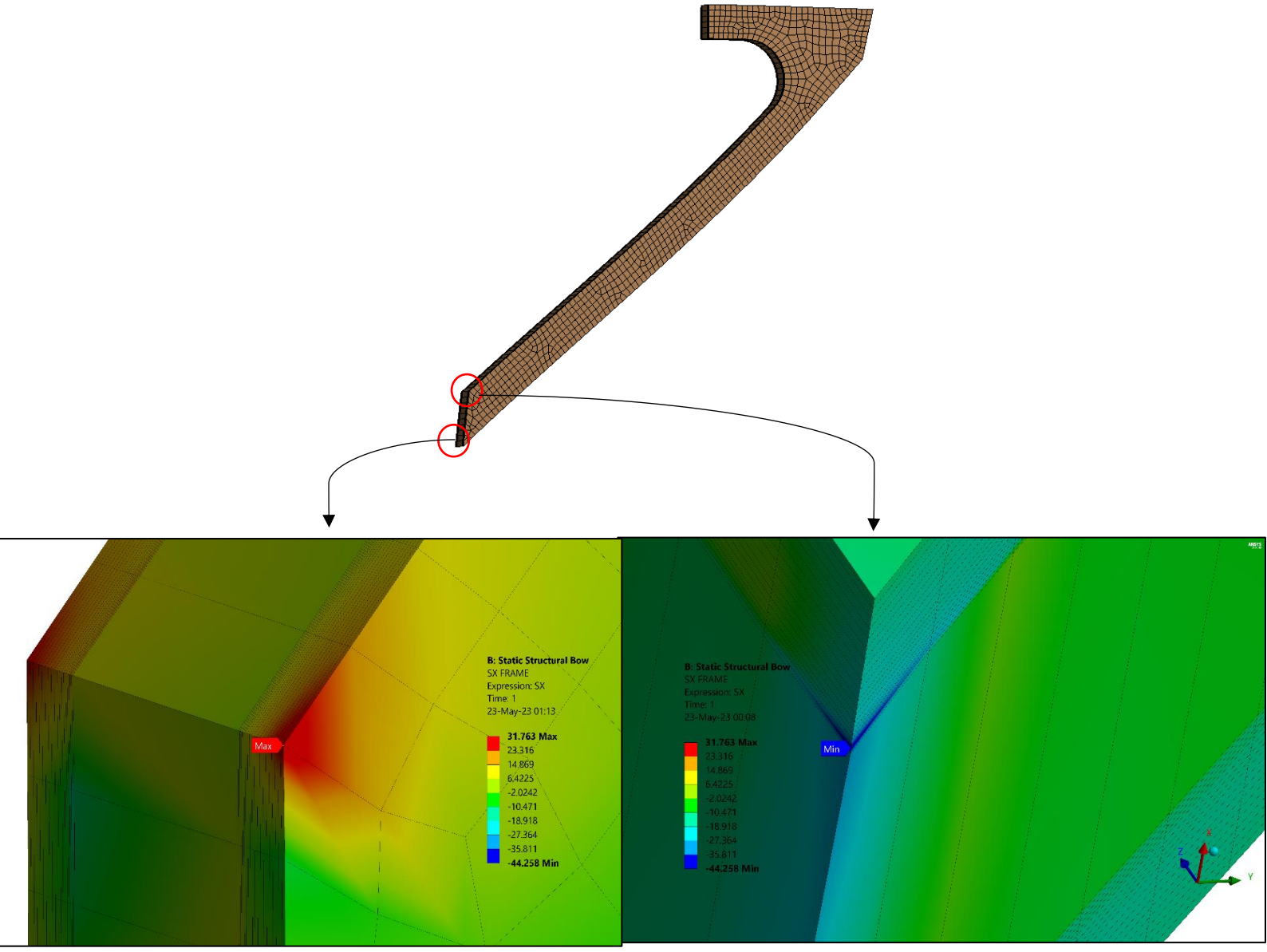

Figure 41:Model(A): Stress concentration area of Middle Transverse Frame

The area where these stresses are generated is at the connection between the frame and longitudinal bulkhead. Based on the abrupt change of the geometry of this area (acute edges), these stresses have no real impact on this construction since they are considered as stress concentrations. For this reason, and since at this area there is the presence of the hull as well, they can be excluded from the results. Similar phenomena are expected for Model(B).

Instead, the frame in Figure 43,can be considered as the range of maximum and minimum stresses s1:

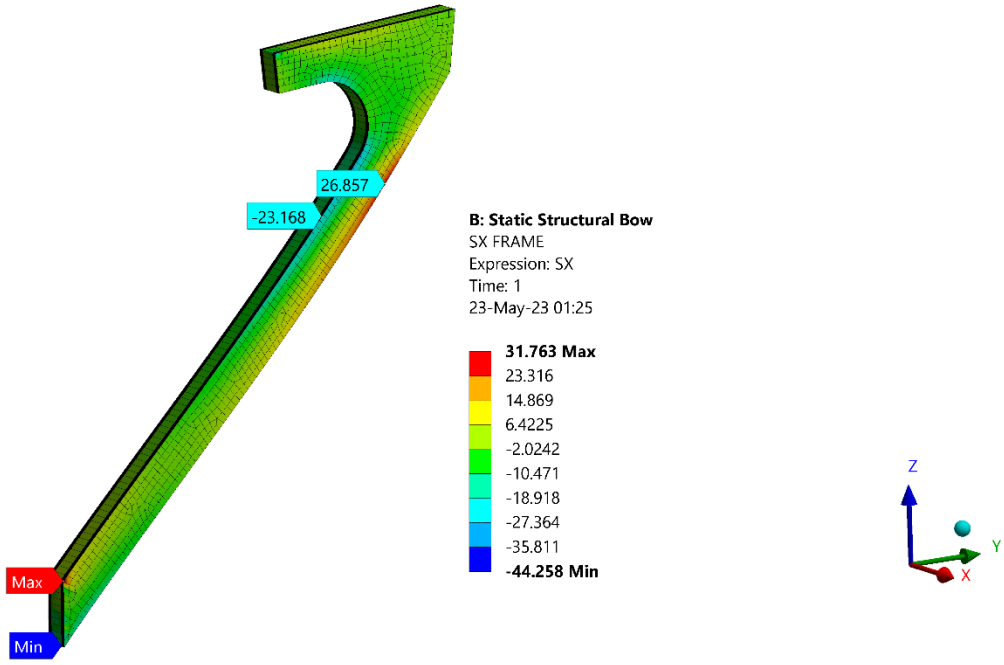

Figure 42:Model(A):Areas of smooth stress values of Middle Transverse Frame

In contrast to the previous stresses (Figure 42), it is observed that there is a smooth distribution in many finite elements and these regions are not areas of stress concentration. This phenomenon with stress concentrations is also observed for different stress types as expected.

Excluding other stress concentration regions from the results, the stress distributions for the middle transverse frame, as shown above, are smooth and symmetrical and the results can be considered acceptable. It is worth noting that the symmetry of the values on either side of the core is slightly different towards the fore side of the reinforcement, due to the way the load is applied to the structure.

- Model(B):

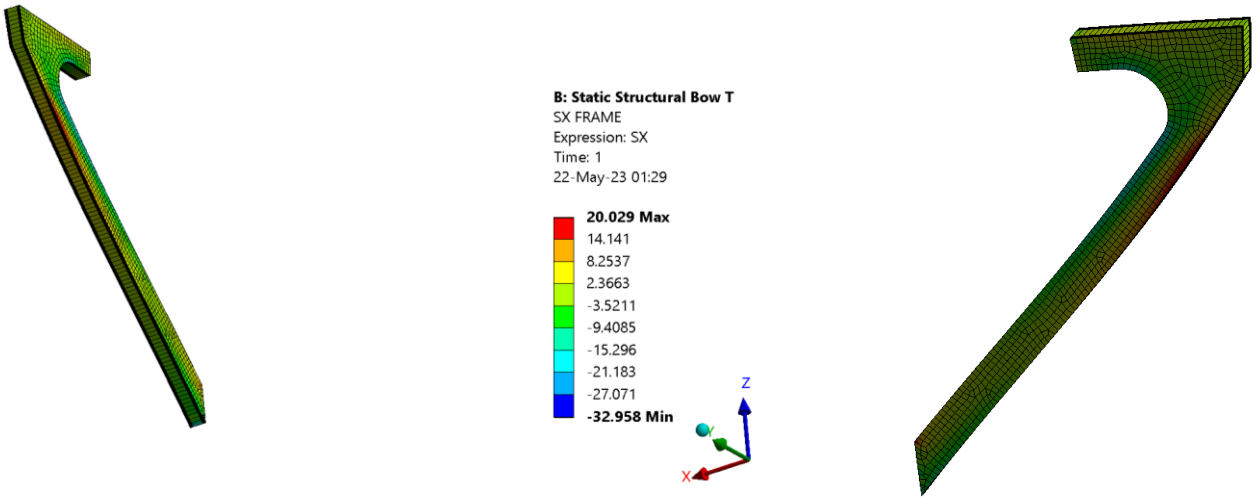

Figure 43: Model(B): Normal Stresses SX of Middle Frame

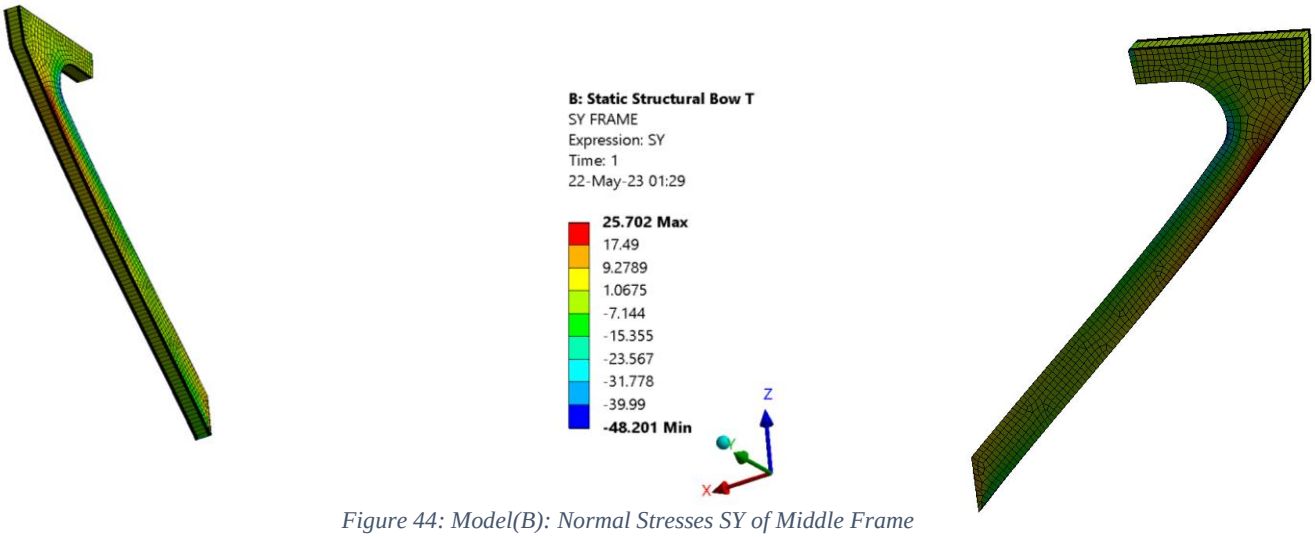

Figure 44: Model(B): Normal Stresses SY of Middle Frame

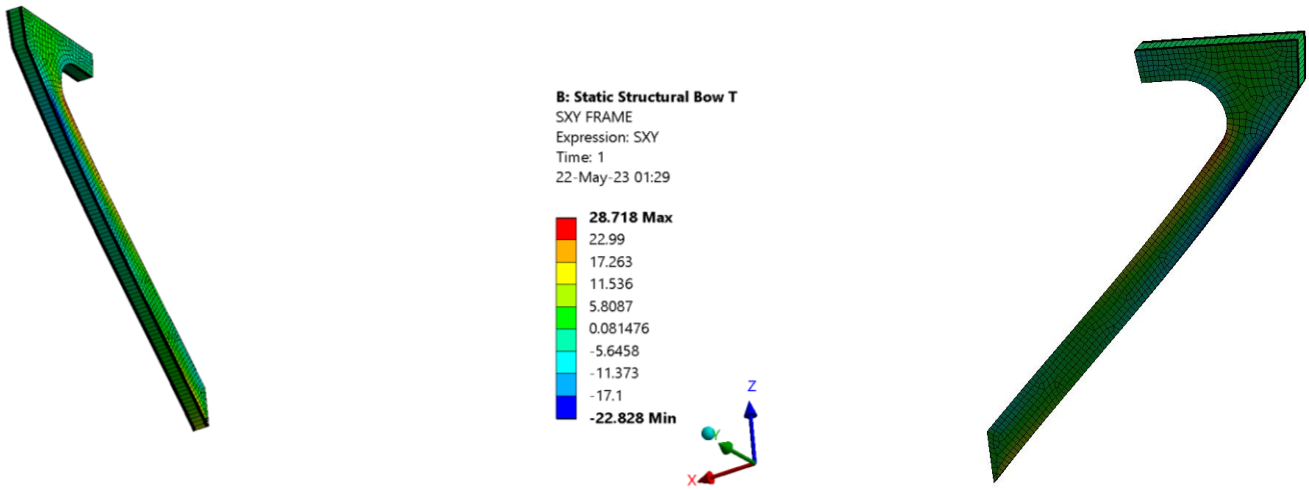

Figure 46: Model(B): Shear Stresses SXY of Middle Frame

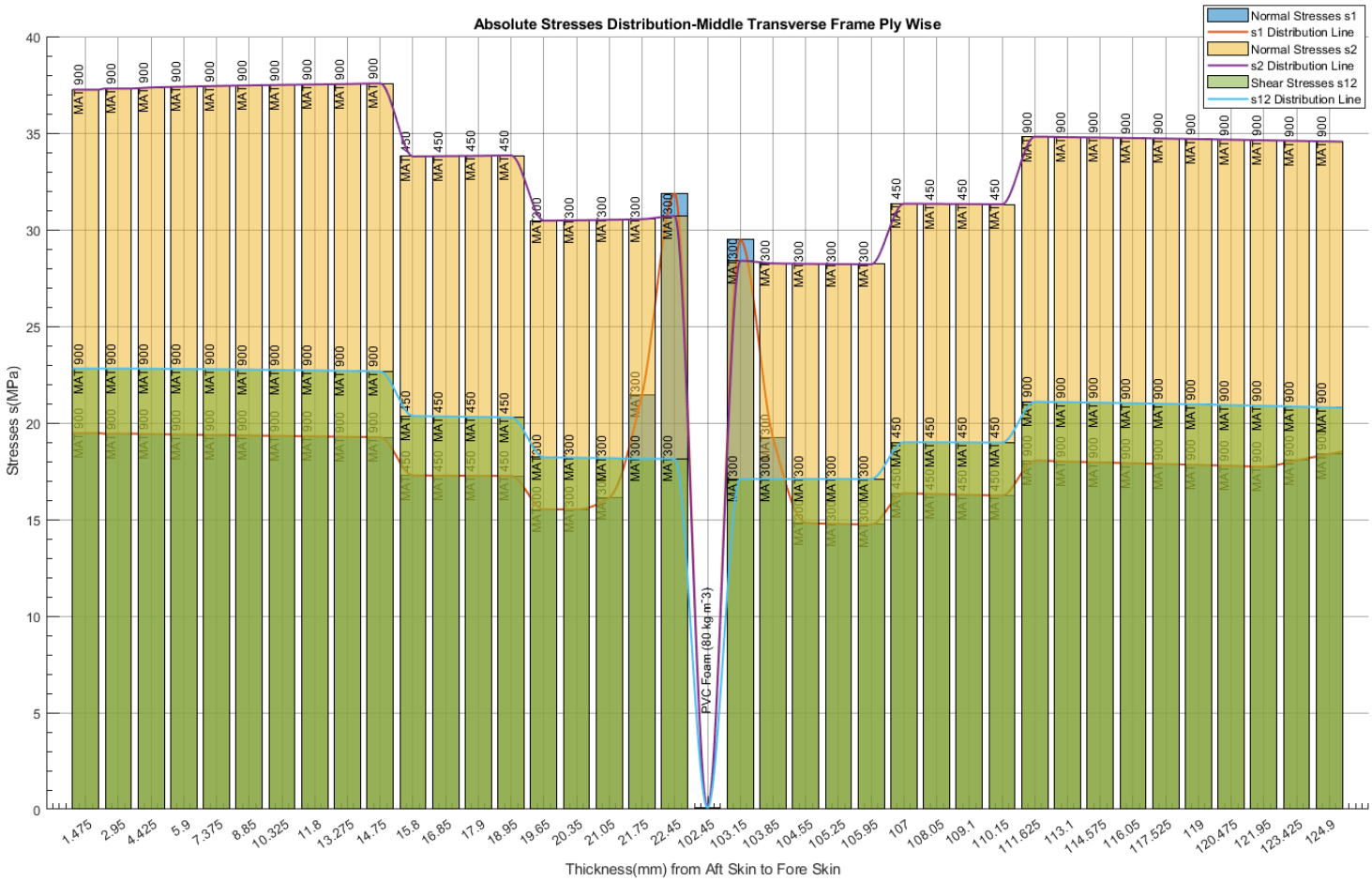

Figure 45: Model(B): Absolute Normal and Shear Stresses Distribution of Middle Frame

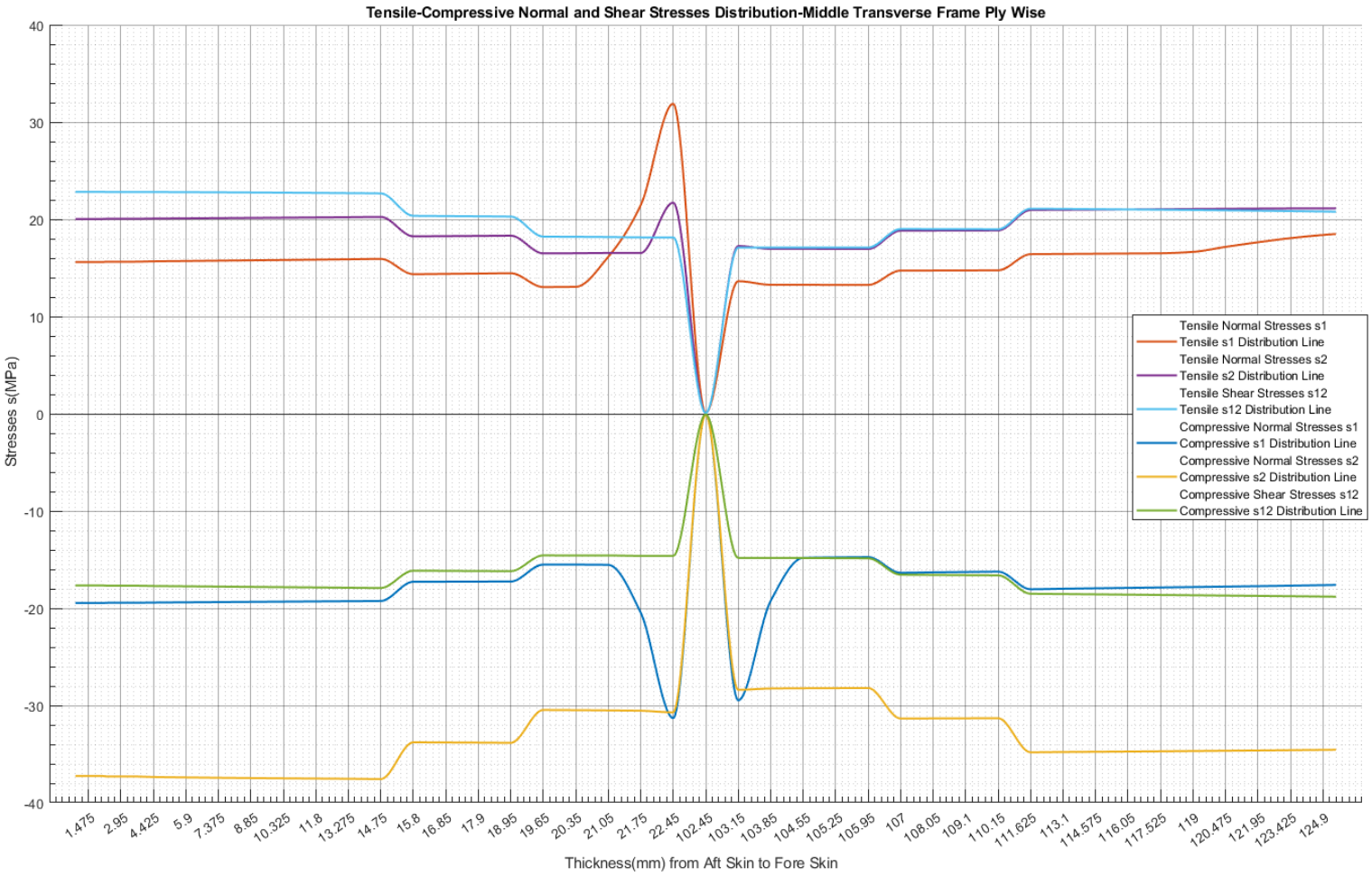

Figure 47: Model(B): Tensile-Compression Normal and Shear Stress Distribution of Middle Frame

From the Figures(44-48) it is observed that in Model(B) the highest stresses are the compression stresses s_2, with a value of about -37MPa. Furthermore, there is a sharp increase of the normal stress s1 in the MAT300 ply on both sides of the core, due to stress concentration, in the same way as in Model(A). Clearer results for the tensile and compression distributions are provided by the corresponding principal stresses diagrams.

5.2.3 Deck

Based on middle transverse frame, the same results currently are shown below for the foredeck which supports the crane.

- Model(A):

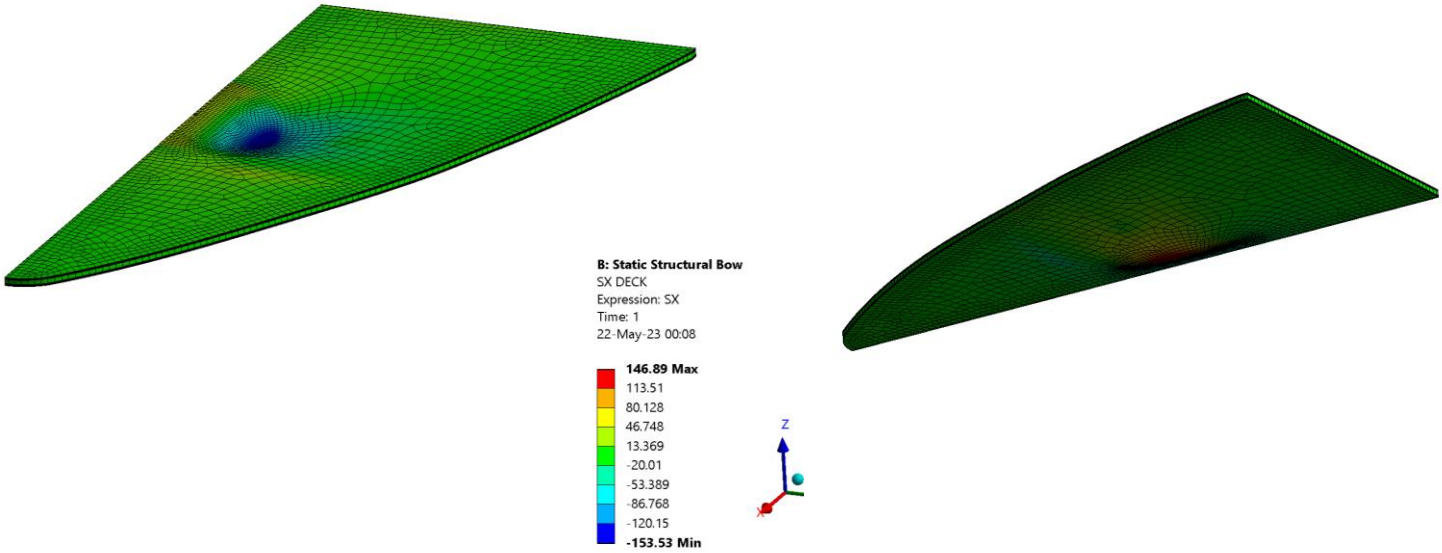

Figure 48: Model(A): Normal Stresses SX of Deck

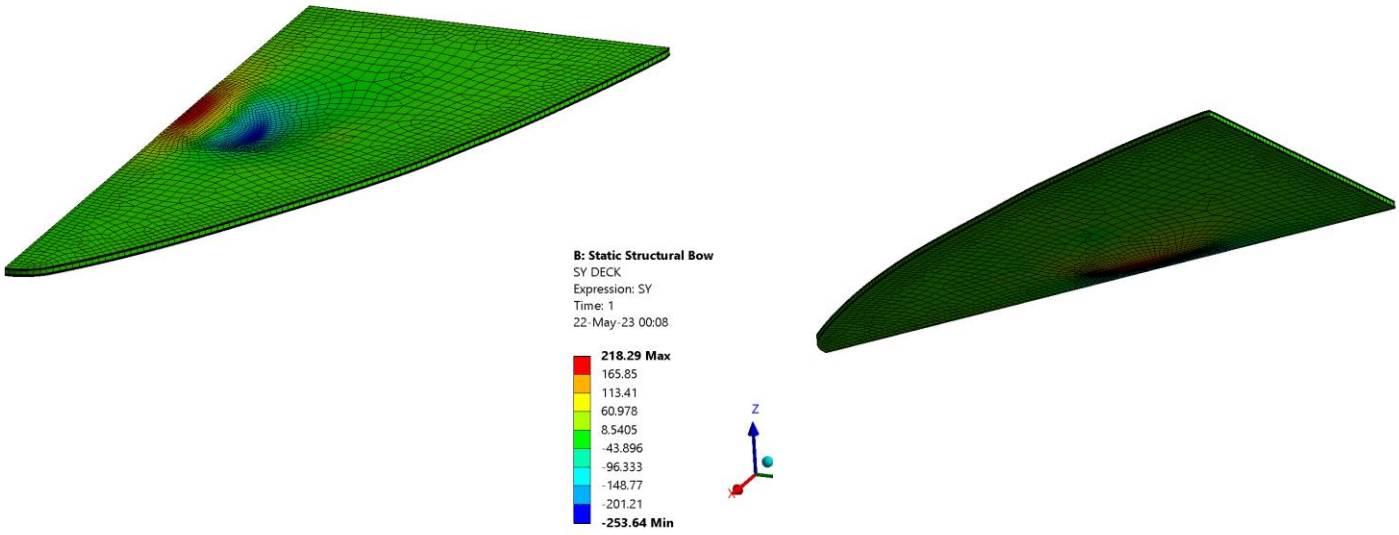

Figure 49: Model(A): Normal Stresses SY of Deck

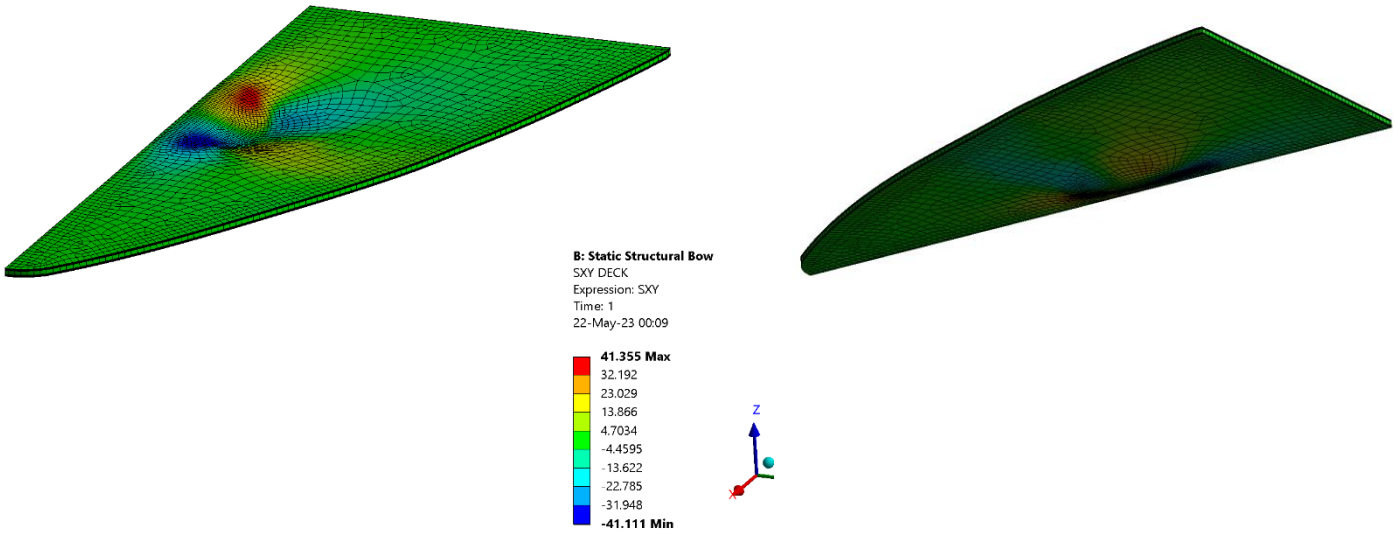

Figure 50: Model(A): Shear Stresses SXY of Deck

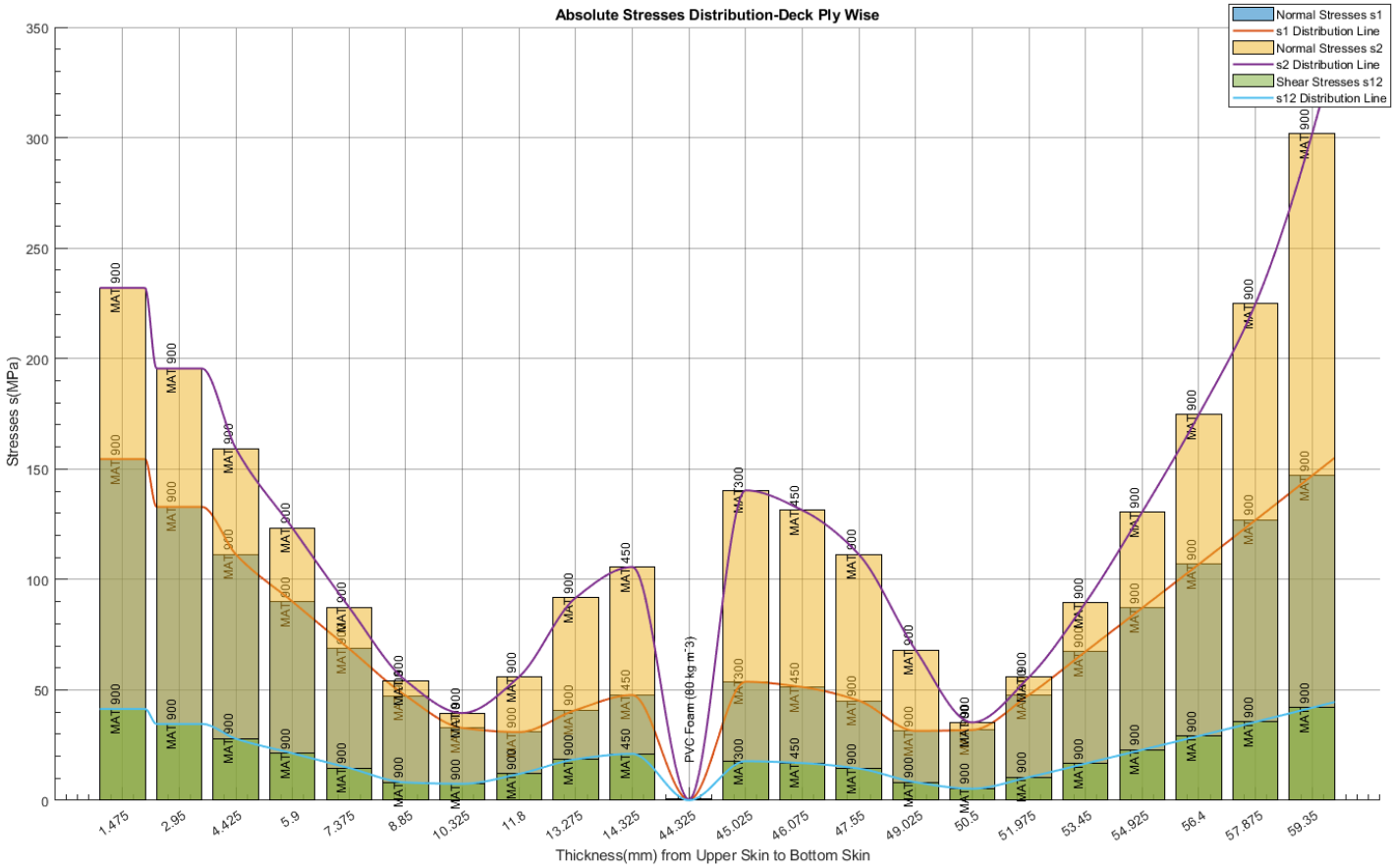

Figure 51: Model(A): Absolute Normal and Shear Stresses Distribution of Deck

An important observation in Figure 52 is the reduction in stresses at thicknesses of 10.325mm and 50.5 mm. This is because the above diagram shows the absolute values of the stresses ranging from negative to positive. The absolute values are calculated since the failure criteria utilized in the study are quadratic, therefore the magnitude plays the most important part in failure.

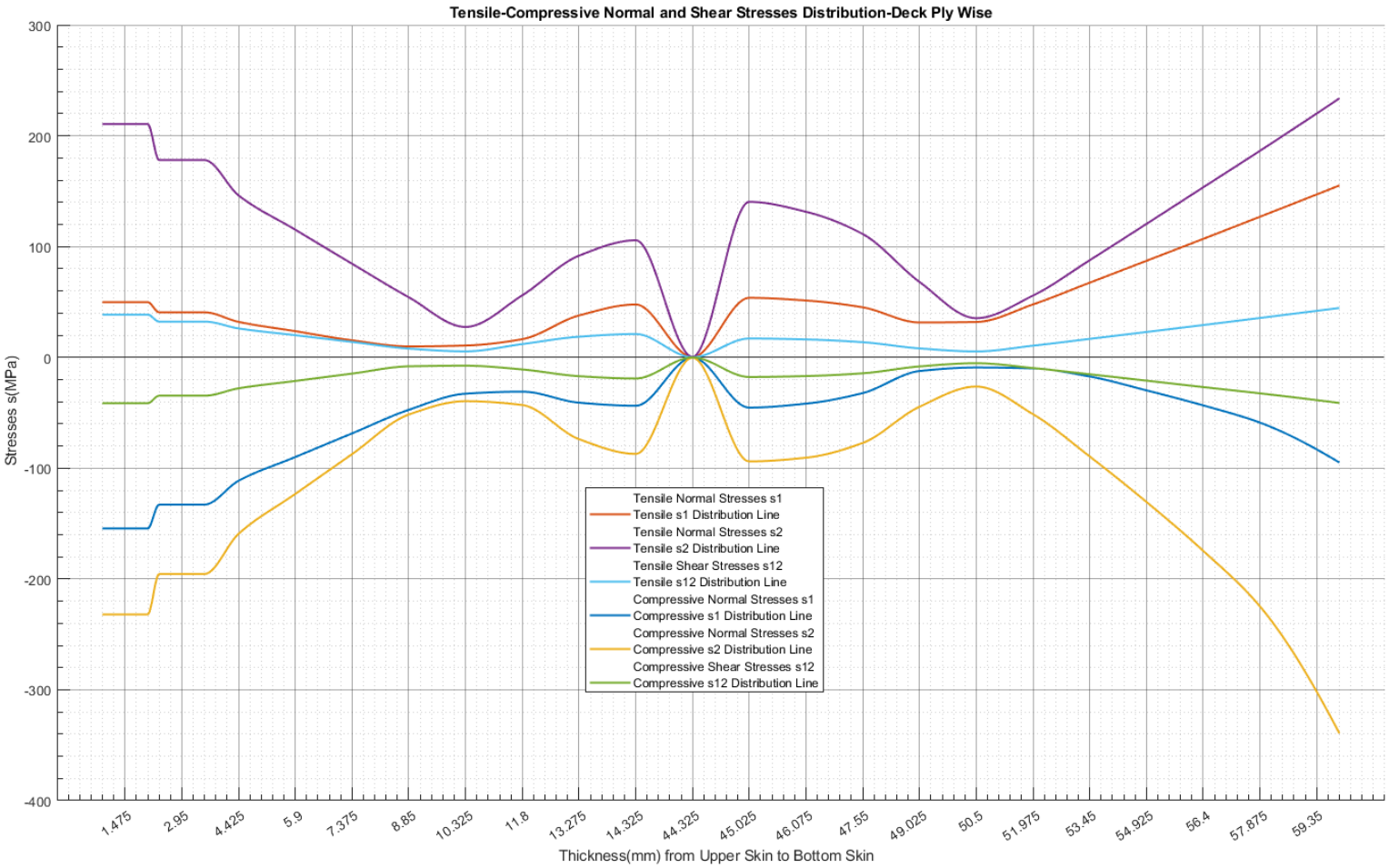

Figure 52: Model(A):Tensile-Compression Normal and Shear Stress Distribution of Deck

The Figures (49-53) reveal that the area of interest in the deck is the crane support area. The stresses with the highest values are the compressive stresses s_2, similar to the frame above. The maximum stress is compressive with a value of -301.7 MPa, at ply MAT900 adjacent to the longitudinal bulkhead and the area of interest located around the crane foundation. The stresses have a symmetrical pattern on each side of the core and can be considered acceptable. Finally, it is observed that in the deck the distributions are more distinct from each other without any alternations, compared to the same diagram for the frame above.

- Model(B):

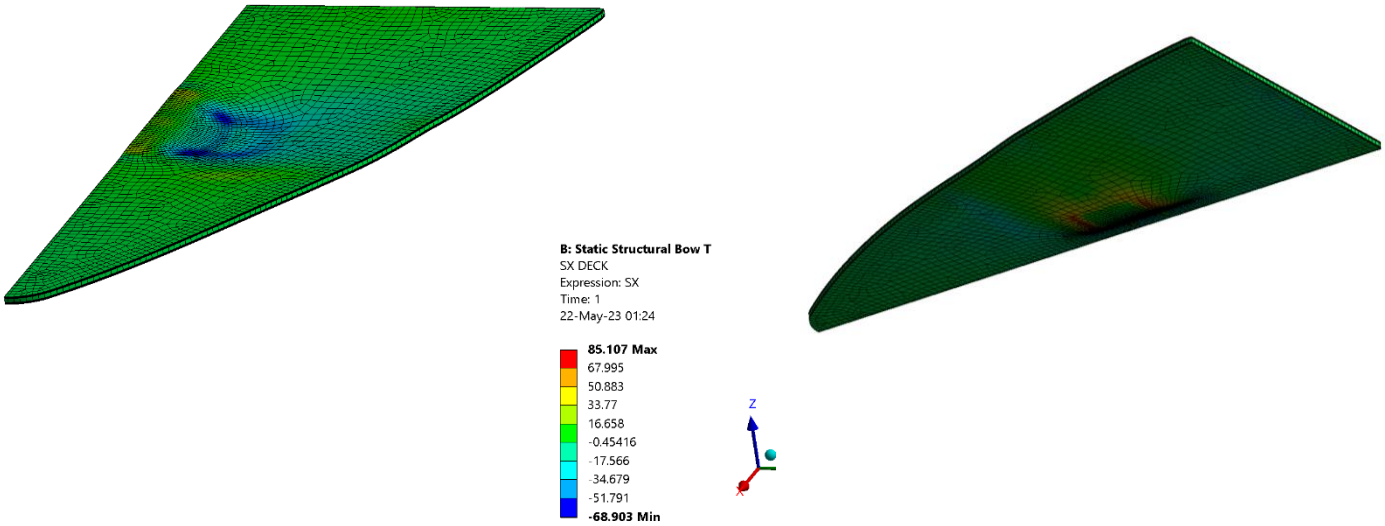

Figure 54: Model(B): Normal Stresses SX of Deck

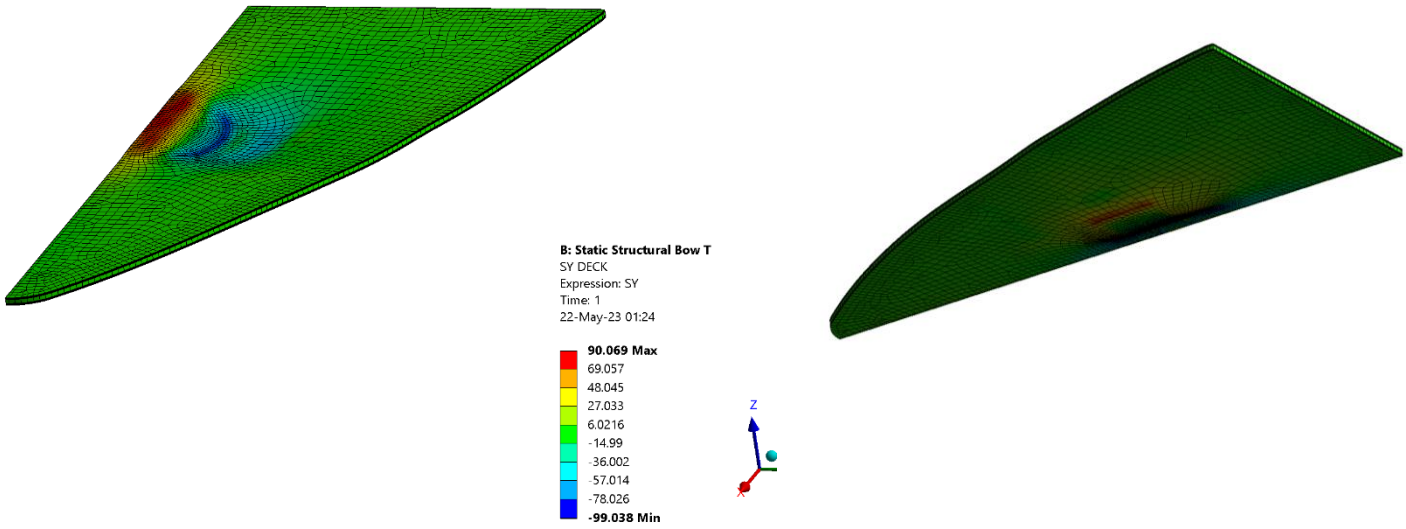

Figure 53: Model(B): Normal Stresses SY of Deck

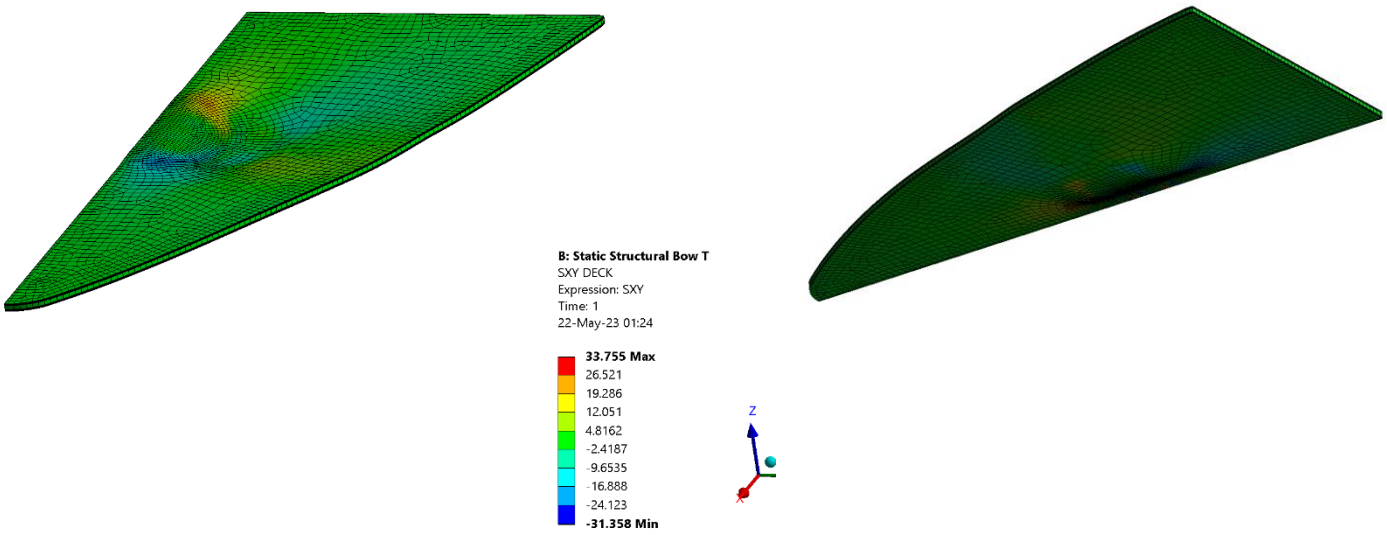

Figure 55: Model(B): Shear Stresses SXY of Deck

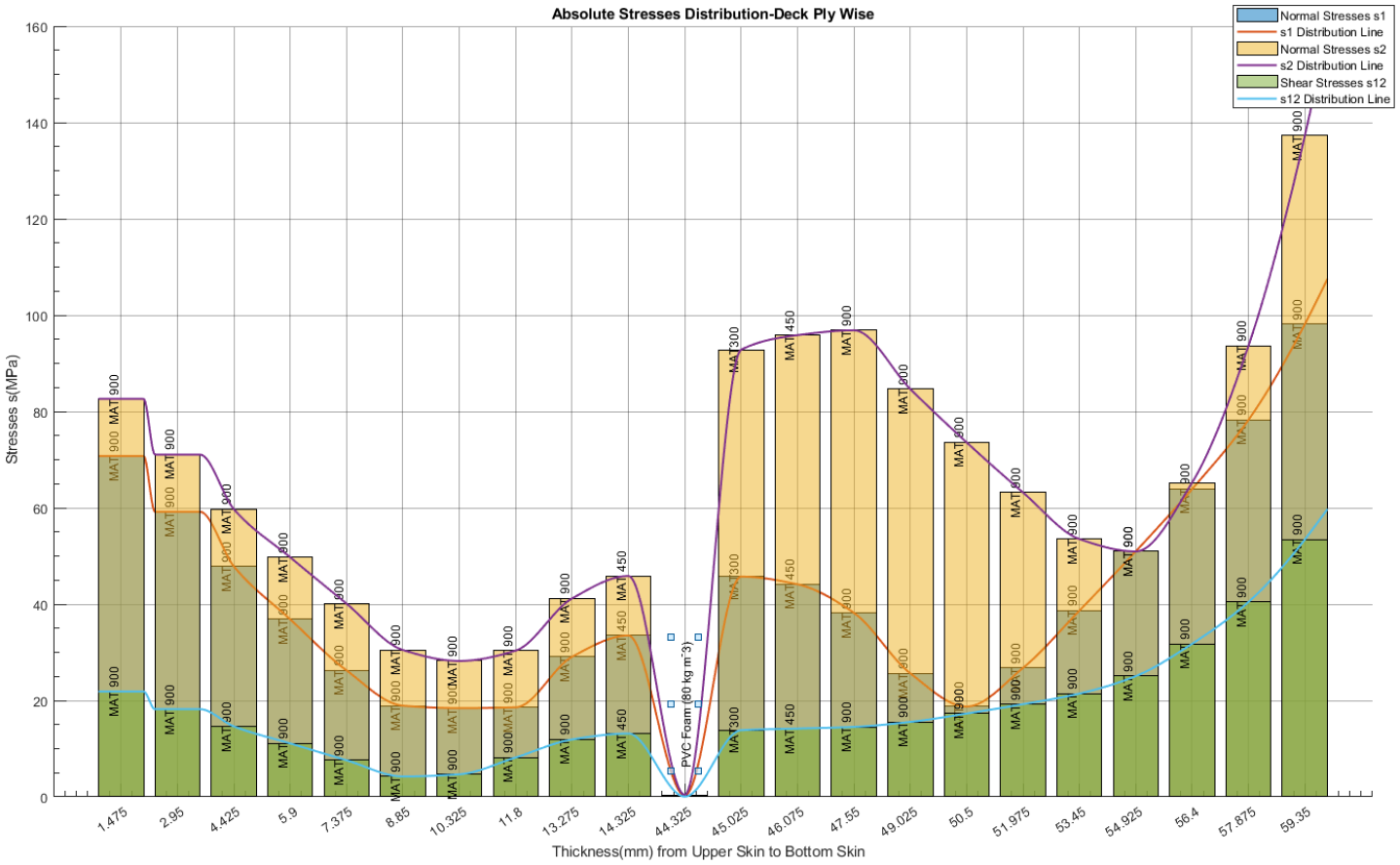

Figure 56: Model(B): Absolute Normal and Shear Stresses Distribution of Deck

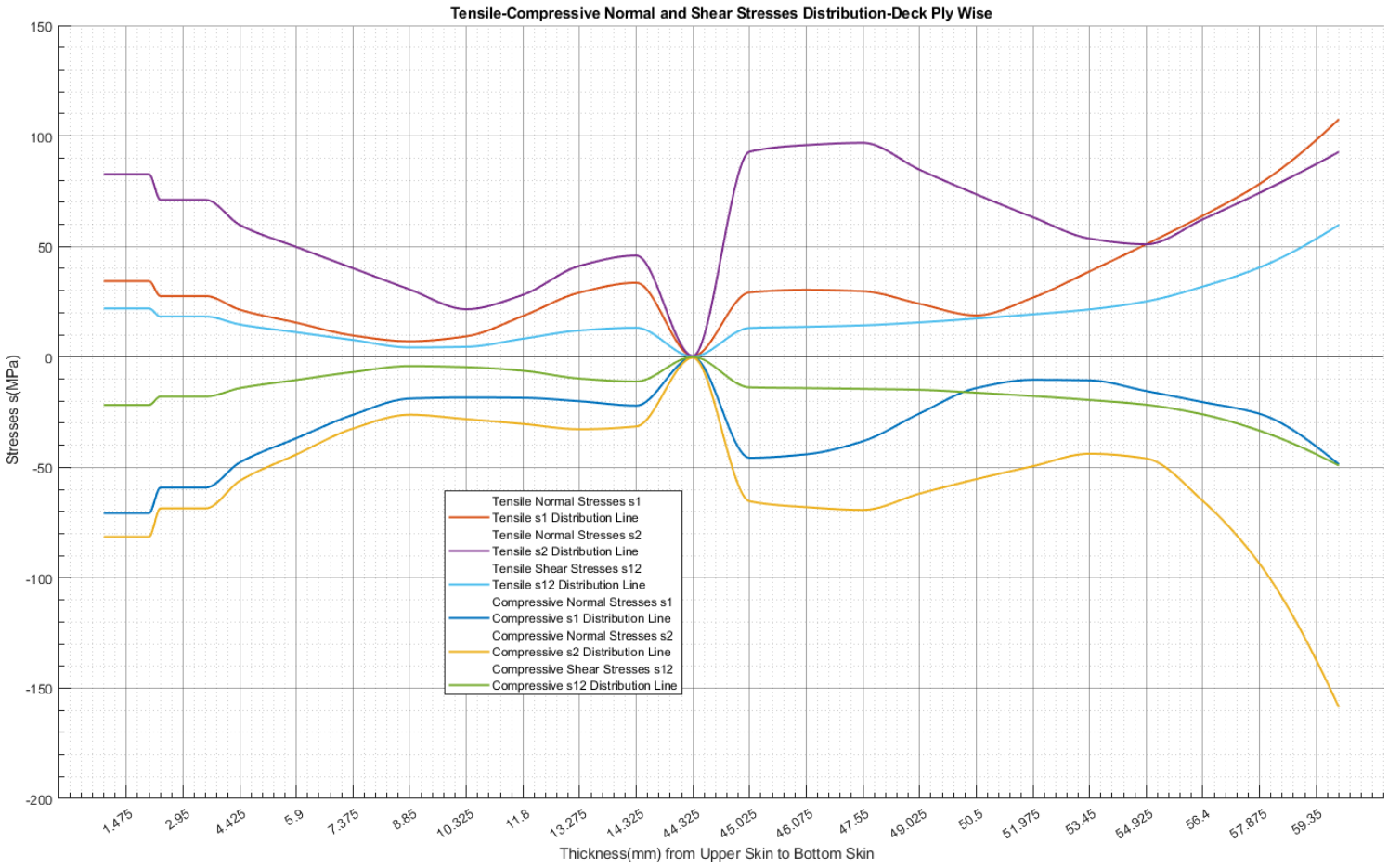

Figure 57: Model(B): Tensile-Compression Normal and Shear Stress Distribution of Deck

In model (B) a distribution of stresses in the finite elements located all-around of the shape of the T-Joint reinforcement and a sharp increase in stresses from the core to the bottom skin of the sandwich exist. The largest stresses are s_2 which are compressive at MAT 900, that is adjacent to the longitudinal bulkhead, and possess a maximum value of -137.3 MPa. It is observed that at model B the compressive stress s1 after thickness 50.5 mm is no longer symmetrical. Similar phenomena apply to the tensile stresses s_1, s_2 after thickness 54.925 mm. The change in symmetry is due to the T-Joint which seems to significantly affect the normal stresses of the deck by significantly reducing them (See par. 5.5 Compare Analysis of Results).

5.2.4 T-Joint Reinforcement

The stress distribution should be studied for T-Joint reinforcement in order to evaluate the strength of the reinforcement.

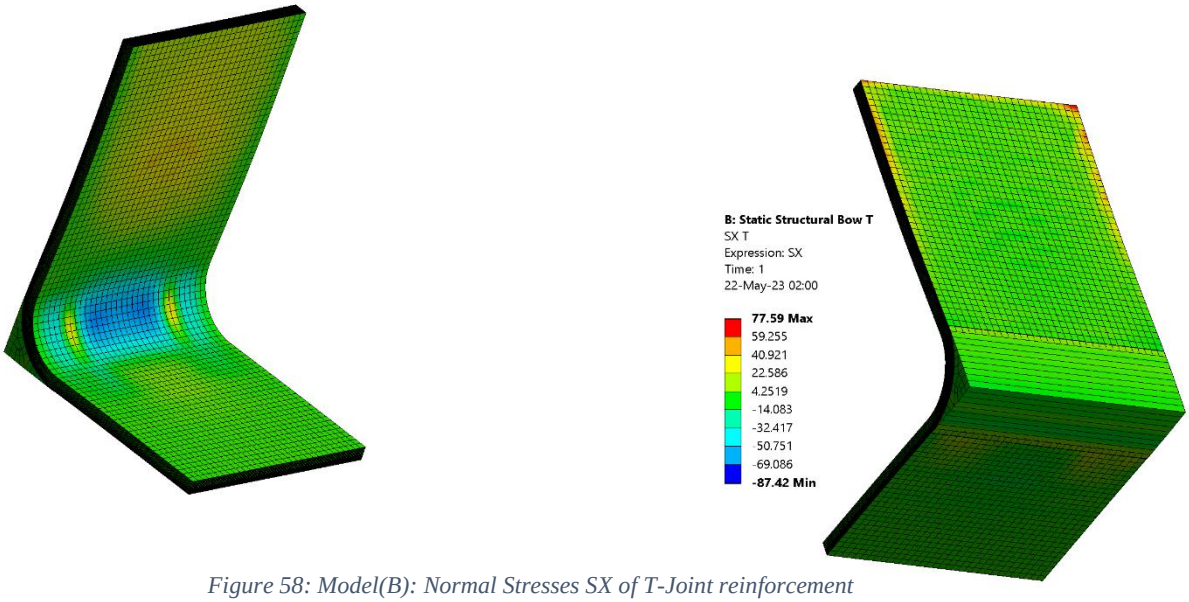

Figure 58: Model(B): Normal Stresses SX of T-Joint reinforcement

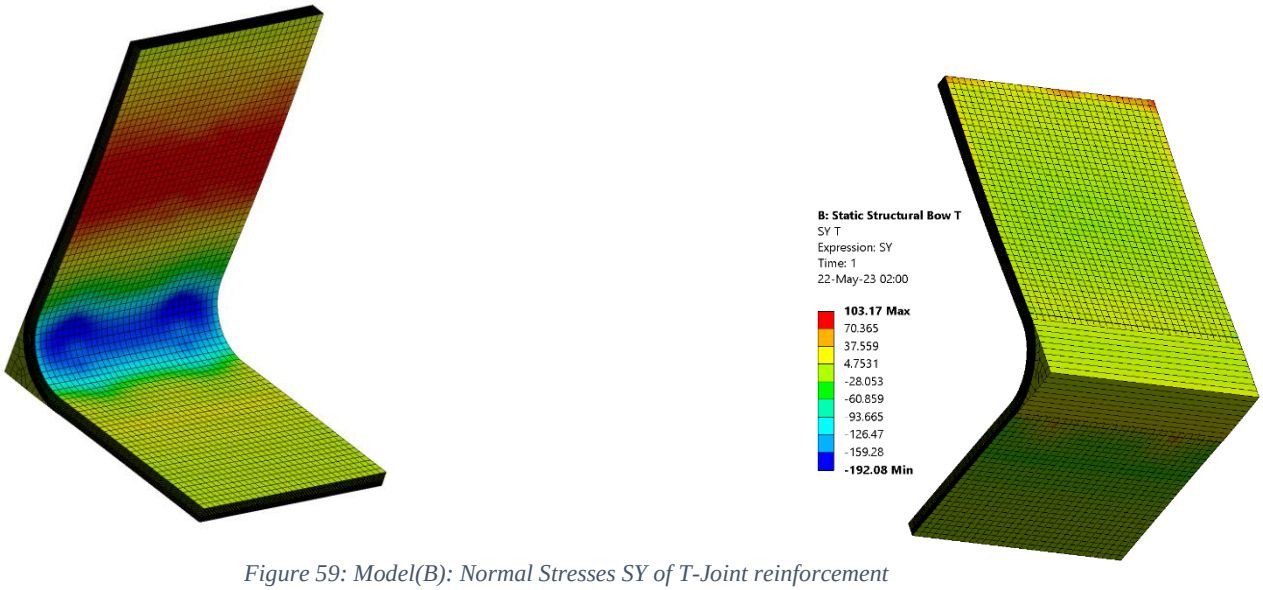

Figure 59: Model(B): Normal Stresses SY of T-Joint reinforcement

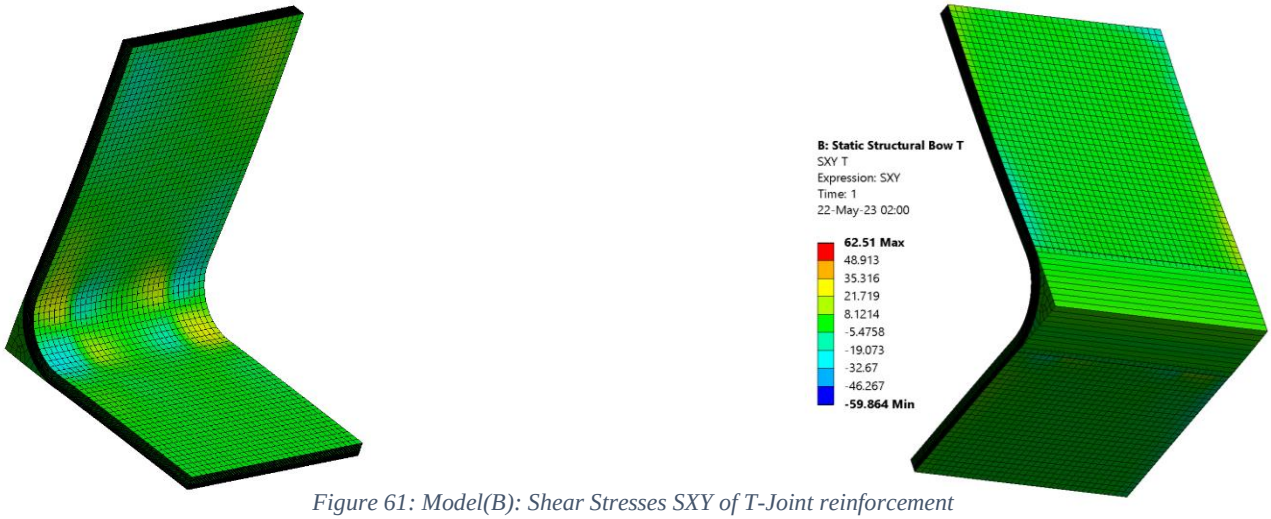

Figure 61: Model(B): Shear Stresses SXY of T-Joint reinforcement

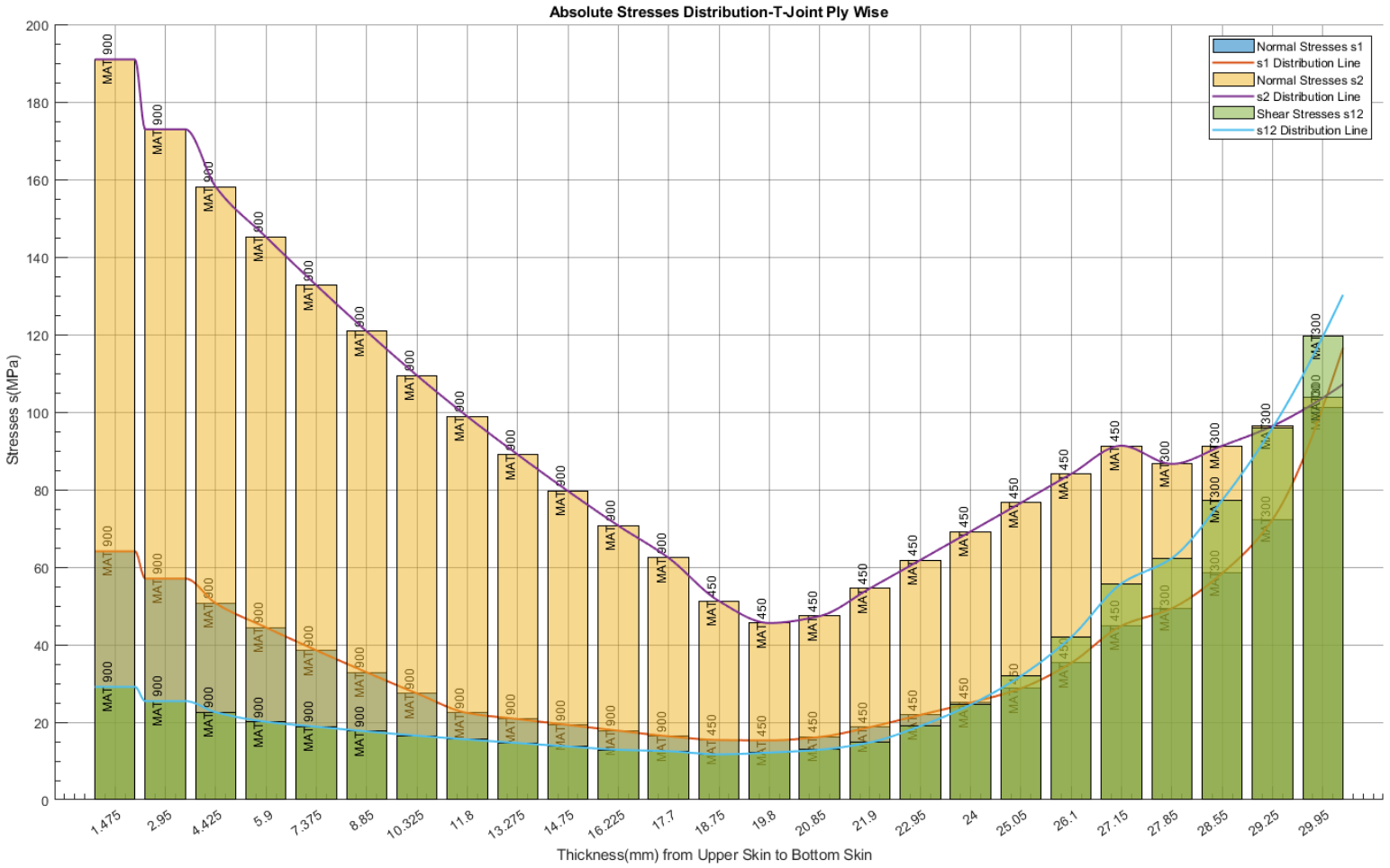

Figure 60: Model(B): Absolute Normal and Shear Stresses Distribution of T-Joint reinforcement

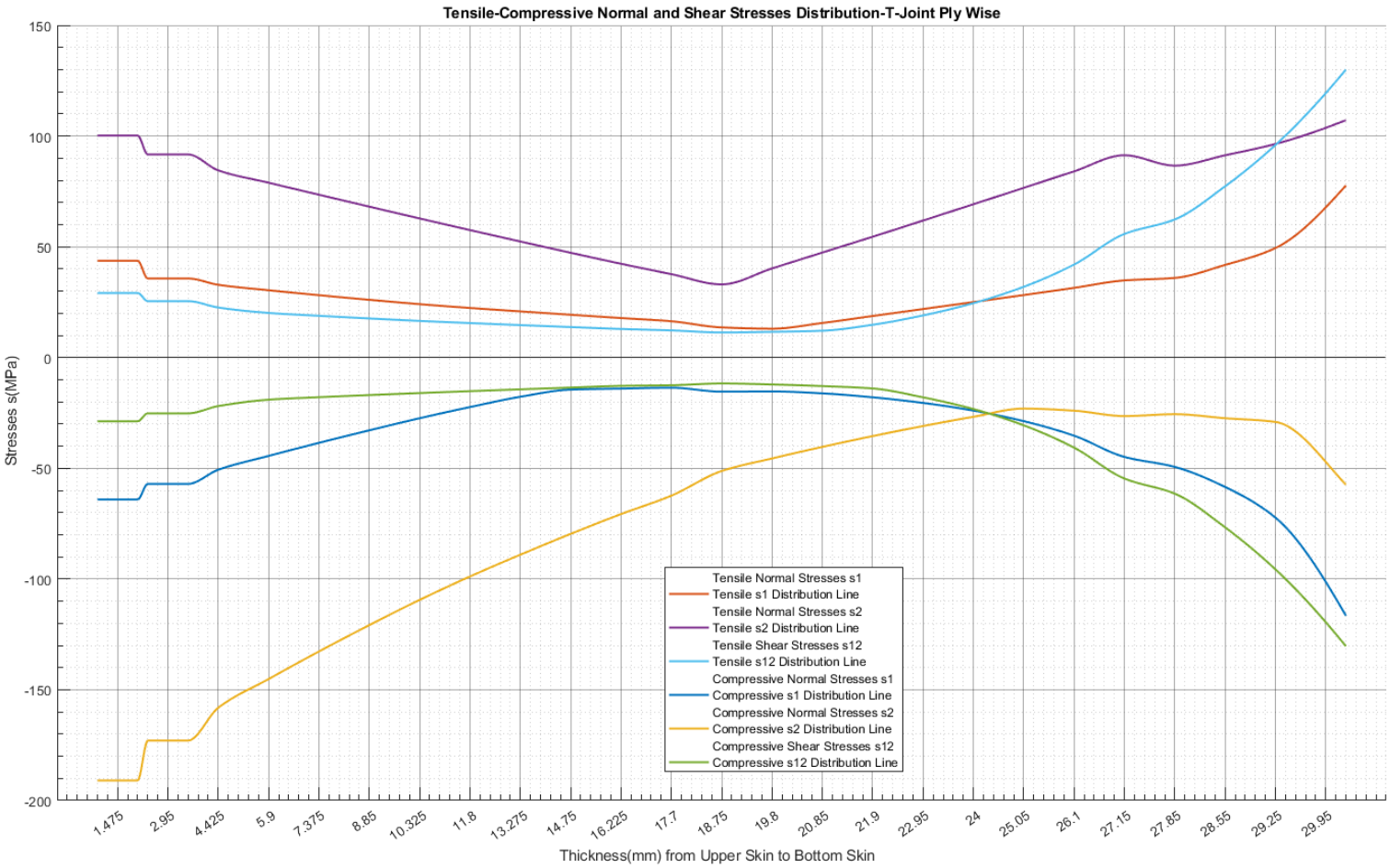

Figure 62: Model(B):Tensile-Compression Normal and Shear Stress Distribution of T-Joint reinforcement

According to the Figures (Figure 60-Figure 61) above, the T-Joint stiffening appears to be stressed mainly in the fillet region (due to the change in geometry) by normal stresses s1 and s2. The largest stress is s2, which appears to be on the outer ply MAT900, while the inner ply MAT300 is stressed by s1 and s12. Also, there is a stress concentration at the acute edge of the T-Joint and deck transverse at stresses s1, which can be neglected because it extends only to one finite element. Finally, as shown in the MAT300 layers, the compressive stresses have similar values to the tensile stresses. The compressive stresses are observed in the fillet region, while the tensile stresses are observed in the other regions of the T-Joint.

5.3 Principal Stresses

Principal stresses are the maximum and minimum normal stresses values that apply to a certain location of the structure according to the principal coordinate system as described in *4.5.2 Coordinate System of Principal Stresses*. For the assessment of structural performance under varied loading conditions, they give crucial information on the critical stress states, in the principal planes, that bear no shear stresses.

5.3.1 Bow Region

- Model(A):

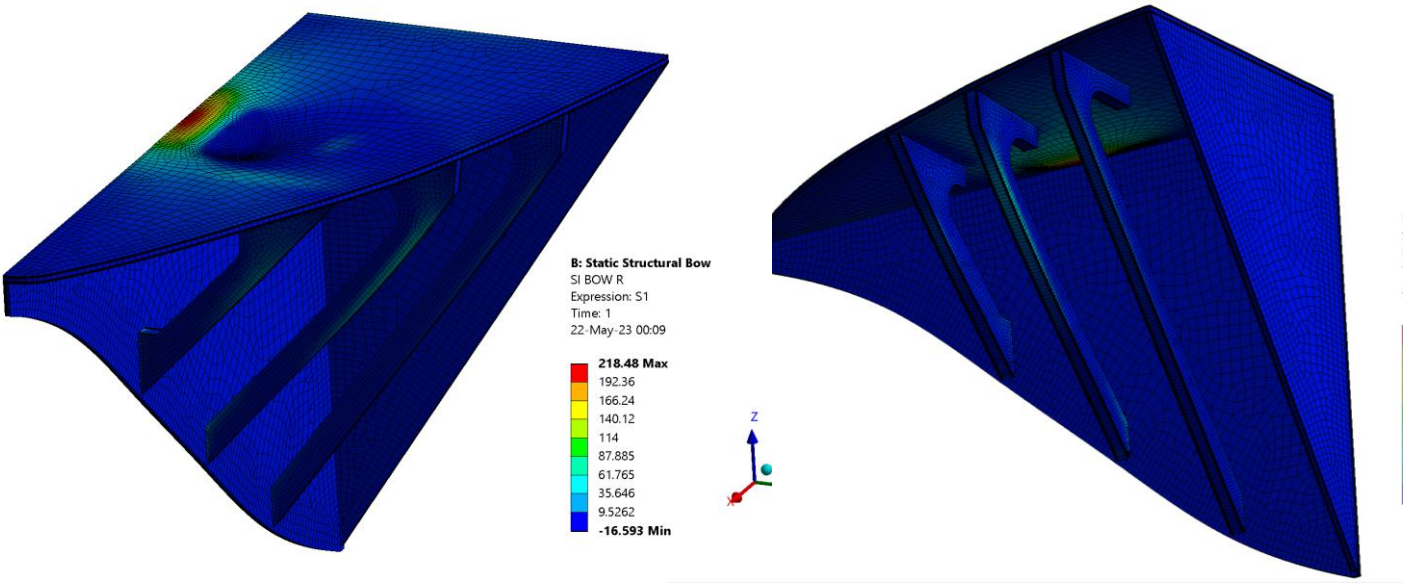

Figure 63:Model(A): Principal Stresses SI of Bow Region

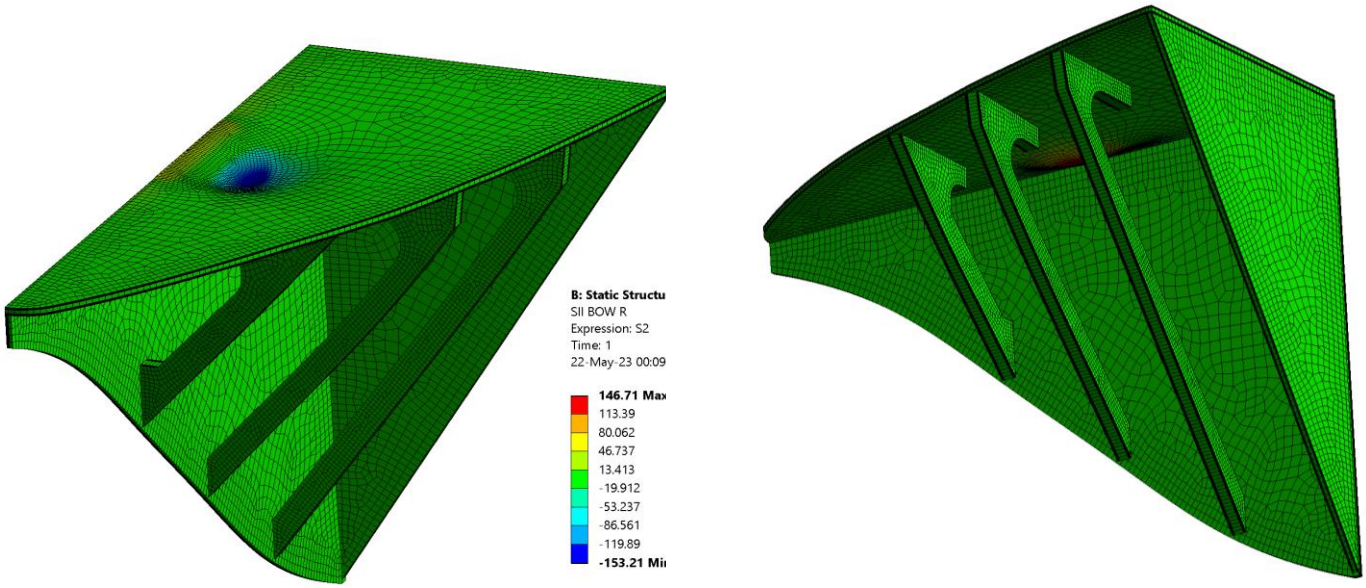

Figure 64:Model(A): Principal Stresses SII of Bow Region

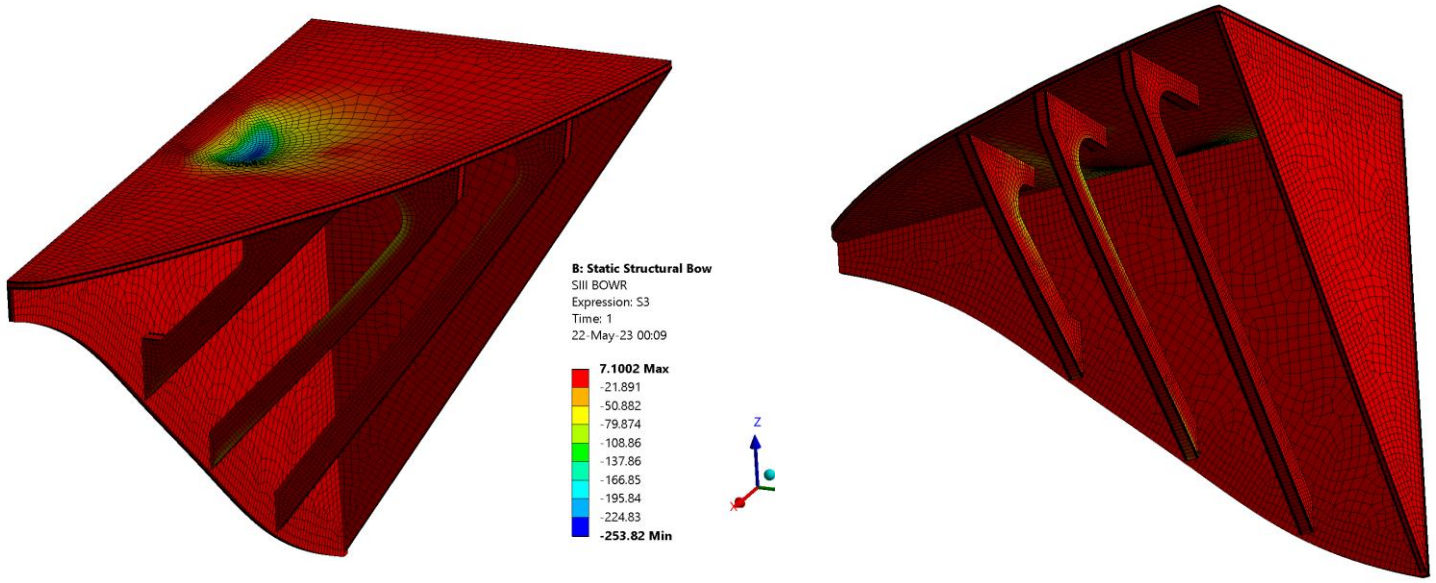

Figure 65:Model(A): Principal Stresses SIII of Bow Region

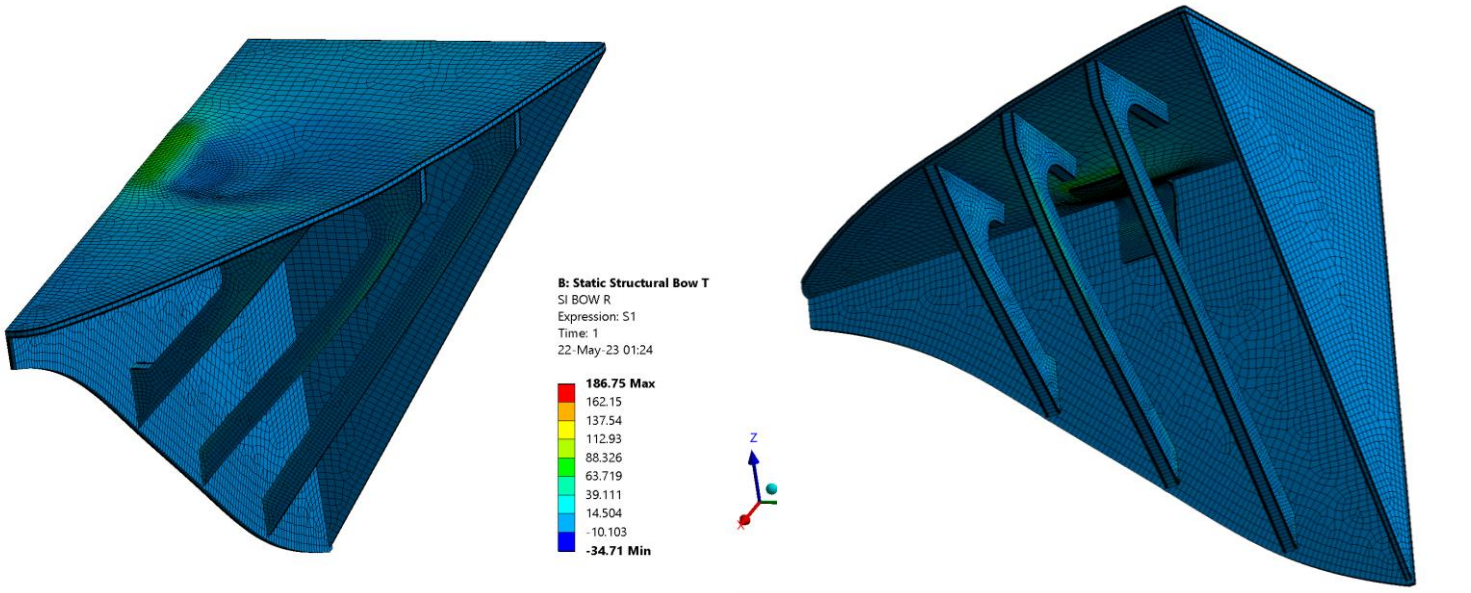

Figure 66:Model(B): Principal Stresses SI of Bow Region

- Model(B):

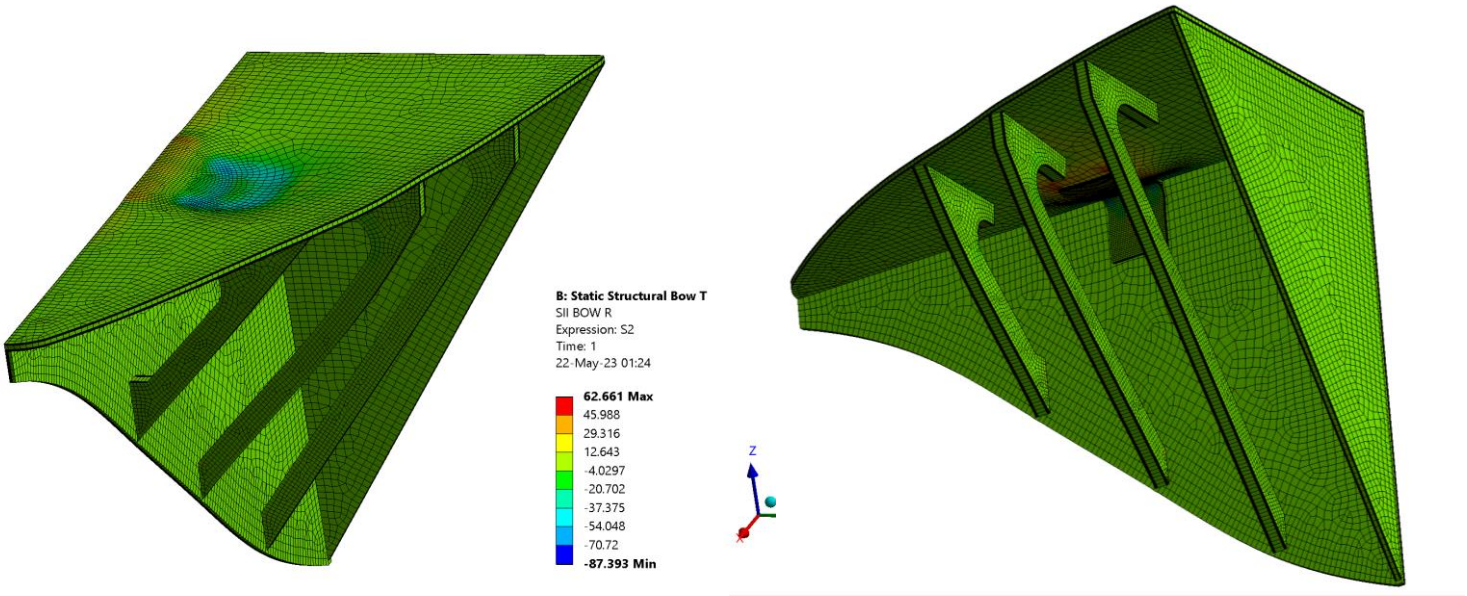

Figure 67:Model(B): Principal Stresses SII of Bow Region

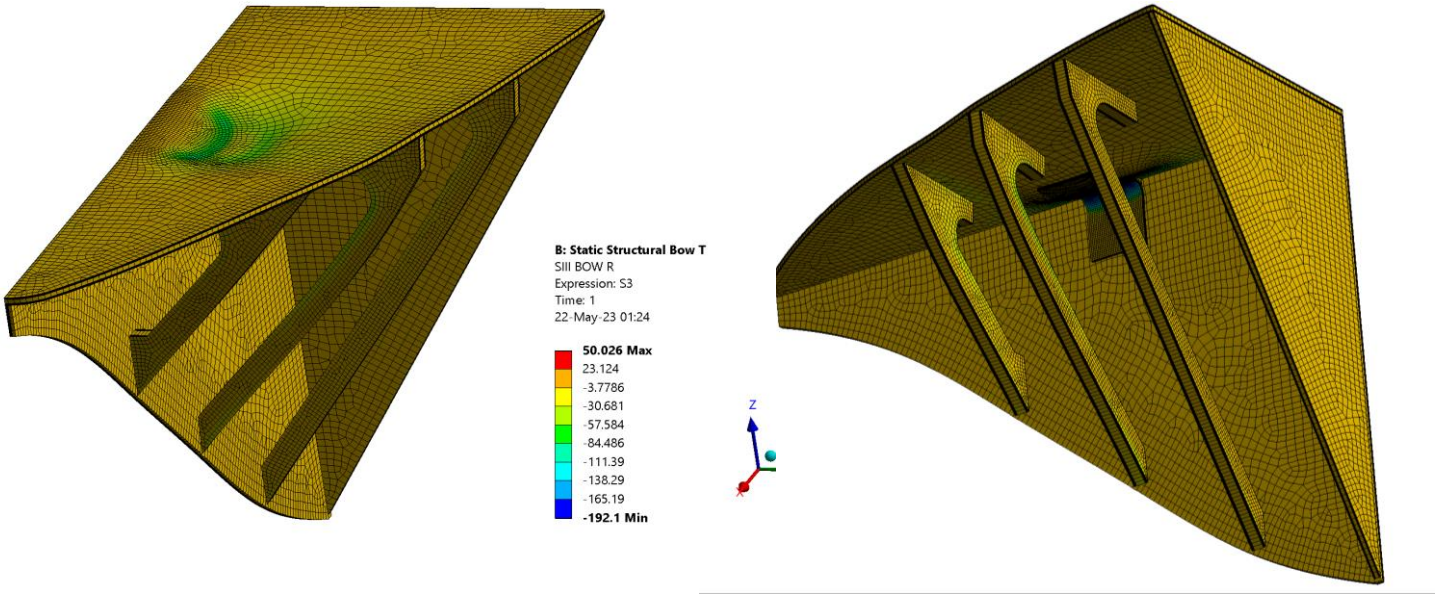

Figure 68:Model(B): Principal Stresses SIII of Bow Region

The reinforcement by GRP attachment in the location of the crane resulted in a very significant reduction in the Principal Stresses. Also, it appears that the longitudinal bulkhead is not significantly stressed. The areas that need to be studied more in terms of stresses are the deck and the middle transverse frame. It is worth noting that the Principal Stresses do not contain shear terms, but as a stress state are similar to the one presented in Normal and Shear Stresses.

5.3.2 Middle Frame

- Model(A):

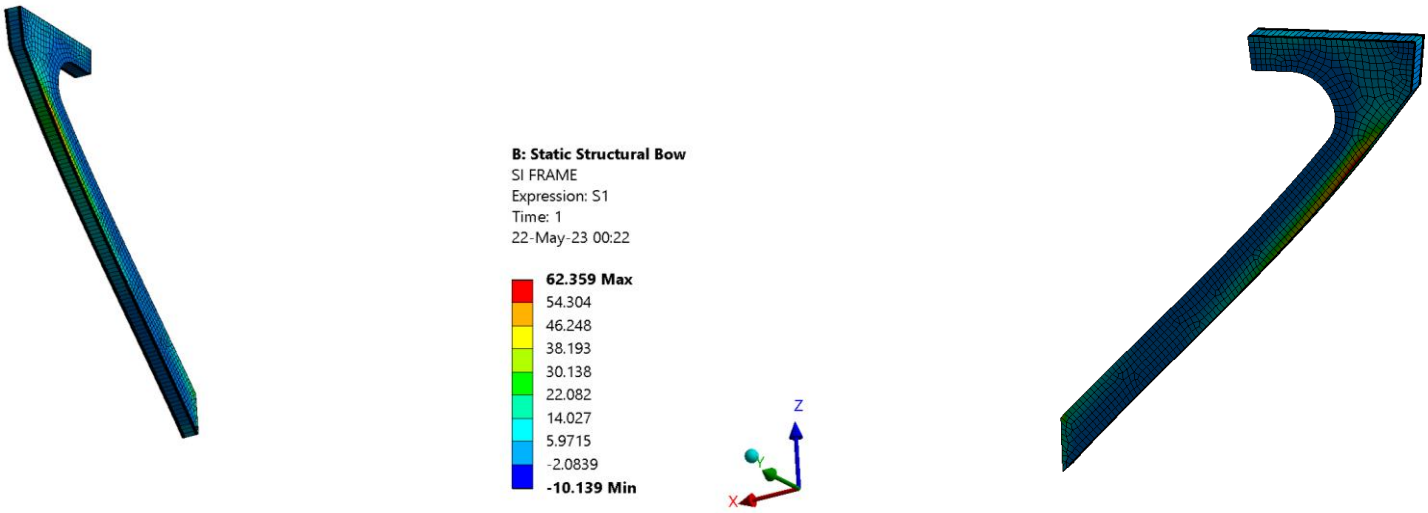

Figure 70:Model(A): Principal Stresses SI of Middle Frame

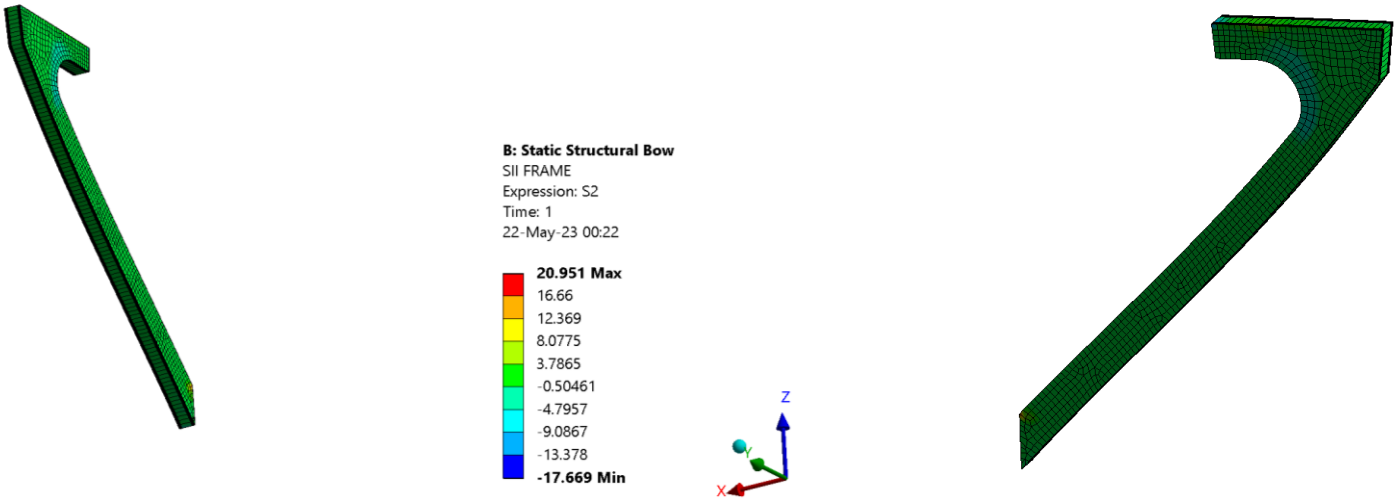

Figure 69:Model(A): Principal Stresses SII of Middle Frame

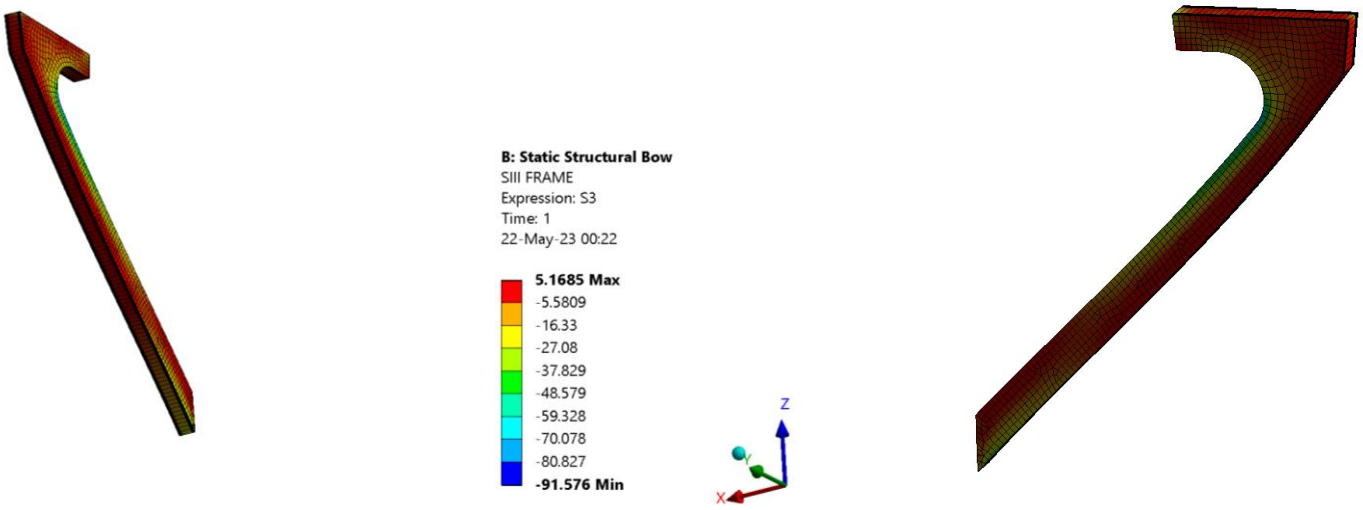

Figure 72:Model(A): Principal Stresses SIII of Middle Frame

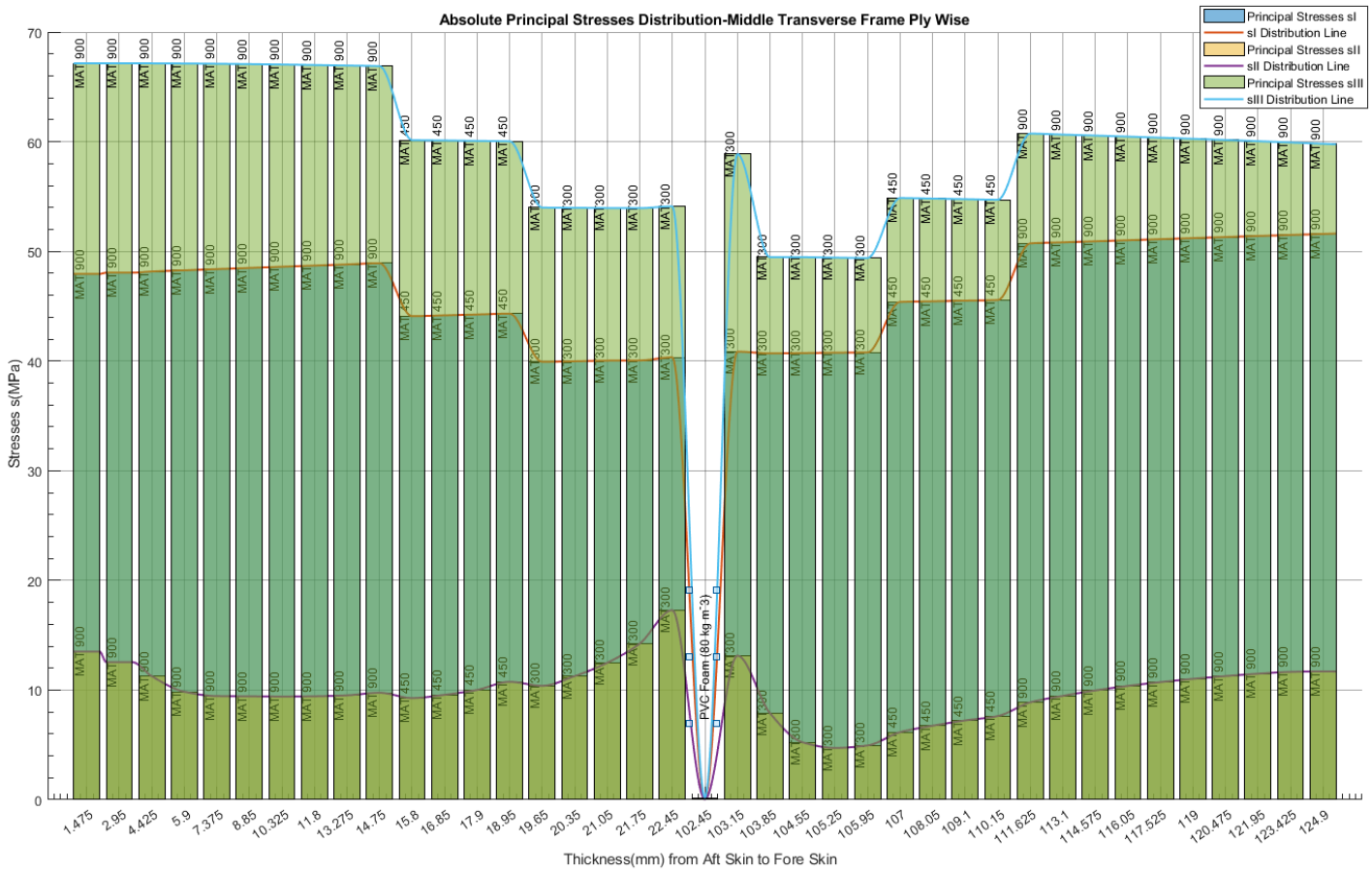

Figure 71: Model(A): Absolute Principal Stresses Distribution of Middle Frame

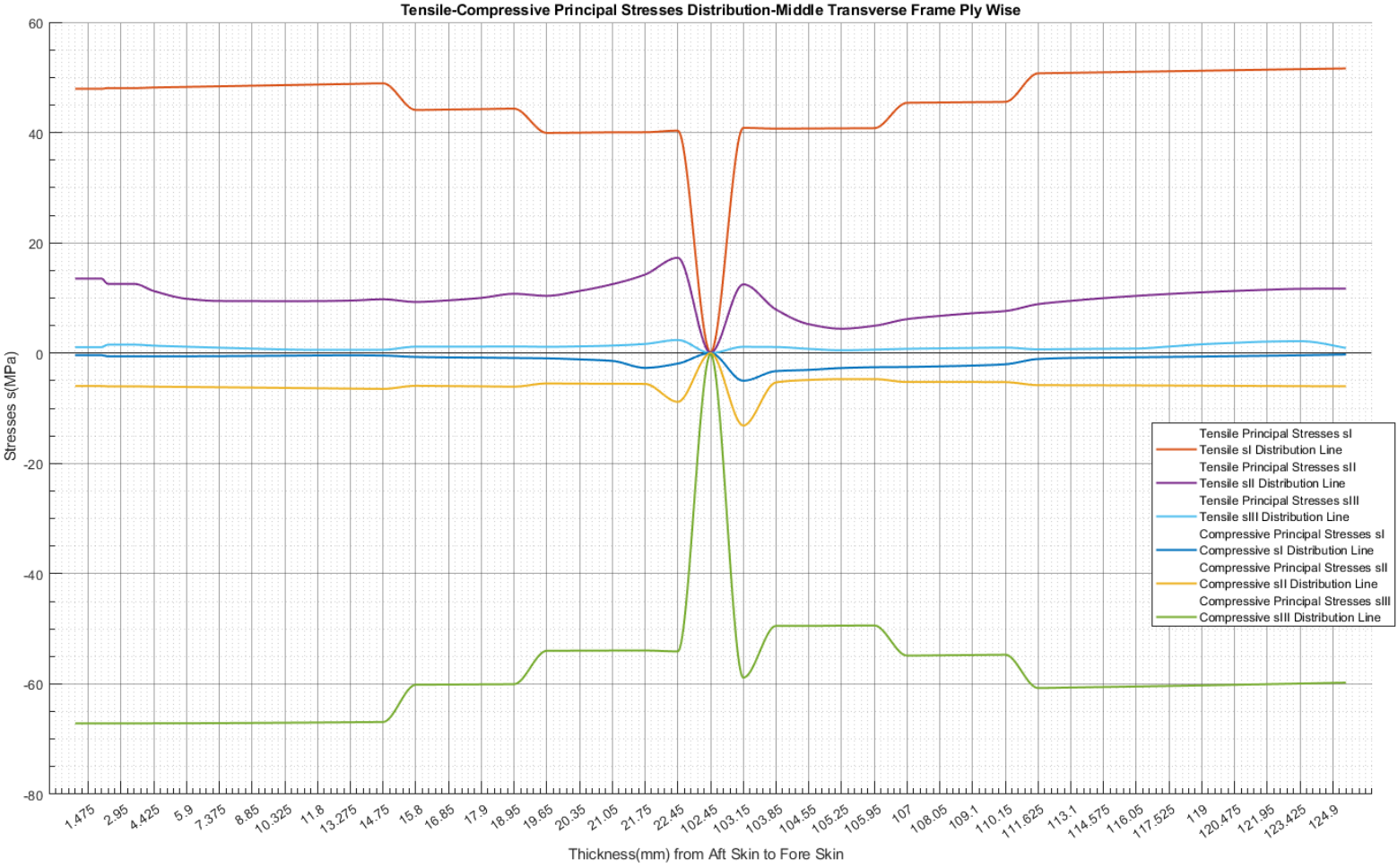

Figure 73: Model(A): Tensile-Compressive Principal Stress Distribution of Middle Frame

The principal stresses that possess the maximum values is the tensile Maximum Principal S_I and the compressive Minimum Principal S_{III}. It is observed that there are stress concentration phenomena at the same points as before. The maximum tensile occurs at the mid-length of the frame at the two outer edges as shown above. The maximum compressive is at the stress concentration point, between frame and longitudinal bulkhead and its maximum value is around -70MPa, after proper evaluation. Finally, an important observation that should also apply to the following principal stress diagrams in order to be valid, is the fact that the stresses should be $S_I > S_{II} > S_{III}$ according to classic mechanics.

Also, a stress concentration point to be further investigated is located at MAT300, on either side of the Middle Principal S_{II} stress core. This point is shown as following:

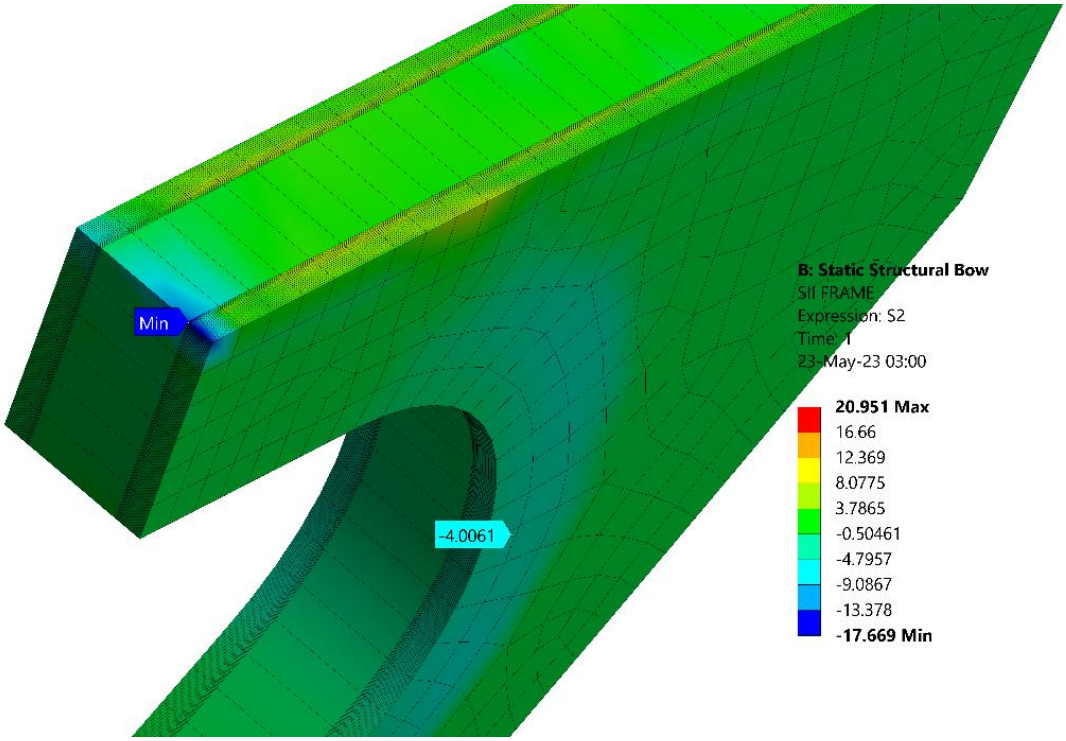

Figure 74:Model(A): Stress Concentration of Middle Principal Stress SII

Excluding the stress concentrations, the distributions are acceptable, since they show a symmetry of values on both sides of the core and have a smooth distribution.

- Model(B):

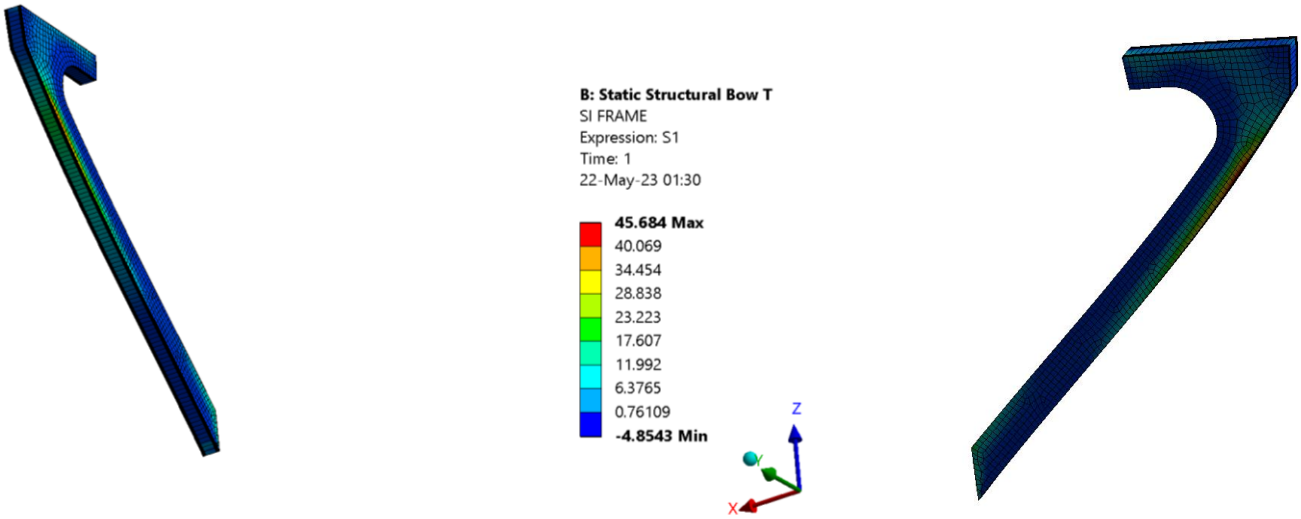

Figure 75:Model(B): Principal Stresses SI of Middle Frame

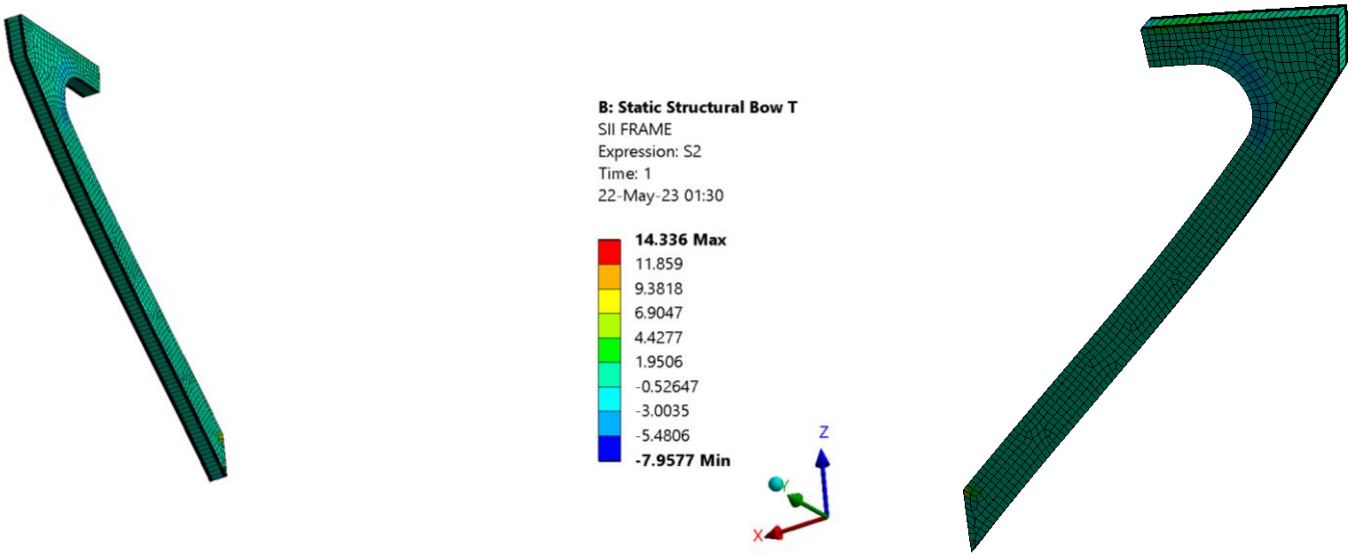

Figure 76:Model(B): Principal Stresses SII of Middle Frame

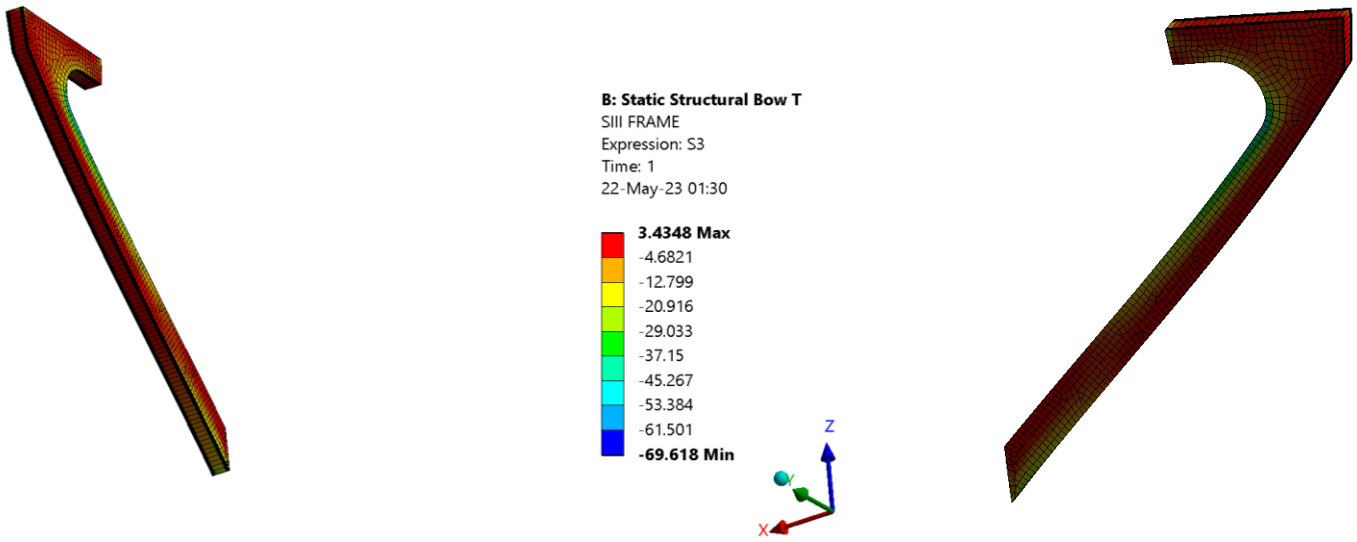

Figure 77:Model(B): Principal Stresses SIII of Middle Frame

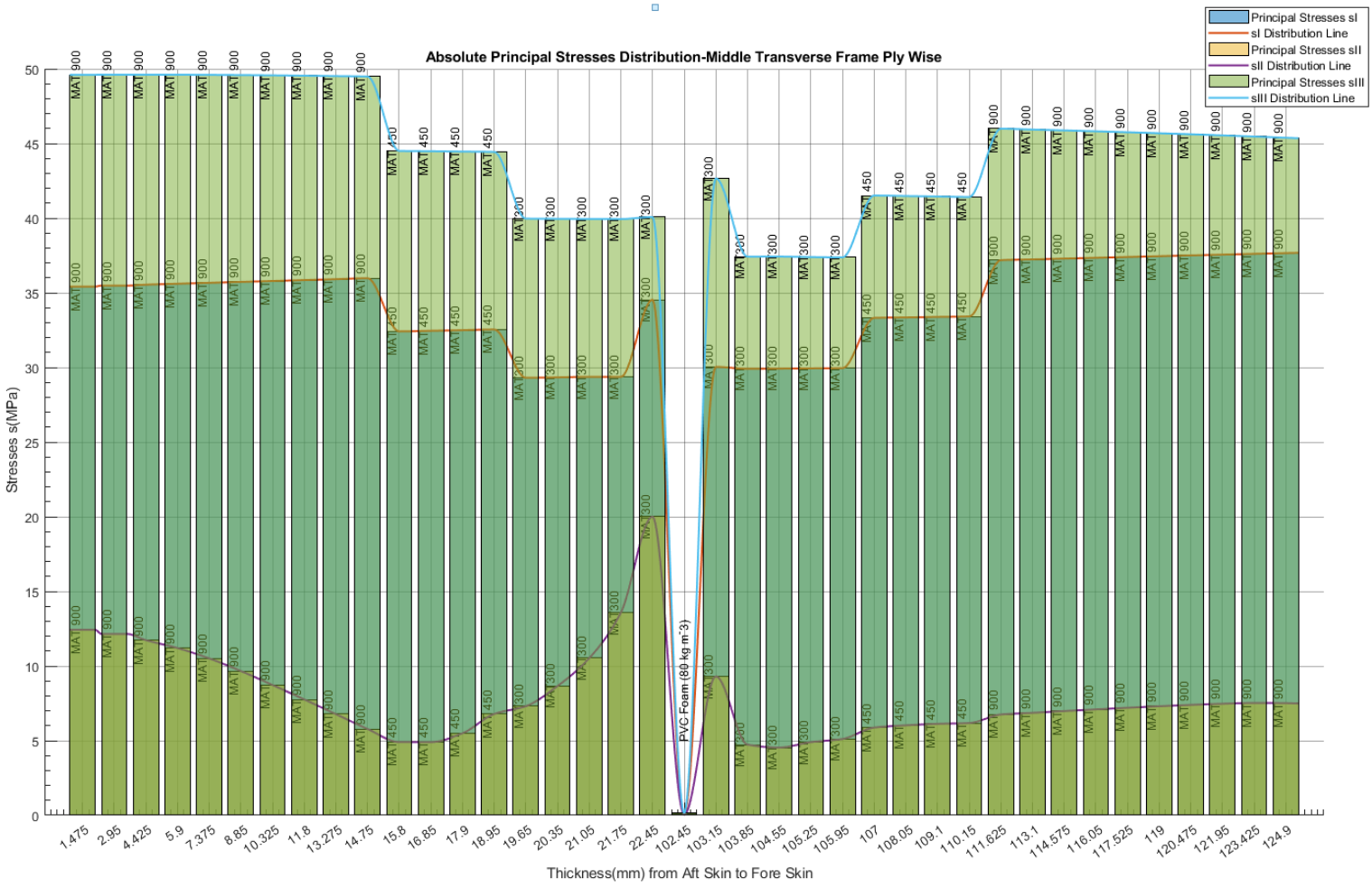

Figure 78: Model(B): Absolute Principal Stresses Distribution of Middle Frame

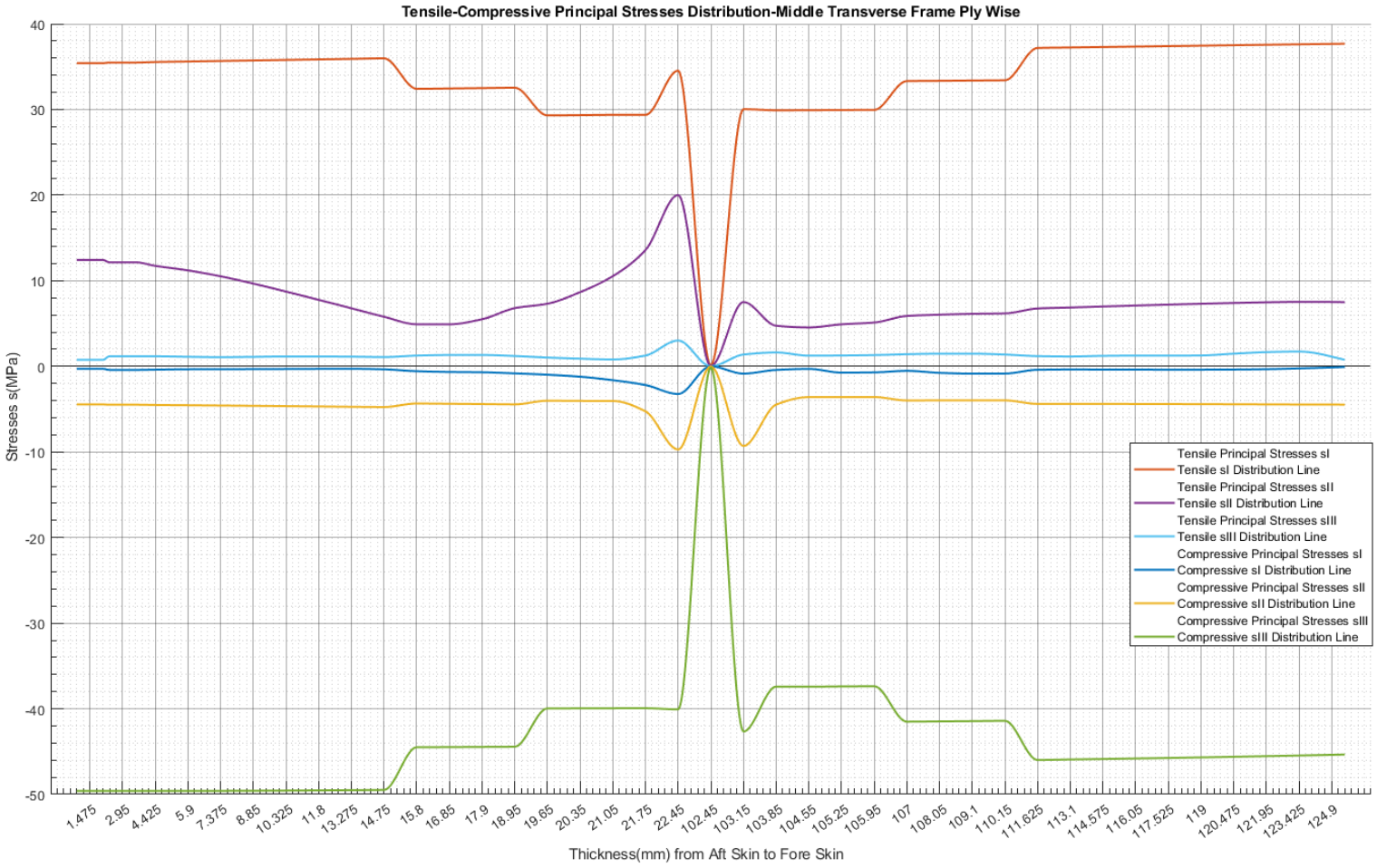

Figure 79: Model(B): Tensile-Compressive Principal Stress Distribution of Middle Frame

According to the illustrations above, the distribution of principal stresses in the finite elements is similar to Model(A). The distributions of values in each ply follow the same pattern, but with decreasing values. The symmetry that exists in the stress distribution is a positive indicator for the load transfer through the reinforcement. Finally, a decrease in principal stresses SI, SII and SIII of 25%,33% and 33.5% accordingly is observed.

5.3.3 Deck

In the deck shear stresses dominate a significant proportion of the stress distribution. Using principal stresses will make it more convenient to detect the maximum stress value in the deck.

- Model(A):

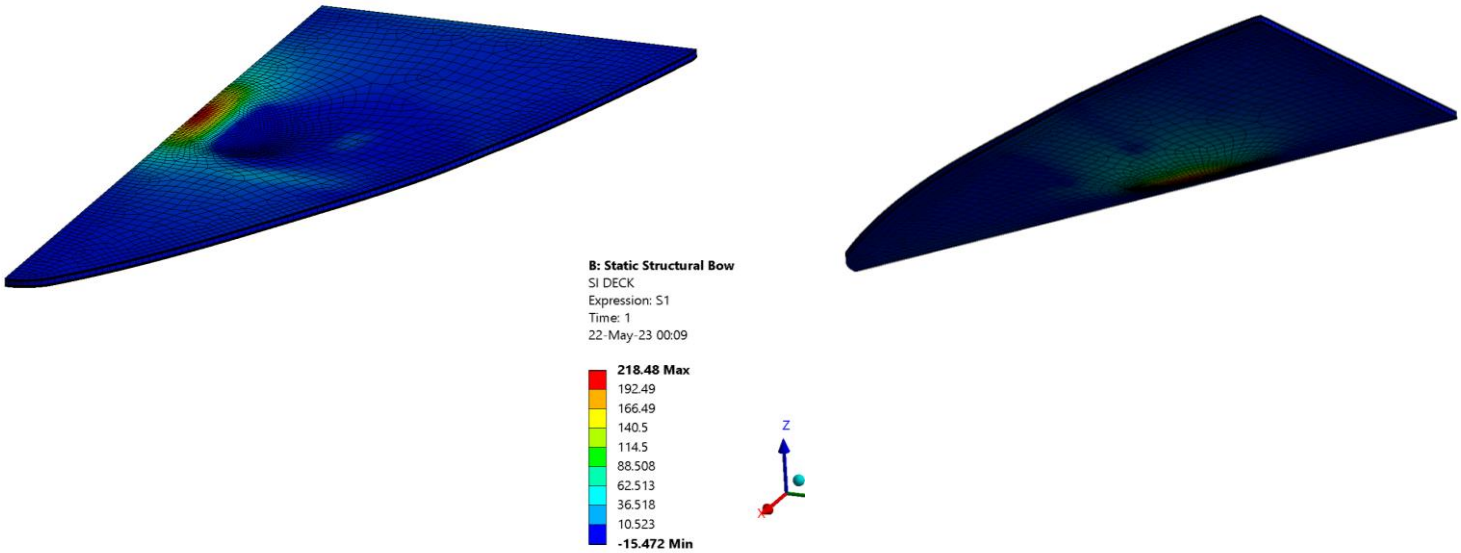

Figure 80:Model(A): Principal Stresses SI of Deck

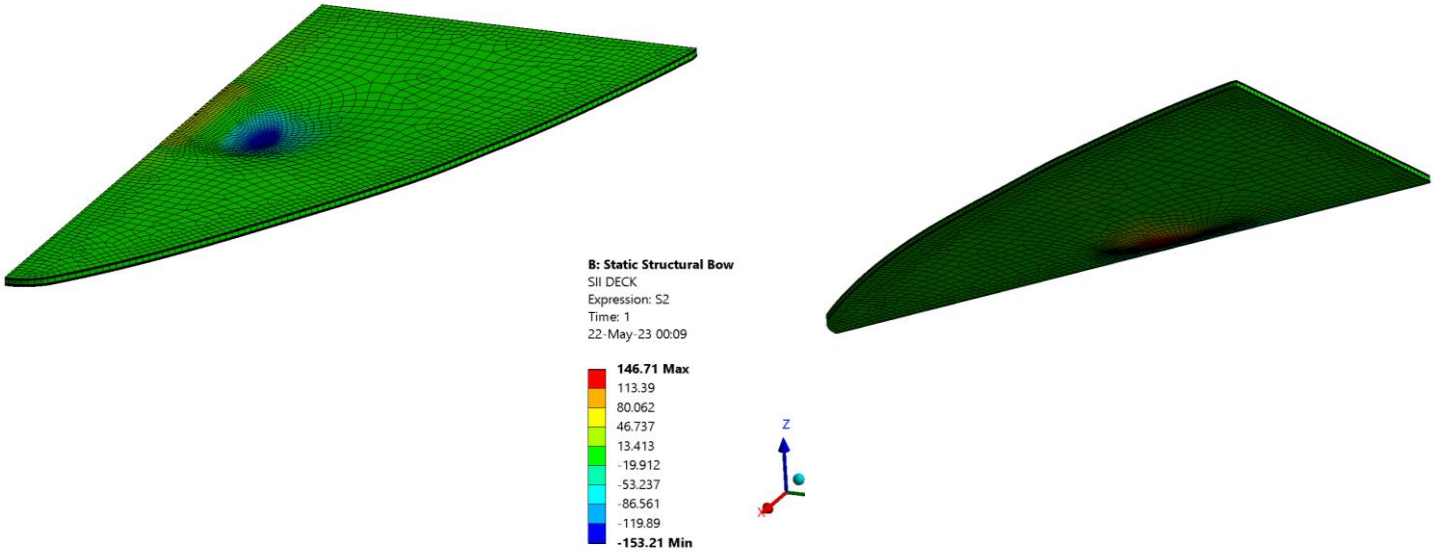

Figure 81:Model(A): Principal Stresses SII of Deck

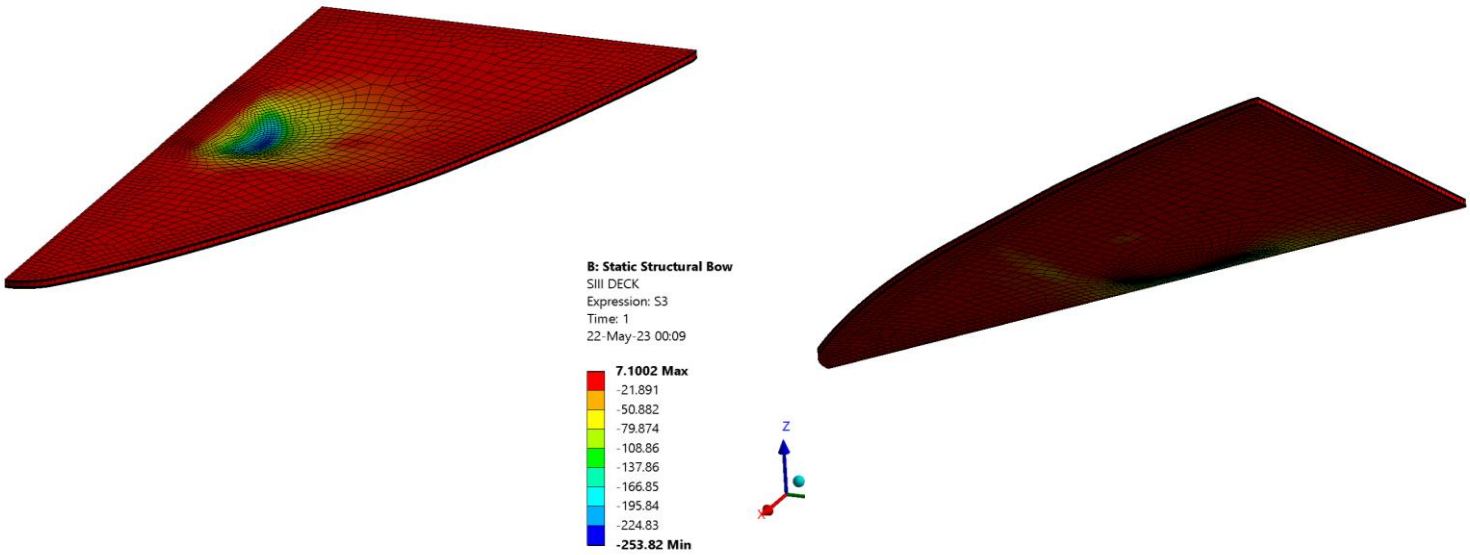

Figure 82:Model(A): Principal Stresses SIII of Deck

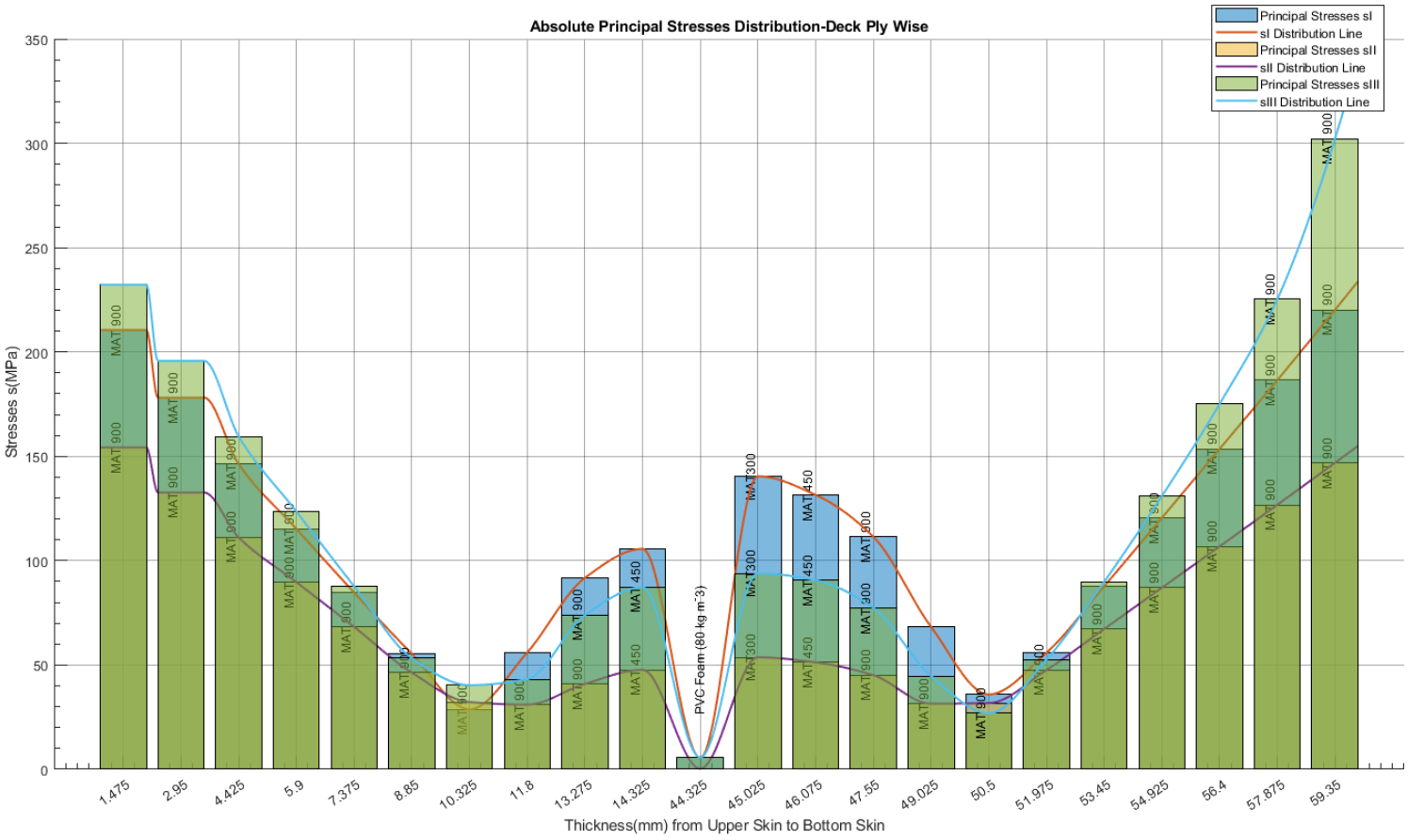

Figure 83: Model(A): Absolute Principal Stresses Distribution of Deck

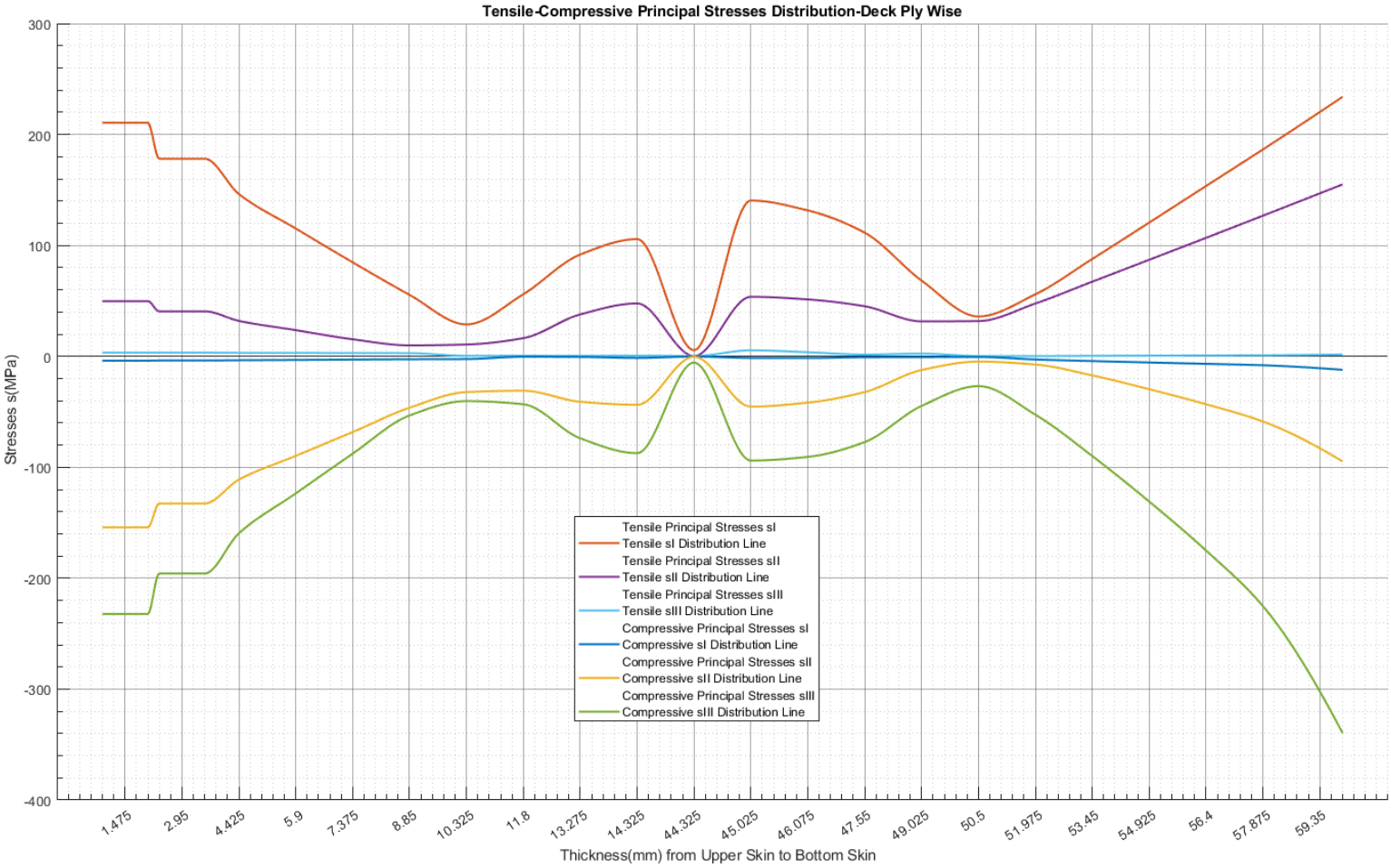

Figure 84: Model(A): Tensile-Compression Principal Stress Distribution of Deck

The principal stresses on the deck are distributed at the crane support base but are more concentrated towards the longitudinal bulkhead, as opposed to the normal and shear stresses analyzed previously. Also, approaching the core from both sides, the Maximum Principal S_I seem to prevail as maximum stresses, whereas the Maximum Principal S_I prevails towards the outside of the sandwich. Finally, as expected, the maximum stresses are the compressive Minimum Principal S_{III} and prevail at the contact of the deck with the longitudinal bulkhead.

- Model(B):

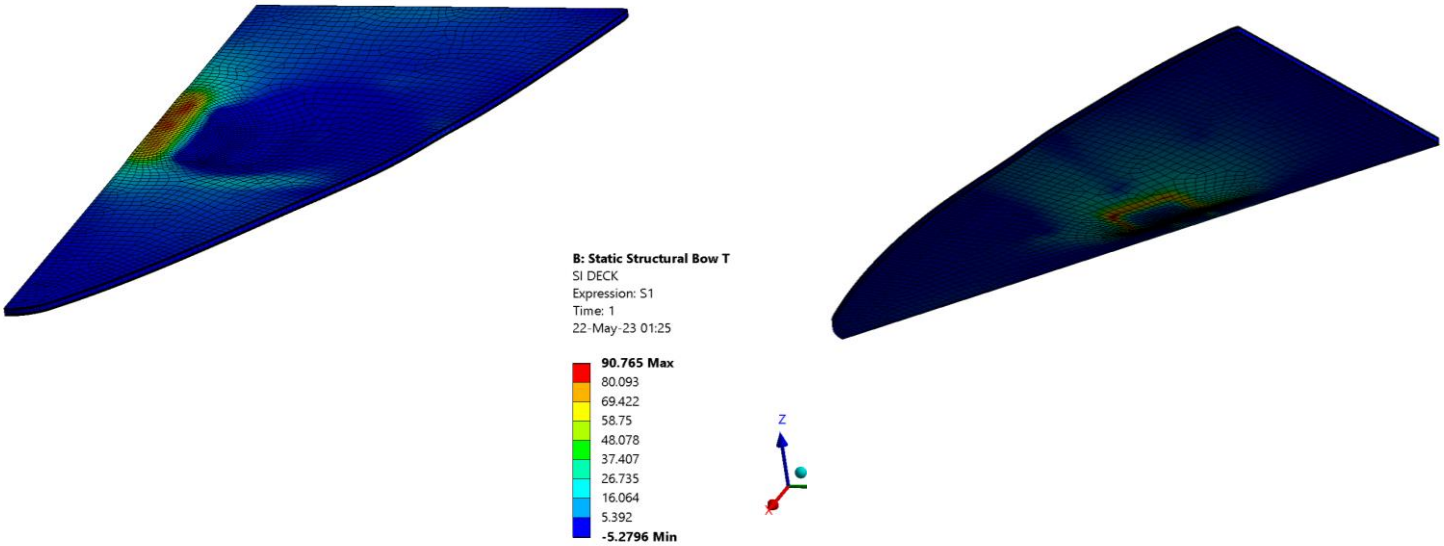

Figure 86:Model(B): Principal Stresses SI of Deck

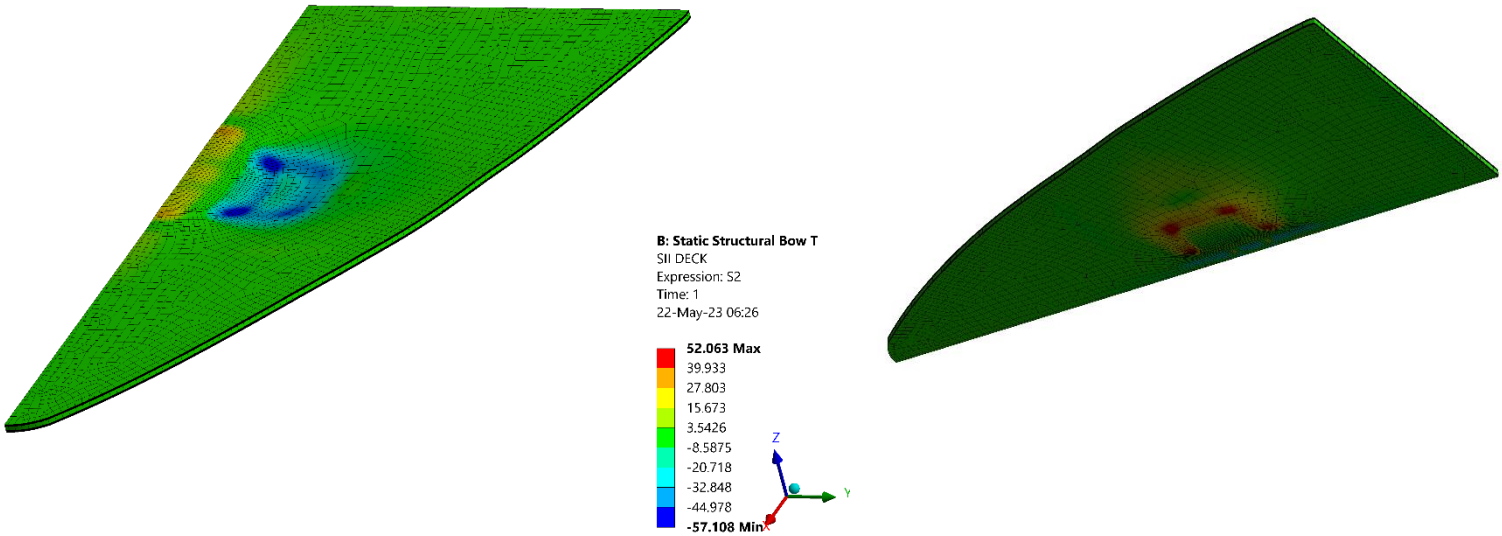

Figure 85:Model(B): Principal Stresses SII of Deck

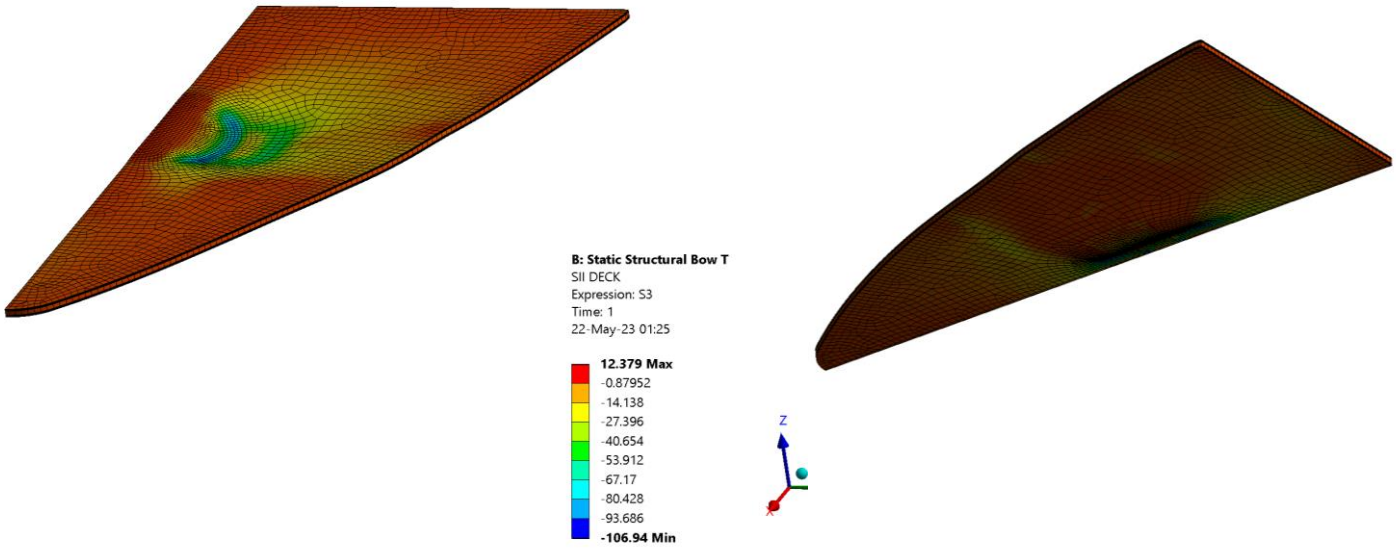

Figure 88:Model(B): Principal Stresses SIII of Deck

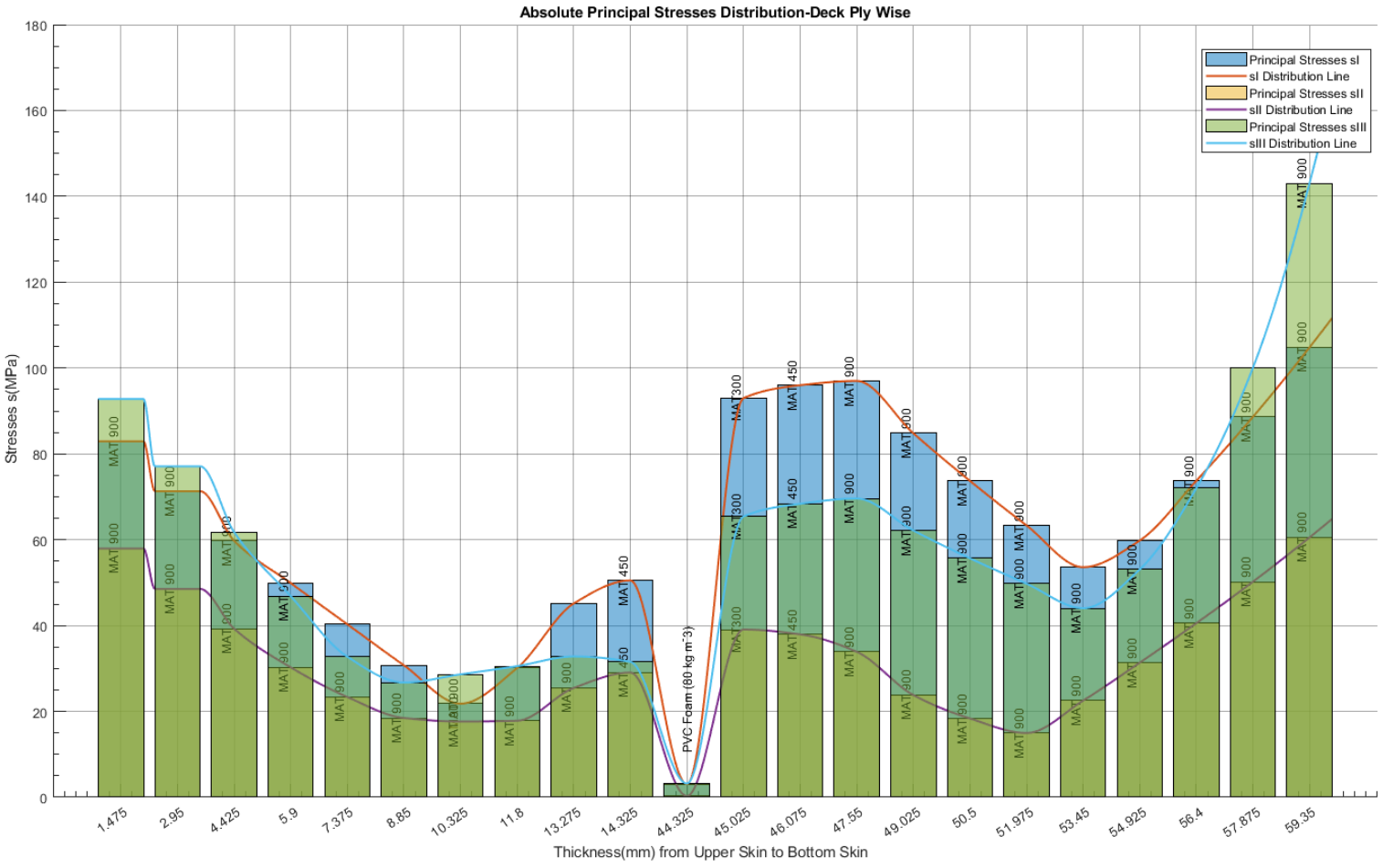

Figure 87: Model(B): Absolute Principal Stresses Distribution of Deck

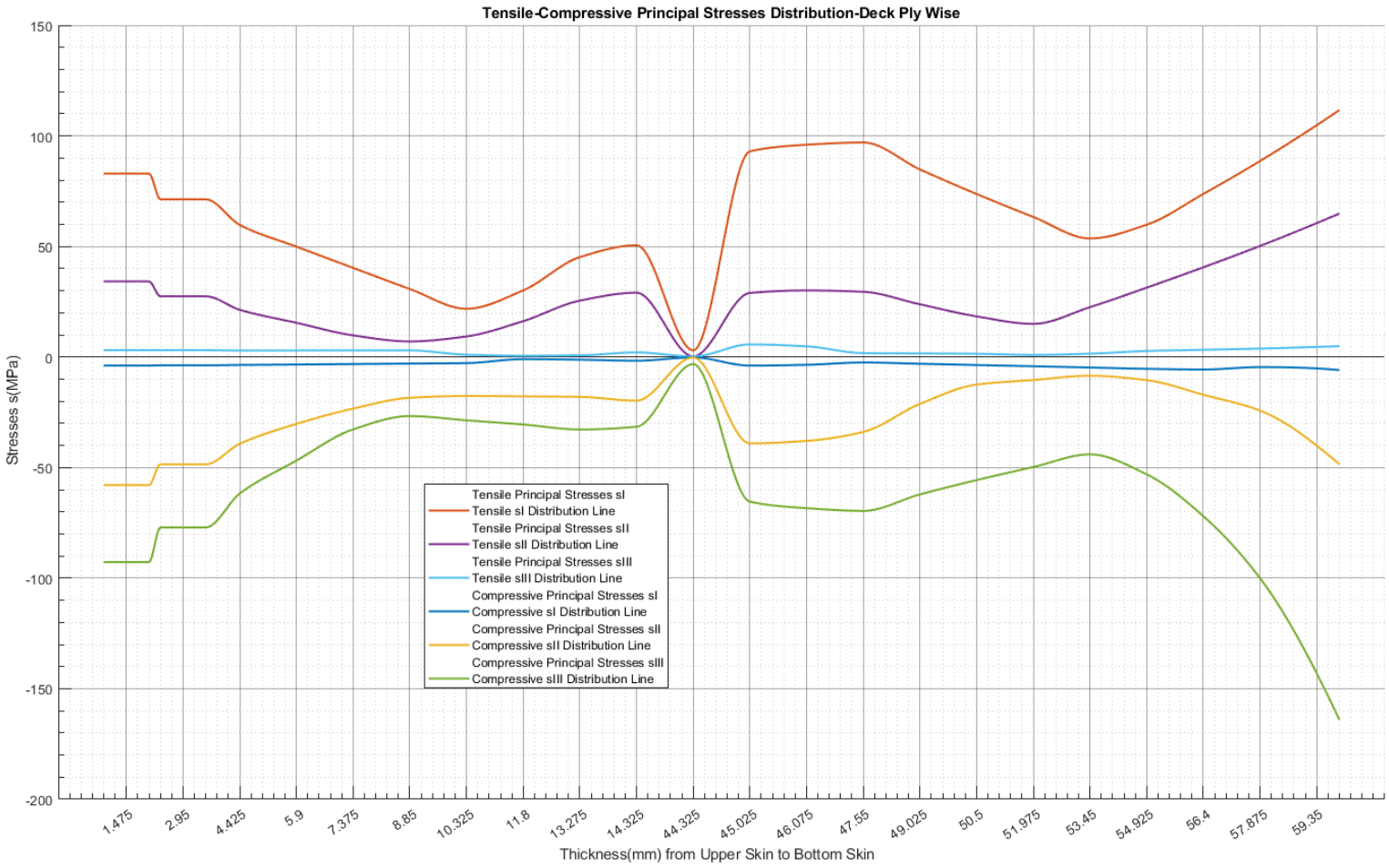

Figure 89: Model(B):Tensile-Compression Principal Stress Distribution of Deck

For Model(B), it is observed that the distribution of stresses in the finite elements around the T-Joint is smooth. In this region, the upper skin of the sandwich is subjected to compression, while the bottom skin is subjected to tension, which is perfectly reasonable. The distribution pattern is similar to Model(A), showing reduced maximum values from about 300MPa to 140MPa. Also, a decrease in compressive S_I, S_{II} and S_{III} of 58.7%,64% and 58% accordingly exists.

Finally, the same layers appear to present high tensile and compressive stresses simultaneously. This occurs in different regions. For example, the tensile stresses occur above the longitudinal bulkhead region, while the compressive stresses occur above the T-Joint region.

5.3.4 T-Joint Reinforcement

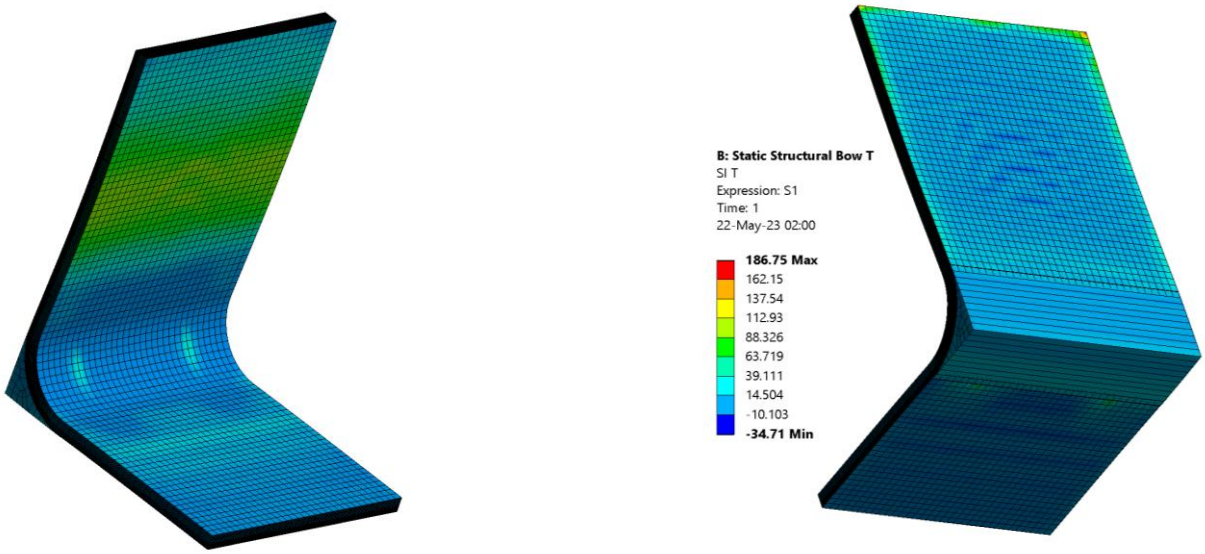

Figure 90:Model(B): Principal Stresses SI of T-Joint reinforcement

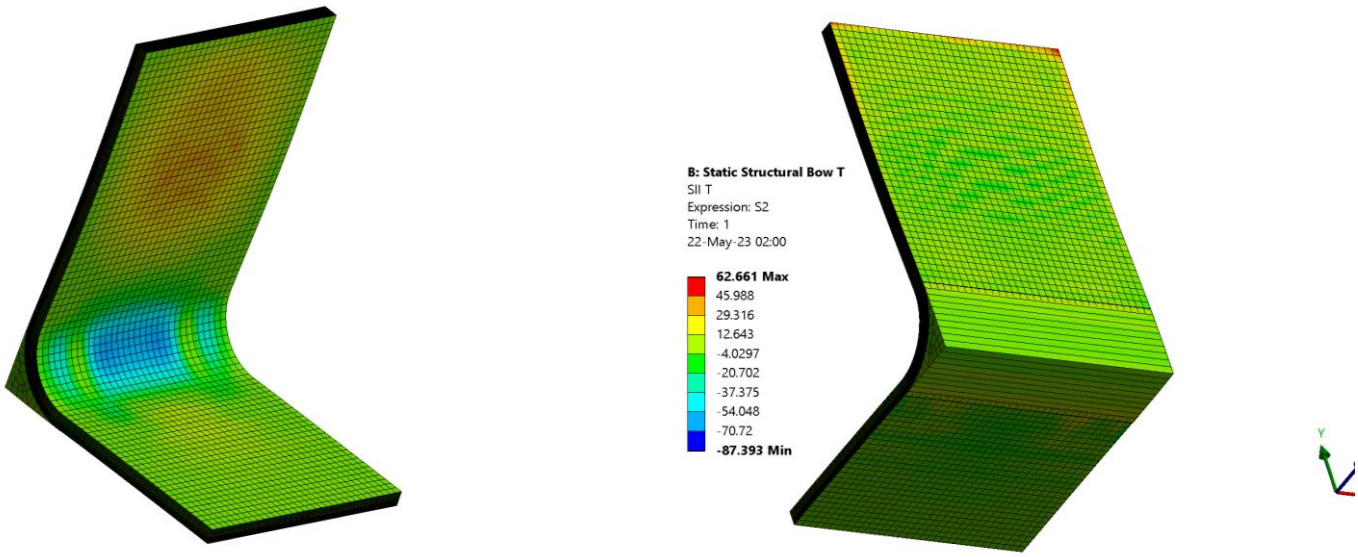

Figure 91:Model(B): Principal Stresses SII of T-Joint reinforcement

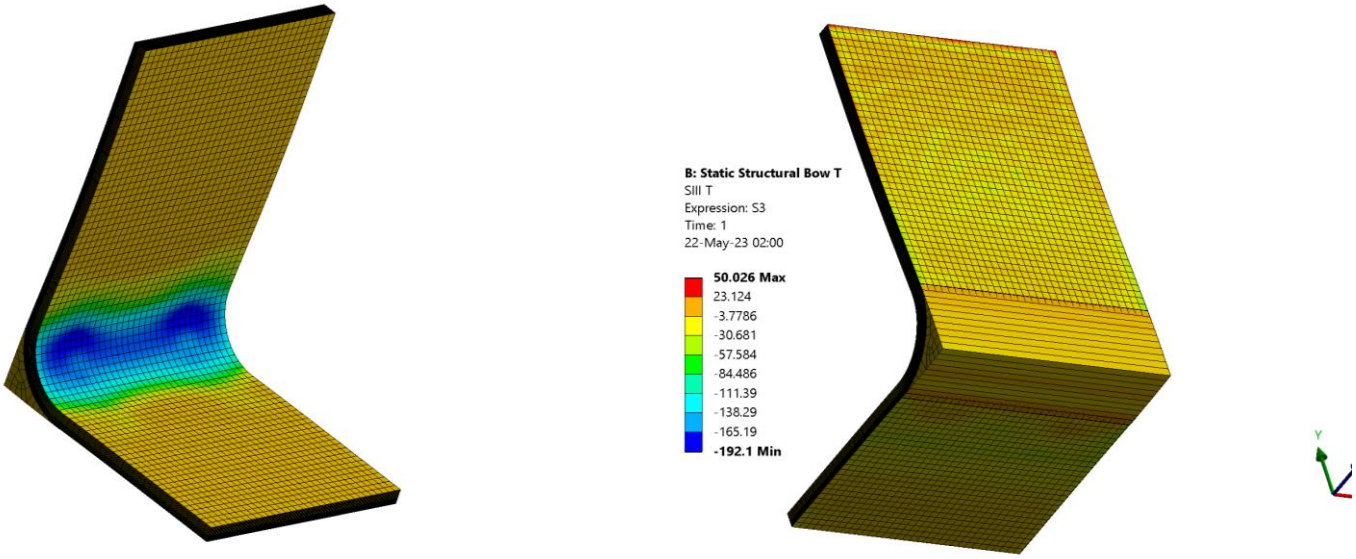

Figure 92:Model(B): Principal Stresses SIII of T-Joint reinforcement

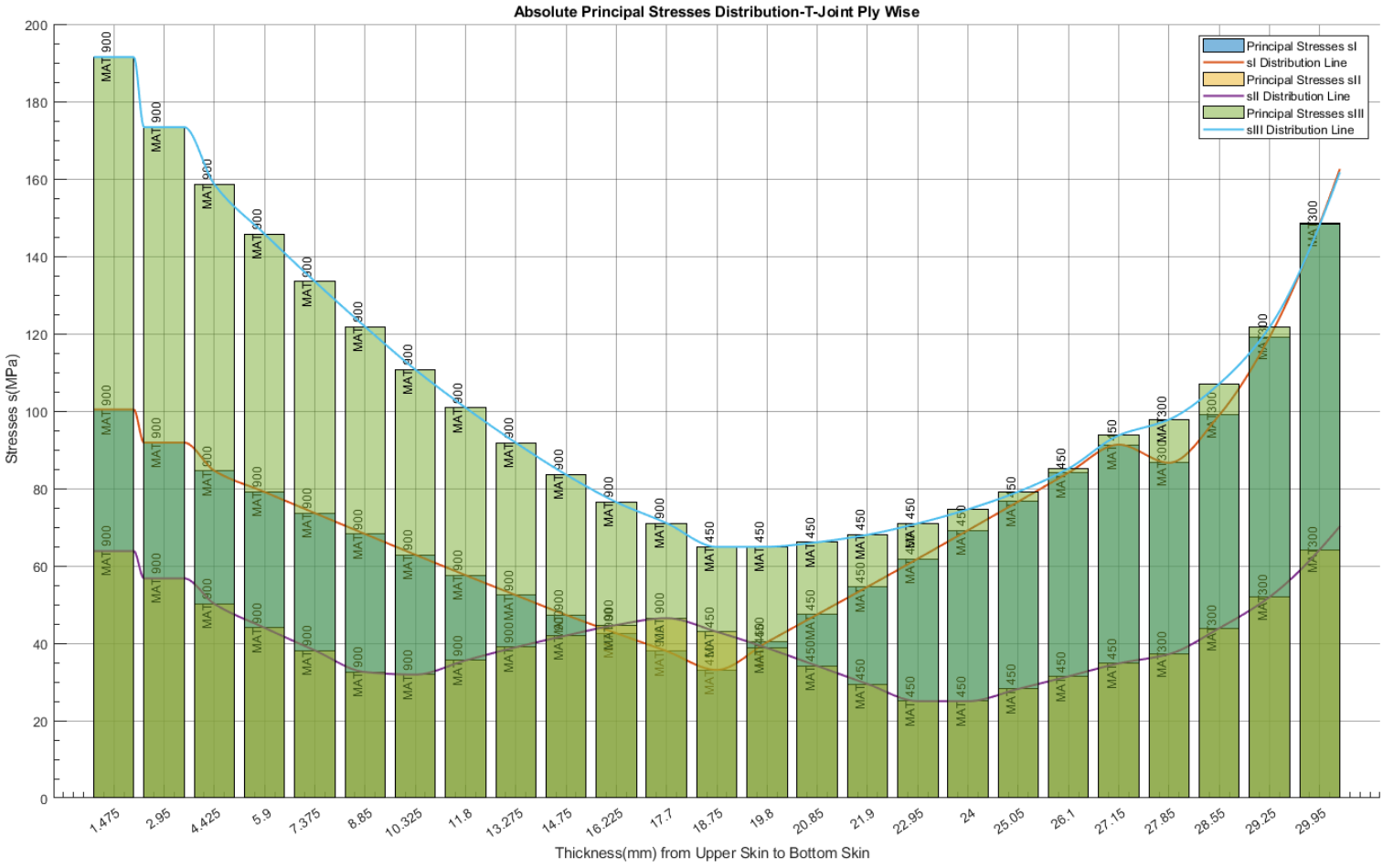

Figure 93: Model(B): Absolute Principal Stresses Distribution of T-Joint reinforcement

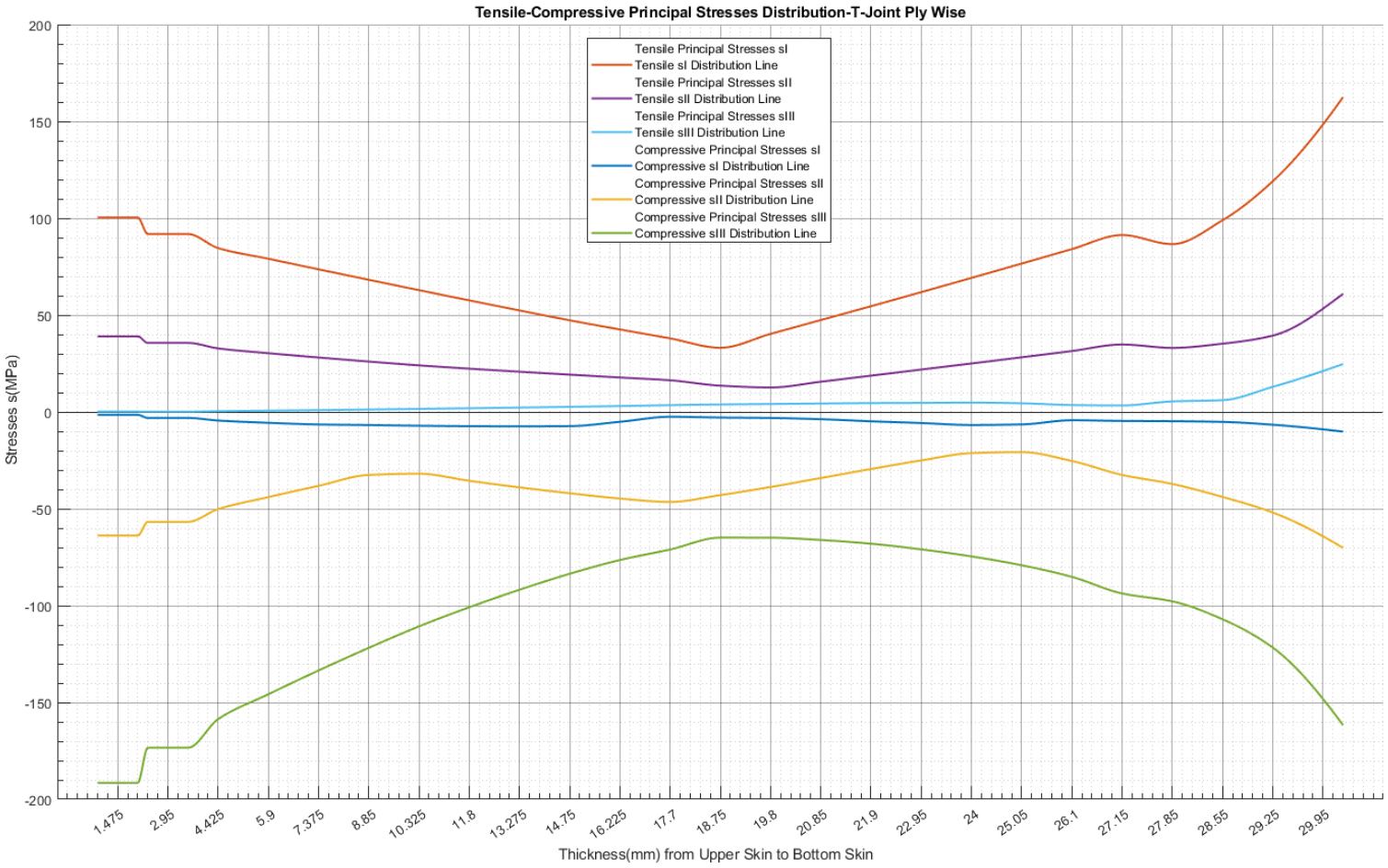

Figure 94: Model(B): Tensile-Compression Principal Stress Distribution of T-Joint reinforcement

According to the Figures (91-95), the stress region at the T-Joint reinforcement is at the fillet, due to principal stresses. Regarding the Maximum SI and Middle SII principal stresses, there is an increase towards the center of the T-Joint overlamination. However, the dominant stress with the highest value for the outer skins is the compressive S_{III}. As it can be seen from the stress distribution, the T-Joint is more likely to fail due to compression, rather than tension.

The stress concentration in this component is still at the acute edge between the T-Joint and deck. Also, in the middle of the plies, and specifically at the last MAT900, there is an unusual increase in the Middle Principal S_{II} stress which is worth investigating for the same reason as the decrease in the Maximum Principal S_I stress at MAT300 when changing from MAT450. Thus, the plies mentioned are presented as following:

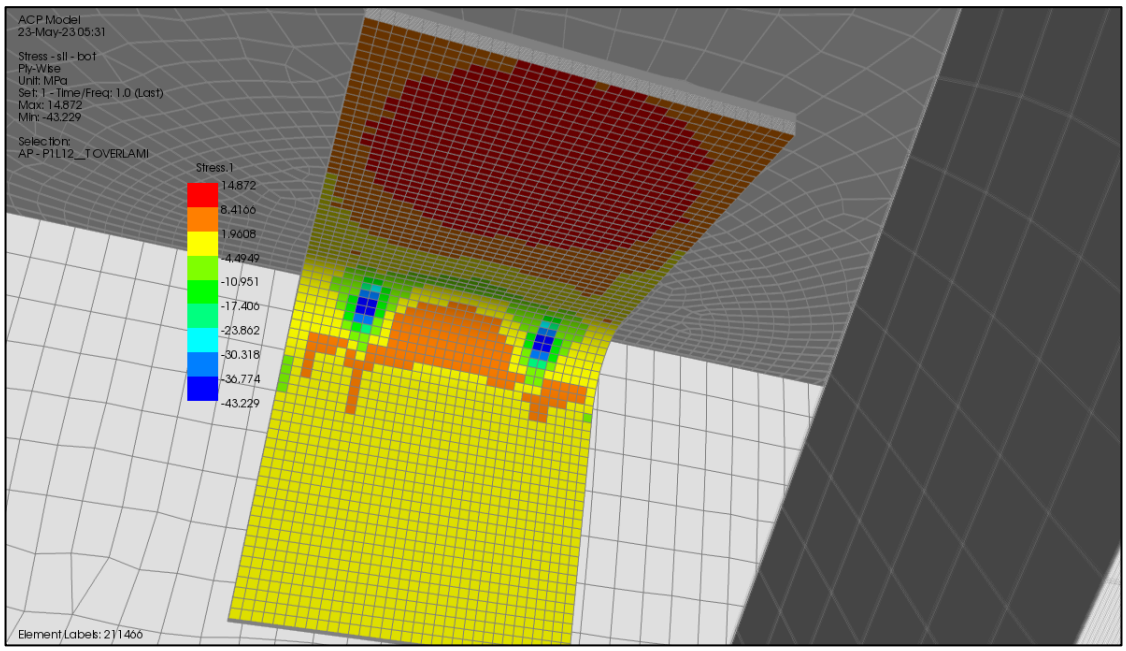

Figure 95:Model(B):MAT900 SII Stress increment

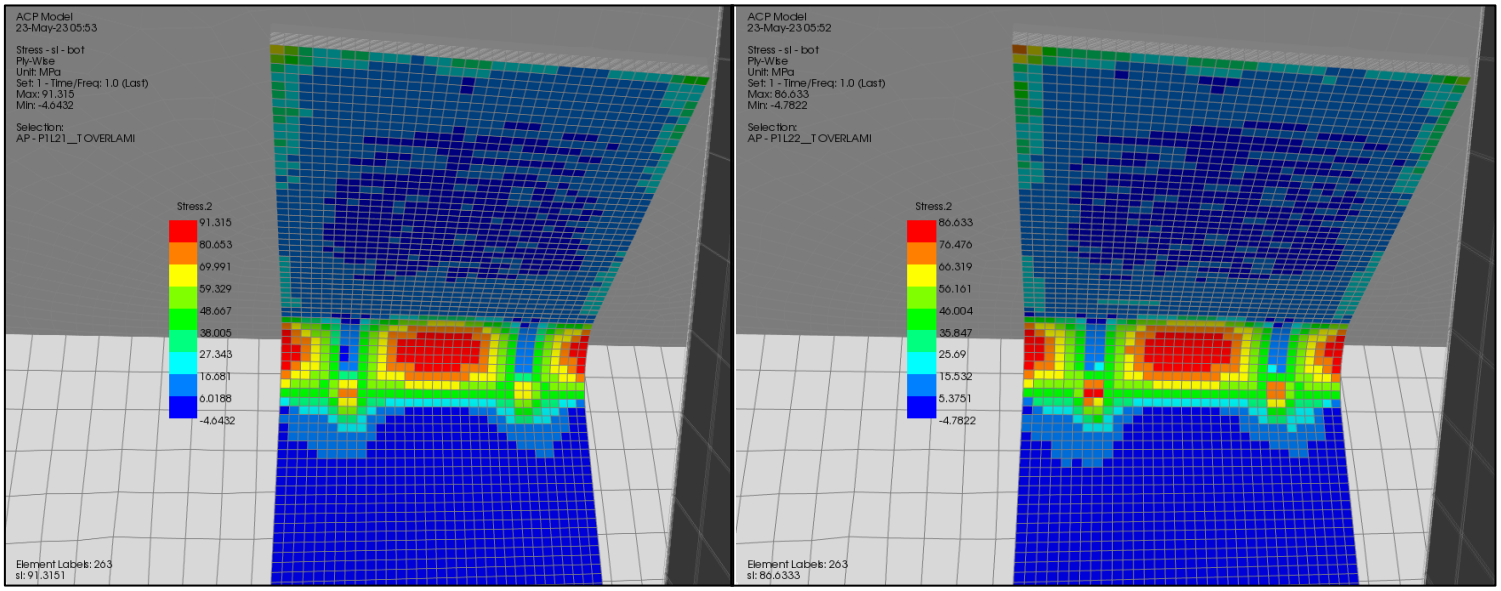

Figure 96:MATT450(Right) to MAT300(Left) SI reduction

This observation is noteworthy, since in all cases the points where the decrease or increase phenomenon occurs, are not stress concentration points. However, at the points where this phenomenon is observed, their common characteristic is the change in the layer material. One explanation for this is that the change in the layer material implies a change in the compliance matrix [S] of the elements, and therefore a variation in the values at these points. These observations will be equally useful when studying the failure based on the Tsai-Wu Failure Criterion.

5.4 Tsai-Wu Failure Safety Factor

An analytical method often used to predict the failure of composite materials is the Tsai-Wu failure criterion. It is a quadratic equation that takes into consideration both material strength in tension and compression as well as interactions between various stress components. Using this criterion may estimate possible failure locations in a composite material by comparing the Tsai-Wu failure index to a threshold value.

5.4.1 Bow Region

- Model(A):

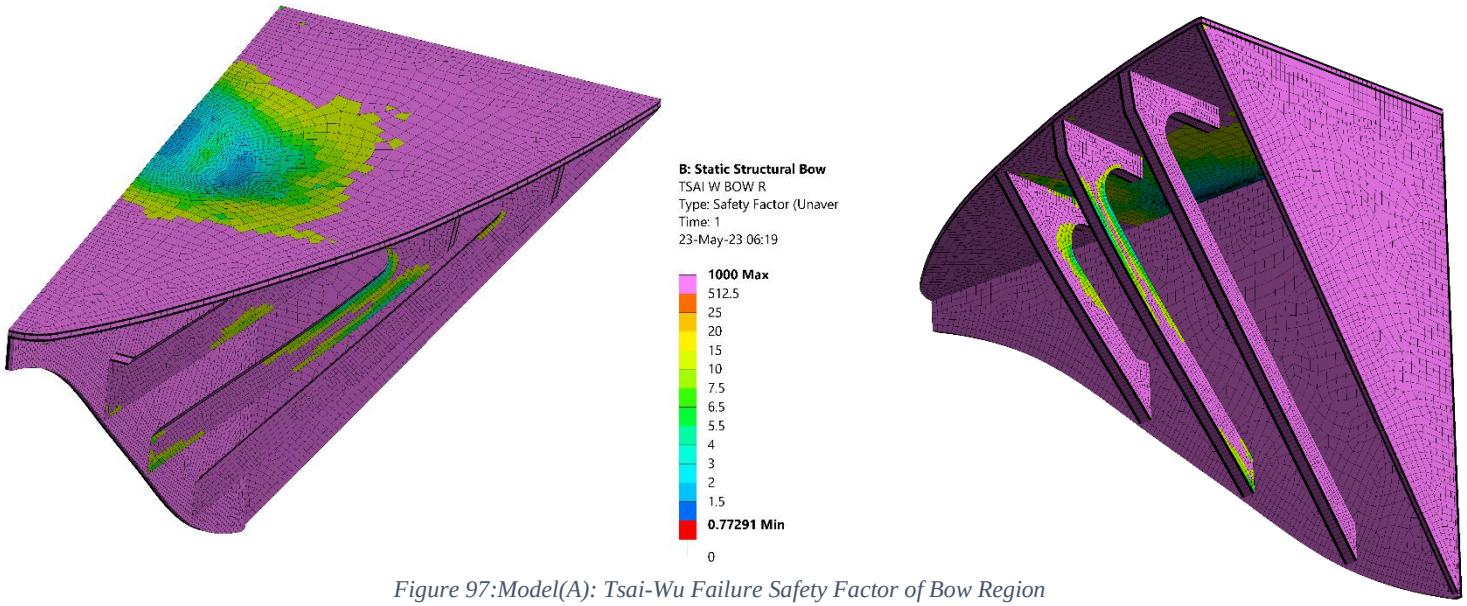

Figure 97:Model(A): Tsai-Wu Failure Safety Factor of Bow Region

- Model(B):

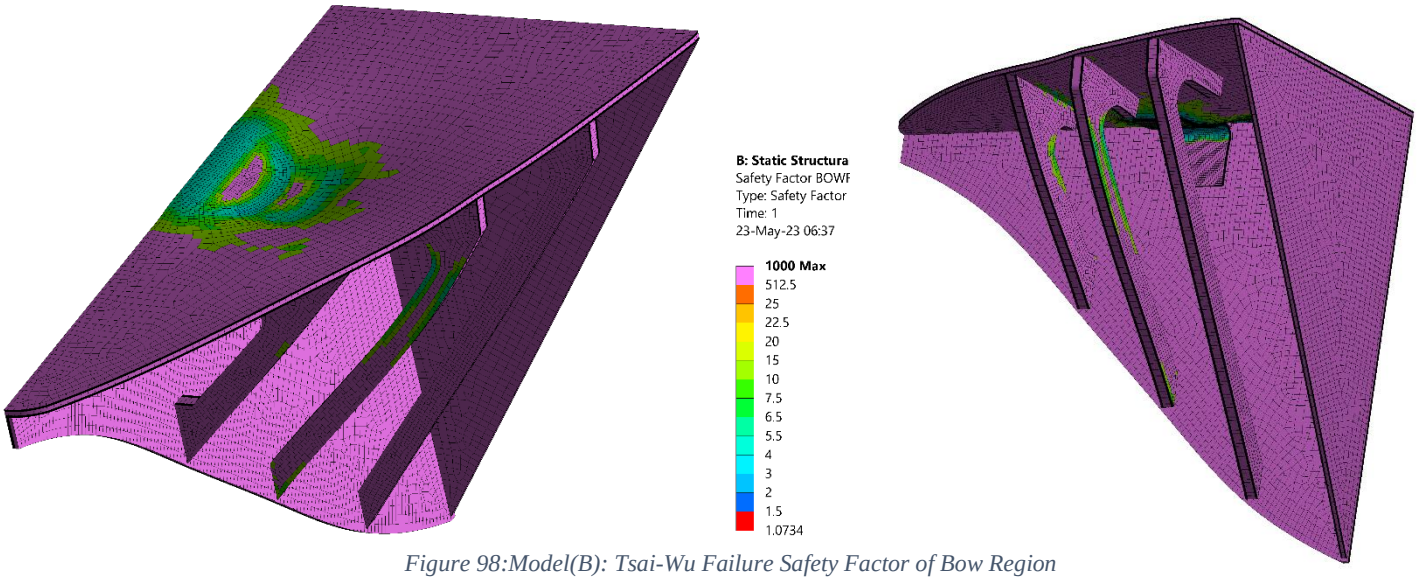

Figure 98:Model(B): Tsai-Wu Failure Safety Factor of Bow Region

The insertion of a T-Joint reinforcement in the structure implies an increase in the Tsai-Wu Failure Safety Factor, i.e., the structure becomes safer. An initial look shows that some component of Model(A) fails, since the Safety Factor becomes less than unity, while Model(B) is marginally safe.

5.4.2 Middle Frame

The potential failure points for the frame are determined by Tsai-Wu using the normal and shear stress results.

- Model(A):

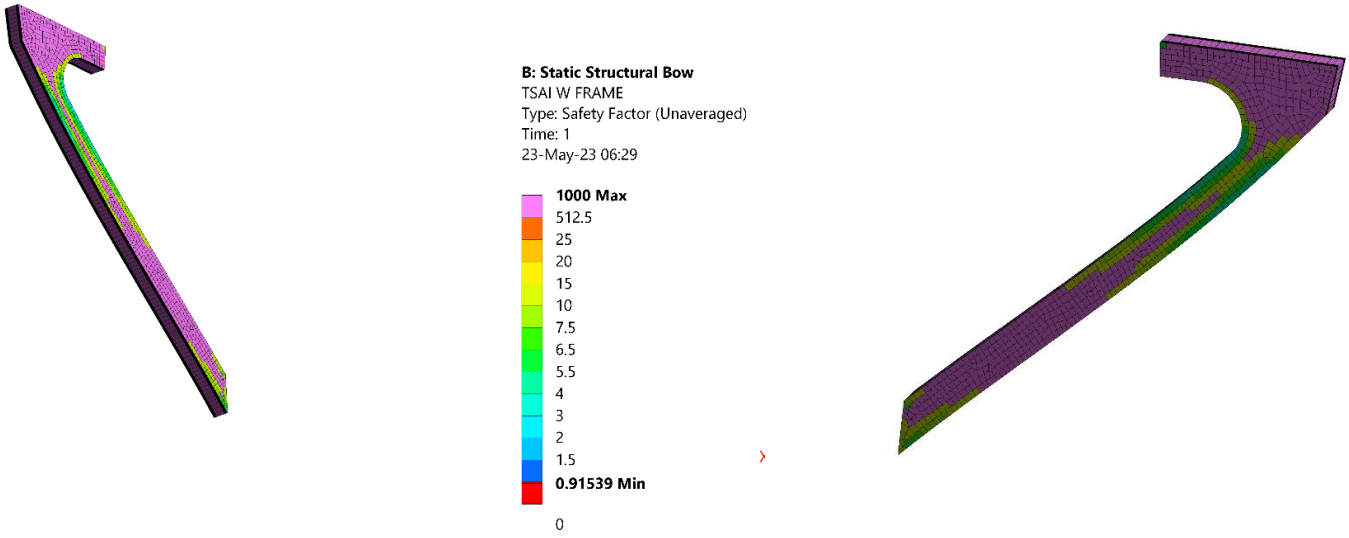

Figure 99:Model(A): Tsai-Wu Failure Safety Factor of Middle Frame

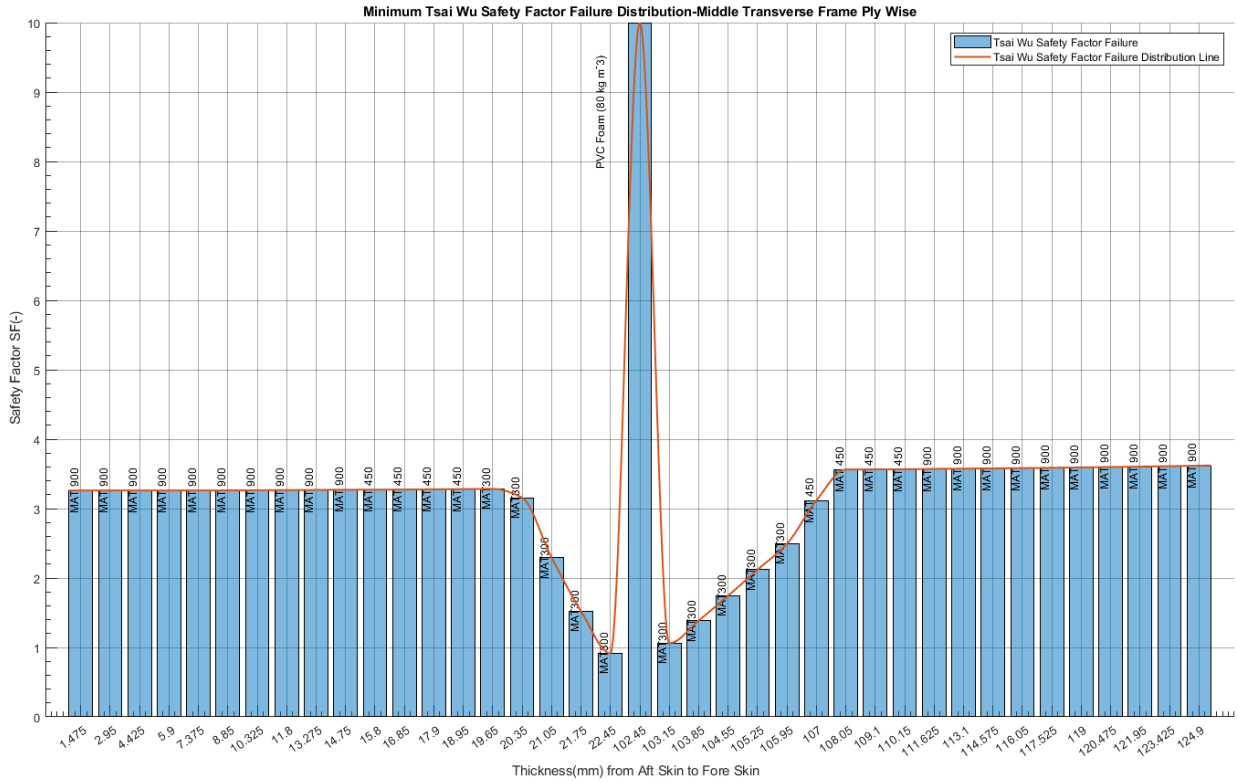

Figure 100: Model(A): Absolute Tsai-Wu Failure Safety Factor Distribution of Middle Frame

According to the above, the failure is in some ply of the structure which should be investigated in depth. The ply which seems to fail is MAT300 next to the core, as shown in Figure 102:

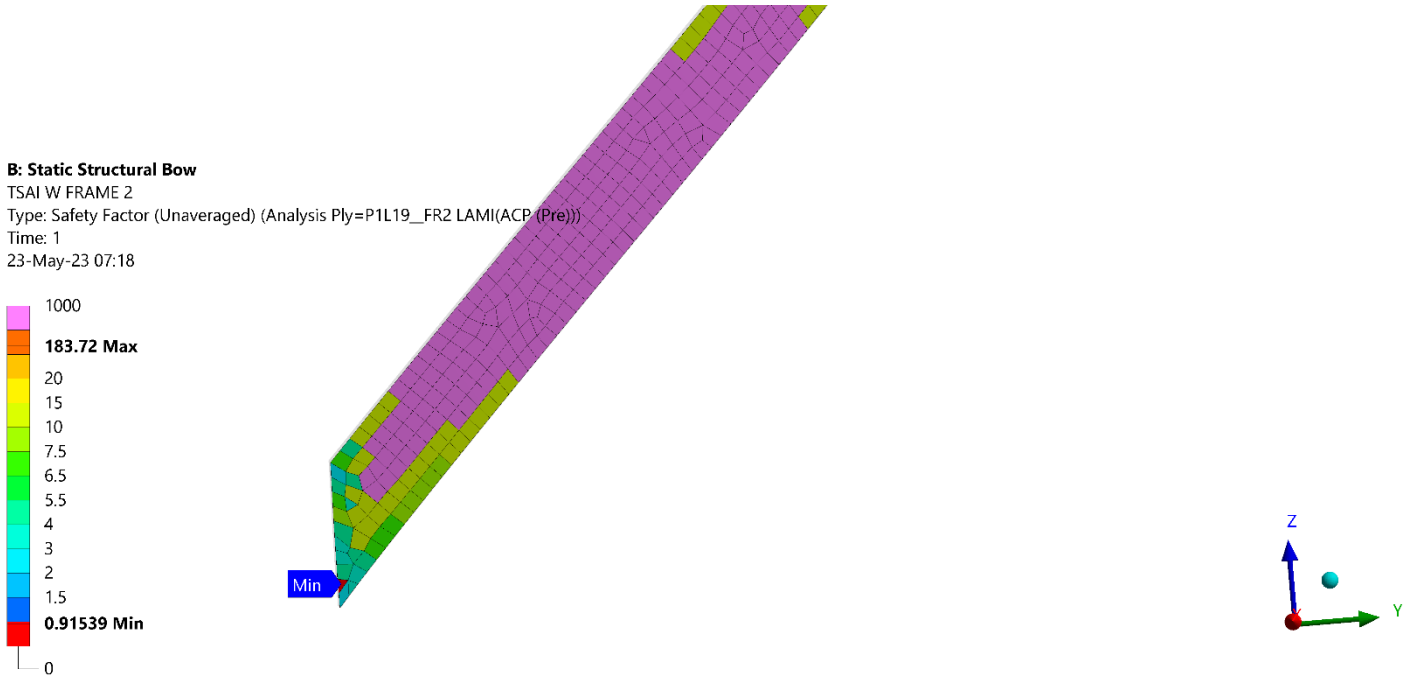

Figure 101:Model(A):Tsai-Wu Ply Failure Examination

This failure is located to a single element close to a free edge therefore it cannot be taken into account for the safety factor evaluation.

With this observation there is serious evidence that Model(A) does not actually fail as it initially appeared. Based on the smooth distributions of the safety factor, its value is found to be approximately 3 for the transverse middle frame.

- Model(B):

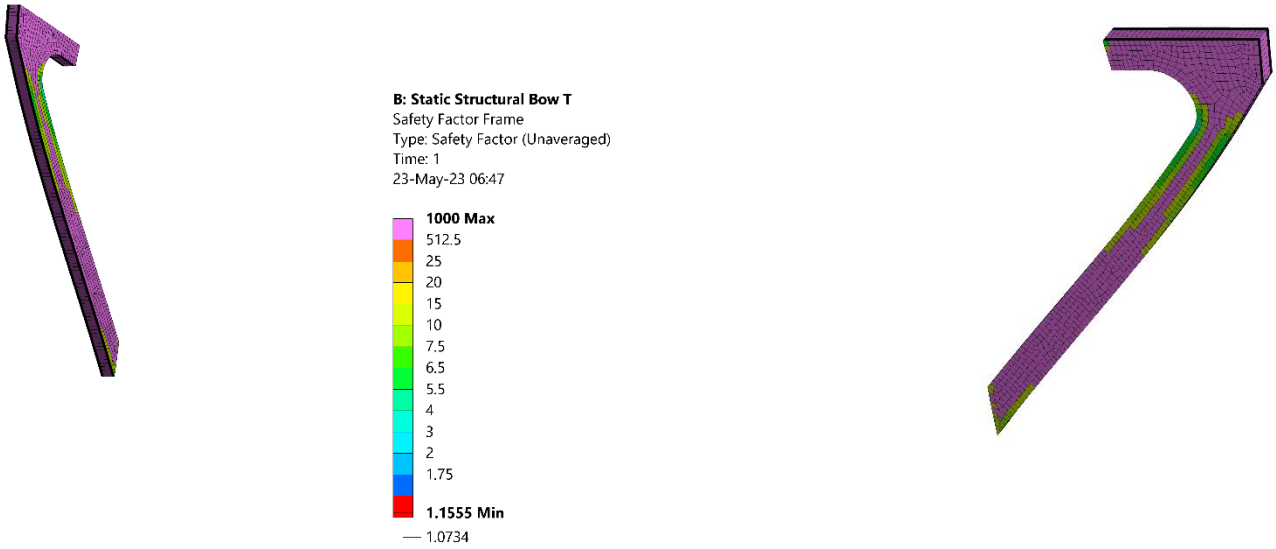

Figure 103:Model(B): Tsai-Wu Failure Safety Factor of Middle Frame

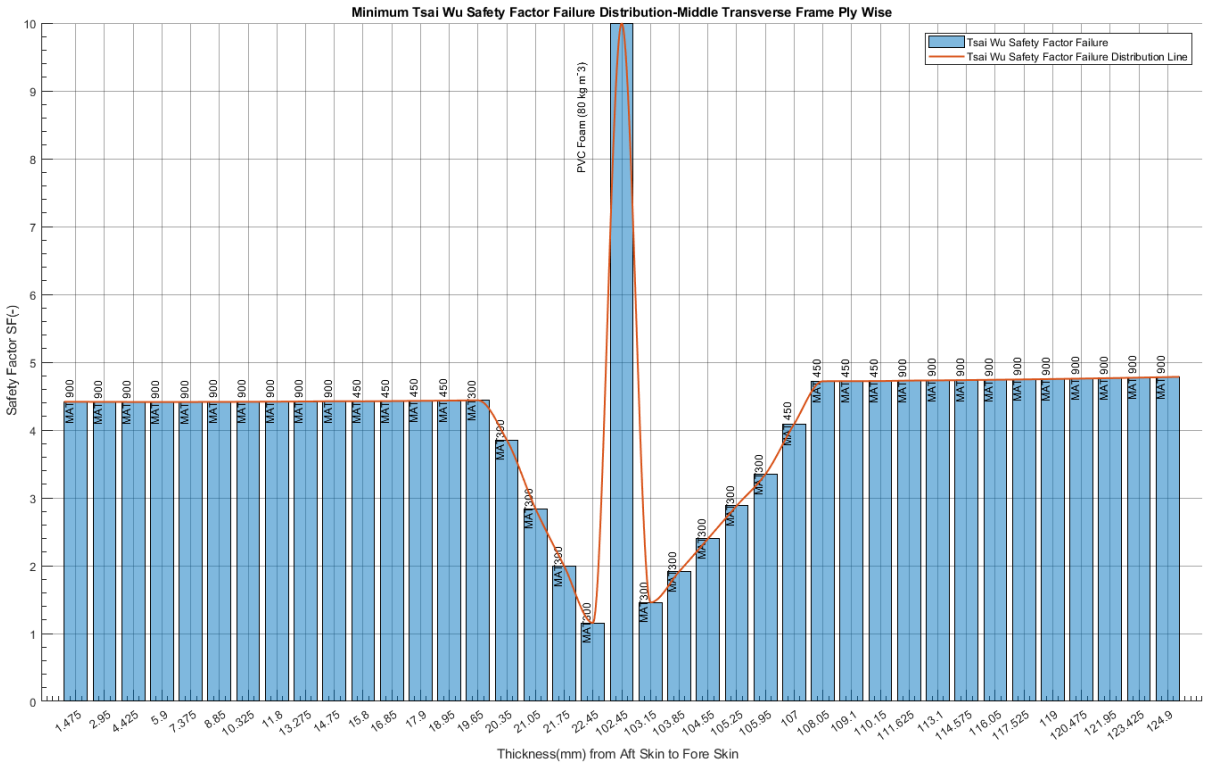

Figure 102: Model(B): Absolute Tsai-Wu Failure Safety Factor Distribution of Middle Frame

In MAT300 of Model(B) the same phenomenon of safety factor reduction occurs as in Model(A). With the exception of these values and as shown in the diagram, the value of the Tsai-Wu Failure Safety Factor is around 4.5, an increase of 1.5 units compared to Model(A).

5.4.3 Deck

The minimum value of the Tsai-Wu safety factor is expected to be at the point where the deck is subject to the largest stresses.

- Model(A):

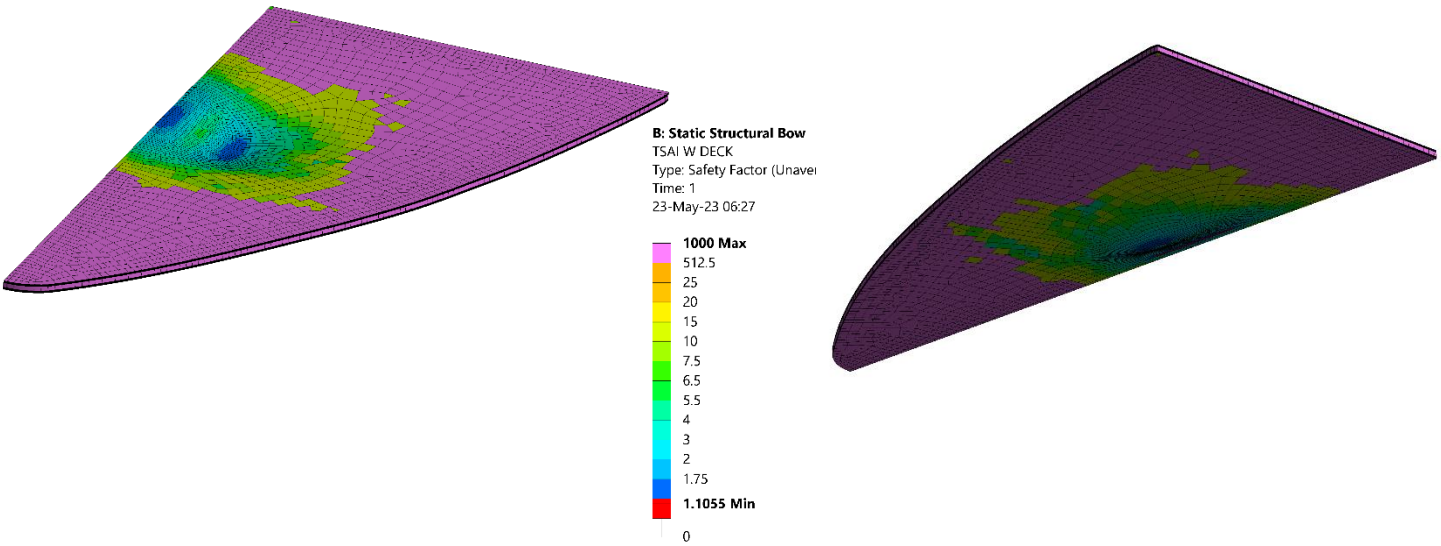

Figure 104:Model(A): Tsai-Wu Failure Safety Factor of Deck

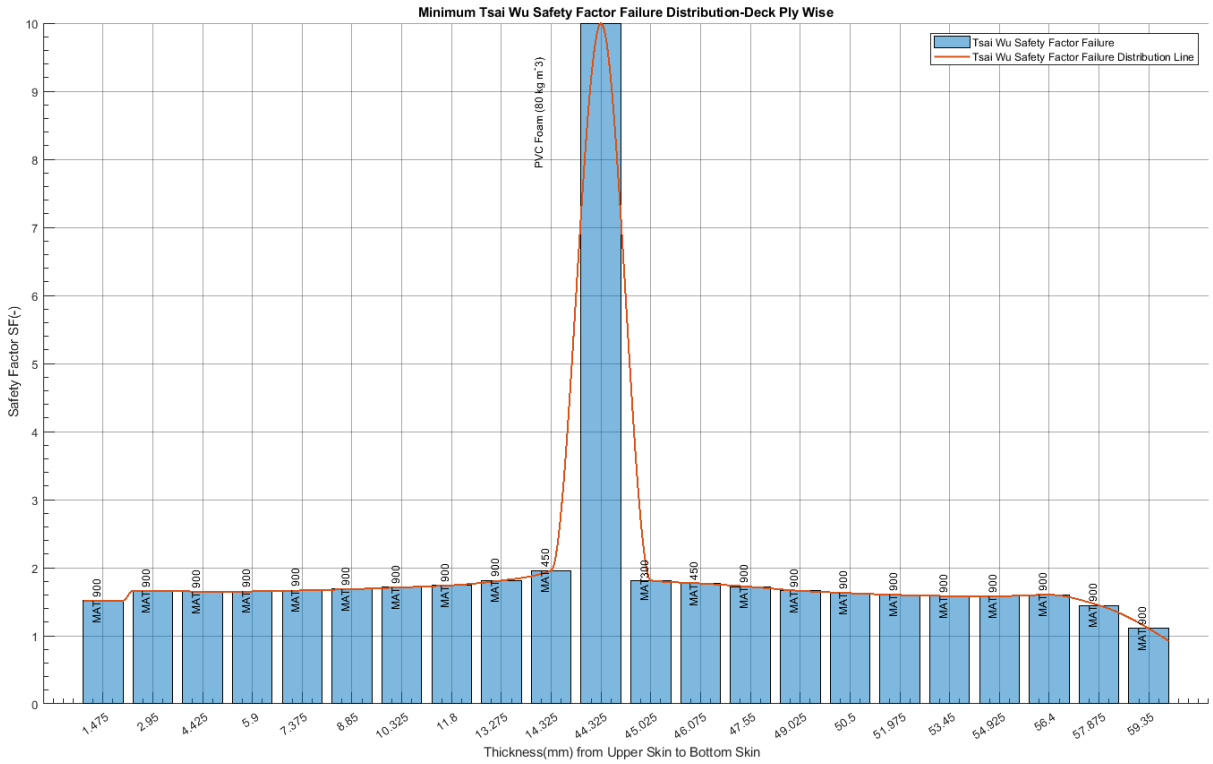

Figure 105: Model(A): Absolute Tsai-Wu Failure Safety Factor Distribution of Deck

- Model(B):

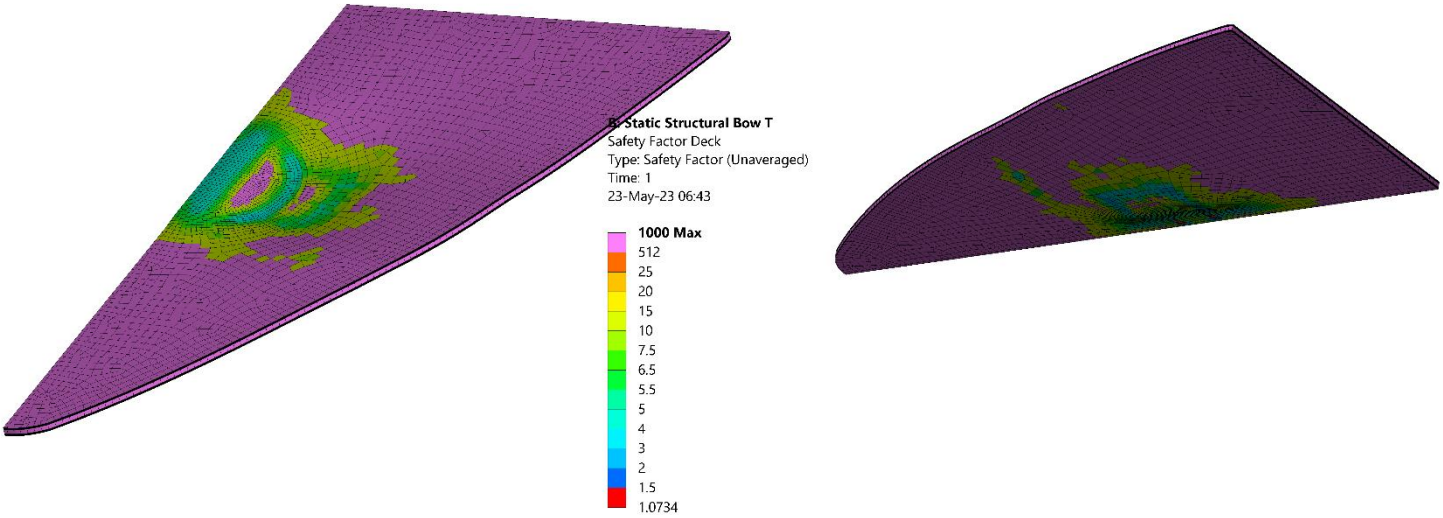

Figure 106:Model(B): Tsai-Wu Failure Safety Factor of Deck

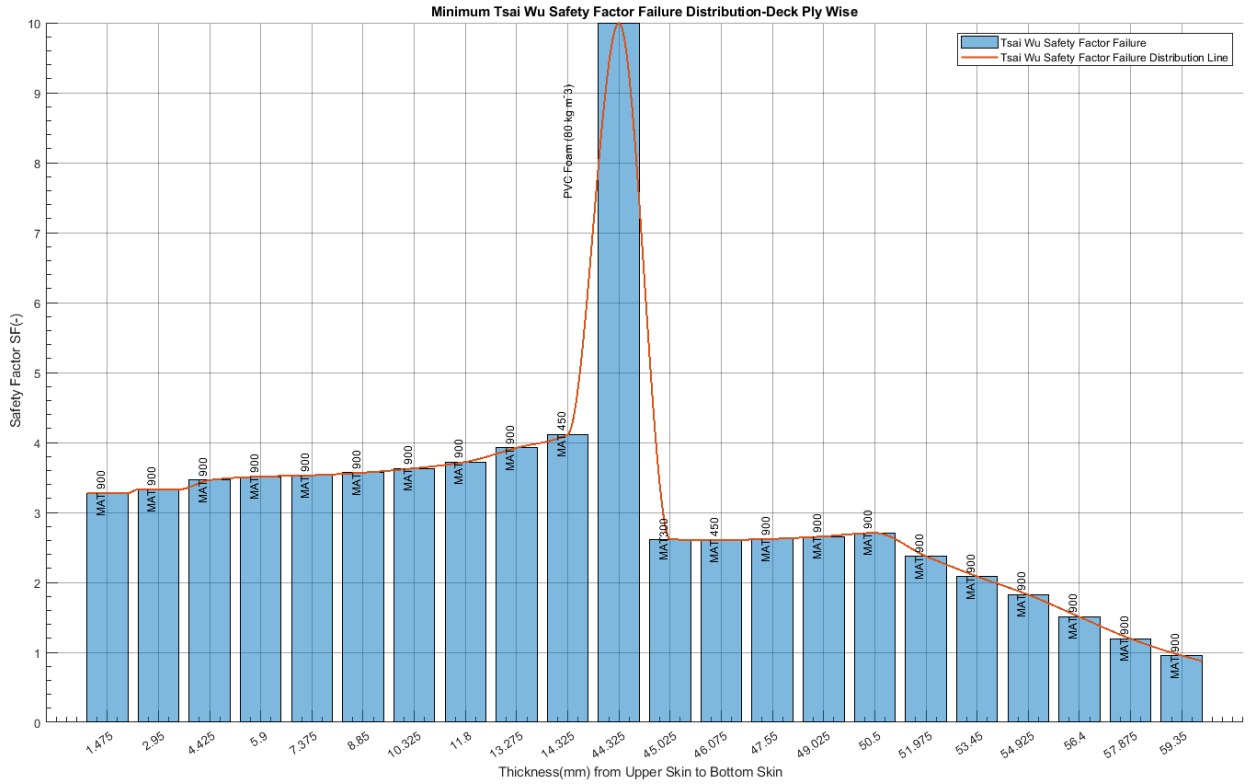

Figure 107: Model(B): Absolute Tsai-Wu Failure Safety Factor Distribution of Deck

The deck of Model(A) shows no signs of failure. In Model(B) the relief of the area underneath the T-Joint is observed. However, the safety factor decreases drastically at MAT900 which rests on the longitudinal bulkhead and needs to be investigated. Inevitably, this decrease is expected, taken into account the Principal Stresses for Model(B).

The ply MAT900 is shown in Figure 109:

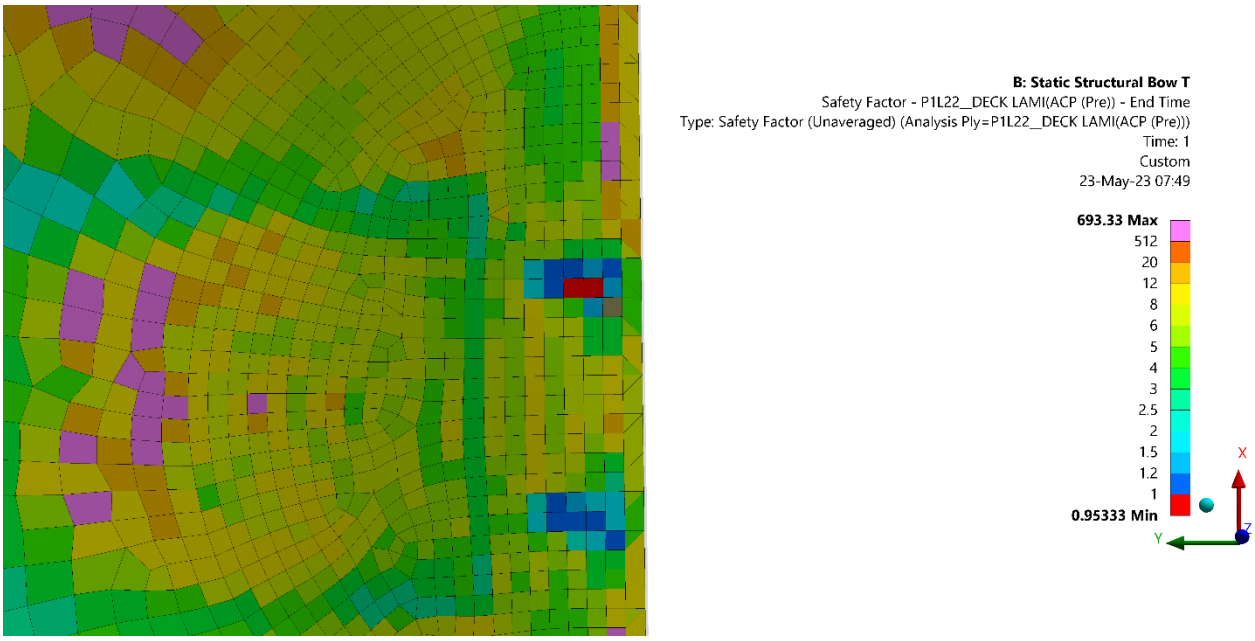

Figure 108:Model(B):Examination of Bottom Ply of Deck for Tsai Wu Failure

From this examination, it appears that the value of 0.95, of the safety factor, cannot be maintained, since only two finite elements own this value. Thus, according to the above, the value of the Tsai Wu Failure Safety Factor for the Deck of Model(B) can be modelled close to 3. For the same region, Model(A) has a safety factor of 1.5. This implies that the reinforcement by the T-Joint increased the Tsai Wu Failure Safety Factor for the Deck by 50%.

5.4.4 T-Joint Reinforcement

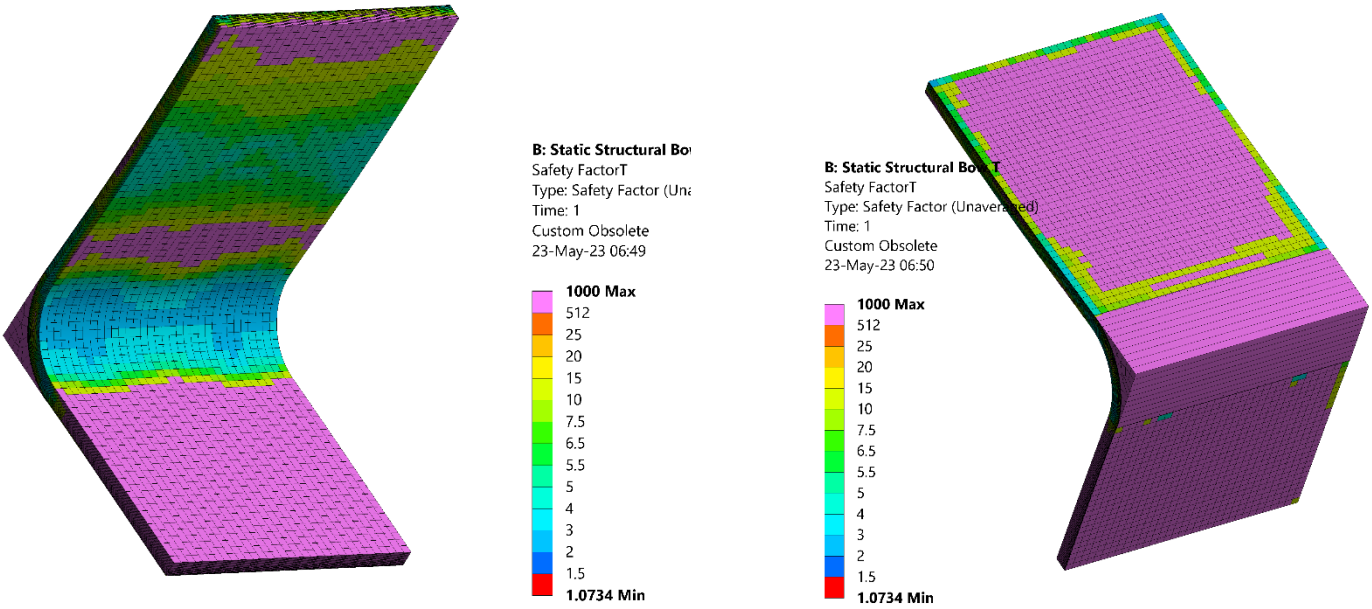

Figure 109:Model(B): Tsai-Wu Failure Safety Factor of T-Joint reinforcement

The **Error! Reference source not found.** depicts a safe state for the T-Joint while the area with the lowest safety factor is at the fillet, as expected. The lowest value of the safety factor is at ply MAT300 and is shown as following:

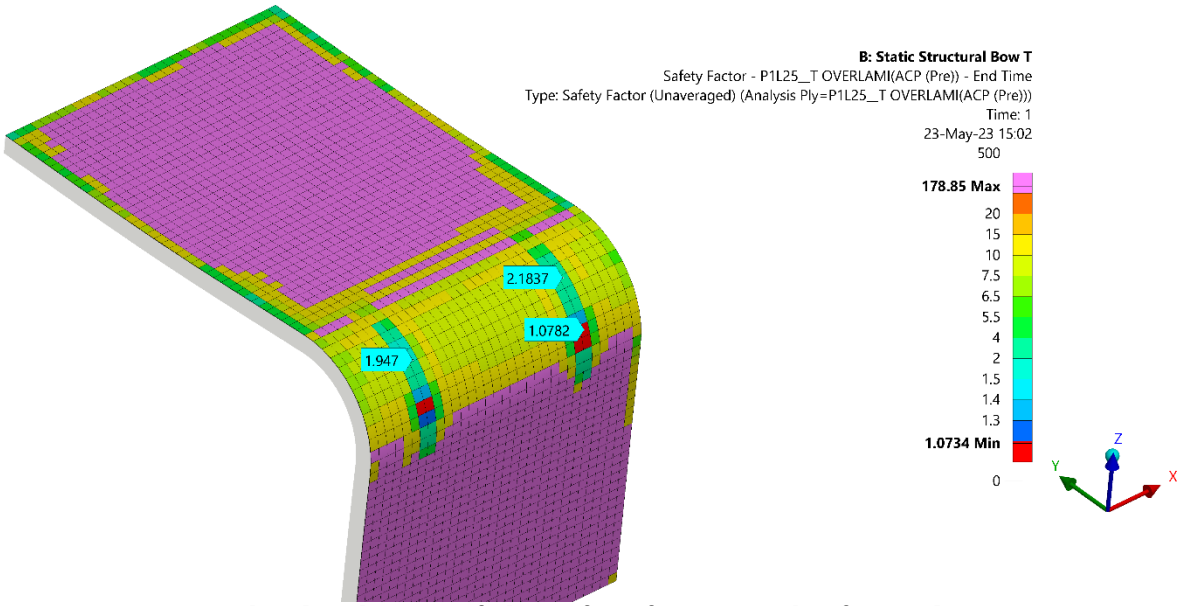

Examining again the distribution of the safety factors in the finite elements, it is observed that the minimum value of the safety factor (~1.07) is found in 6 finite elements, 2 of which are far from the rest. This is an indication that this value is not representative and is excluded. The minimum value of the safety factor is found to be around 2.

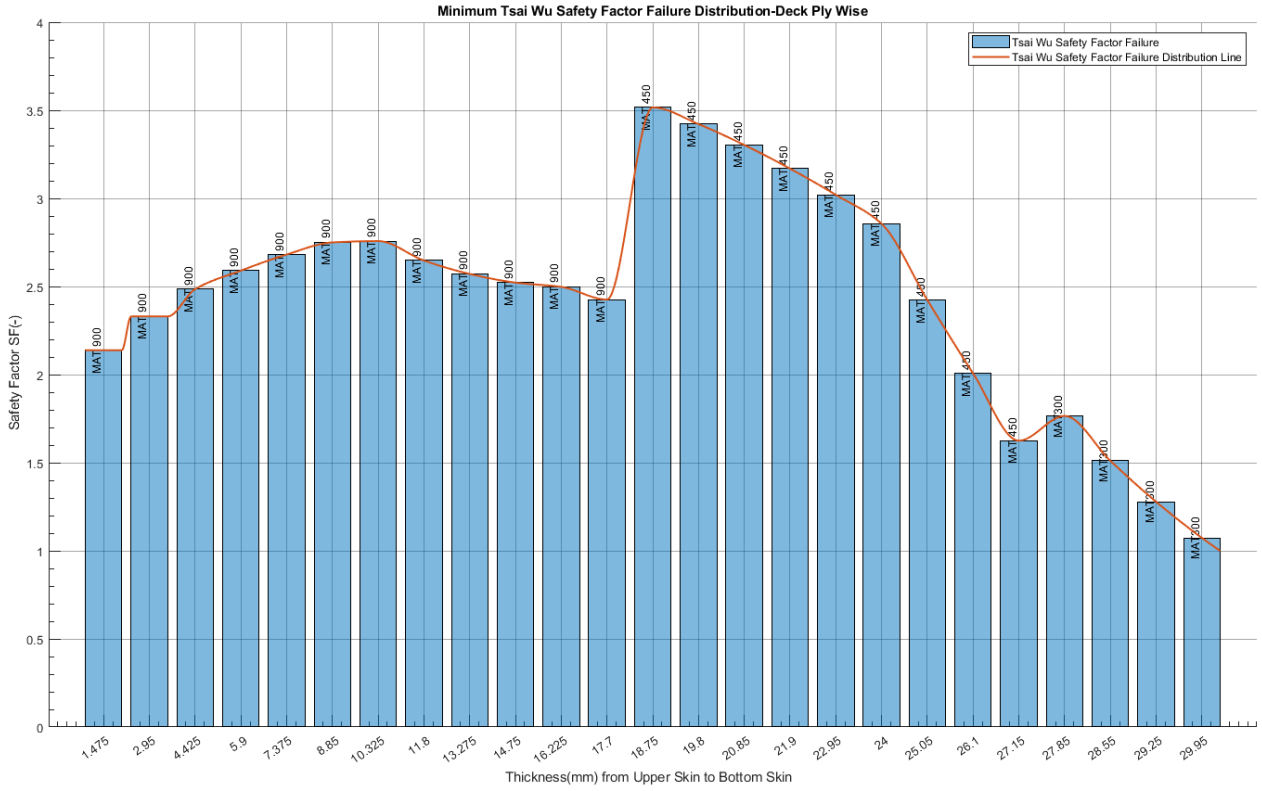

Figure 110: Model(B): Absolute Tsai-Wu Failure Safety Factor Distribution of T-Joint reinforcement

5.5 Compare Analysis of Results

5.5.1 Strength Comparison

The comparison between Total Deformation, Normal-Shear Stresses and Tsai-Wu Safety Factor for deck and middle transverse frame for the maximum values of each size is shown in the table below:

Table 19:Comparison Table between Models (A) and (B)

Deck	Model(A)	Model(B)	% Change	Status (Model (A) Reference)
Total Deformation (mm)	9.36	4.6	50.9%	↓
SX (MPa)	146.8	85	42.1%	↓
SY (MPa)	218	90	58.7%	↓
SXY (MPa)	41.3	33.7	18.4%	↓
Tsai-Wu Safety Factor	1.1	1.5	36.4%	↑

Middle Frame	Model(A)	Model(B)	% Change	Status (Model (A) Reference)
Total Deformation (mm)	10.5	7.8	25.7%	↓
SX (MPa)	31.76	20	37.0%	↓
SY (MPa)	35	25.7	26.6%	↓
SXY (MPa)	38.6	28.7	25.6%	↓
Tsai-Wu Safety Factor	0.9	1.15	27.8%	↑

The values of the table above are based on maximum absolute values of each size.

As presented in Table 19:Comparison Table between Models (A) and (B), a 50.9% reduction of total deformation, 42%,59% and 18 % of SX,SY and SXY accordingly and 36.4% increase of the Tsai-Wu safety factor for the deck. In the same way, 25.7% reduction of total deformation, 37%, 27% and 26% of SX, SY and SXY accordingly and 28% increase of Tsai-Wu Safety Factor for middle frame. Reinforcing by the T-Joint the crane base, the overall strength of the bow region is increased. The increase in SX normal stress is due to the placement of T-Joint, as discussed above. The longer the length reinforcement of the T-Joint is, the smaller the deformations and stresses. The T-Joint has an effect on the construction after 250cm length, whereas for lengths less than this a negative effect on the construction is presented.

Based on the above studies, the following comparative graphs for the magnitudes of stresses and safety factors are depicted:

- Frame

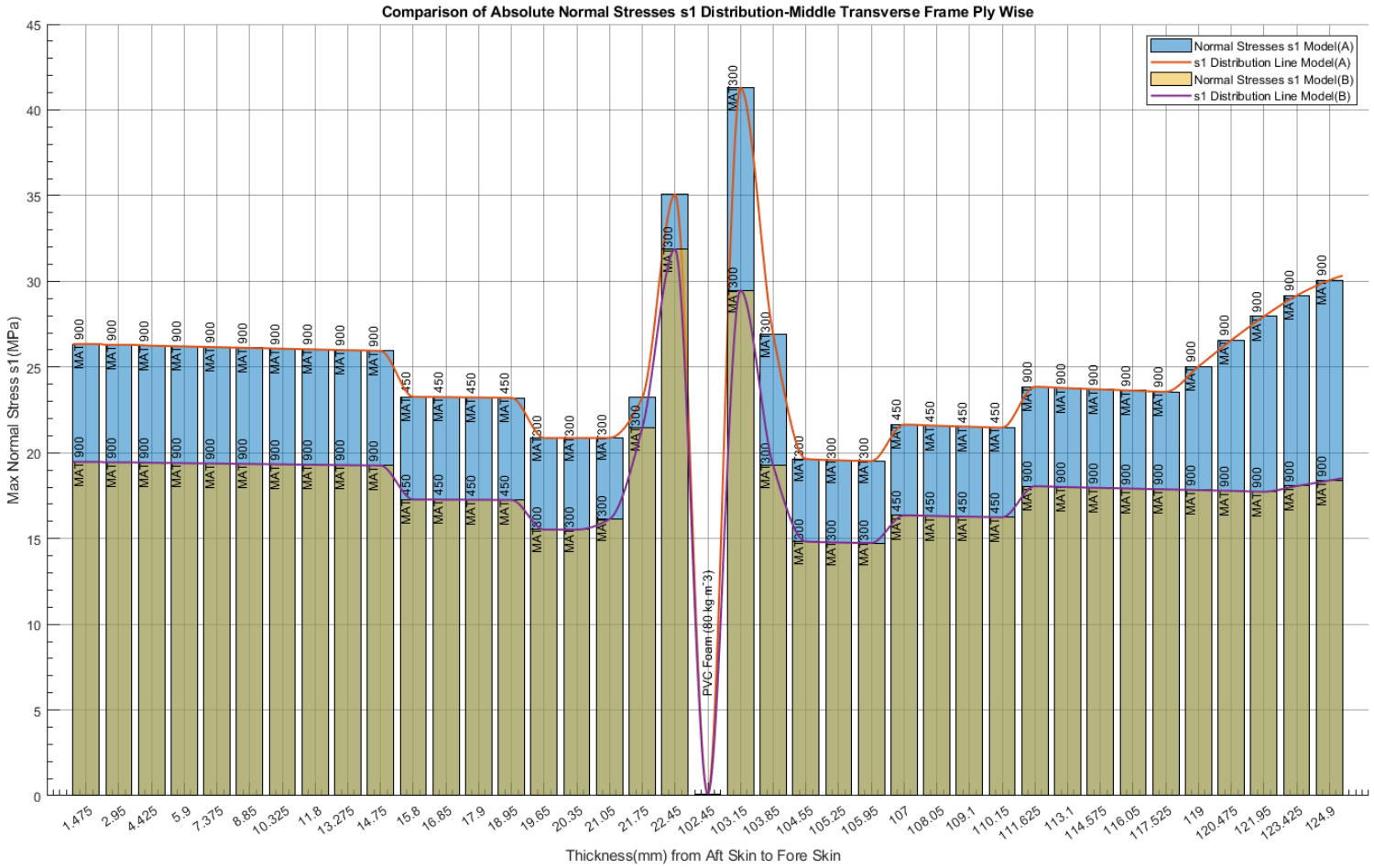

Figure 111: Comparison Model(A)-Model(B): Absolute Normal Stresses SX Distribution of Middle Frames

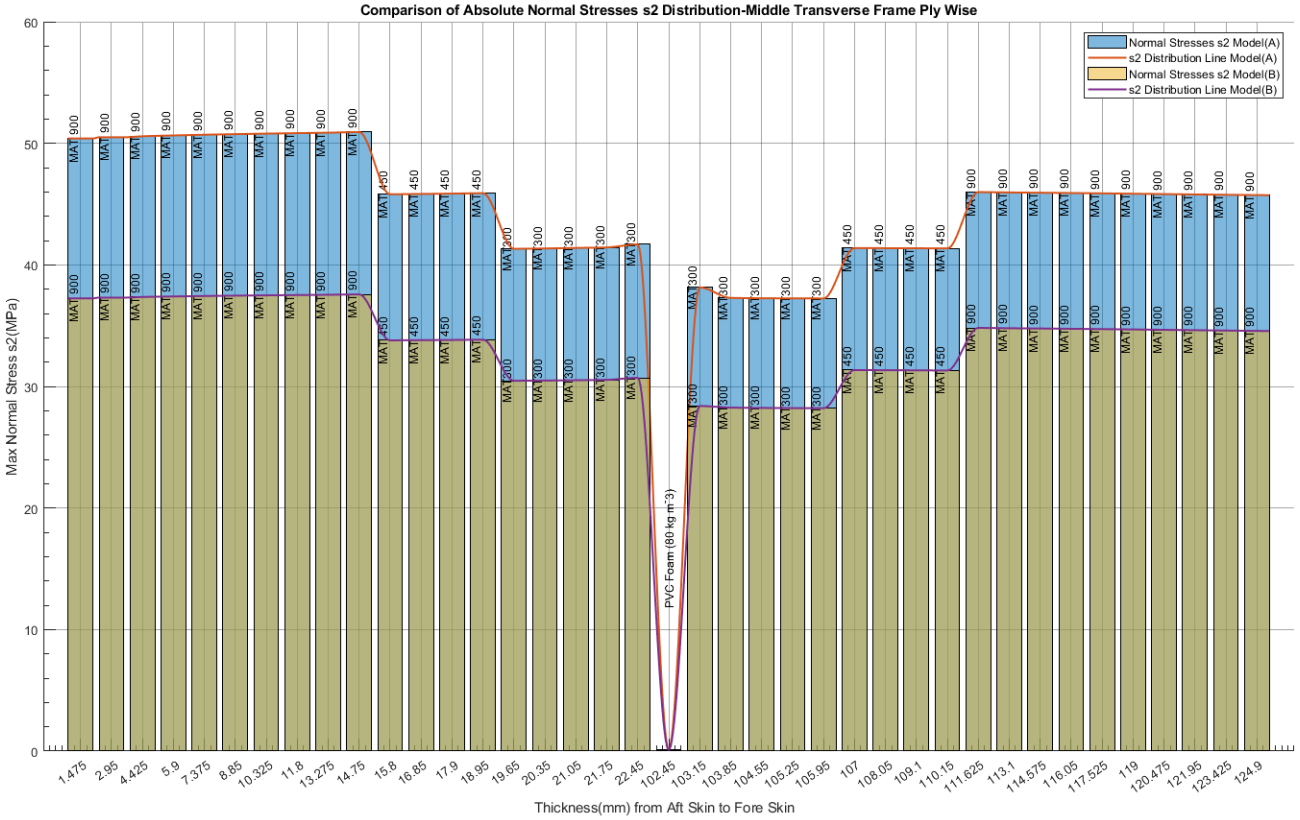

Figure 112: Comparison Model(A)-Model(B): Absolute Normal Stresses SY Distribution of Middle Frames

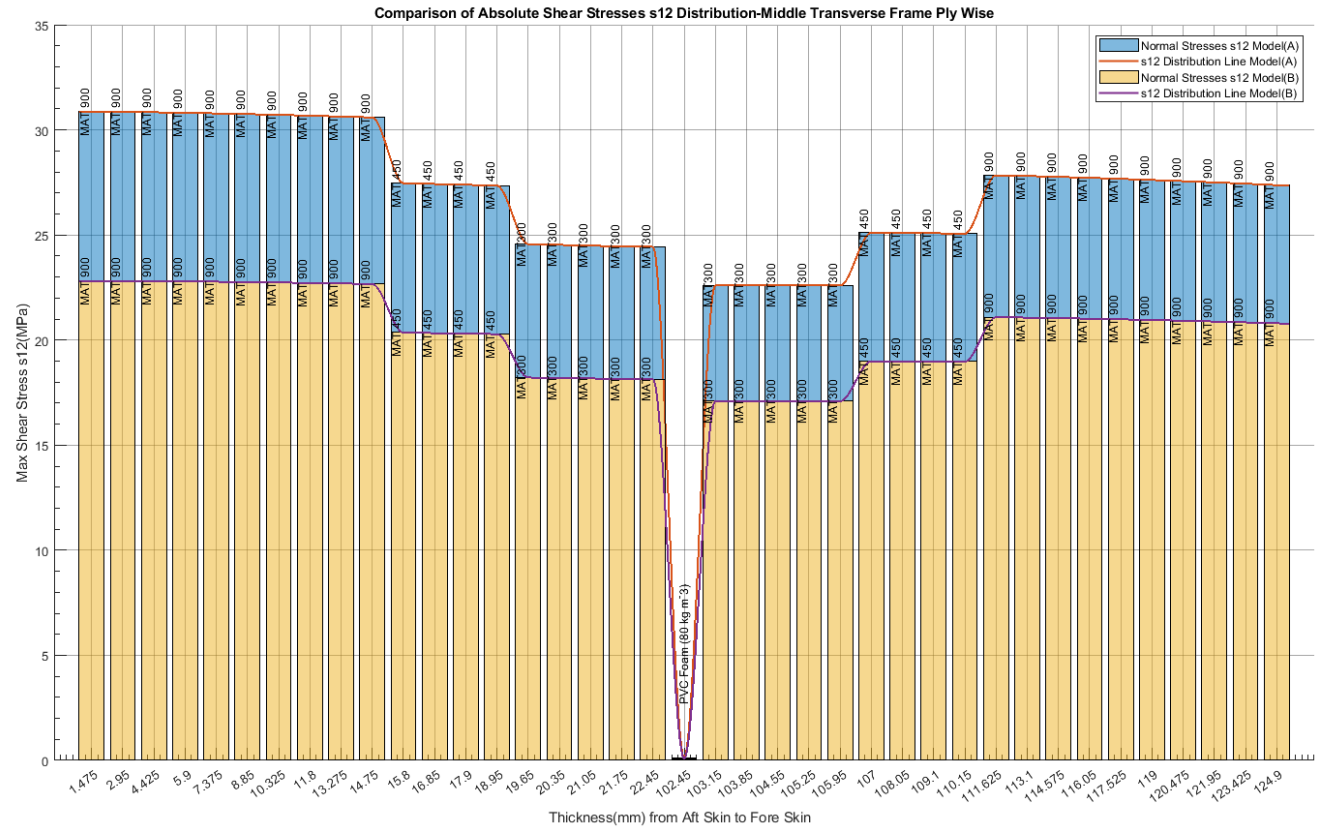

Figure 113: Comparison Model(A)-Model(B): Absolute Shear Stresses SXY Distribution of Middle Frames

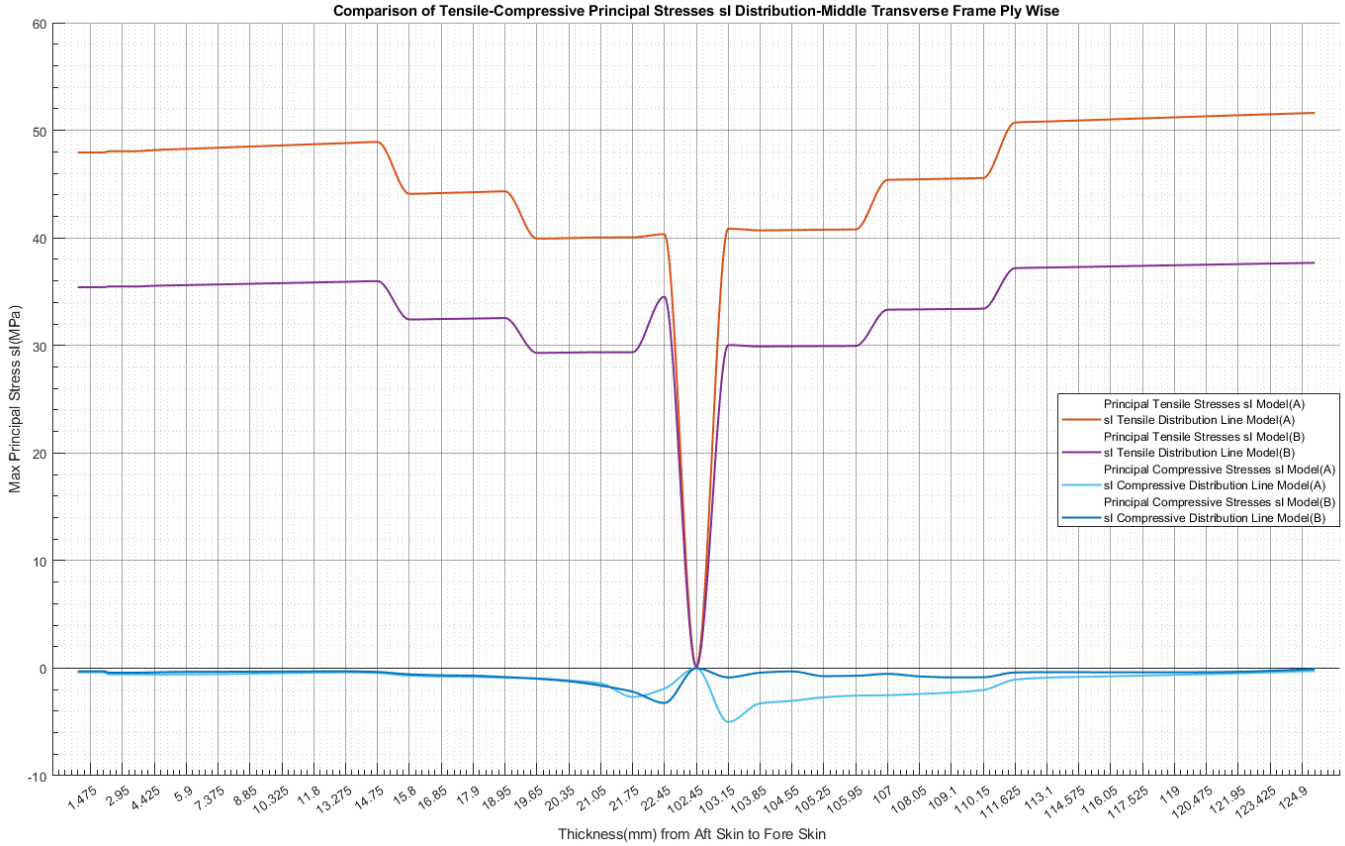

Figure 114: Comparison Model(A)-Model(B): Tensile-Compressive Principal Stresses SI Distribution of Middle Frames

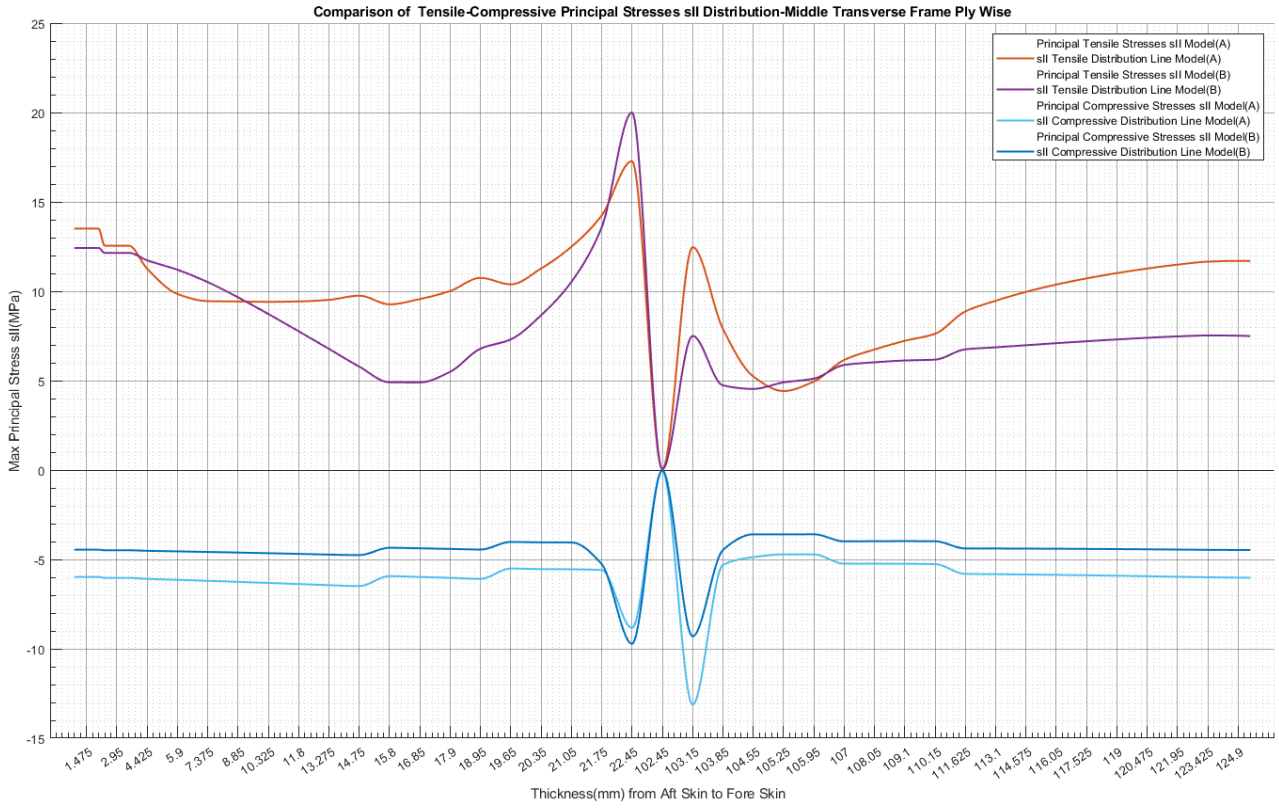

Figure 115: Comparison Model(A)-Model(B): Tensile-Compressive Principal Stresses SII Distribution of Middle Frames

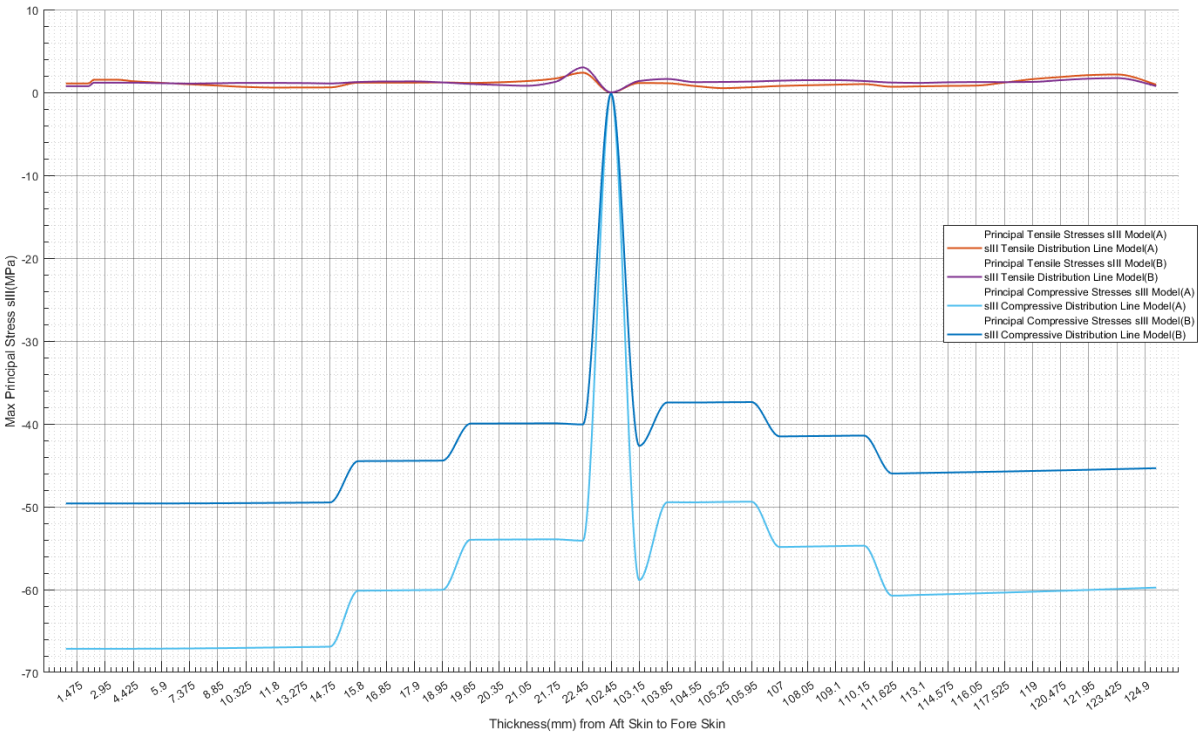

Figure 117: Comparison Model(A)-Model(B): Tensile-Compressive Principal Stresses SIII Distribution of Middle Frames

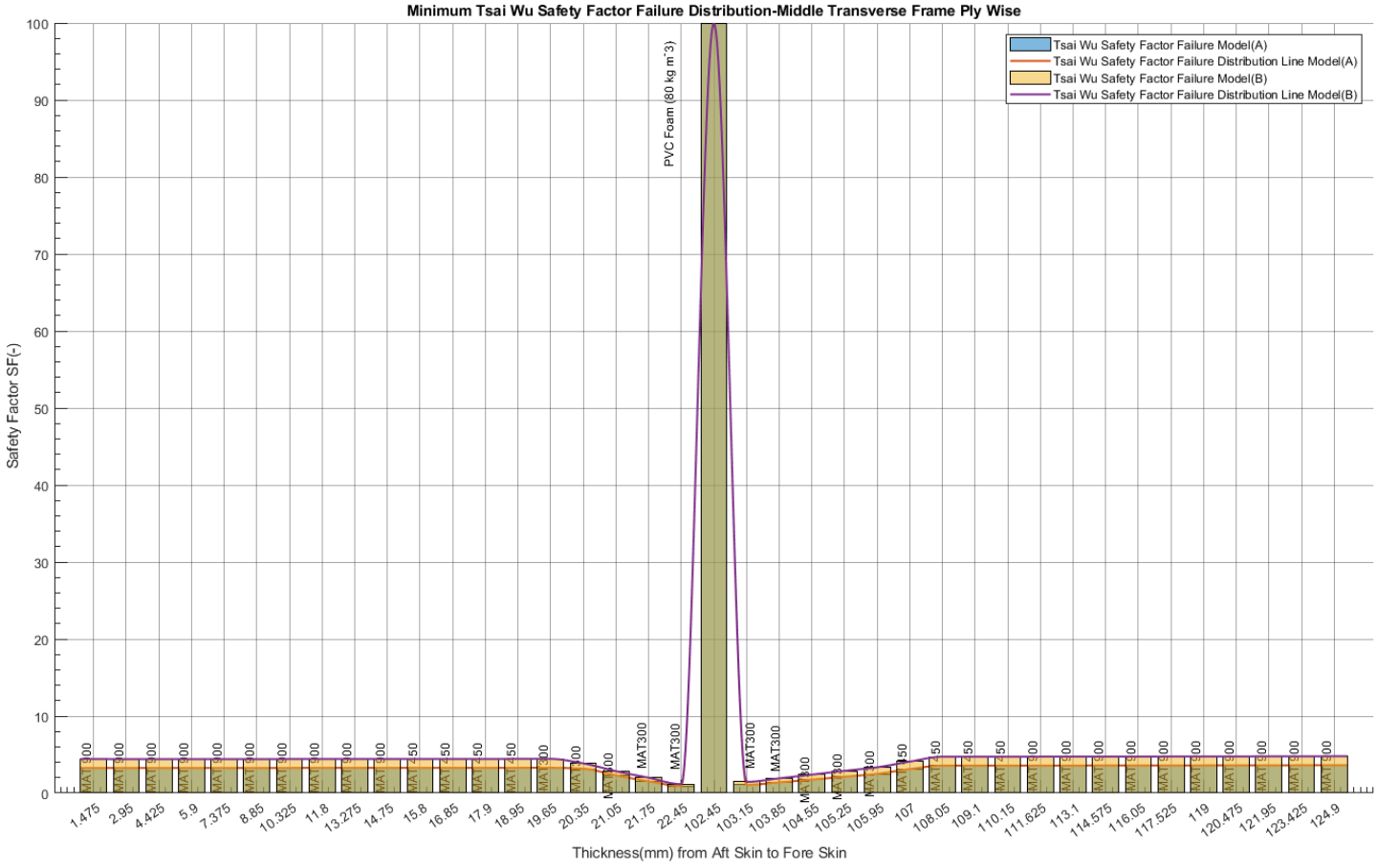

Figure 116: Comparison Model(A)-Model(B): Absolute Tsai-Wu Failure Safety Factor Distribution of Middle Frames

The above diagrams are enlightening with regard to drawing conclusions and performing a representative evaluation between Model(A) and Model(B). The comparison of the results is based on the reduction of stresses and the increase of the safety factor. Some values present peculiarities for the reasons mentioned above. The principal stresses are compared through the Tsai Wu Failure Safety Factor, since their values come under this criterion.

For the transverse middle frame, the normal stress SX, SY and the Shear Stress SXY show a significant decrease in the presence of a T-Joint. A positive feature is that in the SY and SXY stresses the pattern is the same and there is simply a decrease in the values. As for the SX stresses the pattern changes slightly in the areas marked as stress concentration areas. As it can be seen from the principal stresses S_I, S_{II}, the compressive stresses do not change dramatically in contrast to the principal stresses S_{III}. **Thus, it can be assumed that the T-Joint significantly reduces the compressive stresses in the transverse middle frame, while it greatly reduces the tensile principal S_I**. The T-Joint does not significantly affect the pattern of the stress distribution.

The comparison for the Tsai Wu Failure Safety Factor shows an increase which means an improvement in the failure margin of the frame, for the loading conditions that result from the crane installation.

In summary, regarding the transverse middle frame, the reinforcement of the T-Joint to the structure has positive results.

- Deck

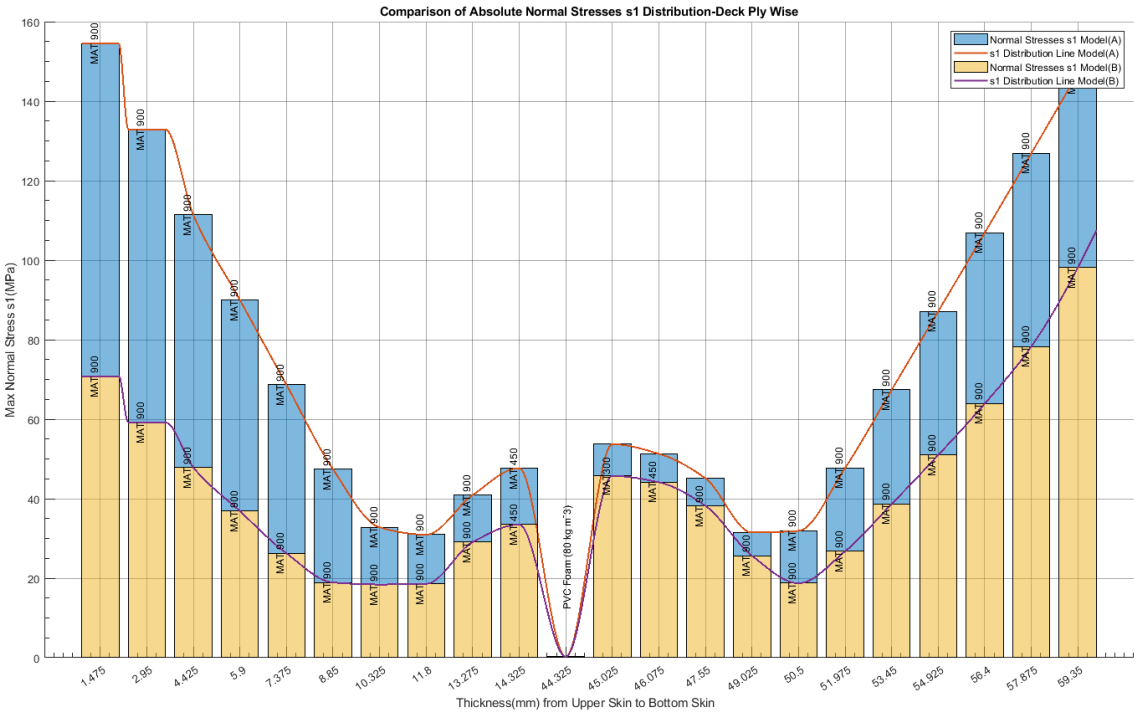

Figure 119: Comparison Model(A)-Model(B): Absolute Normal Stresses SX Distribution of Deck

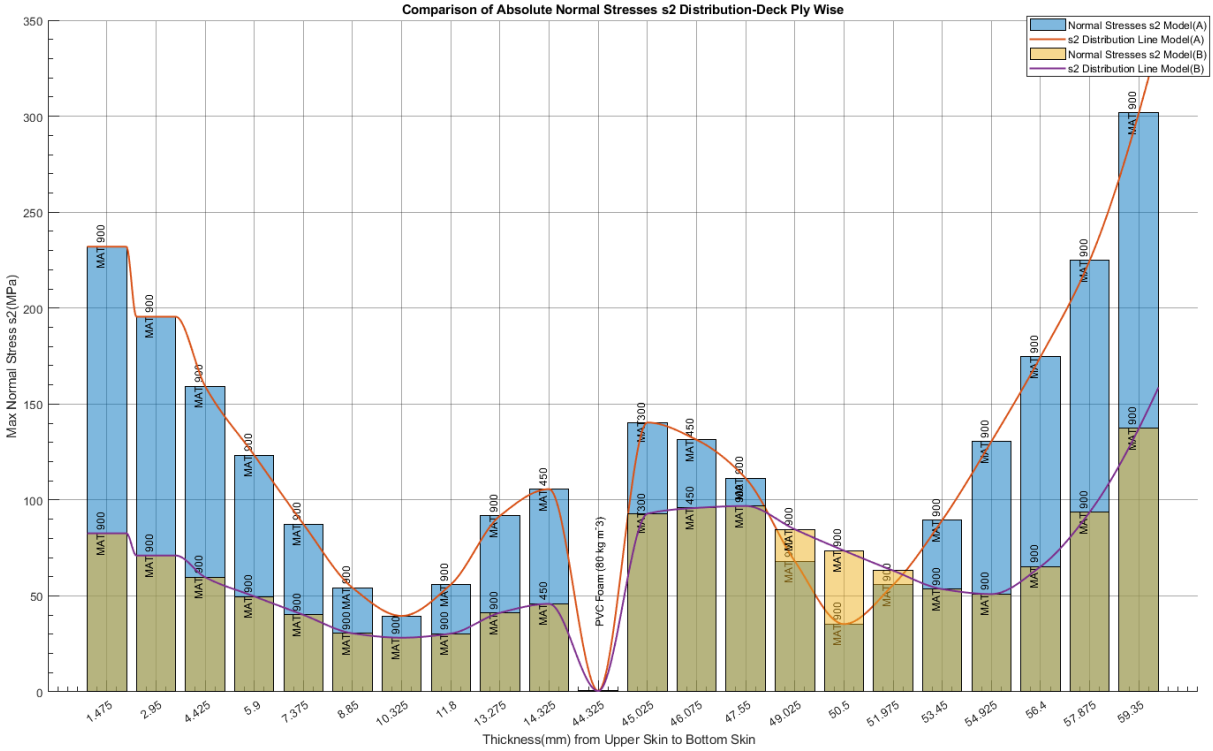

Figure 118: Comparison Model(A)-Model(B): Absolute Normal Stresses SY Distribution of Deck

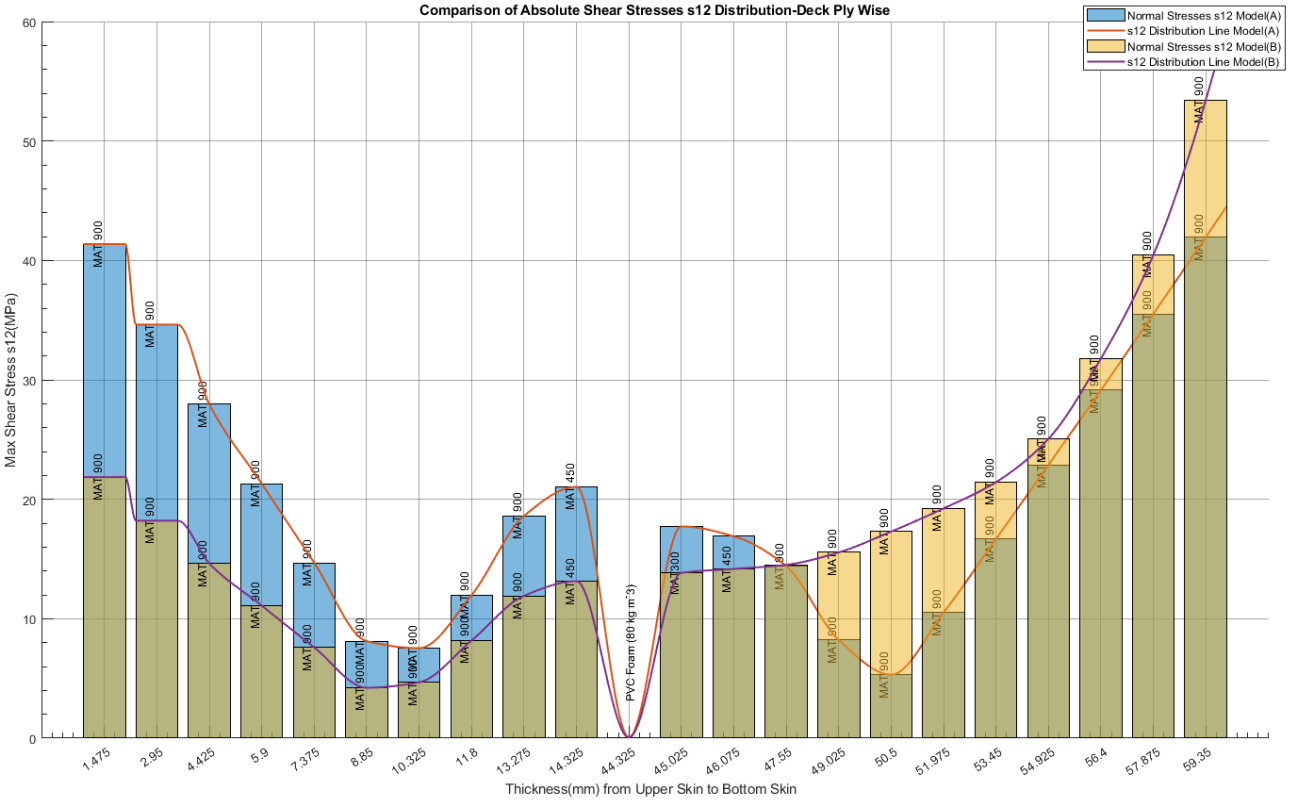

Figure 121: Comparison Model(A)-Model(B): Absolute Shear Stresses SXY Distribution of Deck

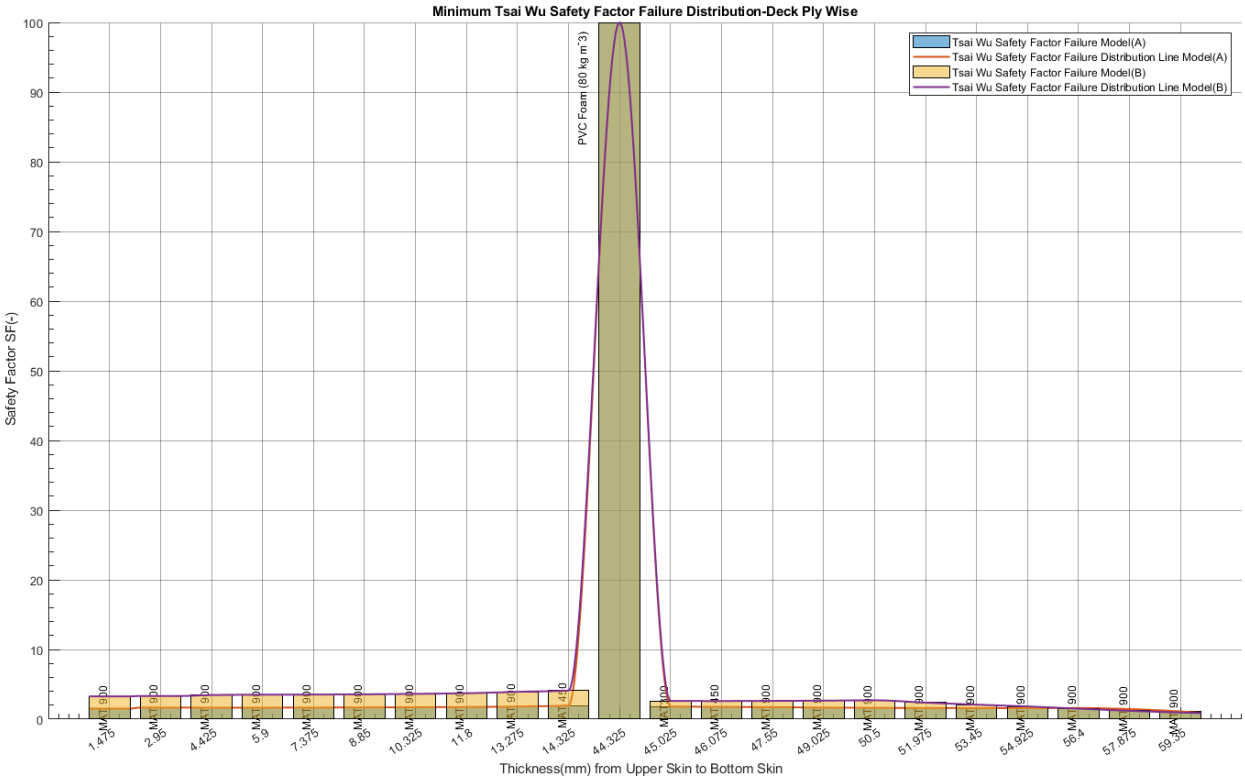

Figure 120: Comparison Model(A)-Model(B): Absolute Tsai-Wu Failure Safety Factor Distribution of Deck

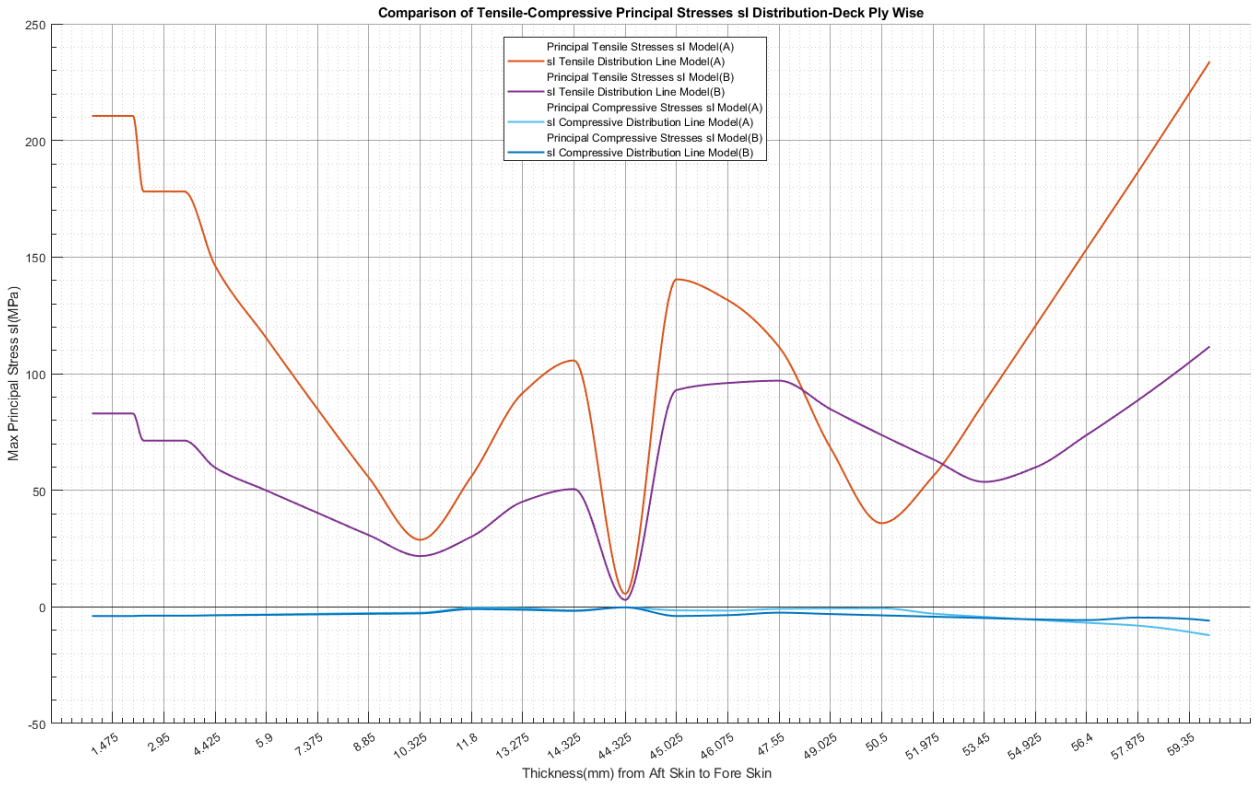

Figure 123: Comparison Model(A)-Model(B): Tensile-Compressive Principal Stresses SI Distribution of Deck

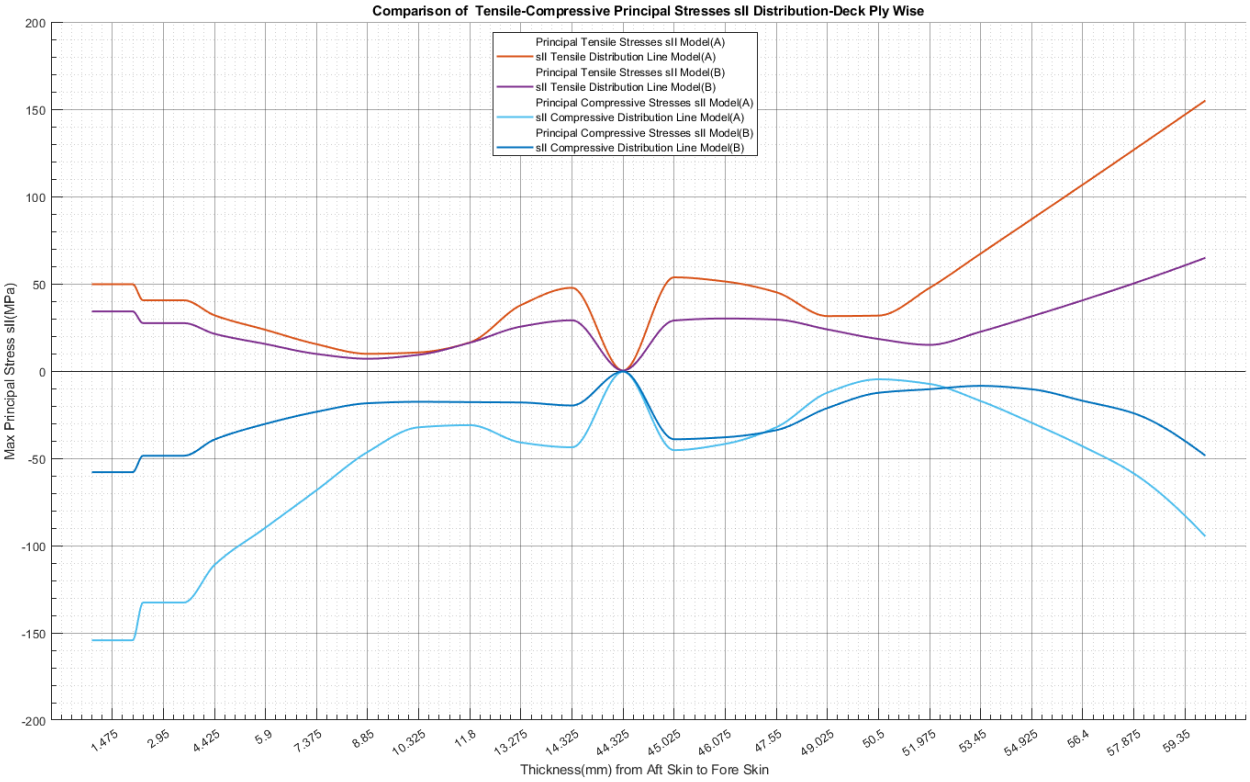

Figure 122:Comparison Model(A)-Model(B): Tensile-Compressive Principal Stresses SII Distribution of Deck

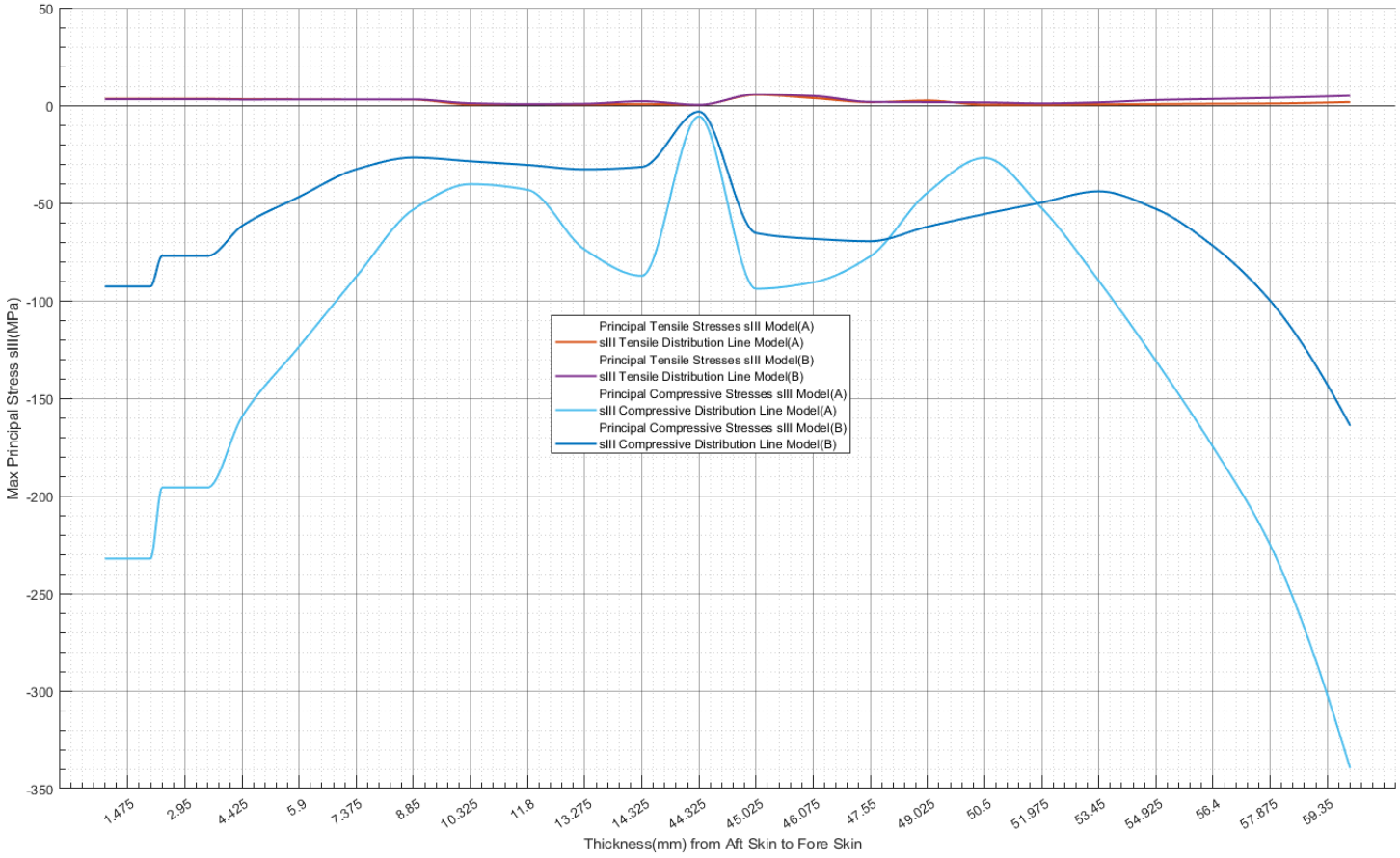

Figure 124 :Comparison Model(A)-Model(B): Tensile-Compressive Principal Stresses SII Distribution of Deck

Similar to the middle transverse frame, the reinforcement of the T-Joint in the structure has positive effects and reduces the stresses and strains. The normal stresses SX, SY and shear stresses show a very smooth distribution and similar pattern between them. From the principal stresses it is clearly understood that the reinforcement of the T-Joint in the deck construction reduced the tensile stresses SI, as well as the compressive stresses SIII. The stresses SII did not change significantly as a whole but only in specific layers.

An important observation that could not be detected before is the alternation of SY, S_I and SXY values from ply MAT900 at 50mm thickness. According to the pattern, the trend of Model(B) should be lower than Model(A), but at these points, the opposite is the case. Thus, this point needs to be further investigated and the illustration to be examined is:

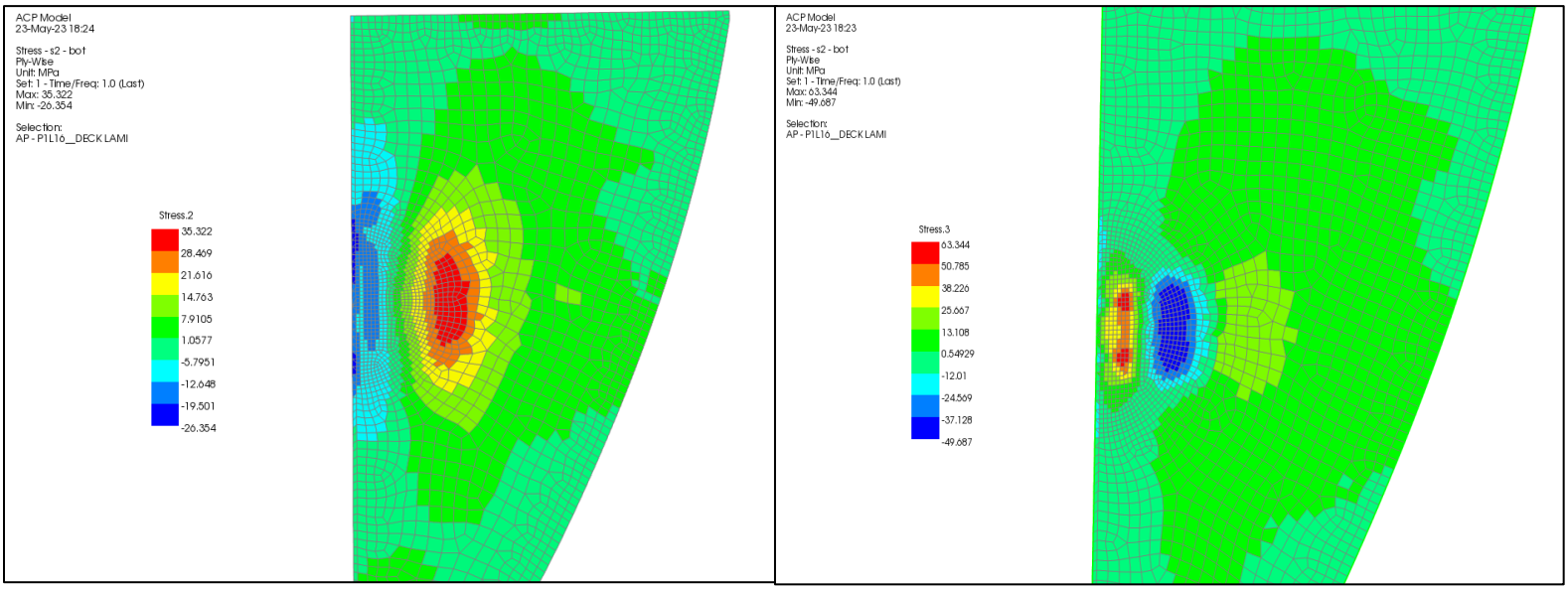

Figure 125:Comparison Model(A)(Left)-Model(B)(Right):Deck Ply Stress Comparison

The values shown as opposite in the diagram are the tensile 35 MPa for Model(A) and the tensile 63 MPa for Model(B). The observation that provides the explanation for this phenomenon is the fact that when the T-Joint reinforcement is placed, the areas that appear to be tensile in Model(A) turn to compressive. This leads to the conclusion that the reinforcement of the T-Joint in the structure affects the pattern of the stress distribution of SY, SXY and converts the tensile regions to compressive. This phenomenon is observed in the MAT900 layers that are closer in contact with the T-Joint.

Despite this happening, the structure remains safe according to the Tsai Wu Failure Safety Factor, where again Model(B) has increased failure margins compared to Model(A).

To summarize, regarding the deck, the reinforcement of the T-Joint has positive effects on the structure, by reducing the stresses and deformation. However, it may change the pattern of stress distribution, since after the insertion of the T-Joint reinforcement that experienced tensile stresses, it was shown that areas were experiencing compressive stresses.

Finally, as a general comment on the deck, it should be emphasized that, the stresses have a larger distribution in the area around the crane support, due to the fact that more emphasis was given to the specific loads using the appropriate assumptions in the study.

Conclusions

This thesis is focused on the installation of a yacht crane at the bow, using Finite Element Method (FEM) analysis for strength and failure evaluation encompassing fracture mechanics through VCCT Theory and Ansys software. Three different geometry models were created to investigate the behavior of the T-Joint connection located under the deck.

The first model referred to as Model A, simulated the bow region without the T-Joint stiffener configuration. The second model, Model B, incorporated a T-Joint connection between the deck and the longitudinal bulkhead. Finally, the third sub-model, Model C, featured a voided T-Joint to simulate a scenario involving crack propagation during the construction phase. This is presented in Appendix(A). The initial crack was assumed to be located between the over-lamination skin and deck region of the T-Joint.

The primary focus of this study was to compare the strength and structural performance of Model(A) and Model(B). Various parameters were evaluated, including total deformation, normal and shear stresses, principal stresses and Tsai-Wu failure safety factor. The most important results for Models A and B are presented in the following lines:

1. The reinforcement of the bow area below the crane by a T-joint, leads to a reduction in stresses and an increase in the safety factor against failure.
2. The longer the length reinforcement of the T-Joint, the smaller the deformations and stresses. The T-Joint has an effect on the construction after 250cm length, whereas for lengths less than this the consequences have a negative effect on the construction.
3. Considering the maximum values of the components studied, it is concluded that the reinforcement of the T-Joint generally leads to a 50% reduction in total deformations, 40%, 43% and 22% reduction in stresses S_X, S_Y and S_{XY} respectively. Also, the maximum increase in Tsai Wu Failure Safety Factor is found to be 32%.
4. Several simulation related remarks were made, specifically regarding stress concentrations in single elements and careful evaluation of material and geometry parameters variations.

Additionally, the investigation of crack propagation and delamination in Sub Model C revealed important insights of failure mechanisms. However, due to the limited relevance of Model C in the context of this study, detailed results for this sub-model can be found in Appendix A.

Overall, the results highlight the importance of the T-Joint connection in strengthening the yacht crane installation. The incorporation of the T-Joint reinforcement significantly improves structural performance, reducing deformation and stress levels while increasing the Tsai-Wu safety factor. These findings have practical applications on the design and optimization of yacht crane installations, enhancing safety and reliability in naval architecture and marine engineering applications.

In conclusion, the comparison between Model A and Model B demonstrated that the T-Joint configuration provides notable improvements in structural performance. Further analysis of the crack propagation and delamination in Sub Model C can be found in Appendix A, along with specific results and data for all models. The insights gained from this study contribute to the advancement of naval architecture marine engineering practices, particularly in the design and implementation of yacht crane installations at the bow.

Future Work

Future work related to this study could include further optimization of the T-Joint stiffener configuration to enhance the structural performance of yacht cranes. This could involve investigating alternative stiffener shapes and configurations to minimize the potential for crack propagation and delamination, while also reducing weight and material usage.

Another potential avenue for future research is to explore the strength of various loading scenarios on the behavior of the T-joint. Dynamic loads that create fatigue cycles can affect the structural integrity of the T-Joint. Therefore, it would be valuable to assess the behavior of the t-joint under these loading conditions and develop design guidelines to ensure safety and durability.

Furthermore, the use of advanced manufacturing techniques, such as additive manufacturing, could offer new possibilities for T-Joint design and construction. Future studies could investigate the feasibility and effectiveness of using these techniques to optimize T-Joint performance.

In general, future research should continue focusing on developing optimized T-Joint designs and construction techniques to enhance the structural performance and durability of yacht cranes and other marine structures, while also considering the impact of various loading scenarios and incorporating advanced analysis methods.

A. Appendix of Fracture Mechanics-Results of Cracked T-Joint

A.1 Basics of fracture Mechanics

Fracture mechanics contain three important variables:

i. Applied Stress
ii. Fracture Toughness
iii. Flaw Size

To obtain results from a fracture study, the binding and combination of these variables must be provided.

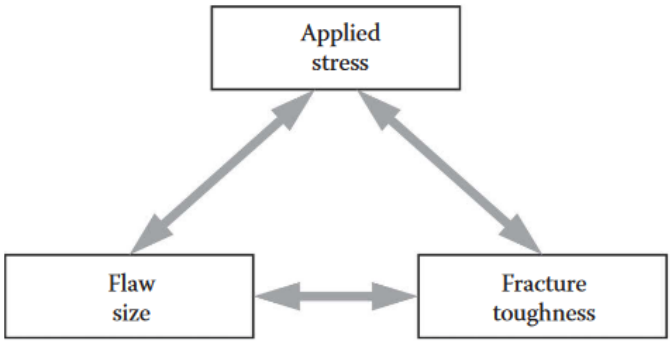

Figure 126: Fracture Mechanics approach [61]

A.1.1 Energy Criterion

According to the energy criterion, when the available energy from the crack growth becomes greater than the resistance of the material the crack is extended. The term material resistance includes all relevant energy sizes of the material related to the propagation of cracks, such as surface energy and plastic work, as well as other diffusion actions.

First Griffith [56], and then Irwin [58] developed the energy criterion in the currently presented form. For an infinite plate that lengthens and contains a crack of 2α length, the relation of energy release rate is as following [57]:

$$G = \frac{\pi \cdot \sigma^2 \cdot a}{E} \tag{58}$$

While in fracture, $G = G_c$, and the relationship describing the critical combination of crack size and stress leading to failure is:

$$G_c = \frac{\pi \cdot \sigma_f^2 \cdot a_c}{E} \tag{59}$$

The relations above describe the rate of change in potential energy with the crack area or the energy release rate G, while at the time the fracture is happening, $G = G_c$, with G_c counting fracture toughness. A key assumption is the fact that the fracture toughness G_C is dependent on the geometry and size of the cracked body. The experimental determination of fracture toughness in a test specimen should correspond to the fracture toughness of an entire construction. Since the behavior of the material is linear elastic, the fracture is mainly influenced by G which, in a sense, constitutes the driving force of the fracture [59],[60],[61].

A.1.2 Modes of fracture

Cracks are possible in three loading scenarios. The major force supplied in mode I loading, which is normal to the crack plane, tends to spread the crack. In-plane shear loading is represented in Mode II, which slides one crack face relative to the other. The third mode is out-of-plane shear. Any one of these modes, or a combination of two or three modes, can be used to load a fractured body [61].

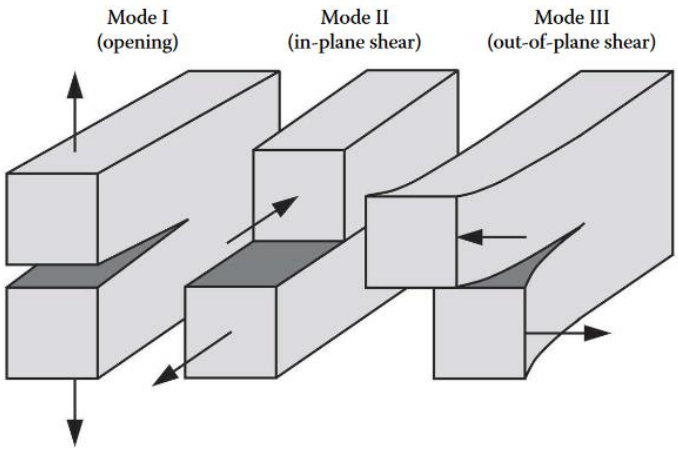

Figure 127:Fracture Opening Modes [61]

A.2 Linear Elastic Fracture Mechanics (LEFM)

This chapter discusses the methods energy criterion, stress energy approach and J-integral in the case of study of fracture with linear elastic fracture mechanics theory in more detail. Also, the way in which LEFM theory can be applied to composite sandwich constructions is presented.

In general, the three most well-known and widely calculated parameters characterizing the fracture are the following:

1. Stress Intensity Factors
2. Strain energy release rate

A.2.1 Strain energy release rate

Irwin's [58] energy release rate, G, is a measure of the energy available for an increase in crack extension:

$$G = -\frac{d\Pi}{\delta A} \tag{60}$$

G is the rate of change in potential energy with crack area. G is also known as the crack extension force or the crack driving force. Once G reaches a certain point, the crack expansion occurs, as in [61]:

$$G_c = \frac{dW_s}{dA} = 2w_f \tag{61}$$

where G_c is a measure of the crack resistance of the material.

The potential energy of an elastic body, Π, is defined as following:

$$\Pi = U - F \tag{62}$$

where U is the strain energy stored in the body and F is the work done by external forces. Considering a dead-loaded fractured plate, the structure is referred to as load controlled, since the load is fixed at P. In this instance,

$$F = P \cdot \Delta \tag{63}$$

$$U = \int_0^{\Delta} P \cdot d\Delta = \frac{P \cdot \Delta}{2} \tag{64}$$

While:

$$\Pi = -U \tag{65}$$

$$G = \frac{1}{t} \cdot \left(\frac{dU}{d\alpha}\right)_P = \frac{P}{2t} \cdot \left(\frac{d\Delta}{d\alpha}\right)_P \tag{66}$$

When displacement is fixed, the plate is displacement controlled:

$$F = 0 \text{ and } \Pi = U$$

Thus,

$$G = -\frac{1}{t} \cdot \left(\frac{dU}{d\alpha}\right)_{\Delta} = -\frac{P}{2t} \cdot \left(\frac{d\Delta}{d\alpha}\right)_{\Delta} \tag{67}$$

The term of the inverse of plate stiffness is indicated below, since it is useful:

$$C = \frac{\Delta}{P} \tag{68}$$

A more realistic approach for both, load control and displacement control, is the strain energy release rate. Therefore, both the load control and the displacement control have the same rate of energy release.

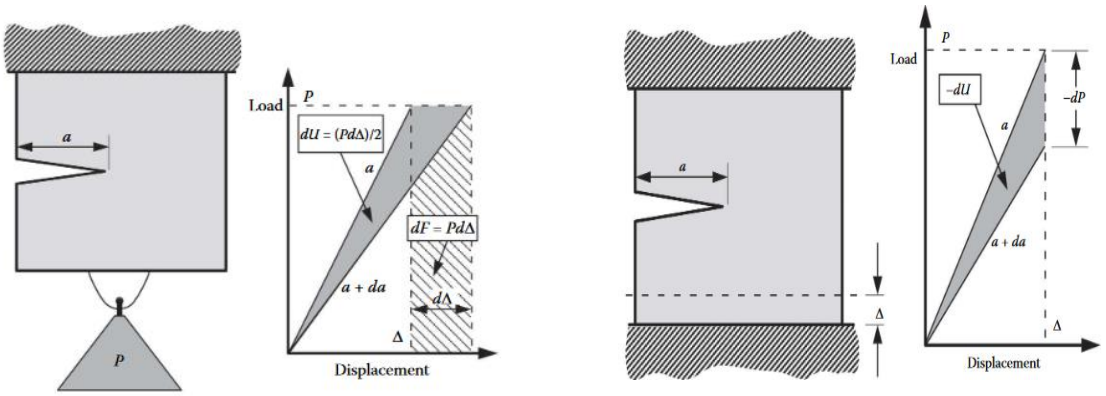

Figure 128: Cracked plate fixed load and fix displacement approach [61]

For a body with constant thickness, t, the strain energy release rate, G, is given by:

$$G = \frac{P^2}{2t} \cdot \frac{dC}{d\alpha} \tag{69}$$

Where P is the load and α is the crack length.

Where δ is the displacement at the point of application of the load. Therefore, the primary benefit of the strain energy release rate is the absence of the requirement for fracture tip stress field analysis.

Additionally, it should be noted that the strain energy release rate is related to the stress intensity factors K_I , K_{II} ,and K_{III} . The relationships for these opening modes are the following:

A.2.1.1 Fracture Mode I:

$$G_I = \frac{K_I^2 \cdot (1 - v^2)}{E} \quad (plane\ strain) \tag{70}$$

$$G_I = \frac{K_I^2}{E} \quad (plane\ stress) \tag{71}$$

A.2.1.2 Fracture Mode II:

$$G_{II} = \frac{K_{II}^2 \cdot (1 - v^2)}{E} \quad (plane\ strain) \tag{72}$$

$$G_{II} = \frac{K_{II}^2}{E} \quad (plane\ stress) \tag{73}$$

A.2.1.3 Fracture Mode III:

$$G_{III} = \frac{K_{III}^2 \cdot (1 + v)}{E} \quad (plane\ strain) \tag{74}$$

$$G_{III} = \frac{K_{III}^2}{E} \quad (plane\ stress) \tag{75}$$

It is obvious that the above equations may be used to calculate the stress intensity factors, if the strain energy release rate mode components are specified. When the fracture tip stress field analysis is difficult, this is incredibly helpful [62]-[69].

The crack growth initiation criteria based on the strain energy release rate has the following form for a specific set of loading conditions:

$$G = G_c \tag{76}$$

The material parameter Gc is the critical value of the strain energy release rate. Thus, if $G < G_c$, the crack is stable and if $G > G_c$, the crack is unstable and should propagate [70],[71].

The superposition method can be used to determine the overall value of the strain energy release rate for a fracture under mixed mode loading conditions. Thus, we the following relation for a crack under general mixed-mode I/II/III loading is provided:

$$G = G_I + G_{II} + G_{III} \tag{77}$$

Where G_I , G_{II}, and $G_{III}$are the mode I, mode II, and mode III components of the strain energy release rate, respectively.

Finally, the following is assumed in LEFM [72]:

1. Material behavior is linear elastic and exhibits little plasticity at the tip of the crack.
2. There is a single dominant flaw in the material.
3. Crack growth of this flaw is self-similar.
4. The material is homogeneous along the crack plane.

A.3 Theory of VCCT

For more complex fracture phenomena, the virtual crack closure approach may be used to compute the strain energy release rate. This technique, which is often utilized, relies on the applicability of linear-elastic fracture mechanics. The results of the finite element analysis provide the basis for its application. This method allows individual computation of the strain energy release rate components linked to each of the three fundamental mechanisms of crack formation. The primary benefit of this method is that it only requires one finite element model study. The components of the strain energy release rate mode must be calculated using the nodal forces at the tip of the crack and the displacement of the nodal behind the tip of the crack, which is given by the finite element analysis [69]. The VCCT method was developed by Rybicki and Kanninen (1977) on the basis of the energy method of Irwin (1958). The development and recent application of the VCCT were reviewed by Krueger (2002) [4].

A.3.1 Overview of VCCT

The use of finite elements is one of the most useful techniques for solving fracture mechanics problems. The composition of the VCCT method is based on the numerical calculation of the following sizes and is one of the most modern and easy methods to calculate the stress intensity factors, including all three fracture modes, according to Rybicki and Kanninen [73]. Finite-element approaches to fracture mechanics can be described as either direct or indirect methods. In the direct method the stress intensity factors are calculated directly from the solution. In the indirect method an energy release rate is calculated and stress intensity factors are inferred from it. A two-step analysis and a one-step analysis are designed as two alternative VCCT implementations. In the two-step analysis the energy required to create the kinking crack can be evaluated by computing the strain energy change according to two cases corresponding to the crack length α and $\alpha+\Delta\alpha$. Then, the total strain energy release rate for a kinking fracture may be determined using Irwin's definition. Two distinct FEAs corresponding to two different fracture lengths, that are infinitesimally different from each other are conducted in order to use a two-step analysis. However, the fundamental concept of the one-step analysis in the first step is to replace the displacement opening behind the parent crack with the displacement opening along the kinking crack line in the second step. Then, in a single step, all the variables are calculated. The current one-

step technique is considered to be as accurate as the two-step VCCT. Although there are some differences, they are minimal compared to the efficiency obtained by employing a one-step VCCT computation, as opposed to a two-step VCCT technique [74]. Most of the challenges that come with conventional approaches, such as the requirement of singularity components at the crack front, or the creation of elements that are normal to the curved crack front, can be avoided with 3D VCCT [75].

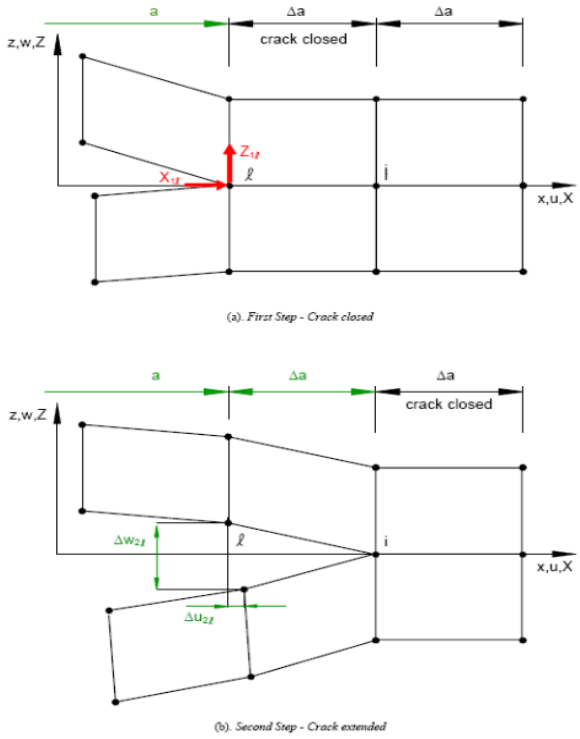

Figure 129:Two Step VCCT Method [4]

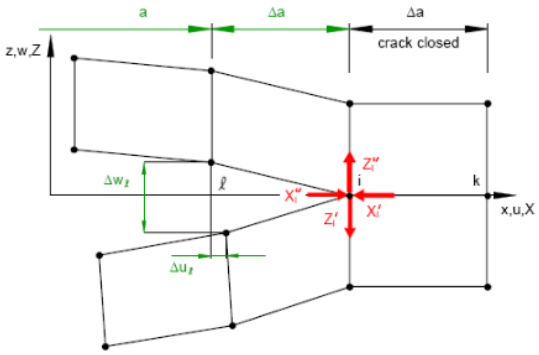

Figure 130:One Step VCCT Method [4]

The VCCT has a considerable advantage over other approaches. SIF is generated using this approach for the following three fracture modes from the equation:

$$G_i = \frac{K_i^2}{E} \cdot \beta \quad (i = I, II, II) \tag{78}$$

where G_i is the energy release rate for mode i, K_i the stress intensity factor for mode I, E the elastic modulus, ν the Poisson ratio, $\beta = 1$ for plane stress, and $\beta = 1 - \nu^2$ for plane strain.

It should also be emphasized that, according to Krueger [76], the two-step approach is occasionally called VCCT. This terminology in literature is frequently confusing. It may be more appropriate to call the two-step analysis method the crack closure method, because the crack is physically extended, or closed, during two complete finite element analyses. This is because the finite crack extension method requires two complete analyses. As mentioned above, the fracture in the model is extended for a limited amount of time prior to the second study. The technique calculates the energy available

for the fracture to progress by multiplying the global forces on the structural level by global deformations. This generates a single global total energy release rate. The integral crack closure of Irwin is the foundation of the crack closure technique. However, the modified, or virtual, crack closure method (VCCT) needs only one complete analysis of the structure to determine the deformations, although it shares the same underlying assumptions as the crack closure method. Only the stiffness matrix of the elements impacted by the virtual crack extension must be calculated in addition to the overall energy release rate, which is calculated locally at the crack front.

However, practically speaking, VCCT determines mixed-mode energy release rates based on the calculated forces and displacements acquired from a finite element analysis [77]. The Virtual Crack Closure Technique is a useful technique for determining the stress intensity factor. The primary benefit of the VCCT is that a particular mesh configuration around the crack front is not necessary. The primary drawback of the VCCT is that it can only be used to solve cases involving linear elastic fracture mechanics. It is simple to integrate VCCT into any commercial FE program. The result of the commercial FE solver determines how complicated the user subroutine will be. Following the FE analysis, calculating SIF requires very little work if all necessary data are present [75].

A.3.2 Three-Dimensional VCCT

The general form of energy release rate for a 3D-crack geometry is defined as:

$$G_I = -\frac{1}{2\Delta A} \cdot R_y \cdot \Delta v \tag{85}$$

$$G_{II} = -\frac{1}{2\Delta A} \cdot R_X \cdot \Delta u \tag{86}$$

$$G_{III} = -\frac{1}{2\Delta A} \cdot R_Z \cdot \Delta w \tag{87}$$

where G_I , G_{II} and G_{III} are Mode I, II and III energy-release rates. Respectively, Δu, Δv and Δw are relative displacement between the top and bottom nodes of the crack face in local coordinates x,y and z. Respectively, Rx, Ry, Rz are reaction forces at the crack-tip node. ΔA is crack-extension area[78].

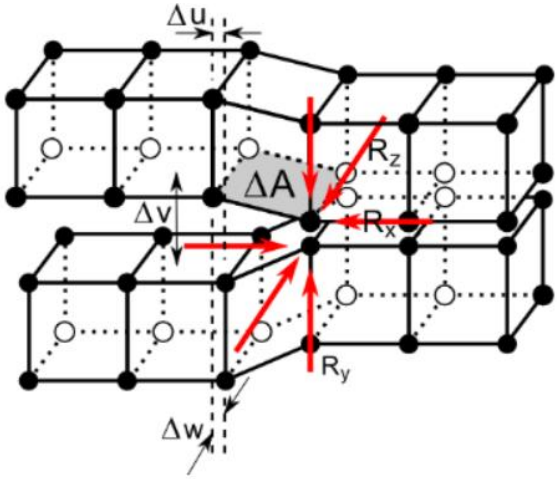

Figure 131: 3D Crack Geometry for VCCT [78]

Considering a 3-D problem, schematic of a crack front area is depicted in the figure above. Eight-nodded spatial elements are used. The strain energy release rate mode components at node i can be expressed as:

$$G_I = \frac{1}{2\Delta a \Delta b} \cdot [Z_i \cdot (w_r - w_s)] \tag{88}$$

$$G_{II} = \frac{1}{2\Delta a \Delta b} \cdot [X_i \cdot (u_r - u_s)] \tag{89}$$

$$G_{III} = \frac{1}{2\Delta a \Delta b} \cdot [Y_i \cdot (v_r - v_s)] \tag{90}$$

where X, Y and Z are components of the nodal force. u, v, and w are components of the displacement of the nodal in the x, y, and z directions respectively.

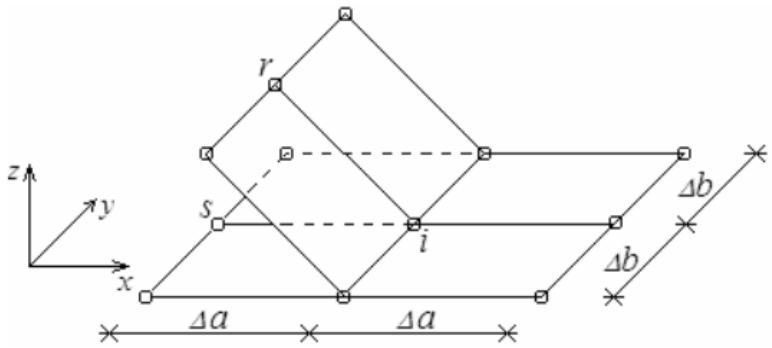

Figure 132: 3D mesh with eight-nodded elements in crack front area [69]

When the model is meshed using twenty-nodded finite elements, the mode components of the strain energy release rate can be obtained as:

$$G_I = \frac{1}{2\Delta a \Delta b} \cdot \left[Z_i \cdot (w_r - w_s) + Z_k \cdot (w_m - w_n) + \frac{1}{2} \cdot Z_l \cdot (w_p - w_q) + \frac{1}{2} \cdot Z_j \cdot (w_d - w_t) \right] (91)$$

$$G_{II} = \frac{1}{2\Delta a \Delta b} \cdot \left[X_i \cdot (u_r - u_s) + X_k \cdot (u_m - u_n) + \frac{1}{2} \cdot X_l \cdot (u_p - u_q) + \frac{1}{2} \cdot X_j \cdot (u_d - u_t) \right] (92)$$

$$G_{III} = \frac{1}{2\Delta a \Delta b} \cdot \left[Y_i \cdot (v_r - v_s) + Y_k \cdot (v_m - v_n) + \frac{1}{2} \cdot Y_l \cdot (v_p - v_q) + \frac{1}{2} \cdot Y_j \cdot (v_d - v_t) \right] (93)$$

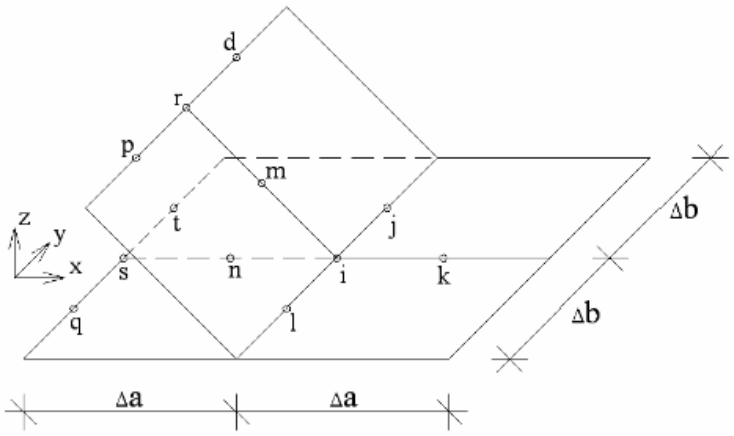

Figure 133:3D mesh scheme with twenty-nodded elements in crack front area [69]

A.4 Theory of VCCT in ANSYS

A.4.1 Energy release rate VCCT

The approach for evaluating the energy-release rate is based on the virtual crack-closure technique (VCCT). The analysis solution step involves calculating the energy-release rate, while the findings are kept for post-processing. The software employs the modified crack closure approach (a VCCT-based method, one-step analysis), and it further assumes that when a crack extends by a little amount Δa, the stress values near the tip of the crack do not change considerably. It is often advised to use linear elements. The meshes determine how accurate the VCCT computation will be. VCCT requires the finite element mesh to be in the crack extension direction. It is essential to define the crack extension precisely in order to guarantee the precision of the energy-release rate computation. Given that mesh size has an impact on the solution, it is wise to review the mesh size convergence before trying the finite element solution [78].

The following material characteristics are supported by the VCCT technique for calculating the energy release rate:

i. Linear isotropic elasticity
ii. Orthotropic elasticity
iii. Anisotropic elasticity

A.4.2 Crack growth VCCT

The virtual crack closure technique (VCCT) was initially developed to calculate the energy release rate of a cracked body. Since then, it has been extensively used to simulate the interfacial crack growth of laminate composites on the presumption that cracks always propagate along a predetermined path, namely the interfaces. It is possible to simulate crack development using VCCT with linear elements.

The underlying assumptions for a VCCT-based crack-growth simulation are the following:

i. Crack growth follows a predetermined path of cracks.
ii. The path is defined through interface elements.
iii. The analysis is quasi-static and does not account for transient effects.
iv. The material must be anisotropic, orthotropic, or linearly elastic.
v. The model experiences little rotation or deformation.

The crack can be located in a material, or along the interface of the two materials. Fracture criteria are based on energy release rates calculated using VCCT. There are several fracture criteria available, including one that is user defined. An analysis can define several cracks [78].

A VCCT-based crack-growth simulation uses:

i. Interface elements INTER202 (2-D) and INTER205 (3-D).
ii. The CINT command is used to calculate the energy release rate
iii. The CGROW command to define the set of crack growth, the fracture criterion, the crack growth path and the control parameters of the solution.

VCCT-based crack growth simulation has become a popular method for simulating interface delamination of laminate composites for crack propagation along the interfaces. Given that fracture may be considered as a separation process between two surfaces, the approach is also well suited for simulating the fracture process in homogeneous media.

A.4.3 Interface elements generation

In this technique, the surfaces can be separated using interface or contact elements. The cohesive material model is used to explain how the surfaces separate. This method may be used to simulate both interfacial delamination at a material interface and fracture in a homogeneous material. Adding interface elements across the full interface, including the original crack and the predefined crack line, when using the CZMESH command to produce interface elements along the predefined crack path, then the interface elements on the initial crack are removed.

A.5 Fracture examination for model(C)

A.5.1 Geometry-Meshing and Boundary Conditions of Cracked Model (C)

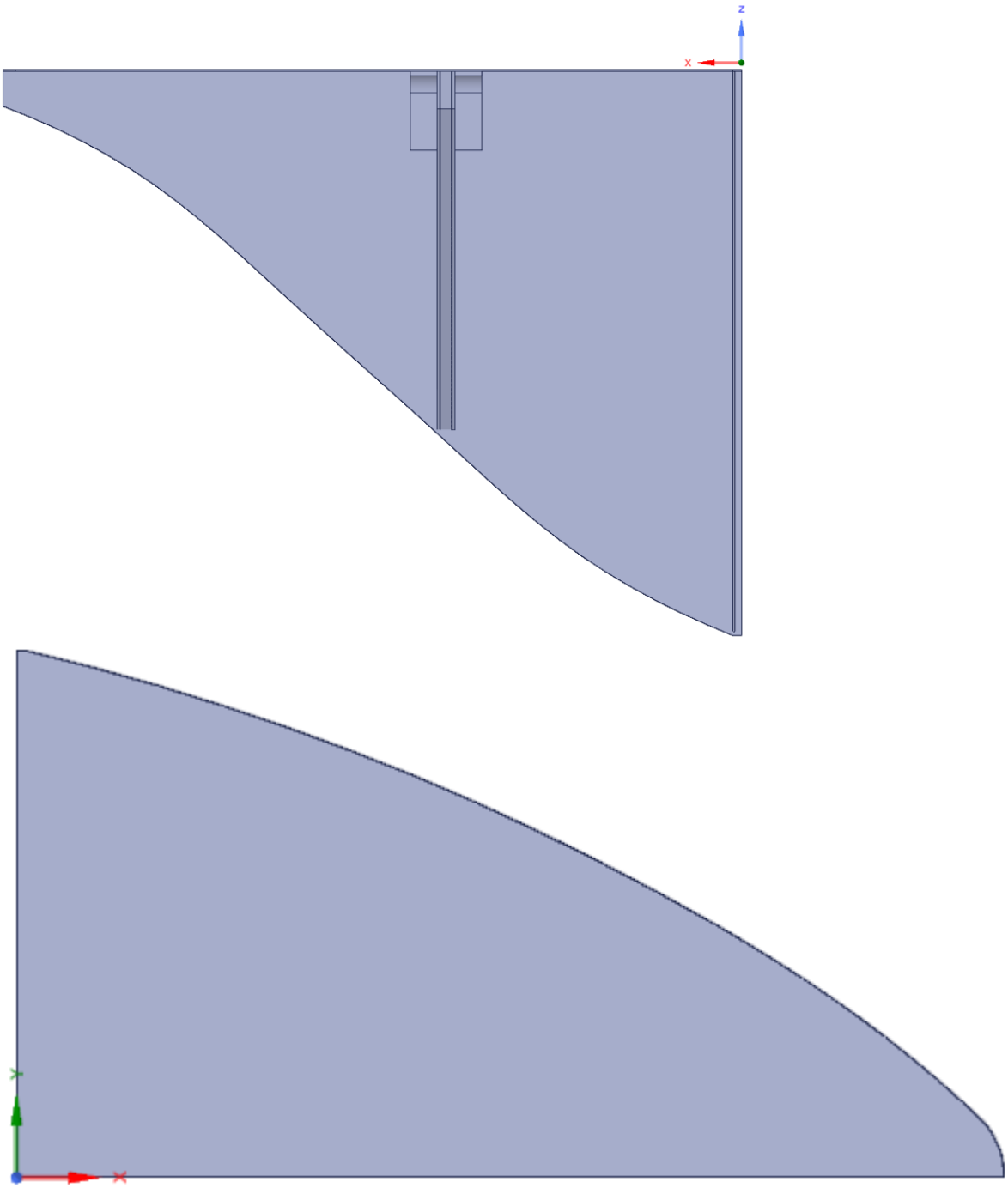

Figure 134:Geometry of Cracked Model(C)

The Cracked Model(C) consists of 79134 elements and 82722 nodes. This shows a very fine mesh for smaller areas. This is necessary in order to study the fracture correctly. Also, in the fracture area, the nodes should be coincident with each other and the element size should be relatively small. These conditions result from the application of the VCCT method and the delamination between the two surfaces.

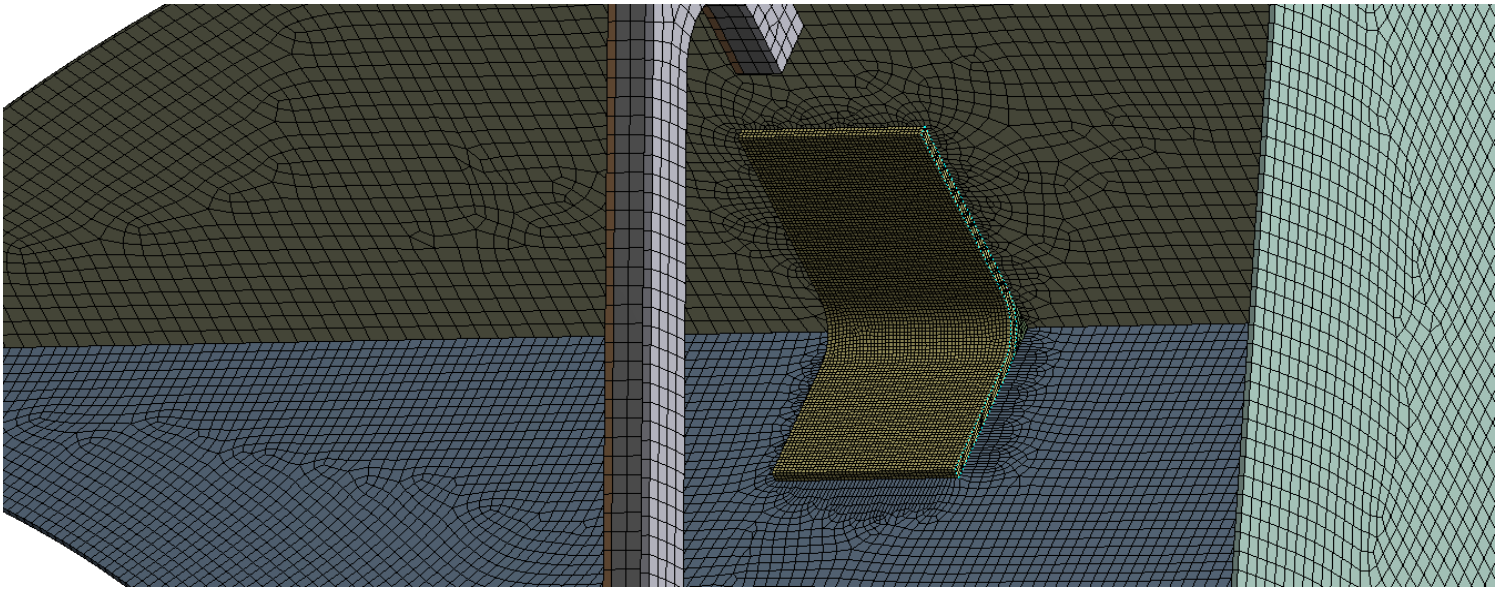

Figure 135:Meshing of Cracked Model (C)

For Cracked Model (C) the boundary conditions and load respond to the above cases. However, they are imported to the model using the Model(B) solution file. Therefore, the displacements of the previous solution are transferred in Sub Model (C).

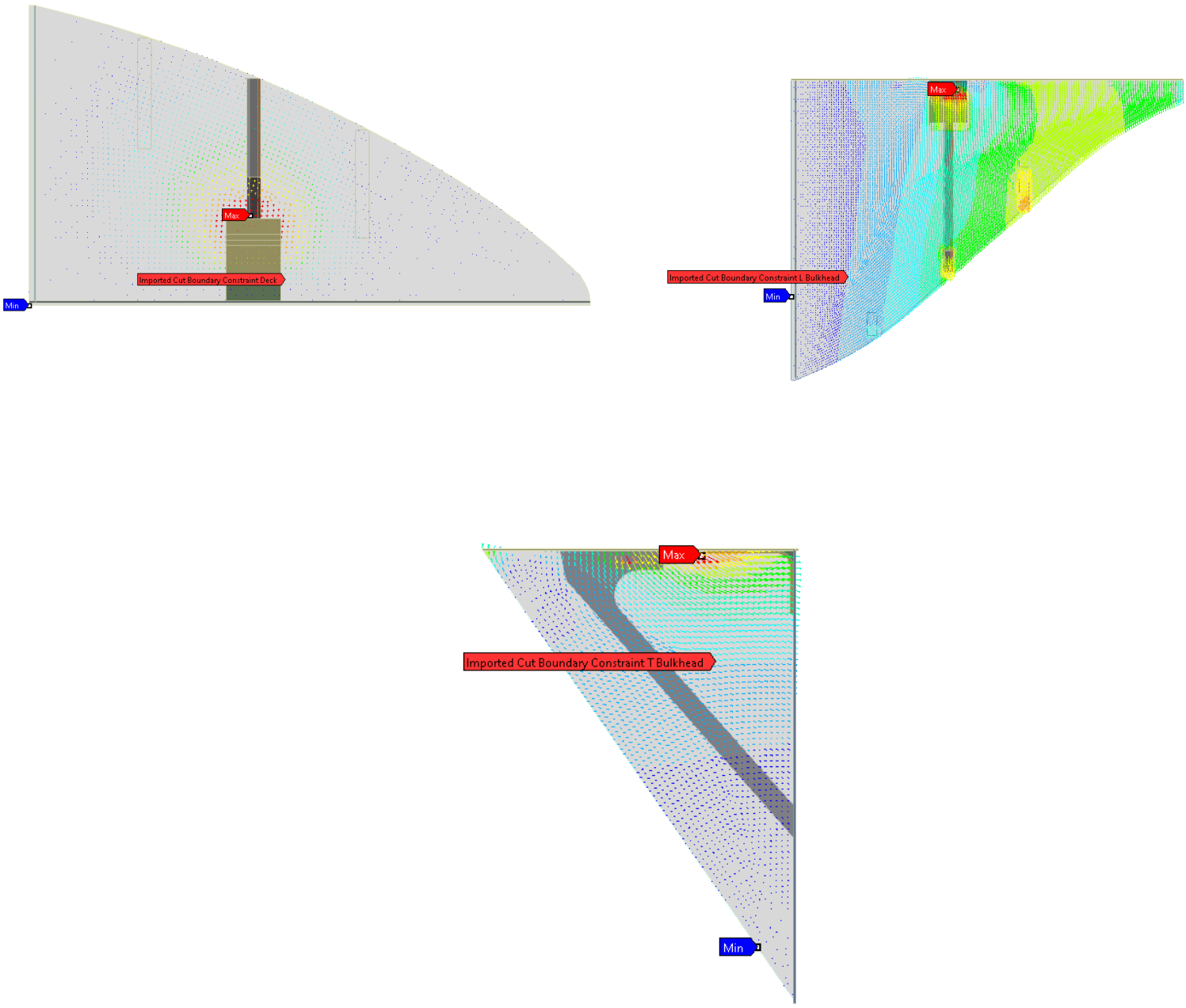

Figure 136:Displacement Boundary Conditions of Cracked Model (C) imported from Model(B)

A.5.2 Fracture Set-up for Sub Model(C)

The fracture model is based on VCCT theory. With the help of Workbench GUI, the process of defining the parameters for fracture and delamination based on VCCT is very simple. The crack placed in the construction belongs to the pre-meshed crack category, i.e. the crack is selected from the geometry and then translated into nodes and elements. The crack has its own coordinate system, which determines the position and direction of the crack. Delamination belongs to the interface delamination category. i.e. the program defines the surfaces of the components that touch each other. The interface is created by interface elements and is essentially the path on which the crack will move. In the interface area, the specified material contains a fracture criterion which controls whether the crack will spread. In this particular work, a linear fracture criterion is used and delamination is based on the results of the VCCT fracture.

Thus, the fracture and delamination regions are:

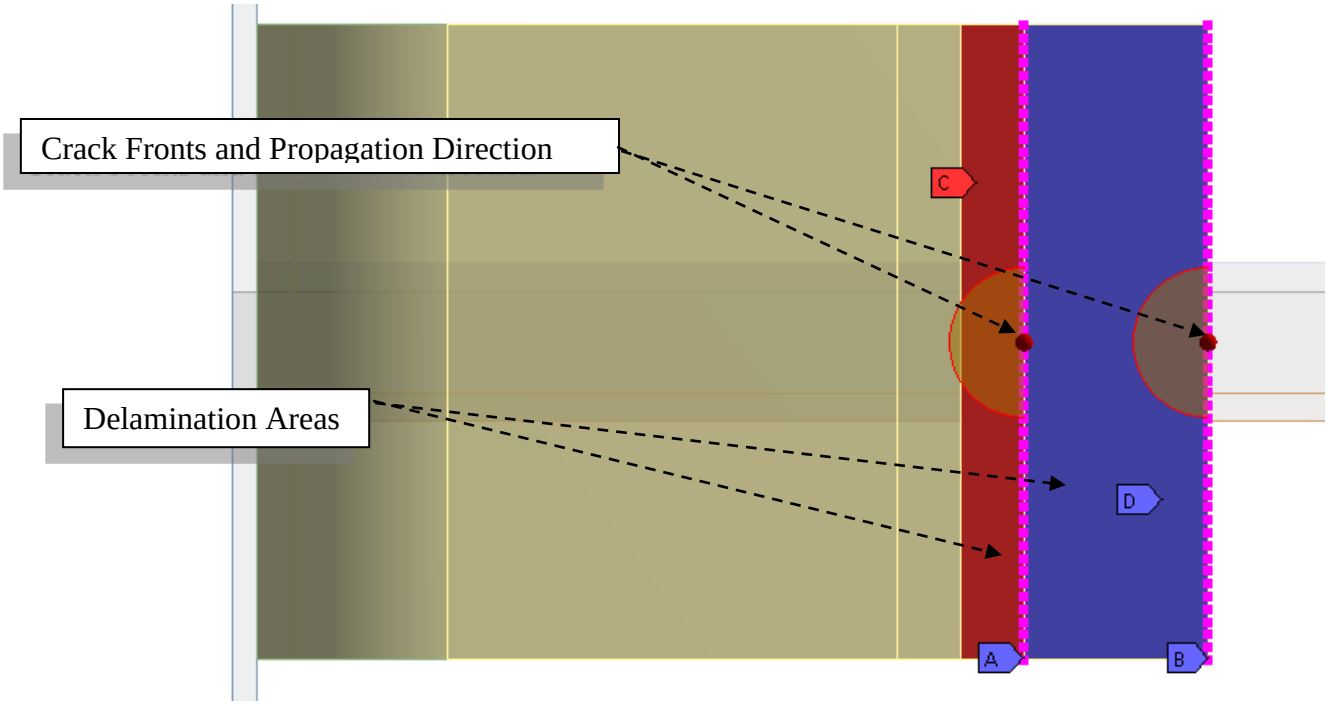

Figure 137:Crack Fronts and Delamination Areas of T-Joint

The results for two crack fronts demonstrated below. Crack 1 is located at the end of the T-Joint and between deck and T-Joint overlamination. Crack 2 is located 145mm away from Crack 1, in the direction of inside of the bow, according to Model (C).

A.5.3 Energy Release Rates before Delamination

A.5.3.1 Crack 1

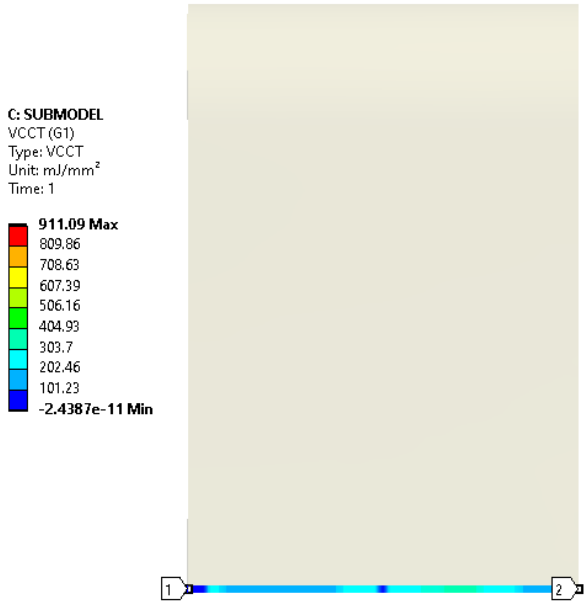

Figure 138:Crack 1 Energy Release Rate Visualization before delamination

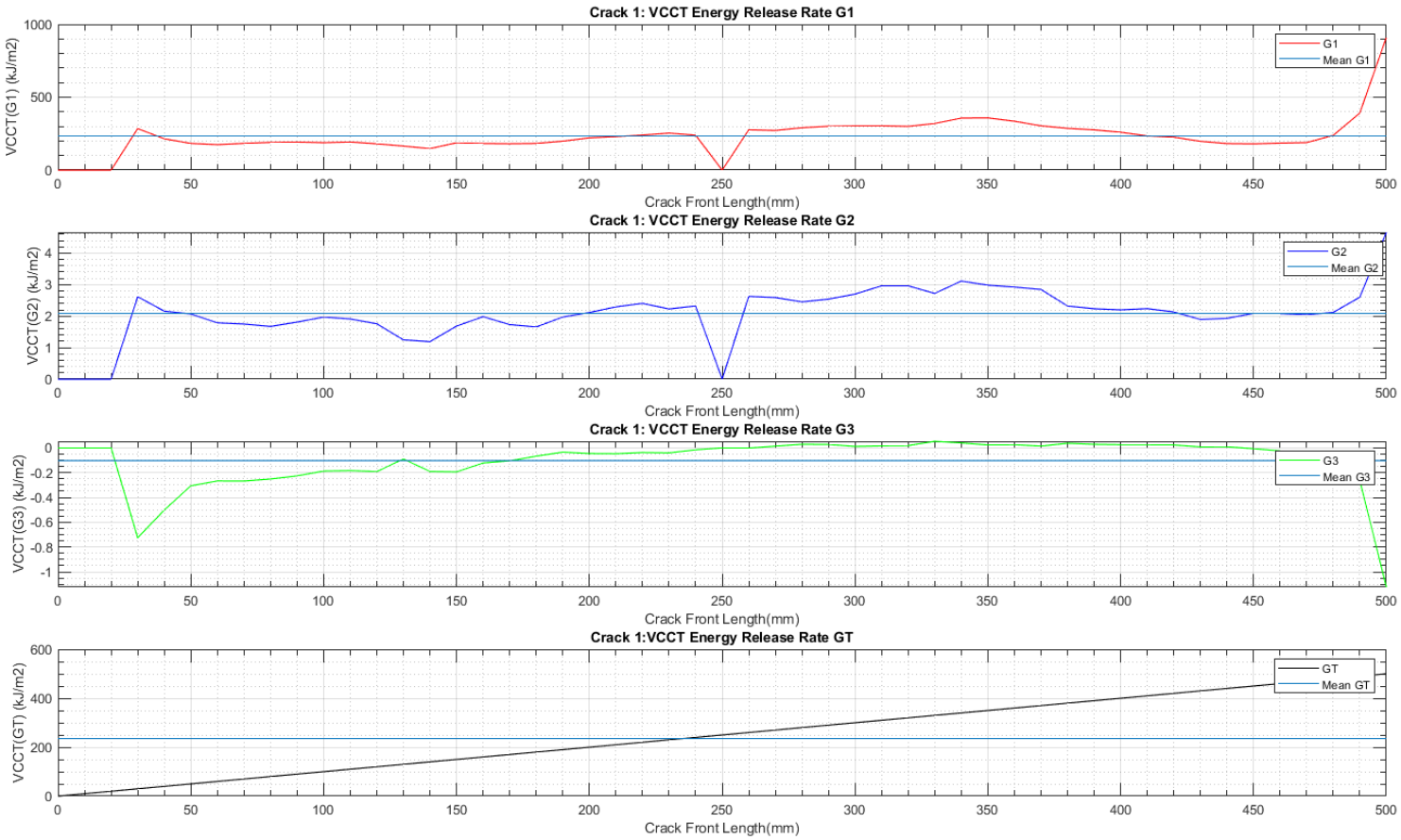

Figure 139:Graph of VCCT Energy Release Rates of Crack 1

A.5.4 Energy Release Rates after Delamination

A.5.4.1 Crack 2

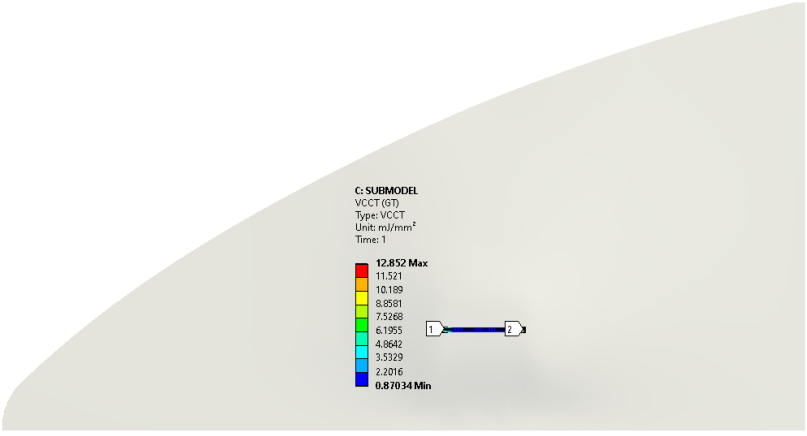

Figure 140: Crack2 Energy Release Rate Visualization after delamination

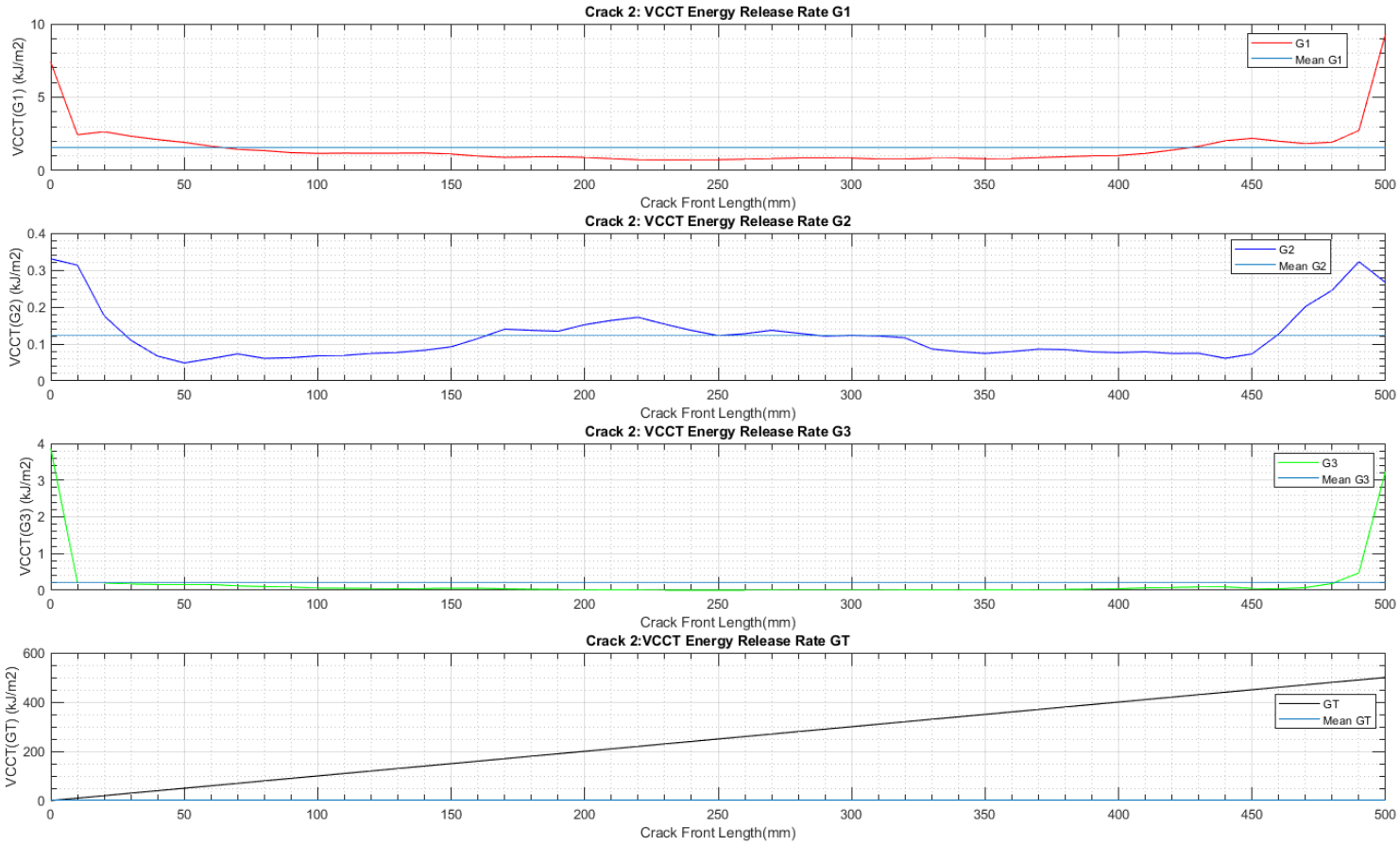

Figure 141: Graph of VCCT Energy Release Rates of Crack 2

A.5.5 Total Deformation of Cracked T-Joint Reinforcement

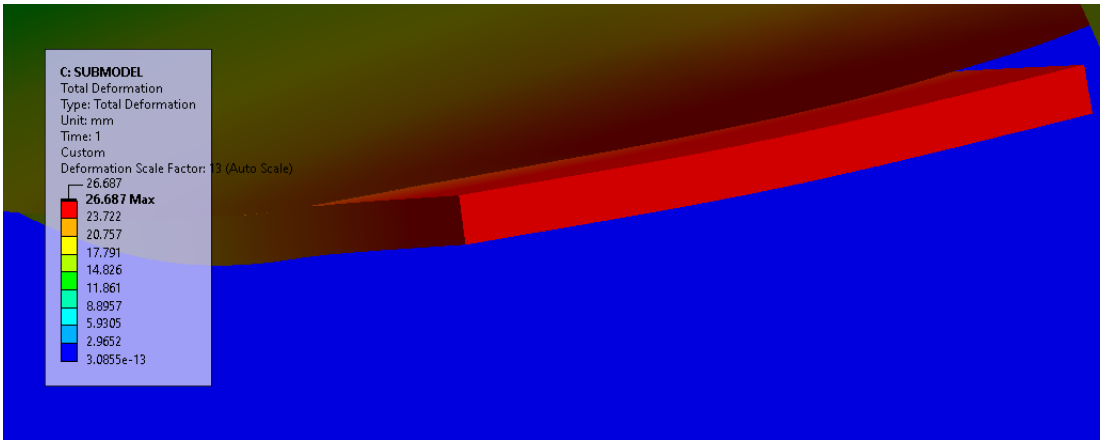

Figure 142: T-Joint Reinforcement Total Deformation of Sub Model(C)

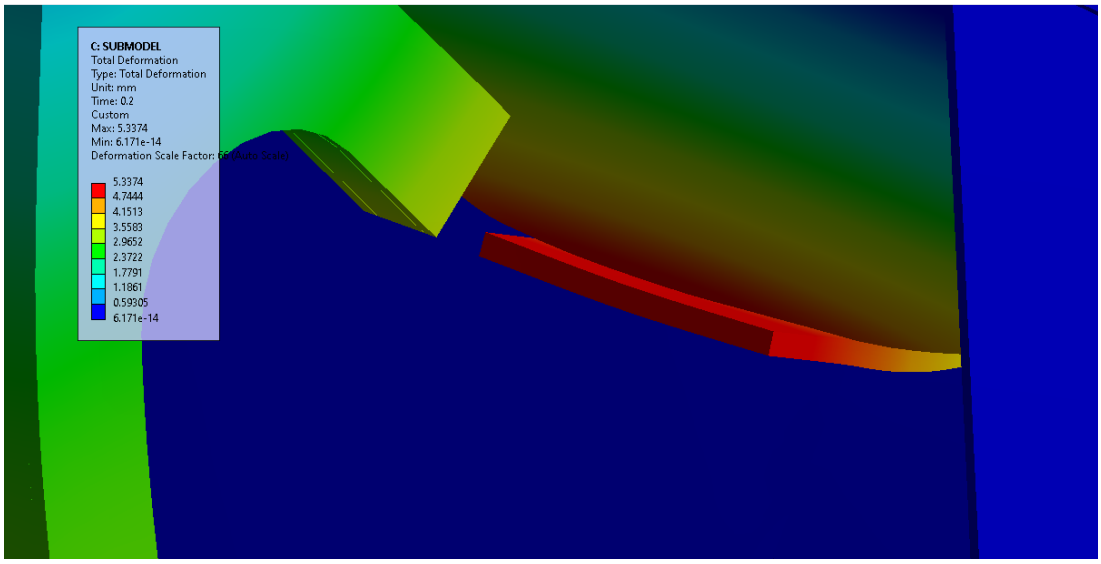

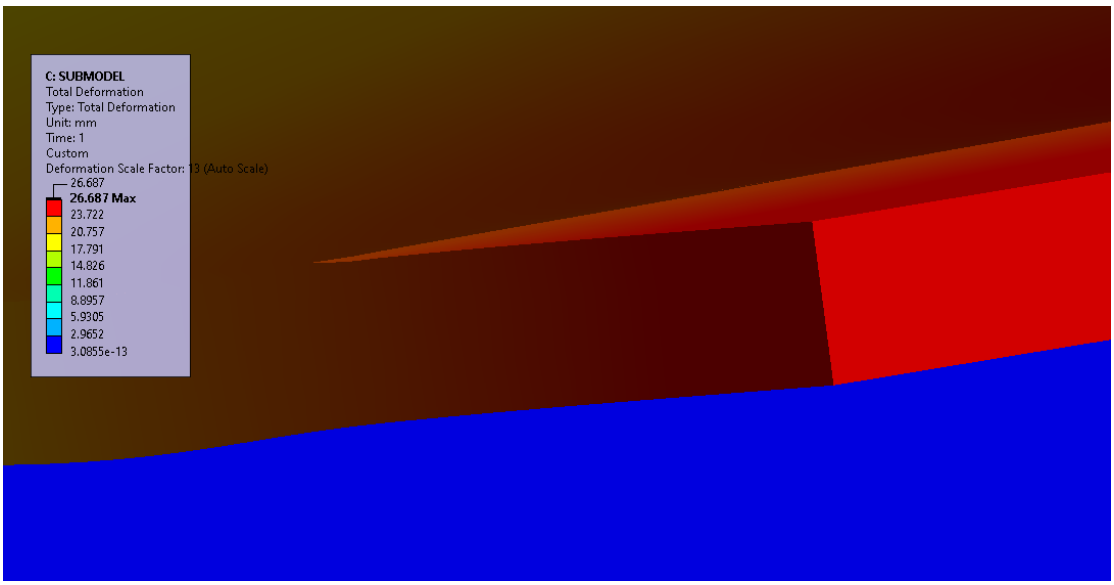

Figure 143:Stop of delamination in crack front 2

Minimum [mm]	Maximum [mm]	Average [mm]
3.0855e-014	2.6687	0.5626
6.171e-014	5.3374	1.1252
1.0799e-013	9.3405	1.969
1.7742e-013	15.345	3.2346
2.4298e-013	21.016	4.4299
3.0855e-013	26.687	5.6253

Based on the Ansys GRANTA Material Library, the single skin E-Glass material has a Fracture Toughness of 18 kJ/m^2.

According to VCCT, the theory is that the energy release rate is larger than the critical value of the linear fracture criterion of 18 kJ/m2. A crack propagation is expected for this region starting from crack 1 (EER $_{at}$ crack $_1$ > 18 kJ/m^2) and stopping at crack 2 (EER $_{at}$ crack $_2$ < 18 kJ/m^2). Therefore, the assumption that delamination will occur at the edge between the end of the T-joint overlamination and the deck, is validated numerically with the above results. Finally, the dominant mode of Energy Release Rate is the Mode I (G1).

A.5.6 Failure of T-Joint under fracture and effects

As expected, the insertion of a crack strip at the end of the edge between the T-Joint and the deck led to the propagation of the crack and the total delamination of the 145cm-long region of the T-Joint overlamination. The crack propagation based on the VCCT Energy Release Rate, shows that the dominant mode of fracture is Mode I, as validated from the shape and results of the cracked region. Also, delamination occurred until the calculated energy release rate became smaller than the critical fracture strength of the E-Glass material. After this, the T-Joint cannot transfer any load to the rest of the bow components. Therefore, we generally conclude that when the T-Joint is cracked in the same manner as in this study, the bow region decreases its mechanical properties from Model(B) to Model(A) with negative results in overall strength.

B.Appendix of Simulation and Materials

B.1. Finite elements for 3D VCCT analysis

SOLID 185

Is used for 3-D modeling of solid structures. Eight nodes are used to define it. Each node has three degrees of freedom: x, y, and z translations. The element is capable of big deflection, large strain, large deflection, plasticity, hyperelasticity, stress stiffening and creep. Additionally, it offers the ability to use mixed formulations to simulate the deformation of completely incompressible hyperelastic materials and virtually incompressible elastoplastic materials [87].

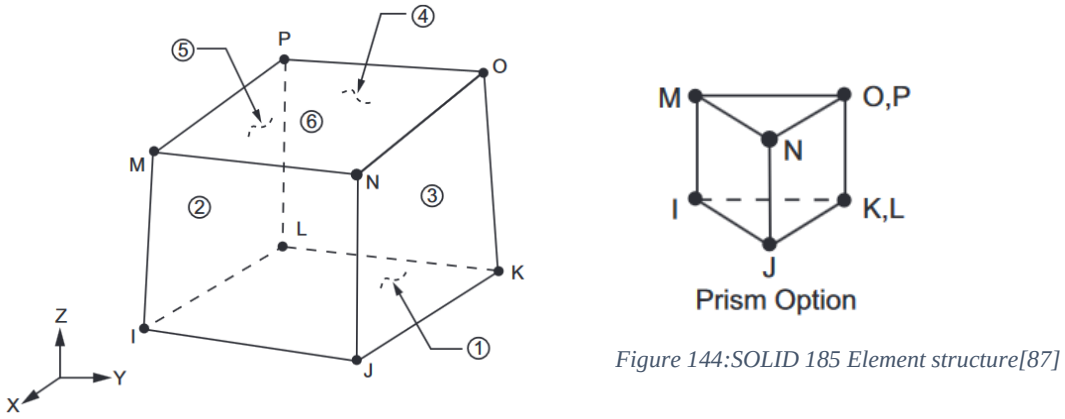

Figure 144:SOLID 185 Element structure[87]

INTER 205

is a linear 3-D interface element with 8 nodes. INTER205 models an interface between two surfaces and the following delamination process when combined with 3-D linear structural components like SOLID185. The separation is represented by a progressive displacement between nodes inside the interface element. At first, the nodes are coincident. Eight nodes that have three degrees of freedom each (translations in the nodal x, y, and z directions) define the element which is a linear 3-D interface with 8 nodes. INTER205 models an interface between two surfaces and the following delamination process when combined with 3-D linear structural components like SOLID185. The separation is represented by a progressive displacement between nodes inside the interface element. At first, the nodes are coincident. Eight nodes that have three degrees of freedom each (translations in the nodal x, y, and z directions) define the element [87].

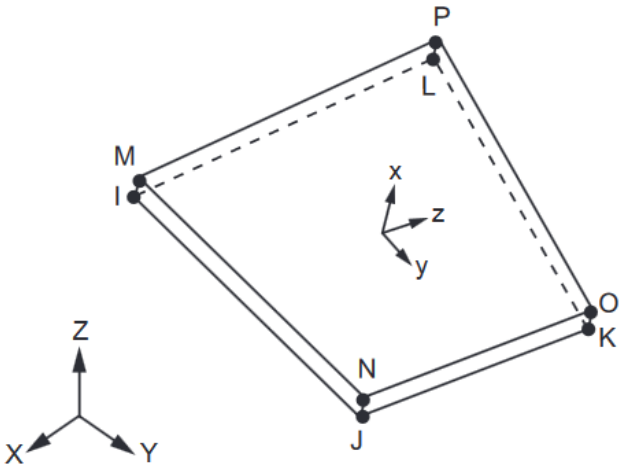

Figure 145:INTER 205 Element Structure [87]

TARGE 170

It is used to represent various 3-D "target" surfaces for the associated contact elements (CONTA173, CONTA174). Contact with the target surface, as described in TARGE170, is possible between contact elements and solid, shell, or line elements that characterize the border of a deformable entity. This target surface is connected to its related contact surface by a shared set of real constants and discretized by a collection of target segment elements (TARGE170).

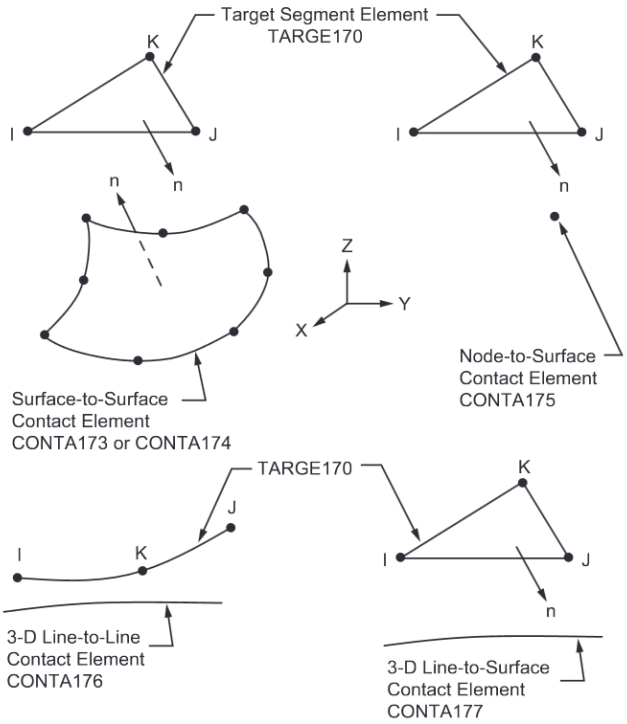

Figure 146:TARGE 170 Element Structure[87]

CONTA 173

It is used to represent contact and sliding between 3-D "target" surfaces (TARGE170) and a deformable surface defined by this element. The element can be used in coupled field contact studies and 3-D structural assessments. This component is found on the surfaces of 3-D solid or shell elements like SOLID185 that are missing mid-side nodes. When an element surface penetrates one of the target segment elements (TARGE170) on a given target surface, contact has occurred. Additionally, this component enables the separation of bonded contacts to simulate interface delamination [87].

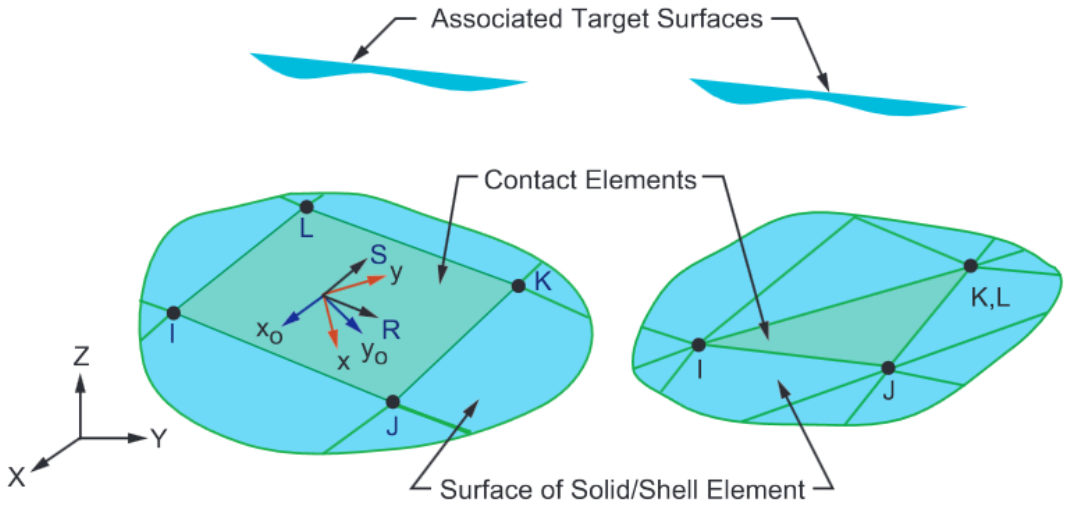

Figure 147:CONTA 173 Element Structure[87]

B.2.Experimental Data of PVC Core

To better evaluate the results of this study, an experimental procedure for PVC core material was conducted. The experiments concern PVC specimens that were subjected to the following mechanical tests:

i. Tensile test
ii. Bending test

The testing procedures were executed in University of West Attica at the Department of Naval Architectures and Marine Engineers in the laboratory of Materials, under the supervision of the professor Isidoros Iakovidis. To retrieve the results five specimens were used for each testing. Only the data of successful specimens were taken into account. These data are used as validation for the materials used.

Tensile test of PVC Specimens

The geometrical characteristics of the tensile specimens are given below.

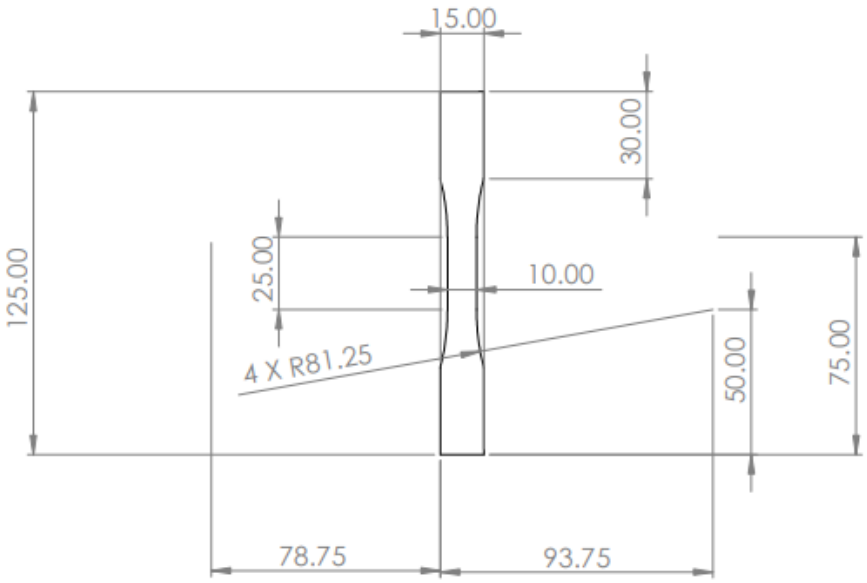

Figure 148:PVC Tensile Specimen dimensions

The data results from the testing of three successful samples are shown below:

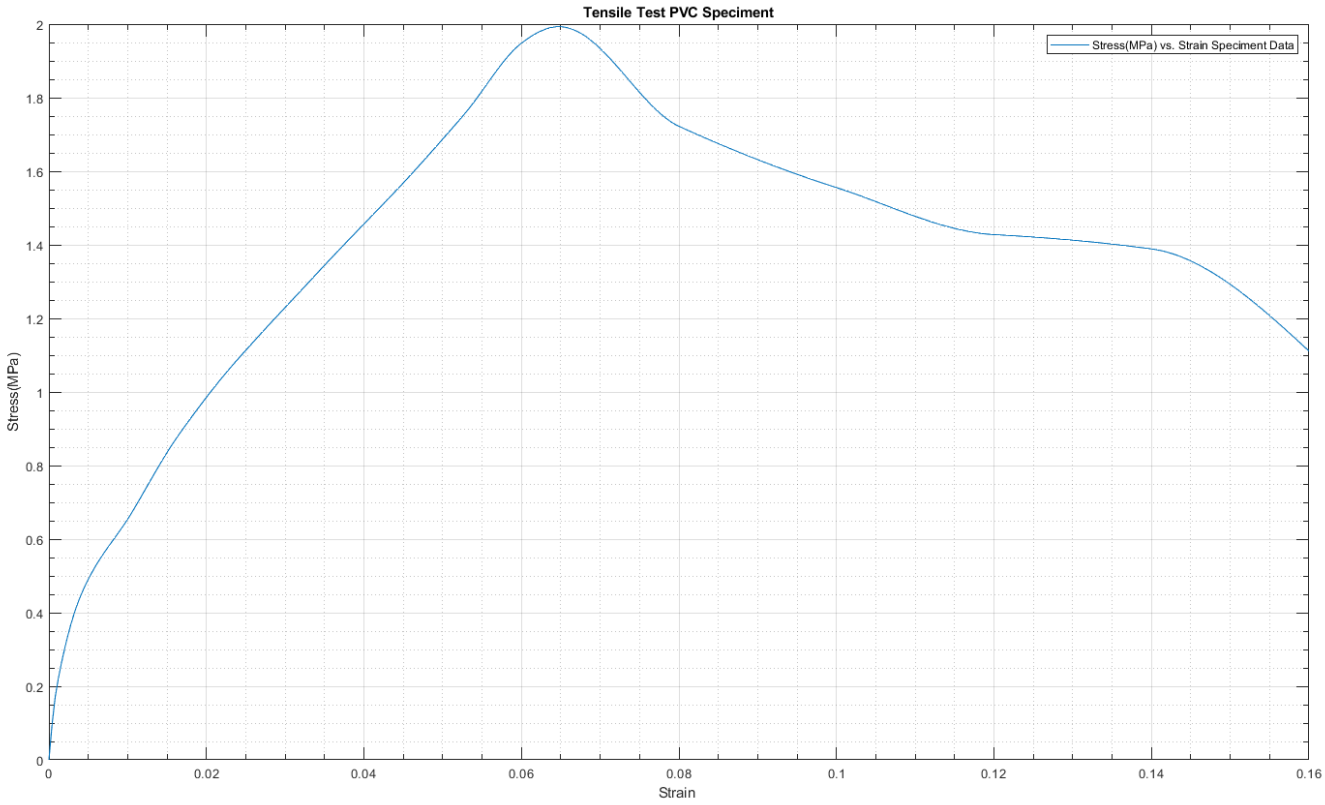

Figure 149:Stress-Strain graph of PVC Tensile Specimen

Bending test of PVC Specimens

The geometrical characteristics of the bending specimens are given below:

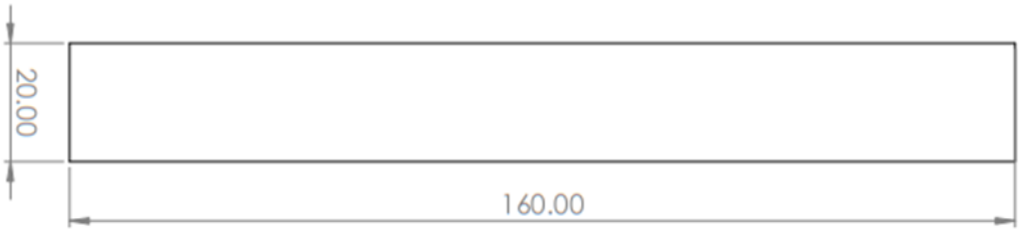

Figure 150:PVC Bending Specimen dimensions

Bending tests were executed for one failed specimen. Due to the large elasticity of the pvc bending specimen, no breaking occurred. After the unloading, the specimen returned to its initial dimensions. Therefore, the data results of the bending testing conclude that there is no breaking of the pvc core material in the bending mode. This is a main reason for which composite sandwich materials are resistant to bending.

C.Appendix of Ply Wise Analysis

C.1.Model(A)

- Frame

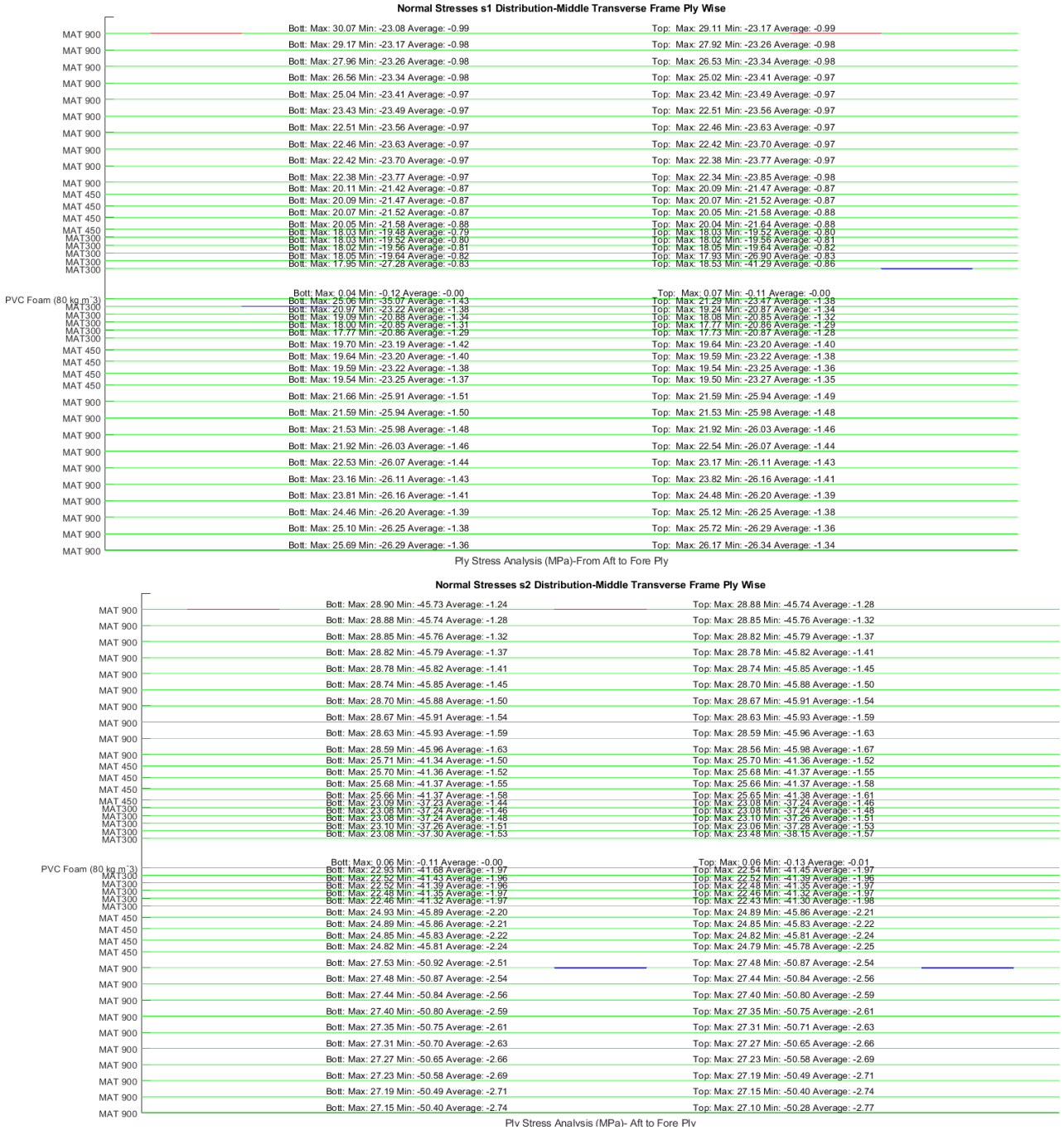

Figure 151: Model(A): Ply Analysis of Normal and Shear Stresses Distribution of Middle Frame

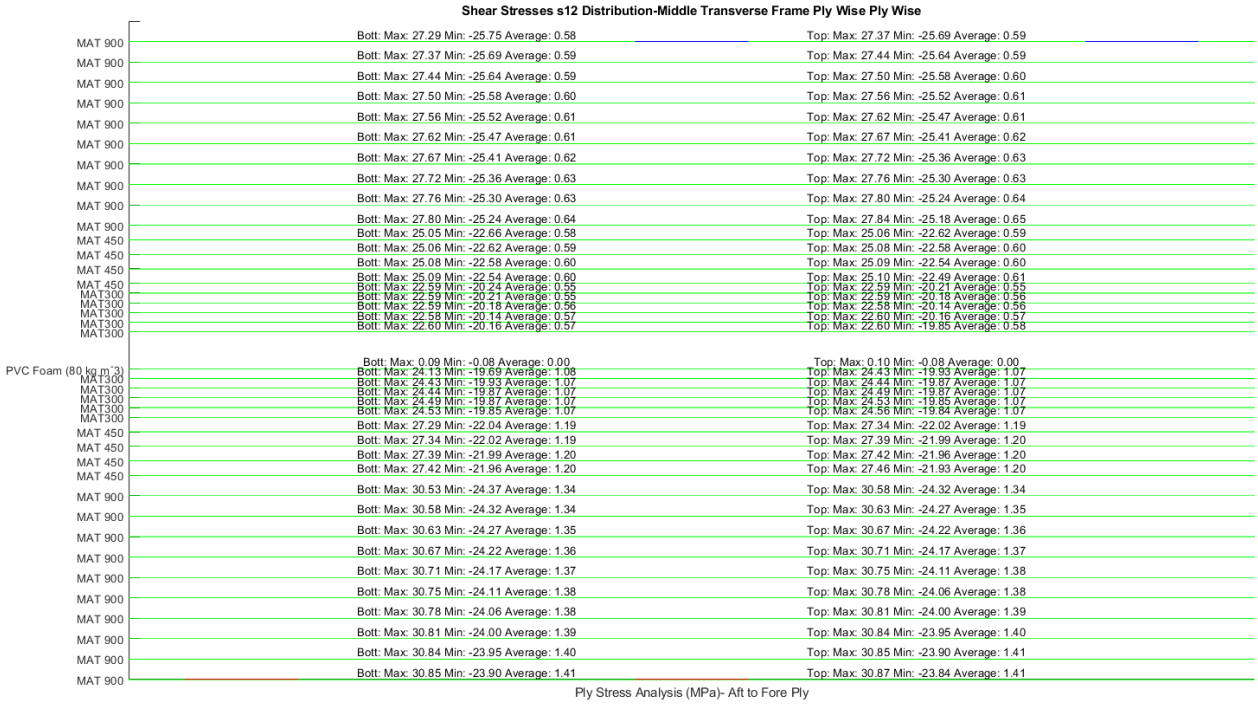

Figure 152: Model(A): Ply Analysis of Tsai Wu Failure Safety Factor Distribution of Middle Frame

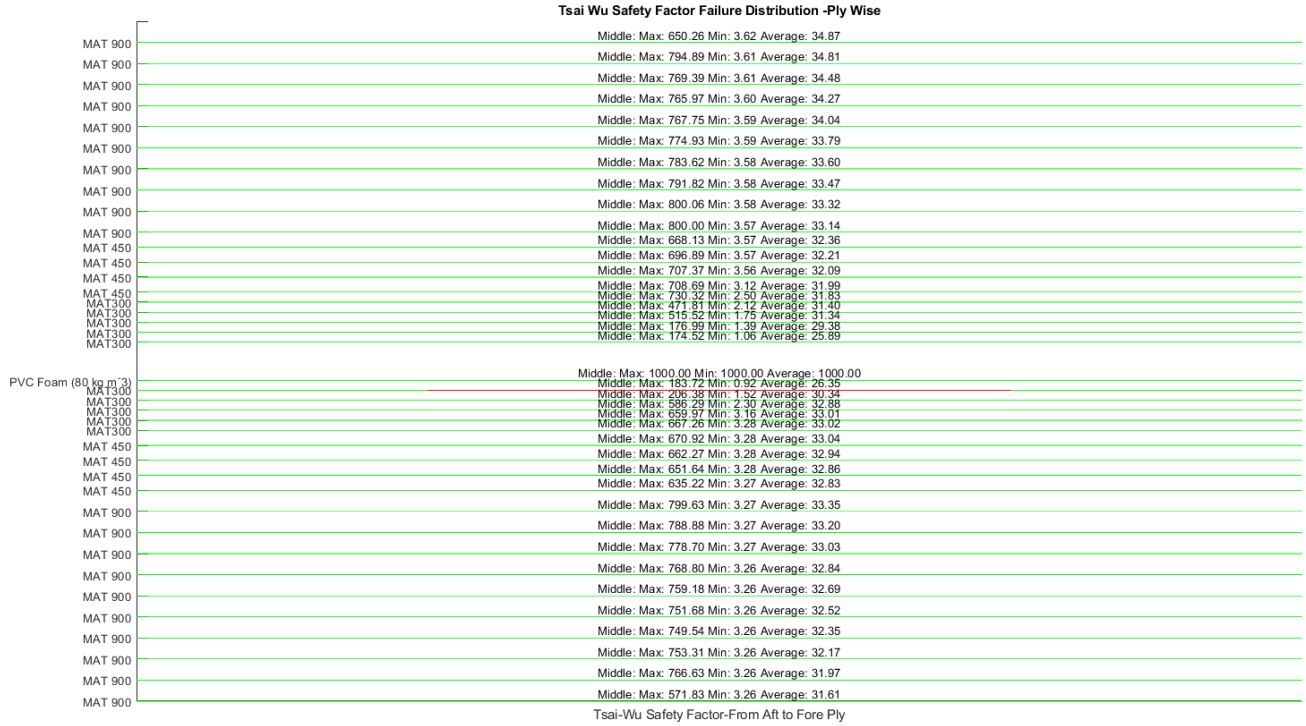

- Deck

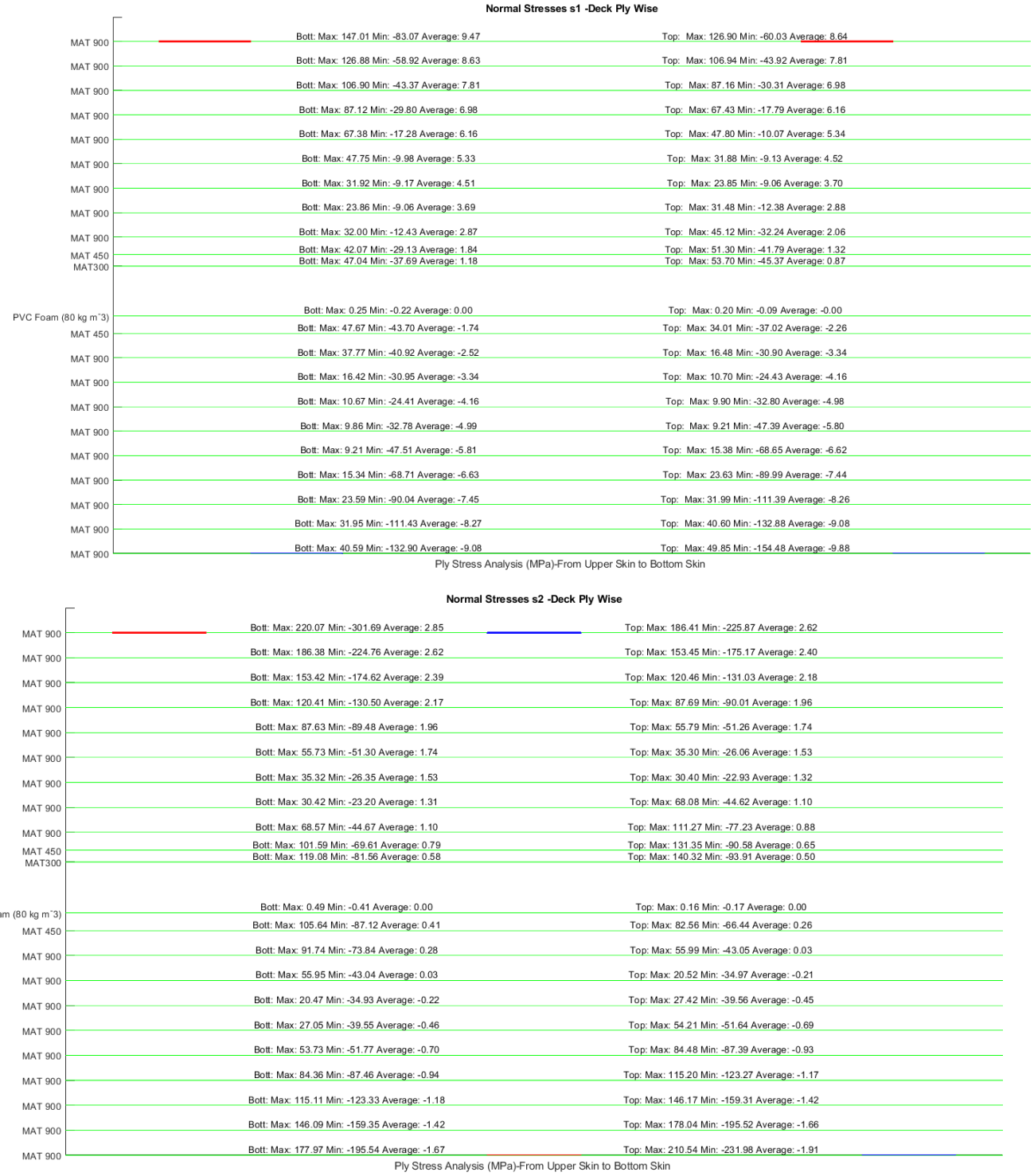

Figure 153: Model(A): Ply Analysis of Normal and Shear Stresses Distribution of Deck

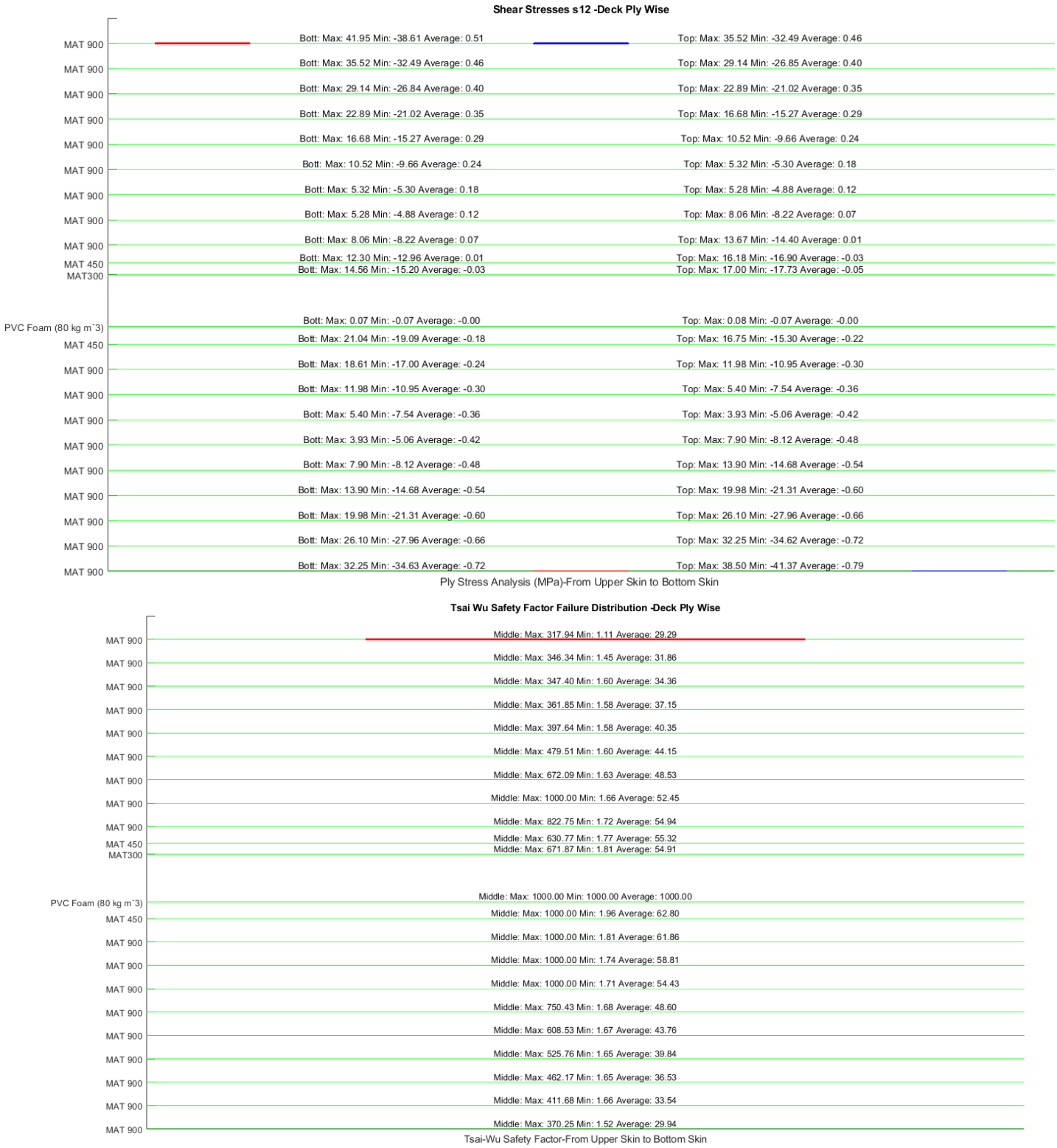

Figure 154: Model(A): Ply Analysis of Tsai Wu Failure Safety Factor Distribution of Deck

C.2.Model(B)

- Frame

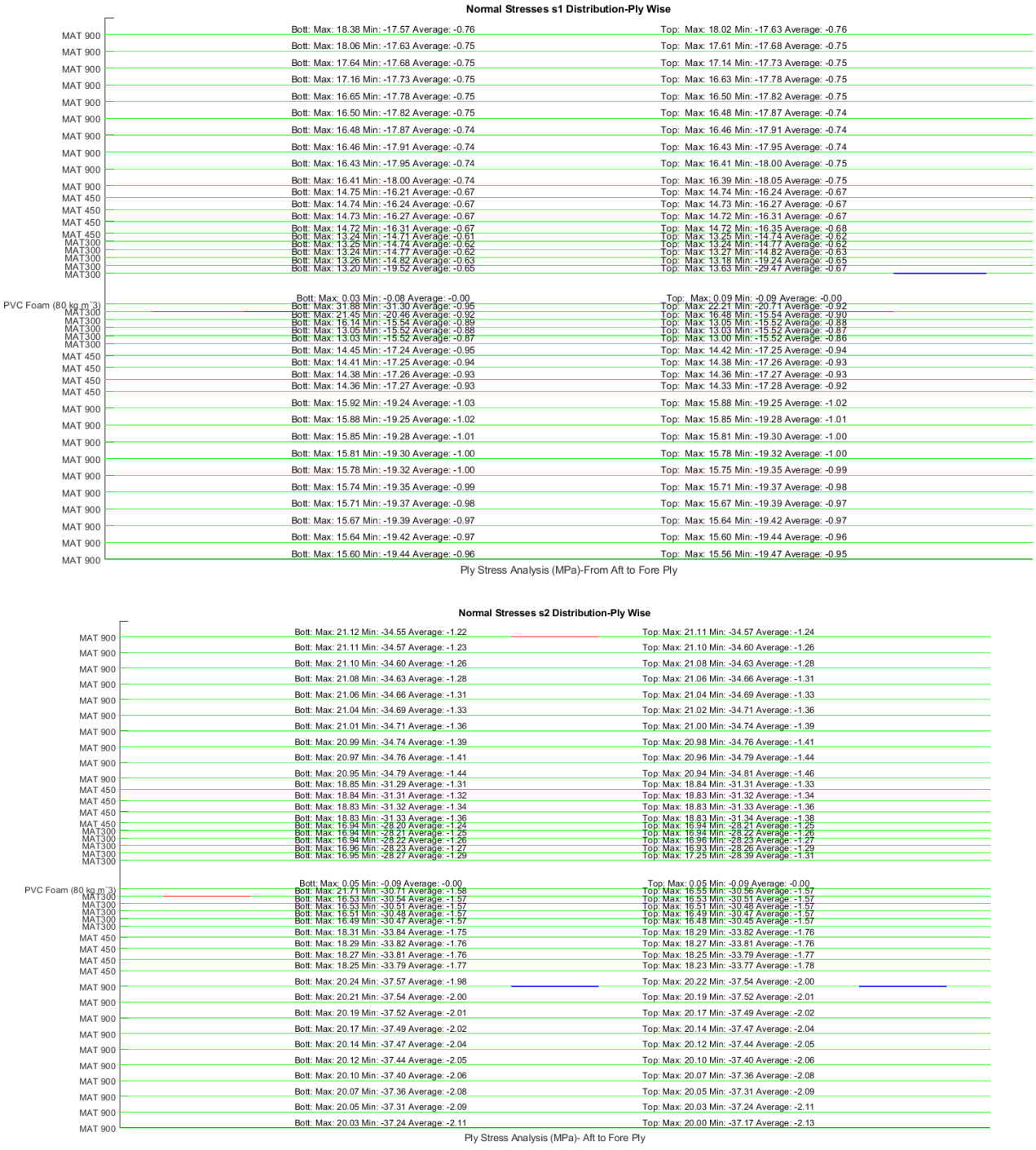

Figure 155: Model(B): Ply Analysis of Normal and Shear Stresses Distribution of Middle Frame

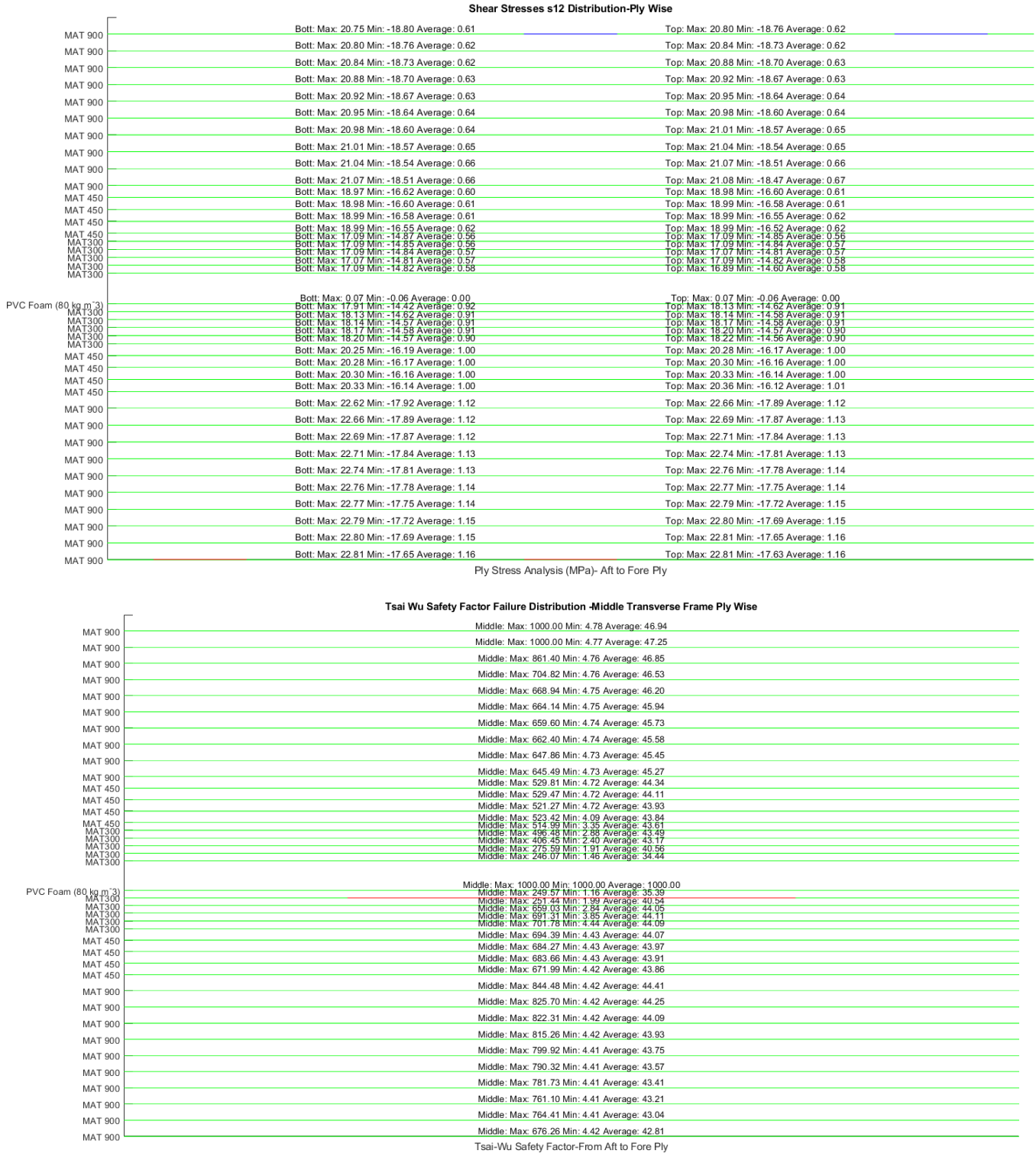

Figure 156: Model(B): Ply Analysis of Tsai-Wu Failure Safety Factor Distribution of Middle Frame

Πανεπιστημιούπολη
Άλσους Αιγάλεω
Αγίου Σπυρίδωνος, Αιγάλεω 12243
τηλ: 210 5385100

- Deck

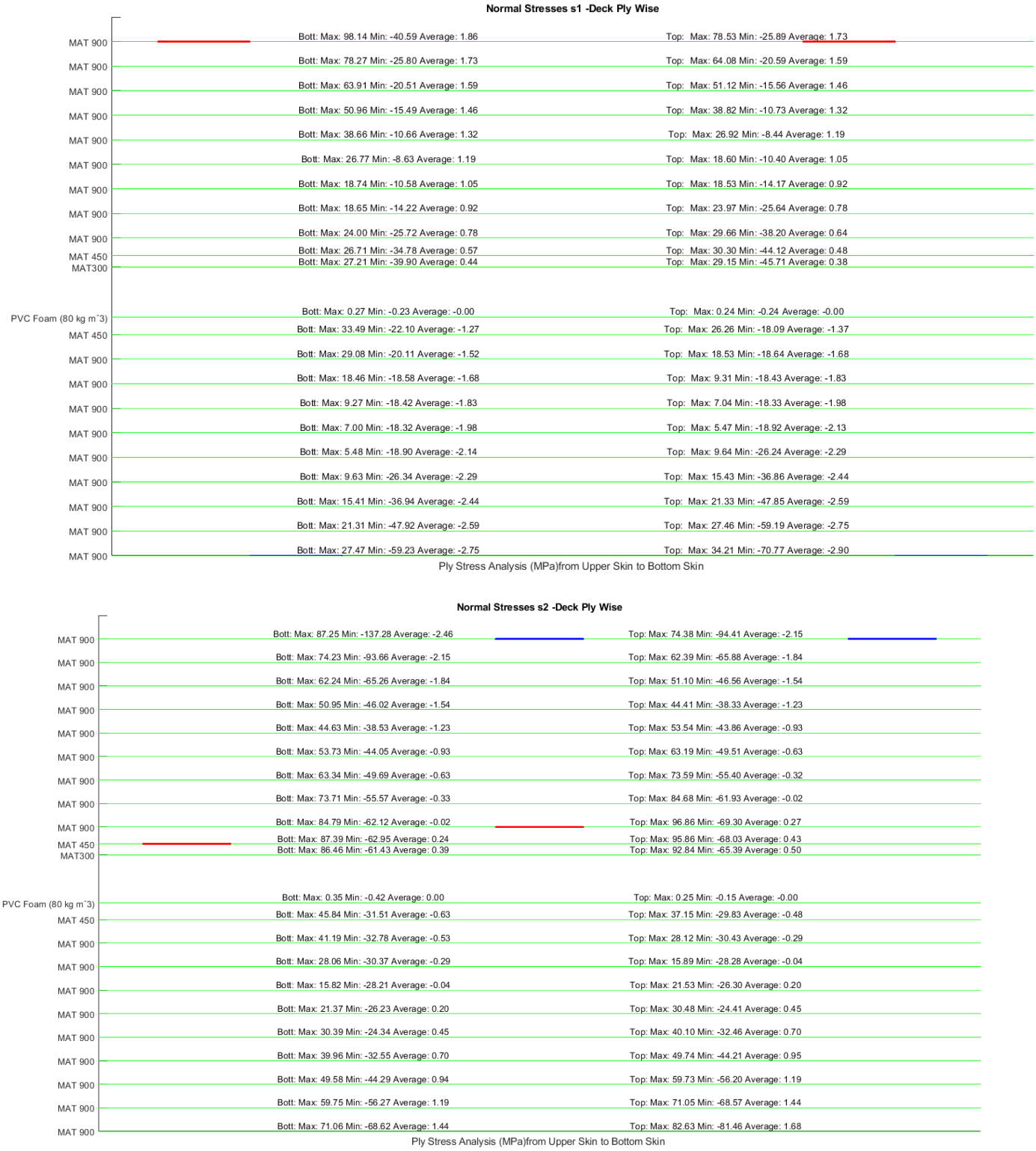

Figure 157: Model(B): Ply Analysis of Normal and Shear Stresses Distribution of Deck

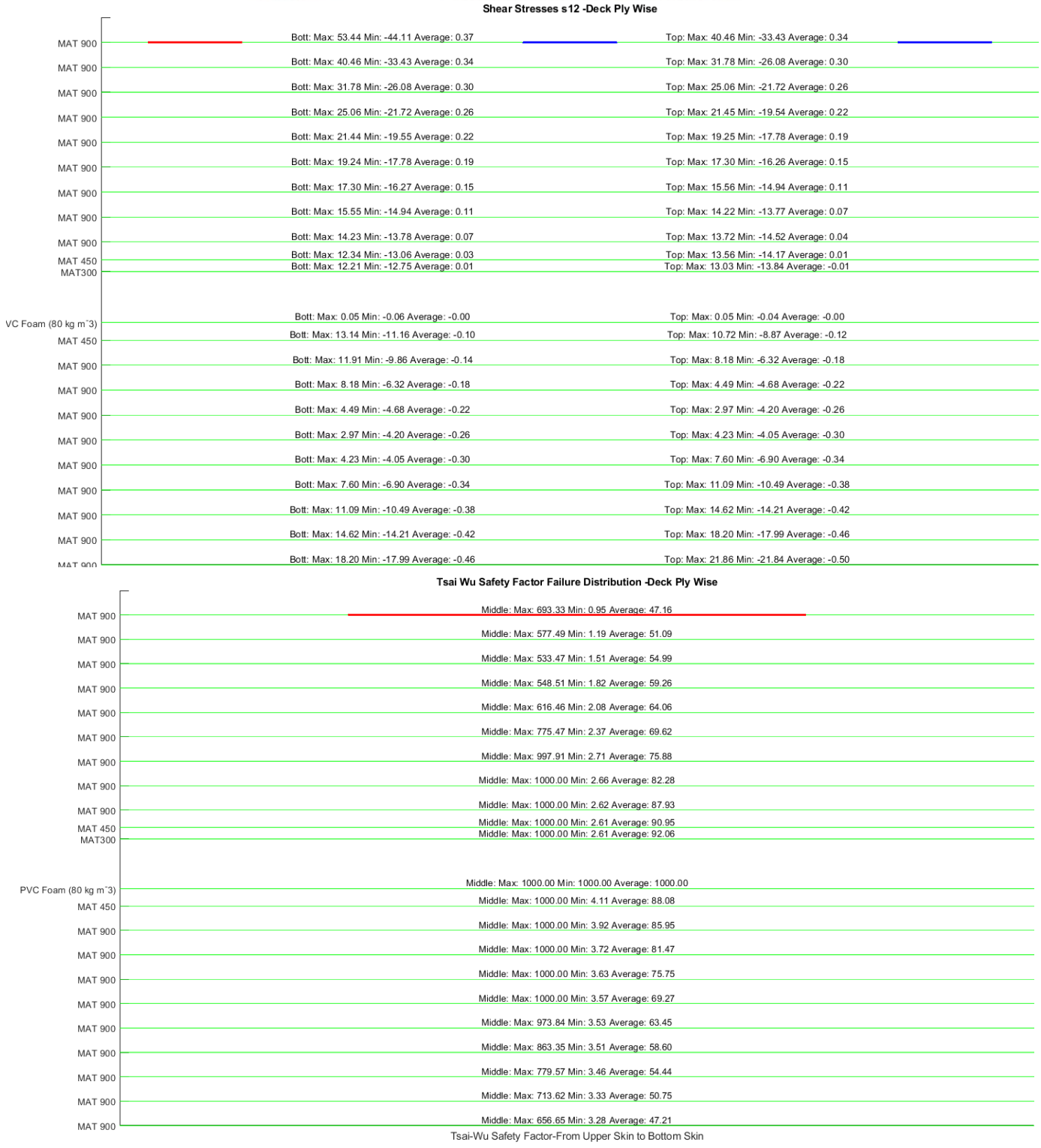

Figure 158: Model(B): Ply Analysis of Tsai-Wu Failure Safety Factor Distribution of Deck

Πανεπιστημιούπολη
Άλσους Αιγάλεω
Αγίου Σπυρίδωνος, Αιγάλεω 12243
τηλ: 210 5385100

- T-Joint

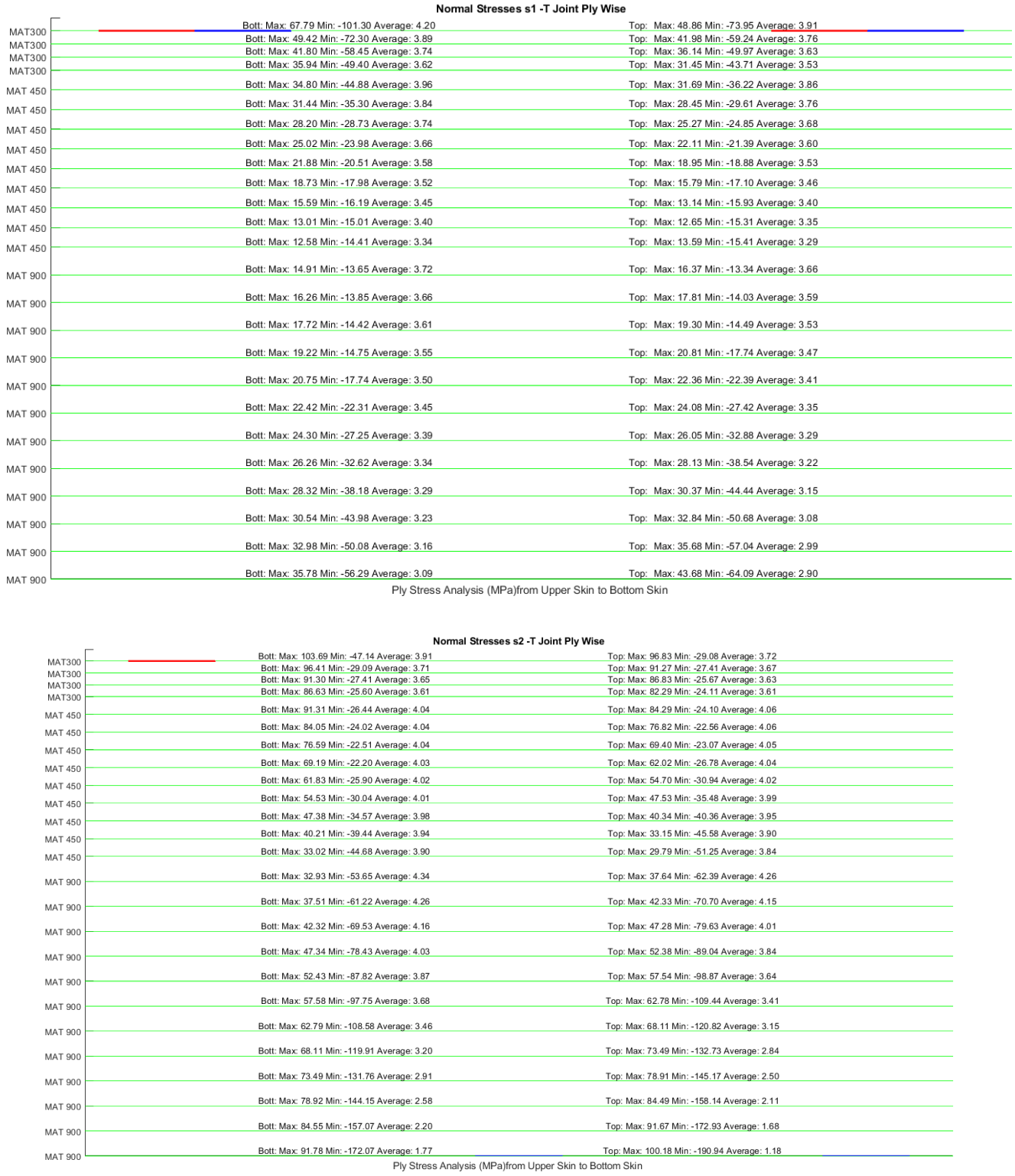

Figure 159: Model(B): Ply Analysis of Normal and Shear Stresses Distribution of T-Joint

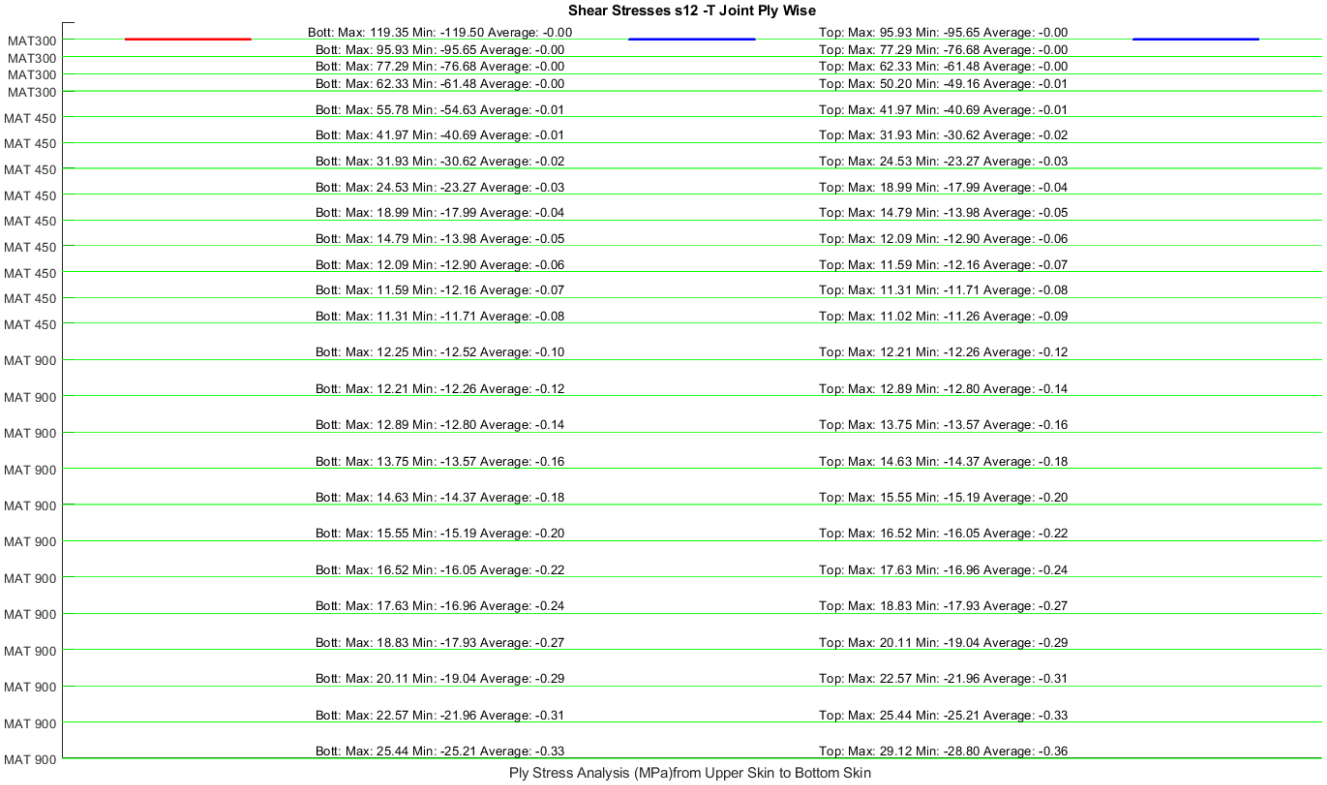

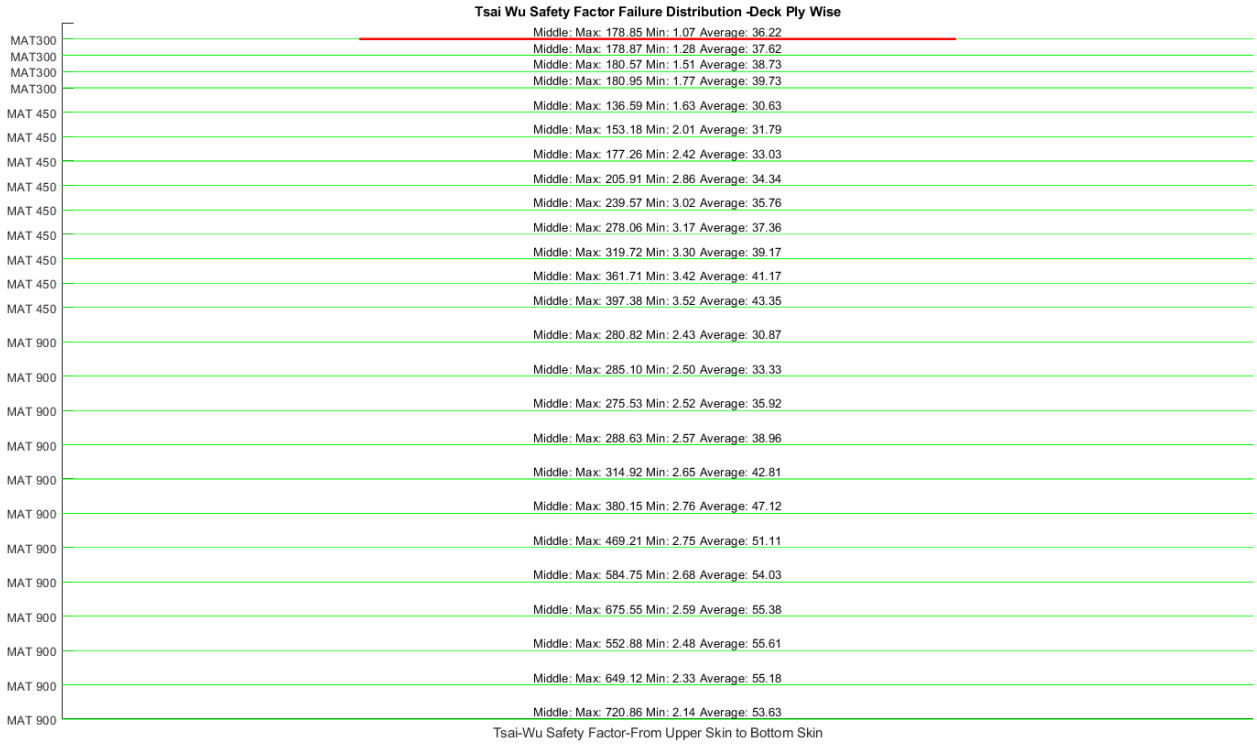

Figure 160: Model(B): Ply Analysis of Tsai-Wu Failure Safety Factor Distribution of T-Joint

Πανεπιστημιούπολη
Άλσους Αιγάλεω
Αγίου Σπυρίδωνος, Αιγάλεω 12243
τηλ: 210 5385100

References

[1] A. P. Mouritz, E. Gellert, P. Burchill, and K. Challis, "Review of advanced composite structures for naval ships and submarines," *Compos. Struct.*, vol. 53, no. 1, pp. 21–42, Jul. 2001, doi: 10.1016/S0263-8223(00)00175-6.

[2] G. Neşer, "Polymer Based Composites in Marine Use: History and Future Trends," *Procedia Eng.*, vol. 194, pp. 19–24, 2017, doi: 10.1016/j.proeng.2017.08.111.

[3] G. Di Bella, G. Galtieri, E. Pollicino, and C. Borsellino, "JOINING OF GFRP IN MARINE APPLICATIONS," in *Advances in materials science research: Volume 12*, M. C. Wythers, Ed., New York: Nova Science Publishers, Inc, 2013.

[4] F. Dharmawan, "Structural integrity and damage tolerance of composite t-joints in naval vessels," RMIT University, 2008.

[5] A. Riccio and A. Sellitto, "Analytical Tool for the Preliminary Design of an Adhesively Bonded T Joint," *Key Eng. Mater.*, vol. 665, pp. 285–288, Sep. 2015, doi: 10.4028/www.scientific.net/KEM.665.285.

[6] M. D. Banea and L. F. M. da Silva, "Adhesively bonded joints in composite materials: An overview," *Proc. Inst. Mech. Eng. Part J. Mater. Des. Appl.*, vol. 223, no. 1, pp. 1–18, Jan. 2009, doi: 10.1243/14644207JMDA219.

[7] S. K. Panda and P. K. Mishra, "Adhesion failure resistance techniques in T-type composite joints," p. 13, 2019.

[8] R. Masoudi Nejad, D. Ghahremani Moghadam, M. Hadi, P. Zamani, and F. Berto, "An investigation on static and fatigue life evaluation of grooved adhesively bonded T-joints," *Structures*, vol. 35, pp. 340–349, Jan. 2022, doi: 10.1016/j.istruc.2021.11.025.

[9] M. R. Khosravani and K. Weinberg, "Characterization of sandwich composite T-joints under different ageing conditions," *Compos. Struct.*, vol. 197, pp. 80–88, Aug. 2018, doi: 10.1016/j.compstruct.2018.05.043.

[10] M. R. Khosravani, D. Anders, and K. Weinberg, "Influence of strain rate on fracture behavior of sandwich composite T-joints," *Eur. J. Mech. - ASolids*, vol. 78, p. 103821, Nov. 2019, doi: 10.1016/j.euromechsol.2019.103821.

[11] M. R. Khosravani, "Influences of Defects on the Performance of Adhesively Bonded Sandwich Joints," *Key Eng. Mater.*, vol. 789, pp. 45–50, Nov. 2018, doi: 10.4028/www.scientific.net/KEM.789.45.

[12] S. M. R. Khalili and A. Ghaznavi, "Numerical analysis of adhesively bonded T-joints with structural sandwiches and study of design parameters," *Int. J. Adhes. Adhes.*, vol. 31, no. 5, pp. 347–356, Jul. 2011, doi: 10.1016/j.ijadhadh.2010.12.005.

[13] M. Omidali and M. R. Khedmati, "Numerical investigation on novel geometrical configuration for adhesively bonded T-joint between aluminum and sandwich panel," *Thin-Walled Struct.*, vol. 131, pp. 122–134, Oct. 2018, doi: 10.1016/j.tws.2018.06.039.

[14] P. Fernandes, G. Viana, R. J. C. Carbas, M. Costa, L. F. M. da Silva, and M. D. Banea, "The influence of water on the fracture envelope of an adhesive joint," *Theor. Appl. Fract. Mech.*, vol. 89, pp. 1–15, Jun. 2017, doi: 10.1016/j.tafmec.2017.01.001.

[15] F. Bianchi, T. M. Koh, X. Zhang, I. K. Partridge, and A. P. Mouritz, "Finite element modelling of z-pinned composite T-joints," *Compos. Sci. Technol.*, vol. 73, pp. 48–56, Nov. 2012, doi: 10.1016/j.compscitech.2012.09.008.

[16] C. Li, Y. Sun, C. Duan, and R. Li, "Study on Properties of Z-pin-reinforced and Rivet-reinforced Composite T-joint: Experiment and Simulation," *Appl. Compos. Mater.*, vol. 28, no. 2, pp. 395–408, Apr. 2021, doi: 10.1007/s10443-021-09866-2.

[17] J. Bigaud, Z. Aboura, A. T. Martins, and S. Verger, "Analysis of the mechanical behavior of composite T-joints reinforced by one side stitching," *Compos. Struct.*, vol. 184, pp. 249–255, Jan. 2018, doi: 10.1016/j.compstruct.2017.06.041.

[18] P. B. Stickler and M. Ramulu, "Parametric analyses of stitched composite T-joints by the finite element method," *Mater. Des.*, vol. 23, no. 8, pp. 751–758, Dec. 2002, doi: 10.1016/S0261-3069(02)00070-5.

[19] Z. L. Liu, P. R. Jia, T. Peng, and Z. L. Yao, "Study on Tensile Mechanical Behavior of Composite T-Joints," *Adv. Mater. Res.*, vol. 1142, pp. 146–151, Jan. 2017, doi: 10.4028/www.scientific.net/AMR.1142.146.

[20] H. Toftegaard and A. Lystrup, "Design and test of lightweight sandwich T-joint for naval ships," *Compos. Part Appl. Sci. Manuf.*, vol. 36, no. 8, pp. 1055–1065, Aug. 2005, doi: 10.1016/j.compositesa.2004.10.031.

[21] E. A. Diler, Ç. Özes, and G. Neşer, "Effect of T-Joint Geometry on the Performance of a GRP/PVC Sandwich System Subjected to Tension," *J. Reinf. Plast. Compos.*, vol. 28, no. 1, pp. 49–58, Jan. 2009, doi: 10.1177/0731684407081378.

[22] S. Yan, X. Zeng, and A. Long, "Experimental assessment of the mechanical behaviour of 3D woven composite T-joints," *Compos. Part B Eng.*, vol. 154, pp. 108–113, Dec. 2018, doi: 10.1016/j.compositesb.2018.08.007.

[23] H. Wu, J. Xiao, S. Xing, S. Wen, F. Yang, and J. Yang, "Numerical and experimental investigation into failure of T700/bismaleimide composite T-joints under tensile loading," *Compos. Struct.*, vol. 130, pp. 63–74, Oct. 2015, doi: 10.1016/j.compstruct.2015.04.019.

[24] X. Li, Z. Liu, L. Hu, Y. Wang, B. Lei, and X. Huang, "Numerical Investigation of T-joints with 3D Four Directional Braided Composite Fillers Under Tensile Loading," *Appl. Compos. Mater.*, vol. 24, no. 1, pp. 171–191, Feb. 2017, doi: 10.1007/s10443-016-9520-5.

[25] J.-B. Bai, C.-H. Dong, J.-J. Xiong, C.-Y. Luo, and D. Chen, "Progressive damage behaviour of RTM-made composite T-joint under tensile loading," *Compos. Part B Eng.*, vol. 160, pp. 488–497, Mar. 2019, doi: 10.1016/j.compositesb.2018.12.069.

[26] L. Burns, A. P. Mouritz, D. Pook, and S. Feih, "Strengthening of composite T-joints using novel ply design approaches," *Compos. Part B Eng.*, vol. 88, pp. 73–84, Mar. 2016, doi: 10.1016/j.compositesb.2015.10.032.

[27] R. S. Trask, S. R. Hallett, F. M. M. Helenon, and M. R. Wisnom, "Influence of process induced defects on the failure of composite T-joint specimens," *Compos. Part Appl. Sci. Manuf.*, vol. 43, no. 4, pp. 748–757, Apr. 2012, doi: 10.1016/j.compositesa.2011.12.021.

[28] X. Ma, K. Bian, H. Liu, Y. Wang, and K. Xiong, "Numerical and experimental investigation of the interface properties and failure strength of CFRP T-Stiffeners

subjected to pull-off load," *Mater. Des.*, vol. 185, p. 108231, Jan. 2020, doi: 10.1016/j.matdes.2019.108231.

[29] T. Ekermann and S. Hallström, "Pull-off tests of CFRP T-joints with conventional and 3D reinforced fillets," *Compos. Struct.*, vol. 223, p. 110893, Sep. 2019, doi: 10.1016/j.compstruct.2019.110893.

[30] U. V. R. S. Turaga and C. T. Sun, "Failure Modes and Load Transfer in Sandwich T-Joints," *J. Sandw. Struct. Mater.*, vol. 2, no. 3, pp. 225–245, Jul. 2000, doi: 10.1177/109963620000200304.

[31] S. M. R. Khalili and A. Ghaznavi, "Behavior and Failure Modes of Sandwich T-Joint Using Cohesive Zone Material Model and Contact Elements," *Appl. Compos. Mater.*, vol. 20, no. 1, pp. 41–54, Feb. 2013, doi: 10.1007/s10443-012-9248-9.

[32] S. Guo and W. Li, "Numerical analysis and experiment of sandwich T-joint structure reinforced by composite fasteners," *Compos. Part B Eng.*, vol. 199, p. 108288, Oct. 2020, doi: 10.1016/j.compositesb.2020.108288.

[33] D. W. Zhou, L. A. Louca, and M. Saunders, "Numerical simulation of sandwich T-joints under dynamic loading," *Compos. Part B Eng.*, vol. 39, no. 6, pp. 973–985, Sep. 2008, doi: 10.1016/j.compositesb.2007.12.002.

[34] H. C. H. Li, F. Dharmawan, I. Herszberg, and S. John, "Fracture behaviour of composite maritime T-joints," *Compos. Struct.*, vol. 75, no. 1–4, pp. 339–350, Sep. 2006, doi: 10.1016/j.compstruct.2006.04.052.

[35] F. Dharmawan, H. C. H. Li, I. Herszberg, and S. John, "Applicability of the crack tip element analysis for damage prediction of composite T-joints," *Compos. Struct.*, vol. 86, no. 1–3, pp. 61–68, Nov. 2008, doi: 10.1016/j.compstruct.2008.03.030.

[36] F. Dharmawan, S. John, H. C. H. Li, and I. Herszberg, "Damage prediction models for composite T-Joints in marine applications," p. 7.

[37] G. Di Bella, C. Borsellino, E. Pollicino, and V. F. Ruisi, "Experimental and numerical study of composite T-joints for marine application," *Int. J. Adhes. Adhes.*, vol. 30, no. 5, pp. 347–358, Jul. 2010, doi: 10.1016/j.ijadhadh.2010.03.002.

[38] Ç. Özes and Ö. Aydin, "Analysis of Sandwich T-Joints under Compression Loads in Marine Applications," *Adv. Compos. Lett.*, vol. 18, no. 3, p. 096369350901800, May 2009, doi: 10.1177/096369350901800301.

[39] F. Dharmawan, R. S. Thomson, H. Li, I. Herszberg, and E. Gellert, "Geometry and damage effects in a composite marine T-joint," *Compos. Struct.*, vol. 66, no. 1–4, pp. 181–187, Oct. 2004, doi: 10.1016/j.compstruct.2004.04.036.

[40] X. Li, Z. Zhu, Y. Li, and Z. Hu, "Design and Mechanical Analysis of a Composite T-Type Connection Structure for Marine Structures," *Pol. Marit. Res.*, vol. 27, no. 2, pp. 145–157, Jun. 2020, doi: 10.2478/pomr-2020-0036.

[41] V. Marcadon, Y. Nadot, A. Roy, and J. L. Gacougnolle, "Fatigue behaviour of T-joints for marine applications," *Int. J. Adhes. Adhes.*, vol. 26, no. 7, pp. 481–489, Oct. 2006, doi: 10.1016/j.ijadhadh.2005.07.002.

[42] R. A. Shenoi, P. J. C. L. Read, and G. L. Hawkins, "Fatigue failure mechanisms in fibre-reinforced plastic laminated tee joints," *Int. J. Fatigue*, vol. 17, no. 6, pp. 415–426, 1995, doi: 10.1016/0142-1123(95)98238-X.

[43] R. A. Shenoi and G. L. Hawkins, "Influence of material and geometry variations on the behaviour of bonded tee connections in FRP ships," *Composites*, vol. 23, no. 5, pp. 335–345, Sep. 1992, doi: 10.1016/0010-4361(92)90333-P.

[44] A. R. Dodkins, R. A. Shenoi, and G. L. Hawkins, "Design of joints and attachments in FRP ships' structures," *Mar. Struct.*, vol. 7, no. 2–5, pp. 365–398, Jan. 1994, doi: 10.1016/0951-8339(94)90031-0.

[45] J. I. R. Blake, R. A. Shenoi, J. House, and T. Turton, "Progressive damage analysis of tee joints with viscoelastic inserts," *Compos. Part Appl. Sci. Manuf.*, vol. 32, no. 5, pp. 641–653, May 2001, doi: 10.1016/S1359-835X(00)00158-5.

[46] E. E. Theotokoglou and T. Moan, "Experimental and Numerical Study of Composite T-Joints," *J. Compos. Mater.*, vol. 30, no. 2, pp. 190–209, Jan. 1996, doi: 10.1177/002199839603000203.

[47] E. E. Theotokoglou, "Study of the Numerical Fracture Mechanics Analysis of Composite T-Joints," *J. Reinf. Plast. Compos.*, vol. 18, no. 3, pp. 215–223, Feb. 1999, doi: 10.1177/073168449901800302.

[48] E. E. Theotokoglou, "Numerical Investigation of Crack Propagation in Sandwich Structures," in *Fracture of Nano and Engineering Materials and Structures*, E. E. Gdoutos, Ed., Dordrecht: Springer Netherlands, 2006, pp. 563–564. doi: 10.1007/1-4020-4972-2_279.

[49] E. E. Theotokoglou, "Strength of Composite T-Joints under Pull-Out Loads," *J. Reinf. Plast. Compos.*, vol. 16, no. 6, pp. 503–518, Apr. 1997, doi: 10.1177/073168449701600602.

[50] E. E. Theotokoglou, "FAILURE MODES IN COMPOSITE JOINTS A FINITE ELEMENT STUDY," p. 7.

[51] B. Bureau Veritas, "HULL IN COMPOSITE, PLYWOOD, AND HIGH DENSITY POLYETHYLENE MATERIALS," Bureau Veritas, Rule Note NR546, Nov. 2022.

[52] J. R. Weitzenböck, Ed., *Adhesives in marine engineering*. in Woodhead Publishing in materials. Oxford ; Philadelphia: Woodhead Pub, 2012.

[53] L. F. M. da Silva and R. D. S. G. Campilho, "Design of adhesively-bonded composite joints," in *Fatigue and Fracture of Adhesively-Bonded Composite Joints*, Elsevier, 2015, pp. 43–71. doi: 10.1016/B978-0-85709-806-1.00002-1.

[54] B. Bureau Veritas, "Adhesive Joints and Patch Repair," Bureau Veritas, Guidance Note 613, May 2015.

[55] D. Zenkert and Nordisk Industrifond, Eds., *The handbook of sandwich construction*. in North European engineering and science conference series. Cradley Heath, West Midlands: Engineering Materials Advisory Services Ltd. (EMAS), 1997.

[56] A. A. Griffith, "VI. The phenomena of rupture and flow in solids," *Philos. Trans. R. Soc. Lond. Ser. Contain. Pap. Math. Phys. Character*, vol. 221, no. 582–593, pp. 163–198, Jan. 1921, doi: 10.1098/rsta.1921.0006.

[57] C. E. Inglis, "Stresses in a plate due to the presence of cracks and sharp corners," Transactions of the Institute of Naval Architects, 1913.

[58] G. R. Irwin, "ONSET OF FAST CRACK PROPAGATION IN HIGH STRENGTH STEEL AND ALUMINUM ALLOYS," Naval Research Lab., Washington, D.C., Technical Report, May 1956.

[59] G. R. Irwin, "Analysis of Stresses and Strains Near the End of a Crack Traversing a Plate," *J. Appl. Mech.*, vol. 24, no. 3, pp. 361–364, Sep. 1957, doi: 10.1115/1.4011547.

[60] H. M. Westergaard, "Bearing Pressures and Cracks," *J. Appl. Mech.*, vol. 49, p. 4953, 1939.

[61] T. L. Anderson, "Fracture Mechanics," p. 680.

[62] G. I. Barenblatt, "The Mathematical Theory of Equilibrium Cracks in Brittle Fracture," in *Advances in Applied Mechanics*, Elsevier, 1962, pp. 55–129. doi: 10.1016/S0065-2156(08)70121-2.

[63] D. S. Dugdale, "Yielding of steel sheets containing slits," *J. Mech. Phys. Solids*, vol. 8, no. 2, pp. 100–104, May 1960, doi: 10.1016/0022-5096(60)90013-2.

[64] J. R. Rice, "A Path Independent Integral and the Approximate Analysis of Strain Concentration by Notches and Cracks," *J. Appl. Mech.*, vol. 35, no. 2, pp. 379–386, Jun. 1968, doi: 10.1115/1.3601206.

[65] J. R. Rice and G. F. Rosengren, "Plane strain deformation near a crack tip in a power-law hardening material," *J. Mech. Phys. Solids*, vol. 16, no. 1, pp. 1–12, Jan. 1968, doi: 10.1016/0022-5096(68)90013-6.

[66] J. W. Hutchinson, "Singular behaviour at the end of a tensile crack in a hardening material," *J. Mech. Phys. Solids*, vol. 16, no. 1, pp. 13–31, Jan. 1968, doi: 10.1016/0022-5096(68)90014-8.

[67] C. F. Shih and J. W. Hutchinson, "Fully Plastic Solutions and Large Scale Yielding Estimates for Plane Stress Crack Problems," *J. Eng. Mater. Technol.*, vol. 98, no. 4, pp. 289–295, Oct. 1976, doi: 10.1115/1.3443380.

[68] C. F. Shih, "Relationships between the J-integral and the crack opening displacement for stationary and extending cracks," *J. Mech. Phys. Solids*, vol. 29, no. 4, pp. 305–326, Aug. 1981, doi: 10.1016/0022-5096(81)90003-X.

[69] V. Rizov, "Fracture in Composites - An Overview (Part I)," *J. Theor. Appl. Mech.*, vol. 42, no. 2, Jan. 2012, doi: 10.2478/v10254-012-0006-z.

[70] E. H. Dill, *The Finite Element Method for Mechanics of Solids with ANSYS Applications*, 0 ed. CRC Press, 2011. doi: 10.1201/b11455.

[71] C. K. H. Dharan, B. S. Kang, and I. Finnie, *Finnie's Notes on Fracture Mechanics*. New York, NY: Springer New York, 2016. doi: 10.1007/978-1-4939-2477-6.

[72] W. C. Kim and C. K. H. Dharan, "A fracture control plan for composite structures," *Eng. Fract. Mech.*, vol. 34, no. 2, pp. 305–324, Jan. 1989, doi: 10.1016/0013-7944(89)90145-8.

[73] E. F. Rybicki and M. F. Kanninen, "A finite element calculation of stress intensity factors by a modified crack closure integral," *Eng. Fract. Mech.*, vol. 9, no. 4, pp. 931–938, Jan. 1977, doi: 10.1016/0013-7944(77)90013-3.

[74] D. Xie, A. M. Waas, K. W. Shahwan, J. A. Schroeder, and R. G. Boeman, "Computation of Energy Release Rates for Kinking Cracks based on Virtual Crack Closure Technique," p. 11, 2004.

[75] A. Leski, "Implementation of the virtual crack closure technique in engineering FE calculations," *Finite Elem. Anal. Des.*, vol. 43, no. 3, pp. 261–268, Jan. 2007, doi: 10.1016/j.finel.2006.10.004.

[76] R. Krueger, "Virtual crack closure technique: History, approach, and applications," *Appl. Mech. Rev.*, vol. 57, no. 2, pp. 109–143, Mar. 2004, doi: 10.1115/1.1595677.
[77] R. Krueger, "The virtual crack closure technique for modeling interlaminar failure and delamination in advanced composite materials," in *Numerical Modelling of Failure in Advanced Composite Materials*, Elsevier, 2015, pp. 3–53. doi: 10.1016/B978-0-08-100332-9.00001-3.
[78] "Fracture Analysis Guide," p. 178, 2020.
[79] Mechanical Failure Prevention and Reliability (MPROVE) Research Center, Faculty of Mechanical and Manufacturing Engineering, Universiti Tun Hussein Onn Malaysia, 86400 Batu Pahat, Johor, MALAYSIA. *et al.*, "An Overview of Fracture Mechanics with ANSYS," *Int. J. Integr. Eng.*, vol. 10, no. 5, Oct. 2018, doi: 10.30880/ijie.2018.10.05.010.
[80] DNV, "DNV-ST-0377 Shipboard lifting appliances," DNV, Standrard ST-0377, 2022.
[81] DNV, "DNV-ST-0378-Offshore and Platform lifting appliances," DNV, Standrard ST-0378, 2022.
[82] I. American Petroleum, "API2C Specification of Offshore Cranes," American Petroleum Institute, Mar. 2005.
[83] DNV, "DNV Ships Part 3 Hull Chapter 4 Loads," DNV, Rules Part 3 Chapter 4, 2022.
[84] DNV, "DNV Yachts Part 3 Hull Chapter 3 Hull design loads," DNV, Rules Part 3 Chapter 3, 2022.
[85] BV, "Compose IT." Bureau Veritas.
[86] Ansys, "Ansys Meshing User's Guide," 2010.
[87] F. Barlat and J. Lian, "Mechanical APDL Element Reference," p. 1426.
[88] A. P. Mouritz, Introduction to aerospace materials. in Woodhead publishing in materials. Oxford (GB): Woodhead publ, 2012.
[89] S. W. Tsai and E. M. Wu, "A General Theory of Strength for Anisotropic Materials," J. Compos. Mater., vol. 5, no. 1, pp. 58–80, Jan. 1971, doi: 10.1177/002199837100500106.
[90] Reddy, J. N. (2004). Mechanics of Laminated Composite Plates and Shells: Theory and Analysis. CRC Press.
[91] Gibson, R. F. (2012). Principles of Composite Material Mechanics. CRC Press.
[92] Ashby, M. F.(2017). Materials selection in mechanical design. Cambridge, MA : Butterworth-Heinemann, an imprint of Elsevier